Fall 2022

Monitoring Titanium Dioxide Engineered Particles in Rural and Urban Surface Waters

Md Mahmudun Nabi

Monitoring Titanium Dioxide Engineered Particles in Rural and Urban Surface Waters

by

Md Mahmudun Nabi

Bachelor of Science
Bangladesh University of Engineering & Technology, 2009

Master of Science
University of Stuttgart, 2014

Submitted in Partial Fulfillment of the Requirements

For the Degree of Doctor of Philosophy in

Environmental Health Sciences

The Norman J. Arnold School of Public Health

University of South Carolina

2022

Accepted by:

Mohammed Baalousha, Major Professor

Geoffrey I. Scott, Committee Member

Susan D. Richardson, Committee Member

R Sean Norman, Committee Member

Cheryl L. Addy, Interim Vice Provost and Dean of the Graduate School

Dedication

To my parents, family, friends, mentors and colleagues.

Acknowledgements

It would have been impossible for me to come this long way without the continuous support, help and encouragement from my parents, my family, many outstanding people at the University of South Carolina, and those whom I met along the way. First and foremost, I would like to thank my advisor Dr. Mohammed Baalousha, who always had faith in me and always looked at the sunny side. I can never fully express my gratitude that how thankful I am to you for always being patient, everything you have taught, constantly guiding, and inspiring me. I also want to thank my co-advisor, Dr. Geoff. Scott. Despite his busy schedule as the chair of Department of Environmental Health Sciences, his door was always open for me. He played an instrumental role in this journey and had always been there for me for anything starting from research-recommendation-life advice.

In addition, I would like to thank my doctoral committee members for finding time amid their busy schedule for my dissertation defense, pointing out short comings in my research, guiding me in the right direction, and inspiring me to always ask for the fundamental aspects of my research.

I express my sincere gratitude to every one of the ENA group, Ferry group and Lead group. We have been a family. Special thanks to Jingjing Wang and Amar Jassim for being more than friends, being compassionate in time of research or personal difficult moments. All those friends around the department who always encouraged me, kept me smiling by smiling back to me. To everyone in the office of Environmental Health Science, who works behind the curtain and take care of all the administrative issues for us and works

tirelessly to ensure friendly work environment. To everyone from the office of International Student Services and Graduate School, who had always been there for any of immigration or academic needs and made my stay in this unknown land easier for all these years and transforming it as my second home.

Finally, a big thanks to my wife and two daughters, who have been there to support me through some of my most difficult hurdles outside of this degree. My daughters are peace to my eyes.

Abstract

Quantifying and characterizing engineered particles in environmental systems is key for assessing their risk but remains challenging and requires the distinction between natural and engineered particles. The Ph.D. dissertation research described in this thesis contributes to the current attempts to improve environmental nanoparticle analysis and better understand nanoparticle behavior in natural systems, with the focus being on natural streams, and the application of single particle inductively coupled plasma-time of flight-mass spectrometry (SP-ICP-TOF-MS) for distinguishing and tracing the origins of environmental nanoparticles. The objective of this dissertation is to characterize and quantify the concentrations of titanium dioxide engineered particles in urban surface water during and following rainfall events, establish a time and cost-efficient surrogate measure to monitor titanium dioxide engineered particles in urban surface water, evaluate the impact of urbanization on the concentrations of titanium dioxide engineered particles, and compare urban and rural river basins.

Four water sampling campaigns were performed to quantify engineered nanoparticle (ENP) concentrations in dynamic natural water systems (i.e., urban runoff impacted Broad, Congaree, and Saluda River and agricultural runoff-impacted Edisto River). The first three campaigns were performed at the discharge event scale in the urban Saluda, Broad, and Congaree Rivers. In contrast, the fourth sampling campaign was a long-term campaign performed between 2017 and 2019 in the Edisto River. The first sampling campaign was performed in 2018 following hurricane Florence to investigate the impact

of rainfall on the concentrations of TiO_2 engineered particles in the Broad River. The second sampling campaign was performed in 2019 during a range of hydrologic settings to investigate the impact of wet and dry weather on the concentrations of TiO_2 engineered particles in the Broad River. The third sampling campaign was performed in 2020 to determine the impact of urbanization on the concentrations of TiO_2 engineered particles in the Saluda, Broad, and Congaree Rivers. The fourth sampling campaign was performed by collecting water samples on a biweekly basis from the Edisto River to investigate the seasonal variability in TiO_2 engineered particle concentrations.

For all field studies, water samples were analyzed for total metal concentrations following acid digestion. Bulk elemental ratios (e.g., Ti/Nb, Ce/La) were determined to determine whether water samples were contaminated with anthropogenic Ti and Ce. The concentrations of anthropogenic Ti and Ce were determined using mass balance calculations and shifts in elemental ratios above the natural background ratios. Selected samples were analyzed for particle number concentration and elemental composition using single particle-inductively coupled plasma-time of flight-mass spectrometer (SP-ICP-TOF-MS). Agglomerative hierarchical analysis was used to group particles into clusters of similar elemental compositions and to compare particles across samples.

In the urban Rivers (Saluda, Broad and Congaree), the elemental ratios of Ti/Nb increased with discharge and with urbanization. In contrast, the elemental ratio of Ti/Nb in the rural Edisto River varied seasonally with increases during spring and summer and decreases during the fall and winter. The elemental composition of multi-element titanium-bearing particles at the single particle level were determined by SP-ICP-MS and were similar throughout rain events in urban Rivers and seasons in the rural River, and consisted

of clusters of FeTiMn, AlSiFe, and TiMnFe, which are typical of naturally occurring iron oxide, clay, and titanium oxide particles. The elemental ratio distributions of Ti/Nb, Ti/Fe, and Ti/Al, determined on a single particle basis using SP-ICP-TOF-MS, were similar between samples during the different rainfall events, indicating that naturally occurring particles had the same elemental ratios and origin. Therefore, the changes in Ti/Nb ratios in the bulk water samples were attributed to the introduction of titanium dioxide engineered particles into the rivers with urban/agricultural runoff during and following rainfall events.

Water samples were collected from the Broad River during seven discharge events in 2018 and 2019. Discharge, bulk elemental concentrations (*e.g.,* Ti, Al, Fe, Nb and Ce), bulk elemental ratios (*e.g.,* Ti/Al, Ti/Fe, and Ti/Nb), TiO_2 engineered particle concentration, and turbidity displayed the same trend of rise and fall as the discharge/runoff following storm events. Linear relationships were established between turbidity and TiO_2 engineered particle concentrations in the Broad River for different flow regimes. The established correlations between turbidity and TiO_2 engineered particle concentrations are important as they can be used to translate the continuously monitored turbidity to TiO_2 concentrations. The concentrations of titanium dioxide engineered particles in the Broad River varied between 20 and 140 μg TiO_2 L^{-1} following the rainfall events in 2018. During a range of hydrologic settings in 2019, the concentrations of titanium dioxide engineered particles in the Broad River varied between 4 and 412 μg TiO_2 L^{-1}.

This study demonstrates that diffuse urban runoff results in high concentration of TiO_2 particles in urban surface waters during and following rainfall events which may pose increased risks to aquatic organisms during these episodic events. The urbanization impacted concentration of anthropogenic TiO_2 increased following the order 0 to 24 μg L^{-}

^{1} in the Lower Saluda River < 0 to 663 µg L^{-1} in the Broad River < 43 to 1051 µg L^{-1} in Congaree River at Cayce <58 to 5050 µg L^{-1} in the Congaree River at Columbia.

On the other hand, in a rural river basin (Edisto River, < 1% urban land cover) in South Carolina, United States, the total concentrations of Ti, Nb, Al, Fe, Ce, and La trended higher during spring/summer compared to autumn/winter, indicating agricultural prep and growing season related increases in TiO_2 engineered particles. Surface water concentrations of TiO_2 engineered particles varied between 0 to 129 µg L^{-1} in the rural Edisto River. Increases in TiO_2 concentrations over the spring/summer were associated with increases in phosphorous, orthophosphate, nitrate, ammonia, anthropogenic gadolinium, water temperature, suspended sediments, organic carbon, and alkalinity, and with decreases in dissolved oxygen. The association between these contaminants together with the timing of the increases in their concentrations is consistent with diffuse wastewater source, such as reuse application overspray, biosolids fertilization, or leaking sewers or septic tanks, as the driver of instream concentrations; however, other diffuse sources cannot be ruled out.

This study provides clear evidence that significant concentrations of TiO_2 engineered nanoparticles enter aquatic systems with urban/agricultural runoff, and that the concentration of TiO_2 engineered nanoparticles entering surface waters via runoffs are expected to increase with the increased applications of TiO_2 engineered particles in consumer products, which may pose higher risks to urban/rural stream aquatic ecosystems during the storm events. Hence, the demonstrated results of this dissertation illustrate the importance of monitoring temporal and/or seasonal variations in engineered particles concentrations in surface waters for a more representative assessment of ecosystem risk.

Table of Contents

List of Tables

List of Figures

List of Abbreviations

ENP .....Engineered nanoparticle

ICP-TOF-MS .....Inductively coupled plasma-time of flight Mass spectrometry

INPs..... Incidental nanoparticles

mmNPs..... Multi-metal nanoparticles

NNPs..... Natural nanoparticles

NP .....Nanoparticle

PNEC .....Predicted no effect concentration

REE .....Rare earth elements

SP ..... Single particle

TEM ..... Transmission electron microscopy

Chapter 1

Introduction

1.1 Nanotechnology, Nanoparticles and Risk

Nanotechnology is anticipated to be one of the major pillars of the next industrial revolution. Nanoparticles (NPs), the building blocks of nanotechnology [1], can be categorized into three types: natural, incidental, and engineered. Engineered NPs (ENPs), designed with very specific properties are tailor made through certain physicochemical processes, including self-assembly (from atoms and molecules) or milling (from their macro-scale counterparts). Due to their nanoscale size (1-100 nm), NPs may possess unique chemical, biological, and physical properties as compared to larger particles of the same material, which gives them an edge in diverse applications [2]. Applications of ENPs include various consumer products from various industries: electronics, medical, environmental, and so on [1]. ENPs may be released into the environment primarily through industrial and environmental applications [3,4] such as diesel engine exhaust, cigarette smoke, indoor pollution, building demolition, cosmetics and other consumer products, manufacturing of engineered nanoparticles etc. [5]. ENPs may thus enter the natural environment (e.g., waters, soils, atmosphere, and sediments) where they may pose risk to environmental and human health [6,7].

Detection and quantification of ENPs in environmental matrices is key for robust risk and lifecycle assessment of ENPs. Risk assessment requires an in detailed understanding of exposure to ENPs and toxicity of ENPs. Plenty of literatures are available on the toxicity of ENPs whereas research on the concentration or exposure assessment of ENPs in the environment including surface waters are scarce and mostly model predicted. Model predicted concentration comes with inherent uncertainties. To validate model prediction several concentration determinations research had been carried out and reported.

However, the research on detection and quantification of ENPs in the environmental samples is in its infancy.

1.2 Engineered Titanium dioxide nanoparticles application and release in the environment

The global consumption of TiO_2 was estimated at 6.1 MMT in 2016 and is projected to reach 8.8 MMT by 2025 [8,9]. A survey of 2012 showed that TiO_2 ENPs are the most produced ENPs worldwide with production volumes of approximately 10,000 tons [10,11]. TiO_2 is widely used in many applications as pigment and engineered particles. It's used as a white pigment because of its brightness and light reflection capacity. There had been 5.3 billion liters $year^{-1}$ paint demand in the United States in 2019, 33% of which (e.g., 1.77 billion liters $year^{-1}$) is used for exterior paint [12]. The United States road markings demand is estimated at 350,000 metric tons $year^{-1}$ in 2018 [13]. White road markings contain at least 10% wt TiO_2 pigments, corresponding at least to 35,000 metric tons TiO_2 pigments per year in 2018. Moreover, road markings demand is projected to be increased to 450,000 metric tons $year^{-1}$ in 2025 [14]. TiO_2 pigments for coatings has an optimum particle size between 100-300 nm in diameter theoretically, but the sizes range from the nano-range to several hundreds of nanometers [15]. Consequently, TiO_2 ENPs are present in most of the TiO_2 pigments in a certain fraction [10]. TiO_2 is used in industrial and architectural paints (60%), plastics (28%), paper (5%), printing ink, roofing granules, ceramics, catalysts, sunscreen, toothpaste, cosmetics, foods etc [16]. TiO_2 used in whitening agent in foods, cosmetics, toothpaste and sun blocks, are ending up in municipal wastewater [17] -a small percentage (*e.g.*, 7% or 0.427 million metric tons) of the global TiO_2 use. TiO_2 is used in

paint in the indoor environment could be released to indoor dust. TiO_2 is also in road marking and thus may be released to surface waters with urban runoff. Many studies in literature shows the presence of TiO_2 ENPs in very low concentration in the surface water of Colorado creek and Danube lake (in the range of 0.4 ng to 27.1 µg per liter range) [17]; but relatively higher TiO_2 ENPs concentration is found in urban runoff (5 to 150 µg per liter) [18], sewage spills (up to 100 µg per liter) [17], stormwater green infrastructures (550 to 1800 mg per kg) [19], and wastewater treatment plants influent (302 to 2057 µg per liter) [20]. These concentrations are in the same order of magnitude in the lower end to higher as the predicted no effect concentration (PNEC) for TiO_2 pigments (*e.g.,* 127-184 µg L^{-1}) and is higher than the PNEC for TiO_2 ENPs to freshwater organisms (*e.g.,* 1-18 µg L^{-1}) [21,22].

1.3 Engineered Cerium dioxide nanoparticles application and release in the environment

Cerium is the most abundant of rare-earth metals found in the Earth's crust. Several Ce-carbonate, -phosphate, -silicate, and -(hydr)oxide minerals have been historically mined and processed for pharmaceutical uses and industrial applications. Of all Ce minerals, cerium dioxide has received much attention in the global nanotechnology market due to their useful applications for catalysts, auto mobile catalytic converter as a censor, fuel cells, solar panels and fuel additives [23]. CeO_2 ENPs are most famously used as a diesel fuel additive (Envirox) to reduce particulate matter emissions and increase fuel economy [24]. CeO_2 ENPs are released in the urban corridors as a result of the combustion of diesel fuel containing the additive Envirox, and hence may be released to surface waters with urban runoff. The estimated concentrations of CeO_2 NPs in WWTP in the San Francisco

Bay area are 10^{-2} to 1 µg/L in effluent and 1 to 10 µg/kg in dry biosolids [25]. In other study by Gottschalk *et al.* (2013) [26], even much lower concentration of CeO_2 NPs in WWTP effluent and biosolid are reported (0.5×10^{-4} µg/L and 10^{-6} mg/kg, respectively). While there are needs in improving the detection and quantification of CeO_2 ENPs in different environmental media, it is imminent that organisms in ecosystem will be exposed to these low concentrations (micro gram per liter or kilogram) [25].

1.4 Engineered Lanthanum oxide nanoparticles application and release in the environment

Among REE applications, lanthanum oxide nanoparticles (La_2O_3 ENP) have been exploited for use in sensors, electronics, fuel cells, magnetic data storage, antimicrobials, catalysis, automobiles, water treatment, phosphate removal and biomedicine [27]. La_2O_3 is being used in automobile exhaust gas converter [28] and fluid catalytic cracking for petrochemical industries and therefore may be released to surface waters with urban runoff [29]. Balusamy et al. (2015) reported that there is significant toxicity of La_2O_3 NP on *D. magna* at concentrations 500 and 1000 mg L^{-1}; and the effective concentration (EC_{50}) and lethal dose (LD_{50}) for aquatic organism had been determined to be 500 and 1000 mg L^{-1} respectively [25].

1.5 Urban Runoff and Hurricanes

Urban runoff is surface runoff of rainwater created by urbanization. This runoff is a major source of flooding and water pollution in urban communities worldwide. Impervious surfaces (roads, parking lots and sidewalks) are constructed from materials

such as asphalt and concrete during land development. ENPs (e.g., TiO_2 used in paint, CeO_2 used in fuel additives and La_2O_3 used in catalytic convertor and in fluid catalytic cracking) are likely to be released to the atmosphere, where they deposit on those hard-impervious surfaces. During rain, hurricanes and other precipitation events, these impervious surfaces, along with rooftops get washed with rain/urban runoff and carry polluted rainwater to storm drains, instead of allowing the water to percolate through soil [30]. Urban runoff typically washes off urban dust and topsoils, which may transfer high concentration of ENPs to receiving surface water [31]. Thus, Urban waters receive large amounts of pollution, including TiO_2 engineered particles, from a variety of sources such as industrial discharges, mobile sources (*e.g.,* cars and trucks), residential and commercial wastewater, and polluted stormwater runoff from urban landscape which is likely to result in high episodic engineered particle concentrations in urban surface waters during and following rainfall events.

In most cases, contaminant, including TiO_2 engineered particle, in urban rivers are not characterized by a constant concentration, but rather by the episodic or random occurrence of rainfall events, snowmelt, and/or return flows and subsequent high river flows [32]. For instance, a recent environmental fate modeling study suggested that stormwater runoff could result in high variability in TiO_2 engineered nanoparticle concentrations in urban rivers, with high flow events generating a large proportion of the total annual TiO_2 engineered nanoparticle loads in rivers [33]. Variables affecting contaminant load in rivers, thus may affect TiO_2 engineered particle concentrations, include antecedent rainfall, duration of the rainfall event, rainfall intensity of the event, succession of rainfall events, time of rise and fall of the hydrograph, runoff duration, peak

discharge and total runoff [34]. Between rainfall events, contaminants in the catchment, including TiO_2 engineered particles, tend to build up via dust blown in by wind, tire wear residue, paint and road marking wear, etc. Thus, the longer period between the antecedent and current rainfall events, the greater the mass of an individual contaminant available for wash-off from surfaces in the basin. In response to the changing intensity, duration, and frequency of rainfall events, some or all the available contaminants are washed off and transported to receiving surface waters [35,36]. While the contaminant mass can increase by storm events, higher peak flows and discharges may end up displaying lower concentrations due to dilution effects.

Hurricane is a special case of runoff when there is a lot of precipitation, resulting in high volume of surface runoff. For example, hurricane Florence (14 to 17 September 2018) achieved Category 4 status over the open Atlantic Ocean, but the storm weakened before it made landfall as a Category 1 with a very large wind circulation. Florence is an example of what meteorologists have come to understand: Category at landfall is not necessarily related to total rainfall. Florence is the new "flood of record" in North Carolina, where 914.4 mm fell in Swansboro, and in South Carolina for tropical storms, where 609.6 mm fell in Loris. There had been 108.2 mm rainfall in Columbia, SC during this event. Recent trends suggest that the number of hurricane events have increased along with the event intensity. The resulted enormous urban runoff during hurricane events washes off urban corridors and may transport high concentration of ENPs to receiving surface water. Pollutants in urban rivers are associated mainly with suspended particles, which act as the transport vector to downstream areas [37]. Neal et al. (2011) reported dissolved (<0.45μm filtered fraction) TiO_2 concentration in urban or industrial, agricultural, and rural rivers in

the UK ranged in the average of 0.9 to 10.8 µg L^{-1} (mean 3.5 µg L^{-1}) [38]. Peters et al. (2017) detected µ-TiO_2 of average particle size 300 nm in Meuse and Ijssel river's surface water within concentration 0.2 to 8.2 µg L^{-1} with an average concentration of 3.1 µg L^{-1} [39]. A recent environmental fate modelling study by Parker et al. (2019) suggested that nano TiO_2 could be present in the peak concentration range of 619 to 1490 µg L^{-1} in urban rivers impacted by stormwater runoff [33]. All of these studies measured the total concentration of Ti by elemental analysis; and reported as the concentration of engineered TiO_2 by identifying the particle size (>150nm, at least) by spICPMS or by scanning electron microscopy (SEM) in a given sample; or are based on ENP fate modelling. The presence of natural Ti has not been considered quantitively. Therefore, it is evident that none of these studies provide measured quantitative concentration of TiO_2 engineered particles in the river surface waters and the contributions of natural and engineered particles to the total Ti concentrations have not been distinguished. Moreover, there have been several studies on the engineered particle, such as TiO_2 fluxes from municipal wastewater treatment plants, urban runoff and sewage spills to urban surface waters, however, these measurements were a proof of concept of the analytical approach and did not investigate the temporal variability of the measured concentrations; or the relationship between TiO_2 engineered particle concentrations and environmental parameters such as flow discharge, temperature, pH, dissolved oxygen, turbidity, or suspended solids; and the roles of urban areas in controlling these fluxes are yet to be evaluated adequately [17,18,40].

1.6 Biosolid amended agricultural soils and septic system

Agriculture land applied biosolids (sewage sludges) are widely recognized as a major vector of chemicals, including heavy metals and nutrients, to biosolid amended soils and nearby surface waters, and therefore biosolids has been shown to contribute significantly to the deterioration of amended soil and surface water quality [41,42]. Engineered nanoparticles present in the municipal wastewater are concentrated in wastewater treatment plants, accumulated in biosolids and eventually ended up in agricultural fields [43–45]. In the United States, there are 7 million dry tons of biosolids are produced annually, and 55% of the produced biosolids (based on 2004 data) are applied for agriculture, silviculture, land restoration etc. [46,47]. Seventy four percent of the total amount of biosolids applied to soils are used for agriculture on farmlands. Treated sludge is usually applied to land as a liquid spray or solid cake which contains Ti-, Fe-, Zn-, Sn- and Pb-containing particles [48,49]. When the rainfall exceeds the infiltration capacity of the soil in an predominantly agricultural watershed, the created surface runoff can transport the engineered nanoparticles from agricultural fields to the surface water [50]. In literature, titanium oxides, iron oxides, and silver and zinc sulfides etc. metal containing particles have already been identified in sewage sludge and sludge-amended soils [45,49,51–53]. A recent modelling study suggested that the concentration of nano-TiO_2 and nano-silver are 42 µg Kg^{-1} and 662 ng Kg^{-1} per year, respectively in biosolid treated soils in USA [54]. However, these modeled concentrations have not been validated by field measurements, therefore suffers from significant uncertainties. Yang et al., (2014) identified TiO_2 in biosolid amended soils in Texas, USA in an average concentration of 2382 ± 422 mg Kg^{-1} [42]. Moreover, the available studies reported the presence of TiO_2 EPs in biosolids, biosolids-amended agricultural soils, and

other relevant environmental compartments by measuring the total concentration of Ti using elemental analysis accompanied with TiO_2 particle identification by electron microscopy techniques, without estimating the relative fractions of engineered and natural Ti particles [55]. Additionally, more than 21 million households in the United States, most commonly in rural areas, use septic systems – not a public sewer – to trap and filter toilet waste [56]. Septic tanks also are widely recognized as an important source of chemicals to ground and surface waters [57,58]. Although it is well recognized that septic tank and agricultural discharges contributes to the loading of contaminants, including TiO_2 [26,59,60], in river surface water, there are currently no field data on the occurrence and concentrations in surface water receiving septic tank and agricultural discharges.

1.7 Challenges for the characterization of engineered nanoparticles

The detection and quantification of ENPs in the environment is challenging because of their small size, low concentration, lack of appropriate methodology and the relatively high background level of incidental and naturally occurring NPs (NNPs, ca. 1-1000mg/l in fresh waters), often with similar elemental composition [61]. However, natural NPs may contain natural tracers that could be exploited to differentiate natural from engineered particles and to estimate the concentration of ENPs. For instance, natural riverine TiO_2 particles had been shown to be associated with at least one of the following elements Al, Fe, Ce, Si, La, Zr, Nb, Pb, Ba, Th, Ta, W and U [62]. The elemental ratios of Ti to these elements, except for Pb, were in good agreement with those of riverine average elemental ratios and average crustal ratios. TiO_2 ENPs are manufactured by removing these elemental impurities from the parent natural TiO_2 minerals by dissolution and reprecipitation as TiO_2

engineered particles. This process finally results in pure TiO_2 engineered particles. Thus, the introduction of TiO_2 engineered particles into the environment, will result in an increase in the elemental ratio of Ti to these natural tracers (e.g., Al, Fe, Nb, Ta, etc.). However, all TiO_2 ENPs, apart from the food additives, contain 1-15% Al, Si, or Zr as coatings on the surface. Thus, elemental ratios of Ti to Al, Ti to Si, and Ti to Zr might result in underestimation of TiO_2 engineered particle concentrations. Nonetheless, other elements such as Nb and Ta have not been reported to be used in TiO_2 engineered particles. Additionally, natural TiO_2 particles such as rutile and ilmenite are major carriers of Nb and Ta (90-95%) [63,64]. However, the Ta concentration is often found below the limit of detection in the natural environmental samples. Therefore, Nb will be used for tracing natural Ti-particles and Ti/Nb ratio will be used for the quantification of TiO_2 ENP's total concentration [17].

Engineered cerium oxide (used in diesel fuel additive) and Lanthanum oxide (used in fluid catalytic cracking for petrochemical industries) nano-particles (CeO_2, La_2O_3 ENPs) are relatively pure [29]. The naturally occurring CeO_2 contains only trace amounts of other rare earth elements (REEs) such as La, Ba, Pr, Nd, Th [65,66]. The elemental ratios of Ce and La to these elements (Pr, Nd) were in good agreement with those of average crustal ratios. Th often fall below the detection limit. Moreover, Salminen et al. (2005) demonstrated that cerium (Ce) and lanthanum (La) are present in a stable 2 : 1 ratio in soils and stream sediments throughout Europe [67]. Therefore, Ce/La ratio will be used to distinguish CeO_2 and La_2O_3 ENPs released from anthropogenic activities to surface waters from CeO_2 and La_2O_3 NNPs. But if both CeO_2 and La_2O_3 ENPs are released at the same time, the Ce/La ratio will be erroneous since proportionally elevated value of both Ce and La can still yield

a stable 2:1 ratio! Hence, Ce/REEs and La/REEs ratios will be used to evaluate the presence of CeO_2 and/or La_2O_3 engineered particles.

1.8 Approaches for the characterization of engineered nanoparticles

The overall arching approach to detect and quantify engineered TiO_2 particles in environmental matrices is based on differentiating natural and engineered particles based on differences in their physicochemical properties. Several methods have been proposed to differentiate natural from engineered TiO_2 particles including 1) elemental ratios of Ti to Nb, Ti to Ta, and Ti to Al [17,68]; 2) geochemical indices such as enrichment factor, contamination factor, and geoaccumulation index [69]; 3) particle morphology [70]; 4) presence of engineered coating [71]. But none of these methods are 'unequivocal' for the characterization of TiO_2 EPs. The TiO_2 EPs are manufactured by removing all the natural impurities from natural parent minerals. Thus, detecting elemental impurities in TiO_2 particles as well as elemental ratio might assist to differentiate between natural and engineered TiO_2 particles. Nevertheless, the environmental processes could alter the elemental associations and ratios by dissolution due to change in pH and redox potential (environmental conditions), or during particle extraction [72]. Several authors suggested geochemical indices to estimate the level of TiO_2 contamination, which is a bulk technique based on background and sample TiO_2 and Fe concentration. Moreover, background concentrations of metals in environmental matrices can vary naturally by several orders of magnitude, hence the use of geochemical indices technique might be misleading in differentiating between the natural and engineered TiO_2 particle [73]. Transmission electron microscopy (TEM) could help in differentiating natural from the engineered TiO_2 particles

by observing the TiO_2 particle morphology (i.e., rough irregular surface for natural nano particles vs. regular surface for ENP). However, the presence of high concentration of natural particles, poor statistical power due to the viability that limited number of particles can be imaged and analyzed within reasonable cost and time frame along with demanding operator time hamper the quantification of TiO_2 EPs in complex environmental matrices [17]. Other studies suggested, the presence of engineered organic coating for engineered particles could differentiate between the TiO_2 natural and engineered particles, but the organic coatings could be easily desorbed in nature with the water interaction [71]. It's feasible in the complex environmental matrices due to the fact that TiO_2 EPs with similar composition as natural counterpart can follow the exact same transformation pathways, thus distinction might be impossible between the TiO_2 natural and engineered particles [69]. On the other hand, sp-ICP-TOF-MS is a promising technique to differentiate ENPs from NNPs based on elemental associations and elemental ratios at the single particle level.

For the metal ENPs, inductively coupled plasma-mass spectrometry (ICP-MS) and energy dispersive spectroscopy (EDS) coupled to transmission electron microscopy (TEM) are the most widely used methods. Multielement-Single particle inductively coupled plasma-mass spectrometry (ME-SP-ICP-MS) are being used to differentiate between natural and engineered particles now a days (e.g. CeO_2 & TiO_2) [17]. These analytical techniques are not beyond limitations, but together as a cross checking measure they provide data on the occurrence, concentration, and properties of ENPs in environmental compartments with adequate level of confidence. The advantages and disadvantages of the analytical techniques are summarized in Table 1.1.

1.9 Dissertation overview

The challenges in detection, quantification and characterization of ENPs in environmental systems are not fully overcome [7]. In particular, the presence of natural nanoparticles has not been addressed quantitatively, and the analytical method to differentiate between the engineered nanoparticles and natural nano particles has not been completely developed. This research is primarily focused on developing analytical approaches to overcome the challenges in detecting, quantifying and characterizing ENPs in environmental system [7], particularly in surface water, focusing on chemical nature, concentration, size and morphology of the nanoparticles and providing a framework to monitor ENPs in surface water. Basically, the physicochemical properties (elemental composition, ratio, size and morphology) of the ENPs which are distinct in comparison to their natural counterparts are characterized and used to distinguish between the ENPs and NNPs. This dissertation is organized into six chapters.

Chapter 1 provides a general overview of NPs in the environment, the possible routes of ENPs from anthropogenic application to the environmental systems, and characterization. It also includes the overall research goals of this work and overall dissertation organization.

Chapter 2 reports a protocol for the characterization of the elemental composition of Ti-containing particles in the Broad River on a single particle basis using SP-ICP-TOF-MS during and following rainfall events, monitoring the occurrence and concentration of TiO_2 engineered particles in the Broad River, and determining the possible source(s) of TiO_2 engineered particles in the Broad River, Columbia, South Carolina, United States.

Chapter 3 describes the quantification of the temporal variability in TiO_2 engineered particle concentrations in the Broad River, Columbia, South Carolina, United States during dry and wet weather conditions under rainfall events of various characteristics, evaluating the impact of rainfall events characteristics on TiO_2 engineered particle concentrations, and determining the correlation between TiO_2 engineered particle concentrations, flow discharge, and environmental indicators with particular emphasis on turbidity as a surrogate for suspended sediment concentration.

Chapter 4 investigates the impact of urbanization on the concentrations of TiO_2 engineered particles in urban surface waters.

Chapter 5 reports the seasonal variability in TiO_2 engineered particles concentrations and explore the relationship between TiO_2 and other contaminant concentrations in a rural river basin (Edisto River, South Carolina) with limited urban development (< 1%).

Chapter 6 discusses the overall conclusions of the dissertation, the environmental implications of the different studies performed as part of this PhD dissertation, and the recommendations for future studies.

Table 1.1: Advantages and disadvantages of the analytical techniques

Method	Advantage	Disadvantage
ICP-MS	- Provide elemental isotopic ratio information	- It is a bulk technique that does not provide information on a single particle basis
ME-SP-ICP-MS	- Provide elemental composition on a single particle basis	- In cases where the environmental matrix includes distinct NNPs containing the same element(s) as the ENPs (e.g. Ce, Ti, Si, Fe), it cannot be used to differentiate ENPs from NNPs because both particle types are detected as signal bursts with high SBRs [74]
FFF-ICP-MS Coupled	- It separates particles, and provide elemental associations & ratios as a function of particle size	- Particle losses in the channel due to particle-membrane interactions.
TEM	- Can detect qualitatively ENPs across the entire nanoscale range and determine particle morphology	- Demanding operator time, the presence of high concentrations of natural particles, the poor statistical power due to limited number of particles that can be imaged and analyzed within a reasonable time and cost frame, hamper the quantification of ENPs in complex matrices

References

1. Zänker, H. & Schierz, A. Engineered Nanoparticles and Their Identification Among Natural Nanoparticles. Annu. Rev. Anal. Chem. 5, 107–132 (2012).
2. Mrowiec, B. Nanomaterials in the environment. E3S Web of Conferences 22, (2017).
3. EPA. Nanotechnology for site remediation fact sheet. Solid waste and emergency response. (2008).
4. Huang, S. H. & Chen, D. H. Rapid removal of heavy metal cations and anions from aqueous solutions by an amino-functionalized magnetic nano-adsorbent. J. Hazard. Mater. 163, 174–179. (2009).
5. Buzea, C., Pacheco Blandino, I. I. & Robbie, K. Nanomaterials and nanoparticles: Sources and toxicity. Biointerphases 2, (2007).
6. Benn, T., Cavanagh, B., Hristovski, K., Posner, J. D. & Westerhoff, P. The release of nanosilver from consumer products used in the home. J. Environ. Qual. 39, 1875–1882 (2010).
7. Baalousha, D. M. Developing Analytical Methods for the Detection and Quantification of Engineered Nanoparticle Release in Complex Environmental Matrices. (2017). Available at: https://calendar.buffalo.edu/event/171117ewrebaalousha/.
8. Cision. Titanium Dioxide (TiO_2) - A Global Market Overview. (2016).
9. Loosli, F. et al. Sewage spills are a major source of titanium dioxide engineered (nano)-particle release into the environment. Environ. Sci. Nano 6, 763–777 (2019).
10. Piccinno, F., Gottschalk, F., Seeger, S. & Nowack, B. Industrial production quantities and uses of ten engineered nanomaterials in Europe and the world. J. Nanoparticle Res. 14, 1109 (2012).
11. Peters, R. J. B. et al. Detection of nanoparticles in Dutch surface waters. Sci. Total Environ. 621, 210–218 (2018).
12. Coatingsworld. Demand for Paint and coatings to reach 1.4 Billion Gallons in 2019 | Statista. (2019). Available at: https://www.statista.com/statistics/684695/united-states-paint-and-coatings-demand-by-market/. (Accessed: 22nd April 2020)
13. Grand View Research. No Title. (2018). Available at: https://www.grandviewresearch.com/industry-analysis/%0Atraffic-road-marking-coatings-market/request. (Accessed: 22nd April 2020)
14. ASTM. ASTM D7942 - 15 Standard Specification for Thermoplastic Pavement Markings in Non Snow Plow Areas. (2015). Available at: https://www.astm.org/Standards/D7942.htm. (Accessed: 22nd April 2020)
15. Weir, A., Westerhoff, P., Fabricius, L., Hristovski, K. & von Goetz, N. Titanium Dioxide Nanoparticles in Food and Personal Care Products. Environ. Sci. Technol. 46, 2242–2250 (2012).
16. Linak, E. & Inoguchi, Y. Chemical Economics Handbook: Titanium Dioxide. (SRI Consulting, Menlo Park, 2005).
17. Loosli, F. et al. Sewage spills are a major source of titanium dioxide engineered (nano)-particle release into the environment. Environ. Sci. Nano 6, 763–777 (2019).
18. Wang, J. et al. Detection and quantification of engineered particles in urban runoff. Chemosphere 248, 126070 (2020).

19. Baalousha, M. et al. Stormwater green infrastructures retain high concentrations of TiO_2 engineered (nano)-particles. J. Hazard. Mater. 392, 122335 (2020).
20. Westerhoff, P., Song, G., Hristovski, K. & Kiser, M. A. Occurrence and removal of titanium at full scale wastewater treatment plants: Implications for TiO_2 nanomaterials. J. Environ. Monit. 13, 1195–1203 (2011).
21. Nowack, B. & Mueller, N. C. Exposure modeling of engineered nanoparticles in the environment. EMPA Act. 41, 63 (2008).
22. Lützhøft, H., Hartmann, N., Brinch, A. & Kjølholt, J. Environmental Effects of Engineered Nanomaterials: Estimations of Predicted No-Effect Concentrations (PNECs). (2015).
23. Dahle, J. T. & Arai, Y. Environmental geochemistry of cerium: applications and toxicology of cerium oxide nanoparticles. Int. J. Environ. Res. Public Health 12, 1253–1278 (2015).
24. Dale, J. G., Cox, S. S., Vance, M. E., Marr, L. C. & Hochella, M. F. Transformation of Cerium Oxide Nanoparticles from a Diesel Fuel Additive during Combustion in a Diesel Engine. Environ. Sci. Technol. 51, 1973–1980 (2017).
25. Dahle, J. T. & Arai, Y. Environmental geochemistry of cerium: Applications and toxicology of cerium oxide nanoparticles. International Journal of Environmental Research and Public Health 12, 1253–1278 (2015).
26. Gottschalk, F., Sun, T. & Nowack, B. Environmental concentrations of engineered nanomaterials: Review of modeling and analytical studies. Environ. Pollut. 181, 287–300 (2013).
27. Balusamy, B. & Uyar, T. Toxicity of lanthanum oxide (La_2O_3) nanoparticles in aquatic environments. Environ. Sci. Process. Impacts (2015). doi:10.1039/C5EM00035A
28. Cao, J. et al. Controllable syntheses of hexagonal and lamellar mesostructured lanthanum oxide. Mater. Lett. 59, 408–411 (2005).
29. Blay, V. et al. Engineering zeolites for catalytic cracking to light olefins. ACS Catal. 7, 6542–6566 (2017).
30. VA: U.S. Geological Survey (USGS), U. W. S. S. R. Runoff: Surface and Overland Water Runoff. Available at: https://www.usgs.gov/special-topic/water-science-school/science/runoff-surface-and-overland-water-runoff?qtscience_center_objects=0#qt-science_center_objects. (Accessed: 30th April 2019)
31. He, W., Odnevall Wallinder, I. & Leygraf, C. A laboratory study of copper and zinc runoff during first flush and steady-state conditions. Corros. Sci. 43, 127–146 (2001).
32. Nabi, M. M., Wang, J. & Baalousha, M. Episodic increases in titanium dioxide engineered particle concentrations in the Broad River following rainfall events (In Preparation). (2020).
33. Parker, N. & Keller, A. A. Variation in regional risk of engineered nanoparticles: nano TiO_2 as a case study. Environ. Sci. Nano 6, 444–455 (2019).
34. Onderka, M., Krein, A., Wrede, S., Martínez-Carreras, N. & Hoffmann, L. Dynamics of storm-driven suspended sediments in a headwater catchment described by multivariable modeling. J. Soils Sediments 2012 124 12, 620–635 (2012).
35. Vercruysse, K. & Grabowski, R. C. Temporal variation in suspended sediment transport: linking sediment sources and hydro-meteorological drivers. Earth Surf. Process. Landforms 44, 2587–2599 (2019).

36. Vercruysse, K., Grabowski, R. C. & Rickson, R. J. Suspended sediment transport dynamics in rivers: Multi-scale drivers of temporal variation. Earth-Science Rev. 166, 38–52 (2017).
37. Smail, E. A., Webb, E. A., Franks, R. P., Bruland, K. W. & Sañudo-Wilhelmy, S. A. Status of Metal Contamination in Surface Waters of the Coastal Ocean off Los Angeles, California since the Implementation of the Clean Water Act. Environ. Sci. Technol. 46, 4304–4311 (2012).
38. Neal, C. et al. Titanium in UK rural, agricultural and urban/industrial rivers: Geogenic and anthropogenic colloidal/sub-colloidal sources and the significance of within-river retention. Sci. Total Environ. 409, 1843–1853 (2011).
39. Peters, R. J. B. et al. Detection of nanoparticles in Dutch surface waters. Sci. Total Environ. 621, 210–218 (2018).
40. Taylor, K. G. & Owens, P. N. Sediments in urban river basins: A review of sediment-contaminant dynamics in an environmental system conditioned by human activities. Journal of Soils and Sediments 9, 281–303 (2009).
41. Smith, I. M., Hall, K. J., Lavkulich, L. M. & Schreier, H. Trace metal concentrations in an intensive agricultural watershed in British Columbia, Canada. J. Am. Water Resour. Assoc. 43, 1455–1467 (2007).
42. Yang, Y. et al. Metal and nanoparticle occurrence in biosolid-amended soils. Sci. Total Environ. 485–486, 441–449 (2014).
43. De La Rosa, G., Laura López-Moreno, M., Hernandez-Viezcas, J., Montes, M. O. & Peralta-Videa, J. R. Toxicity and biotransformation of ZnO nanoparticles in the desert plants Prosopis juliflora-velutina, Salsola tragus and Parkinsonia florida. Int. J. Nanotechnol 8,
44. Judy, J. D. & Bertsch, P. M. Bioavailability, Toxicity, and Fate of Manufactured Nanomaterials in Terrestrial Ecosystems. in Advances in Agronomy 123, 1–64 (Academic Press Inc., 2014).
45. Kim, B., Murayama, M., Colman, B. P. & Hochella, M. F. Characterization and environmental implications of nano- and larger TiO_2 particles in sewage sludge, and soils amended with sewage sludge. J. Environ. Monit. 14, 1129–1137 (2012).
46. US EPA. Biosolids Generation, Use, and Disposal in The United States. (US EPA Washington, DC, USA, 1999).
47. North East Biosolids and Residuals Association (NEBRA). A national biosolids regulation, quality, end use & disposal survey. Final report. Tamworth (NH). (2007).
48. Baertsch, C., Paez-Rubio, T., Viau, E. & Peccia, J. Source tracking aerosols released from land-applied class B biosolids during high-wind events. Appl. Environ. Microbiol. 73, 4522–4531 (2007).
49. Tou, F. et al. Environmental Risk Implications of Metals in Sludges from Waste Water Treatment Plants: The Discovery of Vast Stores of Metal-Containing Nanoparticles. Environ. Sci. Technol. 51, 4831–4840 (2017).
50. Martínez, F., Casermeiro, M. A., Morales, D., Cuevas, G. & Walter, I. Effects on run-off water quantity and quality of urban organic wastes applied in a degraded semi-arid ecosystem. Sci. Total Environ. 305, 13–21 (2003).
51. Westerhoff, P. et al. Characterization, Recovery Opportunities, and Valuation of Metals in Municipal Sludges from U.S. Wastewater Treatment Plants Nationwide. Environ. Sci. Technol. 49, 9479–9488 (2015).

52. You, G. et al. Investigation of the rheological behavior of activated sludge in response to CeO_2 nanoparticles and potential mechanism. Environ. Sci. Pollut. Res. 25, 29725–29733 (2018).
53. Kim, B., Park, C. S., Murayama, M. & Hochella, M. F. Discovery and characterization of silver sulfide nanoparticles in final sewage sludge products. Environ. Sci. Technol. 44, 7509–7514 (2010).
54. Gottschalk, F., Sonderer, T., Scholz, R. W. & Nowack, B. Modeled environmental concentrations of engineered nanomaterials (TiO_2, ZnO, Ag, CNT, fullerenes) for different regions. Environ. Sci. Technol. 43, 9216–9222 (2009).
55. Rand, L. N. et al. Quantifying temporal and geographic variation in sunscreen and mineralogic titanium-containing nanoparticles in three recreational rivers. Sci. Total Environ. 743, 140845 (2020).
56. Bureau, U. C. Historical Census of Housing Tables: Sewage Disposal. (1990).
57. Arnade, L. J. Seasonal Correlation of Well Contamination and Septic Tank Distance. Ground Water 37, 920–923 (1999).
58. Paul, J. H. et al. Rapid movement of wastewater from on-site disposal systems into surface waters in the Lower Florida Keys. Estuaries 23, 662–668 (2000).
59. Boxall, A. et al. Current and future predicted environmental exposure to engineered nanoparticles. (Central Science Laboratory, 2007).
60. Clarke, R., Healy, M. G., Fenton, O. & Cummins, E. A quantitative risk ranking model to evaluate emerging organic contaminants in biosolid amended land and potential transport to drinking water. http://dx.doi.org/10.1080/10807039.2015.1121376 22, 958–990 (2016).
61. Westerhoff, P. et al. Low risk posed by engineered and incidental nanoparticles in drinking water. Nat. Nanotechnol. 13, 661–669 (2018).
62. Gondikas, A. P. et al. Release of TiO_2 Nanoparticles from Sunscreens into Surface Waters: A One-Year Survey at the Old Danube Recreational Lake. Environ. Sci. Technol. 48, 5415–5422 (2014).
63. Nakashima, K. & Imaoka, T. Niobian and Zincian ilmenites in syenites from Cape Ashizuri, Southwest Japan. Miner. Pet. 63, 1–17 (1998).
64. José, C. G. . & Wyllie, P. J. Ilmenite (high Mg, Mn, Nb) in the carbonatites from the Jacupiranga complex, Brazil. Am. Miner. 68, 960–971 (1983).
65. Praetorius, A. et al. Single-particle multi-element fingerprinting (spMEF) using inductively-coupled plasma time-of-flight mass spectrometry (ICP-TOFMS) to identify engineered nanoparticles against the elevated natural background in soils. Environ. Sci. Nano 4, 307–314 (2017).
66. Laycock, A., Coles, B., Kreissig, K. & Rehkämper, M. High precision 142 Ce/ 140 Ce stable isotope measurements of purified materials with a focus on CeO_2 nanoparticles. J. Anal. At. Spectrom. 31, 297–302 (2016).
67. Salminen, R. et al. FOREGS Geochemical Atlas of Europe, Part I* Background Information, Methodology, and Maps. Geol. Surv. Finland, Espoo (2005).
68. Yi, Z., Loosli, F., Wang, J., Berti, D. & Baalousha, M. How to distinguish natural versus engineered nanomaterials: insights from the analysis of TiO_2 and CeO_2 in soils. Environ. Chem. Lett. 18, 215–227 (2020).

69. Gallego-Hernández, A. L. et al. Identification of inhalable rutile and polycyclic aromatic hydrocarbons (PAHs) nanoparticles in the atmospheric dust. Environ. Pollut. 260, 114006 (2020).
70. Pradas Del Real, A. E. et al. Searching for relevant criteria to distinguish natural vs. anthropogenic TiO_2 nanoparticles in soils. Environ. Sci. Nano 5, 2853–2863 (2018).
71. Wagner, S., Gondikas, A., Neubauer, E., Hofmann, T. & von der Kammer, F. Spot the Difference: Engineered and Natural Nanoparticles in the Environment-Release, Behavior, and Fate. Angew. Chemie Int. Ed. 53, n/a-n/a (2014).
72. Regelink, I. C., Weng, L., Koopmans, G. F. & van Riemsdijk, W. H. Asymmetric flow field-flow fractionation as a new approach to analyse iron-(hydr)oxide nanoparticles in soil extracts. Geoderma 202–203, 134–141 (2013).
73. Hamon, R. E. et al. Geochemical indices allow estimation of heavy metal background concentrations in soils. Global Biogeochem. Cycles 18, n/a-n/a (2004).
74. Praetorius, A. et al. Single-particle multi-element fingerprinting (spMEF) using inductively-coupled plasma time-of-flight mass spectrometry (ICP-TOFMS) to identify engineered nanoparticles against the elevated natural background in soils. Environ. Sci. Nano 4, 307–314 (2017).

Chapter: 2

Episodic Surges in Titanium Dioxide Engineered Particle Concentrations in Surface Waters Following Rainfall Events

---

Nabi, M.M., Wang, J., Baalousha, M.," Episodic surges in titanium dioxide engineered particle concentrations in surface waters following rainfall events", Chemosphere, 263 (2021), p. 128261

2.1 Abstract

Quantifying and characterizing engineered particles in environmental systems is key for assessing their risk but remains challenging and requires the distinction between natural and engineered particles. The objective of this study was to characterize and quantify the concentrations of titanium dioxide engineered particles in the Broad River, Columbia, South Carolina, United States during and following rainfall events. The elemental ratio distributions of Ti/Nb, Ti/Fe, and Ti/Al, determined on a single particle basis using inductively coupled plasma-time of flight-mass spectrometry (SP-ICP-TOF-MS), were similar between samples during the different rainfall events, indicating that naturally occurring particles had the same elemental ratios and origin. Therefore, the changes in the Ti/Nb ratios in the bulk water samples were attributed to the introduction of titanium dioxide engineered particles into the Broad River with urban runoff during and following rainfall events. The total concentrations of Ti, Fe, Al, Nb, Ce, and La in the Broad River followed the same trend of rise and fall as the discharge/runoff. The elemental ratios of Ti/Nb were higher (*e.g.*, 330 to 565) than the average crustal values (*e.g.*, 320) and the natural background elemental ratios in surface waters in Columbia, SC (*e.g.*, 266.4 ± 8.9), suggesting contamination with titanium dioxide engineered particles. The concentration of titanium dioxide engineered particles were estimated by mass balance calculations using total titanium concentrations and increases in Ti/Nb ratios above the natural background ratios. The concentrations of titanium dioxide engineered particles in the Broad River varied between 20 and 140 µg TiO_2 L^{-1} during the campaigns. The source of titanium dioxide was attributed to urban runoff due to the absence of sewage contamination as indicated by the low size of the gadolinium anomaly. The findings of this

study demonstrate that urban runoff is a major source of titanium dioxide engineered particles to urban rivers, which results in episodic high concentrations of titanium dioxide engineered particles, which may pose environmental risks during and following rainfall events. This highlights the significance of determining the temporal variations in engineered particle concentrations in surface waters for a more comprehensive risk assessment of engineered particles.

2.2 Introduction

Urban runoff is widely recognized as a major vector of chemicals, including engineered particles, to surface waters, and therefore urban runoff has been shown to contribute significantly to the deterioration of surface water quality [1]. Many studies investigated the release of engineered particles from municipal wastewater treatment plants [2], sewage spills [3], and from sunscreens [4,5] to urban surface waters. However, little attention has been given to the contribution of the built urban environment to the fluxes of engineered particles in urban surface waters, despite the many uses of engineered particles in the urban environment [6]. Titanium dioxide (TiO_2) engineered particles are widely used in the urban environment both as pigments (e.g.,100-300 nm) in paint and nanosized particles (e.g.,1-100 nm) in self-cleaning and photocatalytic surfaces [6]. These uses of TiO_2 engineered particles results in their release, and deposition on surfaces in the urban environment [7-9]. During rainfall events, the deposited particles are washed with urban runoff to the receiving surface waters, which is likely to result in high episodic engineered particle concentrations in urban surface waters during and following rainfall events. For instance, a recent environmental fate modelling study suggested that TiO_2 engineered

nanoparticle concentrations could reach 600 to 1500 µg L^{-1} in urban rivers impacted by stormwater runoff [10]. Another study reported high concentrations (5 to 150 µg L^{-1}) of TiO_2 engineered particles in bridge runoff and in urban rivers dominated by urban runoff [11]. However, these measurements were a proof of concept of the analytical approach and did not take into account the temporal variability of the measured concentrations.

Currently, most available data on engineered particles, including TiO_2, concentrations in environmental systems are predicted based on mass flow and environmental fate modeling [12,13]. These models estimated that the concentrations of engineered nanoparticles, including TiO_2, are likely to be in the ng to low µg L^{-1} range. Nonetheless, a recent modeling study predicted high concentrations (e.g., 619 to 1490 µg L^{-1}) of TiO_2 engineered nanoparticles in urban rivers impacted by stormwater [10]. However, these predictions may suffer from significant uncertainties because they are based on modeling approaches that have not been validated against field measurements. Few studies reported the occurrence and the measured concentrations of TiO_2 engineered nanoparticles in environmental systems and many of them reported low TiO_2 engineered nanoparticles concentrations which are in line with the modeled environmental concentrations [4,5,14]. Early studies reported the occurrence of TiO_2 engineered nanoparticles in surface waters by measuring the total concentration of Ti using elemental analysis accompanied with TiO_2 particle identification by electron microscopy techniques [15,16]. However, these studies did not distinguish between the contributions of natural and engineered particles to the total Ti concentrations. Titanium is the ninth most abundant element in the Earth's crust and is mainly found in minerals such as rutile, ilmenite, sphene, and/or opaque heavy minerals (e.g., titanomagnetite, magnetite, and ilmenite) [17]. These minerals always contain trace

concentrations of other elements [18]. Natural TiO_2 minerals, such as rutile and ilmenite, have been shown to be the dominant carriers (e.g., > 90-95% of the whole rock content) of Ti, Nb, Ta, Sb, and W, as well as, important carriers (5-45% if the whole rock content) of V, Cr, Mo, and Sn [19]. Natural Ti-containing particles form after weathering of parent rocks, and display similar elemental compositions, associations, and ratios as those of the parent rocks. For instance, characterization of naturally occurring Ti-containing particles by single particle-inductively coupled plasma-mass spectrometer (SP-ICP-TOF-MS) demonstrated that natural Ti-particles contain other elements such as Al, Si, Fe, Mn, Ce, La, Zr, Nb, Pb, Ba, Th, Ta, W, and U [3,14]. These natural elemental impurities are typically removed from the natural Ti-containing minerals by dissolution and reprecipitation during the manufacturing of TiO_2 engineered particles [3]. Therefore, mobilization of TiO_2 engineered particles with urban runoff to receiving surface waters will lead to increases in the elemental ratios of Ti to the elements naturally associated with Ti-containing minerals. This approach has been recently implemented to estimate the concentrations of TiO_2 engineered particles in sewage spills [3] and urban runoff [11], and surface waters [4].

This study builds on previous advancements in overcoming some of the challenges in the detection and quantification of titanium dioxide engineered particles in surface waters [3,4,11,14] by evaluating the temporal variability in titanium oxide engineered particle concentrations in an urban river during and following rainfall events. The aims of this study are to: 1) characterize the elemental composition of Ti-containing particles in the Broad River on a single particle basis using SP-ICP-TOF-MS during and following rainfall events, 2) monitor the occurrence and concentration of TiO_2 engineered particles in the

Broad River, and 3) determine the possible source(s) of TiO_2 engineered particles in the Broad River, Columbia, South Carolina, United States.

2.3 Materials and Methods

2.3.1 Sampling

Water samples were collected from the Broad River, Columbia, SC 29201 (34°00'10.4"N 81°03'18.4"W). The Broad River is approximately 240 km long, originates in the Blue Ridge Mountains of eastern Buncombe Country, North Carolina, and flows generally south-southeastwardly in South Carolina. The total catchment area of the Broad River is approximately 14,000 square kilometers. The broad River is a principal tributary of the Congaree River, which is a principal tributary of the Santee River, which discharges in the Atlantic Ocean. Apart from the forested land (66%) in the headwaters of the Broad river basin; the dominant land use throughout the Broad river basin is agricultural (23%); urban (9%): commercial and residential; others (2-4%): mining operations, and logging operations. There are permitted 14 major wastewater treatment plants (WWTP), 30 minor WWTPs, 20 animal operation facilities, 92 general and individual stormwater facilities in the Broad river basin [20].

Water samples were collected from the Broad River during a range of hydrologic conditions (**Table A.3**). The first sampling campaign (C1) was conducted between 09/14/2018 and 09/21/2018 during and following Hurricane Florence, which formed on 08/31/2018, dissipated on 09/19/2018, and made landfall near Wrightsville Beach in North Carolina on September 14th. The hurricane eye moved westward through North Carolina

and the Northern part of South Carolina without any significant impact on Columbia, South Carolina. Nonetheless, hurricane Florence generated rainfall in Columbia, SC of a maximum total daily rainfall of 42 mm between September 15th to 18th 2018 (**Table A.3**) [21]. The second sampling campaign (C2) was performed between 10/25/2018 and 11/02/2018 during which a major rainfall event of a 33 mm occurred on 10/26/2018 (**Table A.3**). The third sampling campaign (C3) was performed between 11/02/2018 and 11/09/2018 during which low intensity rainfall (0 to 3.5 mm) occurred on nearly daily basis except on 11/07/208, where a rainfall with higher intensity (19 mm) occurred. The rainfall data was collected from the USGS station number 021695045 (34°00'24"N 81°01'18"W), nearly 3.1 km from the sampling location. The discharge data was collected from the USGS station number 02162035 (34°02'54"N 81°04'24"W), nearly 5.3 km upstream of the sampling location.

2.3.2 Sample collection, digestion and elemental analysis

Surface water samples were collected from the Broad River in 1 L high density polyethylene bottles (Thermo Scientific, Rockwood, TN, United States). Prior to use, bottles were acid-washed in 10% nitric acid (Sigma Aldrich, St. Louis, MO, United States) for at least 24 hours, and soaked in ultrahigh purity water (PURELAB Option-Q, ELGA, High Wycombe, UK) for 24 hours, air dried, and then double-bagged. In the field, the sampling bottles were rinsed three times in the surface water and then filled with the water sample, samples were individually double-bagged, and returned to the lab the same day and were stored in the dark at 4ºC.

The bulk river water samples were digested in 15 mL Teflon vessels (Savillex, Eden Prairie, MN, United States) on custom-made Teflon covered hotplates placed in a box equipped with double-HEPA filtered forced air in a metal-free HEPA filtered air clean lab. 10 mL water aliquots or 5 mL extracted particle suspensions were placed in the vessel and weighed (Mettler Toledo, Excellence Plus, Columbus, OH, United States). Samples were dried at 110°C and treated with 1 mL of 30% H_2O_2 (Fisher Chemical, Fair Lawn, NJ, United States) for 2 h at 70°C to remove organic matters. H_2O_2 was then evaporated and the sample was digested with 2 mL of HF:HNO_3 (3:1) mixture (ACS grade acids distilled in the laboratory, Sigma Aldrich, St. Louis, MO, United States) for 48 h at 110°C. After evaporation of the acid mixture at 110°C, the residue was reacted with 1 mL of distilled HNO_3 to break up insoluble fluoride salt that may have formed during the sample digestion and HNO_3 was left to evaporate at 110°C. This step was repeated twice before weighing the sample and adding 5 mL of 1% HNO_3. The sample was sonicated for 10 min in a sonication bath (Branson, 2800, 40kHz, Danbury, CT, United States) and warmed for 2 h at 50°C for full dissolution. The solution was transferred to 15 mL polypropylene centrifuge tubes (Fisher Scientific, San Nicolás de los Garza, Nuevo León, Mexico) and stored at 4°C. Samples were centrifuged (Eppendorf, 5810 R, Hamburg, Germany) for 5 min at 3100 g prior to ICP-MS analysis to remove any undigested minerals.

The elemental concentrations of the USGS reference materials BHVO-2 Hawaiian basalts run as unknowns after digestion following the digestion procedure described above demonstrate high recovery (approximately 100%) for most elements. The precision of our method was better than 4% for all isotopes except ^{169}Tm and ^{174}Lu (7 and 8%) and the accuracy was better than 89% for most elements, including Ti and Nb except ^{174}Lu (86%).

Full procedural digestion blanks was < 6.8% for all reported element in this study and < 2.8% for titanium and niobium of samples' analyte signal (**Table A.4**). Therefore, blanks are insignificant to the calculations of Ti concentrations or total Ti/Nb elemental ratios.

Elemental concentrations in the digested river water samples were determined by Perkin Elmer NexION 350D ICP-MS. Standard tuning procedure was performed before analysis for instrument maintenance. Dissolved multi-element standards mixture of ICP Complete Group Calibration Standard (BDH Chemicals, Radnor, PA, USA) and ICP Refractory Element Group Calibration Standard (BDH Chemicals, Radnor, PA, USA) diluted in 1% nitric acid (TraceMetal grade, Fisher Chemical, Fair Lawn, NJ, USA) were used for mass concentration calibration ranging from 0.01 to 1000 μg L^{-1}. Internal standards (ICP Internal Element Group Calibration Standard, BDH Chemicals, Radnor, PA, USA) were monitored at the same time for quality control. The isotopes measured were ^{27}Al, ^{47}Ti, ^{57}Fe, ^{93}Nb, ^{139}La, ^{140}Ce, ^{141}Pr, ^{142}Nd, ^{152}Sm, ^{153}Eu, ^{158}Gd, ^{159}Tb, ^{164}Dy, ^{165}Ho, ^{166}Er, ^{169}Tm, ^{174}Yb, and ^{175}Lu. All isotopes were analyzed in standard mode.

2.3.3 Particle composition on single particle basis

The river water samples were shaken well prior extraction to resuspend any settled particles and to obtain a representative subsample. 10 mL aliquots were transferred into acid-washed 15 mL centrifuge tubes. The transferred samples were bath sonicated for 2 h (Branson, Model 2800, 40 kHz, Danbury, CT, United States), then centrifuged at 775 g for 5 min to remove large particles (> 1000 nm assuming natural particle density, ρ = 2.5 g cm^{-3}) and prevent clogging of the ICP-TOF-MS introduction system. The top 7 mL supernatant was decanted and stored at 4°C in the dark till analysis by SP-ICP-TOF-MS.

The theoretical size of the extracted fractions corresponds to particles < 1000 nm for natural particles (ρ = 2.5 g cm^{-3}), and < 725 nm for TiO_2 particles (ρ = 4.2 g cm^{-3}). All samples were bath sonicated again for 15 min and were diluted by a factor of 100 prior to SP-ICP-TOF-MS analysis.

Single particle analysis of the diluted particle extracts was performed using an ICP-TOF-MS (TOFWERK, Thun, Switzerland) to determine all isotopes within a single particle simultaneously [22]. Element specific instrument sensitivities were measured with a multi-element solution mix prepared from a three multi-element solution (0, 1, 2, 5, and 10 μgL^{-1} multi element standard, diluted in 1% HNO_3, BDH Chemicals, Radnor, PA, USA) as described above. The transport efficiency was calculated using the known size approach [23] using both Au ENMs with a certified particle size of 60 nm (NIST RM8013 Au, Gaithersburg, MD, USA) prepared in UPW and Au standard solutions (0, 1, 2, 5, and 10 μgL^{-1}, diluted in 1% HCl, BDH Chemicals, West Chester, PA, USA). Using a standard tuning solution, the ICP-TOF-MS mass spectra were calibrated using $^{18}H_2O^+$, $^{59}Co^+$, $^{115}In^+$, $^{140}Ce^+$, and $^{238}U^+$ target isotopes in TofDAQ view (TOFWERK) prior analysis or in Tofware (TOFWERK) after analysis if mass shifts occurred during analysis. Particle/baseline signal separation, particle signal, mass, and number concentration were determined from mass-calibrated ICP-TOF-MS spectra using Python script in Tofware as described elsewhere [3]. The particle detection threshold was calculated for each isotope according to Eq. 1[24].

$$\text{Threshold} = \text{Mean} + (3.29\sigma + 2.71) \quad \text{(Eq. 1)}$$

The data for each isotope were treated separately, but the time stamps were kept throughout data processing for every isotope, allowing for identification of isotope

correlations in a single particle. For example, an impure particle (*e.g.*, a particle containing multiple elements) generates several isotope signals spikes in a given time stamp. An "apparently pure" particle generates one isotope signal spike in a given time stamp. The term "apparently pure" is used in this study as such particles might contain elements at concentrations below the sp-ICP-MS size/mass detection limit. Elemental association and elemental ratio distributions were determined using data filtration in Excel.

2.3.4 Estimation of TiO_2 engineered particle concentration

The concentration of TiO_2 engineered particles was calculated based on mass balance calculations according to Eq. 2

$$[TiO_2]_{engineered\ particles} = \frac{TiO_{2\ MM}}{Ti_{\ MM}}\left[Ti_{sample} - Nb_{sample}.\left(\frac{Ti}{Nb}\right)_{background}\right] \qquad (Eq.2)$$

Where, [TiO_2] engineered particles is the concentration of TiO_2 engineered particles, $Ti_{\ MM}$ and $TiO_{2\ MM}$ are the molar masses of Ti and TiO_2, Ti_{sample} and Nb_{sample} are the concentrations of Ti and Nb in a given sample, $Ti/Nb_{background}$ is the natural background elemental concentration ratio of Ti/Nb. Background Ti/Nb ratio was calculated on eight reference samples collected from Lake Katherine and Gills creek in Columbia, SC in the absence of rainfall events [3].

Eq 2 assumes that all Ti occurs in particulate form, engineered Ti occurs as pure TiO_2 engineered particles, and that the natural background elemental ratio of Ti/Nb is the constant through the sampling period. These assumptions are justified for the following reasons. Ti occurrence in The Broad River surface water is expected to occur solely in solid phases because of the very low solubility of TiO_2 [25]. While Ti has numerous industrial applications, from metal alloying to aerospace applications to biomedical devices,

approximately 95% of the mined Ti is refined into nearly pure TiO_2 through the treatment of Ti-bearing ores with carbon, chlorine, or sulfuric acid [26]. Additionally, TiO_2 engineered particle contain trace amount of Nb, which was below the ICP-MS detection limit (e.g., < 7 ng L^{-1}) as demonstrated for two commercially available TiO_2 engineered particles [11]. On the other hand, natural TiO_2 minerals are the dominant carriers (e.g., > 90-95% of the whole rock content) of Ti and Nb [19]. The elemental ratio of Ti/Nb, Ti/Fe, and Ti/Al, determined by SP-ICP-TOF-MS, in naturally occurring particles in the Broad River waters were found to be constant throughout the sampling campaigns *(see results and discussion section 2.4.4)*.

2.3.5 Hydrographs and separation of base flow and runoff

The discharge was separated into base flow and direct runoff using tool "WHAT: Web-based Hydrograph Analysis Tool" [27]. 'WHAT' is linked to USGS data base. The base flow and direct runoff separation was performed for the USGS station number 02162035, and the following method and conditions used: Method: Recursive digital filter, Aquifer type: Perennial streams with porous aquifer, Filter parameter: 0.98, BFI_{max}: 0.80, Date range: 01.10.1939 to 11.02.2019.

2.4 Results and Discussion

2.4.1 Precipitation, hydrograph, and separation of base flow and runoff

Precipitation occurred at the beginning of the first two sampling events and during the third sampling event (**Table A3, Figure A1**), which resulted in runoff events in the

Broad River. Direct runoff accounted for 30 to 60% of the total discharge during the first event, 15 to 70% during the second sampling event, and < 30% of the total discharge in the 3rd sampling event. It is worth noting that baseline flow (i.e., no urban runoff contribution) occurred on 09/21/2018, 10/31/2018, and 11/01/2018.

2.4.2 Elemental pollutographs

Pollutographs (i.e., graphs of pollutant concentrations vs. time) of Ti, Nb, Ce, and La are displayed in **Figure 2.1** to illustrate their transport pathways in the Broad River during rainfall events. Ti, Nb, Ce, and La exhibited a mobility pattern driven by the transport of solids [28]. At the start of the hydrographs, during low flows, concentrations were rather low, increased with increasing flow (transporting more solids) and then declined with diminishing flow and supply of solids on the catchment surfaces (**Figure 2.1**). This suggests that urban runoff contributes a major Ti, Nb, Ce, and La loads to the Broad River. During the first sampling campaign (C1), Ti reached a maximum value of 108.4 ± 4.5 µg L^{-1}, which coincided with the discharge and runoff peaks, then decreased to 35.8 ± 0.4 µg L^{-1} with decreasing discharge (**Figure 2.1a**). The lowest Ti concentration coincided with the decrease in runoff to zero on 09/21/2018 (**Figure A1**). During the second sampling event (C2), the Ti concentration varied between 52.8 ± 0.5 to 297.7 ± 6.2 µg L^{-1} (**Figure 2.1**). The lowest Ti concentration during C2 was observed prior to the runoff peak as this event was preceded by 13 days dry period. The highest Ti concentration during C2 coincided with the second peak of the discharge. During the third sampling event (C3), the lowest Ti concentration was 47.91.4 ± 6.0 µg L^{-1} and coincided with the lowest discharge and lowest runoff (e.g., 14% of the total discharge). Overall, the highest Ti concentration

was measured during the second sampling event due to the long antecedent dry period which might have resulted in higher contaminant accumulation on impervious surfaces in the watershed. Similar increases in the concentrations of particulate matter associated contaminants (e.g., metals) with increases in antecedent dry period was observed for road runoff [29,30]. The maximum Ti concentrations measured in C1 and C3 were lower than that measured in C2, possibly due to short antecedent dry period (2days) and dilutional effect in C1, and the absence of antecedent dry period in C3. These short antecedent dry periods prior to C1 and the absence of antecedent dry period in C3 results in lower contaminant accumulation on impervious surfaces in the watershed.

Unlike other sources of pollutants, such as municipal or industrial wastewaters, where the sources of titanium-containing particles are predominantly anthropogenic in nature [2] significant quantities of titanium-containing particles occur in urban runoff as a result of soil erosion and atmospheric deposition of soil particles on surfaces in the urban environment [31]. Therefore, the differences in the total Ti concentration in the river stream during rainfall events can be attributed to the differences in natural and/or engineered Ti concentrations. The differences in the natural Ti concentration can be affected by the difference in natural sources of sediments to the river, i.e. erosion of soils, channel banks, floodplain deposits; atmospheric dust deposition; landslides and debris flows etc. The differences in the engineered Ti concentrations can be impacted by the difference in sources of TiO_2 to the river, i.e. sunscreens [4,5], urban runoff [11], wastewater treatment plant (WWTP) effluent [2], or sanitary sewage overflows [3].

2.4.3 Elemental ratio profiles

All rainfall events resulted in higher Ti/Nb ratios of relative to the average water reference samples collected in nearby water bodies (266.4 ± 8.9) and to the average crustal value (320) (**Figure 2.2**) [3]. The lowest Ti/Nb ratio of 329.7 ± 4.7 was measured on 31/10/2018, where the river discharge was mainly baseflow (**Figure A.1**) and the highest Ti/Nb ratio of 565.4 ± 1.3 was measured during C1 on 09/18/2018, on which the direct runoff was higher than the baseflow (**Figure A.1**). The lower Ti/Nb ratios observed during C2 might be attributed to the higher proportion of naturally occurring particles compared to engineered particles in urban runoff during C2 due to the long antecedent dry period. It is expected that higher deposition of natural occurring particles than engineered particles on surfaces in urban areas [32]. Ti/Nb was generally low during C3, which might be attributed to the absence of antecedent dry period and the continuous low intensity rainfall, and thus the low input of engineered Ti to the Broad River. In contrast to the variation in Ti/Nb ratios, the elemental ratios of Ce/La varied within a narrow range (2.0 ± 0.02 to 2.3 ± 0.01) throughout the three sampling events (**Figure 2.2b**), which is very close to the average crustal Ce/La ratio (2.13) and the average background water Ce/La (2.15 ± 0.01) ratio near the sampling sites [3], indicating the absence of Ce and La contamination as well as the accuracy of the digestion and analysis procedure used in this study. The nearly constant Ce/La ratio and the high concentration of Ce and La in the Broad River water during rainfall events indicates a significant introduction of natural particles with the urban runoff to the Broad River.

Given the significant contribution of natural particles to urban runoff as indicated by the high Ce and La concentrations, the differences in the Ti/Nb elemental ratios in the

bulk water samples can be attributed to 1) variability in the elemental ratios within natural occurring Ti-containing particles, or 2) the introduction of TiO_2 engineered particles which do not contain Nb [33]. The strong association between Ti and Nb in titanium minerals [18,19,34] suggests that these variations are due to TiO_2 engineered particles contamination. To further confirm this hypothesis the elemental associations and the variability in Ti/tracer in Ti-containing particles were investigated by SP-ICP-TOF-MS.

2.4.4 Particle number concentration and elemental composition

The number concentration of Ti-, Nb-, Ce-, and La-containing particles (**Figure 2.3**) followed the same trend as the corresponding total element concentration in the bulk water (**Figure 2.1**). Fourteen major and trace elements were detected in Ti-containing particles including Al, Si, V, Mn, Fe, Ni, Zr, Nb, Ba, Ce, La, Pb, and Th. These findings are in agreement with elemental associations between Ti and natural tracers observed in surface waters [3] and soils (data not published yet) in South Carolina as well as with occurrence of these elements in TiO_2 natural phases (e.g., rutile, ilmenite, etc.) [18,19,34]. Natural TiO_2 minerals, such as rutile and ilmenite, have been shown to be the dominant carrier (e.g., > 90-95% of the whole rock content) for Ti, Nb, Ta, Sb, and W as well as an important carrier (e.g., 5-45% of the whole rock content) for V, Cr, Mo, and Sn in TiO_2-bearing metamorphic rocks [19]. All the elements detected in Ti-containing particles by SP-ICP-TOF-MS, except Nb, occurred in association with Ti as well as free of Ti. Nb was the only element that occurred only in association with Ti- containing particles, further confirming the strong association between Ti and Nb in natural particles. Therefore, Ti/Nb in the digested samples was used to differentiate natural from engineered Ti-containing

particles and quantify the concentrations of TiO_2 engineered particles in the Broad River during and following different rainfall events.

The elemental ratio distributions of Ti/Nb, Ti/Al, and Ti/Fe in Ti-containing particles displayed the same trend in all samples (**Figure 2.4**), indicating that naturally occurring Ti-containing particles were not different between the different samples. Particles containing Ti and Nb displayed Ti/Nb ratios between 20 and 400, with only a small fraction (< 10%) of particles with Ti/Nb ratios > 400 (**Figure 2.4a**). The mean elemental ratio of Ti/Nb varied between 66.4 ± 49.4 to 242.3 ± 247.0 (standard deviation here is that of the Ti/Nb distribution), lower than the average crustal values (e.g., 320) and the average value measured in reference water samples collected in Columbia, SC (e.g., 266.4 ± 8.9). The variability in the Ti/Nb elemental ratios between the different samples can be attributed to the detection of a small number (4 to 110 particles) of the particles containing both Ti and Nb. Only few particles containing both Ti and Nb were detected by sp-ICP-TOF-MS because of the mass/size detection limit of SP-ICP-TOF-MS (e.g., 30 to 35 nm under the current experimental conditions) and the low concentration of Nb in Ti-containing particles (e.g., 20-400 times lower than Ti, **Figure 2.4a**). On the other hand, significantly higher number of particles containing both Ti and Al (91 to 773) and Ti and Fe (325 to 1688) containing particles were detected by SP-ICP-TOF-MS. This is because Al and Fe concentrations are higher than Nb in Ti-containing particles. The higher number of Ti- and Fe- containing particles compared to Ti- and Al-containing particles is due to the lower size detection limit of Fe (e.g., 44-65 nm under the current experimental conditions) compared to Al (e.g., 138-170 nm under the current experimental conditions). Therefore, a comparison of the elemental ratios of Ti/Al and Ti/Fe among the different

samples was used to evaluate if naturally occurring particles were different during the sampling events.

The elemental ratios of Ti/Al display the same distribution in all samples (**Figure 2.4b**). These elemental ratios are in good agreement with naturally occurring particles such as palygorskite and montmorillonite (Ti/Al = 0.014-0.016); illite (Ti/Al = 0.026); kaolinite and hectorite (Ti/Al = 0.06); vermiculite and corrensite (Ti/Al = 0.090-0.093). Similarly, the elemental ratios of Ti/Fe display the same distribution in all samples (**Figure 2.4c**) and are in good agreement with natural occurring titanium minerals such as titanomagnetite ($Fe_{3-x}Ti_xO_4$, $0 < Ti/Fe < 0.43$, $0 < x < 1$), ulvöspinel (Fe_2TiO_4, Ti/Fe = 0.43), pseudobrookite (Fe_2TiO_5, Ti/Fe = 0.43), ilmenite ($FeTiO_3$, Ti/Fe = 0.86), pseudorutile ($Fe_2Ti_3O_9$, Ti/Fe = 1.29), and ilmenorutile and ferropseudobrookite ($FeTi_2O_5$, Ti/Fe = 1.71).

Collectively these results indicate that the elemental ratios of Ti/Nb, Ti/Al, and Ti/Fe in naturally occurring Ti-containing particles were similar between the different samples. Therefore, there was no variability in natural occurring particles during the sampling period. Thus, any changes in total elemental ratios can be attributed to the occurrence of titanium oxide engineered particles in these samples.

2.4.5 TiO_2 concentrations and sources

The calculated TiO_2 engineered particle concentrations based on shifts in Ti/Nb elemental ratios varied between 21.3 ± 5.0 µg L^{-1} and 142.9 ± 22.3 µg L^{-1} and followed the same trend of rise and fall as the discharge/direct runoff (**Figure 2.5**). The highest TiO_2 concentration was found in the second sampling campaign, likely due to the long

antecedent dry period (13 days) prior to the sampling campaign in comparison to the other sampling campaigns. The occurrence of TiO_2 engineered particles in high concentrations in Broad River stream is in good agreement with the extensive use of TiO_2 engineered particles in the urban environment as engineered nanoparticles in self-cleaning and photocatalytic surfaces and as pigment in paint and coatings [35,36] which have been shown to be released by wear and weathering [9]; and the occurrence of TiO_2 engineered particles in road dust, atmospheric particulate matter [37,38], urban runoff [11], and WWTPs effluent [39]. The TiO_2 concentrations measured in this study are much higher than the predicted TiO_2 engineered particle concentrations in surface waters (0.0002 to 24.5 μg L^{-1}) and the measured TiO_2 engineered particle concentrations in river waters (0.55 to 6.5 μg L^{-1}) [16,40,41].

TiO_2 engineered particles enter surface waters from different sources such as effluent of wastewater treatment plants (WWTP), sanitary sewage overflows, urban runoff, industrial discharge, or construction activities. Gadolinium anomaly is widely used to track effluent from wastewater treatment plants [42]. Gadolinium anomaly sizes > 1.5 has been used as an indicator of wastewater treatment effluent in river waters. The size of gadolinium anomaly throughout the sampling events was < 1.2 (**Figure A.3**), indicating the absence of WWTP effluent or sewage spills. There were no construction activities near the sampling site. There are no industrial discharge sources near the sampling location. Furthermore, both industrial and construction activities would result in a continuous discharge of TiO_2 particles to surface water. However, the observed Ti-contamination in this study was correlated/in response to rainfall events, suggesting that the source of TiO_2 particles here is urban runoff.

2.5 Analytical and environmental perspectives

Characterization and quantification of engineered particles in Rivers draining large watersheds is challenging. Identifying the natural background of elemental ratio of Ti/Nb is quite complicated for large urban rivers such as the Broad River. This is because there are many sources of TiO_2 engineered particles release to surface waters in large urban rivers such as urban runoff, sewage spills, wastewater treatment effluent, and resuspension of contaminated sediment [3,28,43]. For instance, there are 44 WWTPs upstream of the sampling site contributing a total of 144 x 10^6 L of effluent discharge per day [20] Atmospheric particles released within the urban environment can also deposit on the water surface in the Broad River. Additionally, engineered particles could be introduced to the Broad River with urban runoff upstream of the sampling site due to the large watershed area. Even during a dry day within the sampling location in Columbia, a rain event upstream will deliver contaminants, including engineered particles, into the sampling location. The continuous introduction of TiO_2 engineered particles into surface waters result in a shift in the natural elemental ratios toward higher values. The lowest elemental ratio of Ti/Nb in the Broad River in the absence of direct runoff was 329.7 ± 4.7, which was higher than the reference value (e.g., 266±9) measured in smaller creeks in the sampling area and in a rural river in South Carolina monitored for the occurrence and concentrations of TiO_2 engineered particles over a period of two years (data not published yet). The selection of the incorrect background elemental ratio (e.g., at the beginning or the end of the event hydrograph) will results in the underestimation of TiO_2 engineered particles. This requires long term monitoring of the site(s) under consideration to achieve the true (lowest) elemental ratio baseline value. Furthermore, monitoring the concentration of TiO_2 engineered particles in smaller river

reaches with fewer potential sources of TiO_2 engineered particles might be useful to better understand the processes determining the fate and transport of TiO_2 engineered particles in surface waters.

Here we report the concentrations of TiO_2 engineered particles in the Broad River following rainfall events. The TiO_2 concentrations varied between 20 and 140 μg L^{-1} during the sampled events. These concentrations are in the same order of magnitude as the predicted no effect concentration (PNEC) for TiO_2 pigments (e.g., 127-184 μg L^{-1}) and is higher than the PNEC for TiO_2 ENMs to freshwater organisms (e.g., 1-18 μg L^{-1}) [12,13]. Transport of TiO_2 engineered particles with river water to the ocean could also pose a significant risk for coral reefs. TiO_2 engineered nanomaterials have been shown to bioaccumulate in microflora and induce coral bleaching, which could contribute to an overall decrease in coral populations [44]. Further research is needed to further understand the impact of rainfall characteristics and the hydrogeological factors on the temporal variability in TiO_2 engineered particle concentrations in urban rivers.

2.6 Conclusion

This study reports the measurement of TiO_2 engineered particle concentrations in the Broad River, Columbia, South Carolina, United States following rainfall events. The concentration of TiO_2 engineered particle were estimated by mass balance calculations using total titanium concentrations and increases in Ti/Nb ratios above the natural background ratios. The elemental ratios of Ti/Nb (e.g., 330 to 565) were higher than the average crustal values (e.g., 320) and the natural background elemental ratios in surface waters in Columbia, SC (e.g., 266 ± 9) and followed the same trend of rise and fall as the

discharge/runoff, suggesting introduction of TiO_2 engineered particle to the Broad River water with urban runoff. The concentrations of titanium dioxide engineered particles in the Broad River varied between 20 and 140 mg TiO_2 L^{-1} following rainfall events. Such high concentrations of TiO_2 engineered particles to urban rivers may pose environmental risks during and following rainfall events. This study highlights the importance of determining the temporal variations in engineered particle concentrations in surface waters for a more comprehensive understanding of the environmental fate, behavior, and risk assessment of engineered particles.

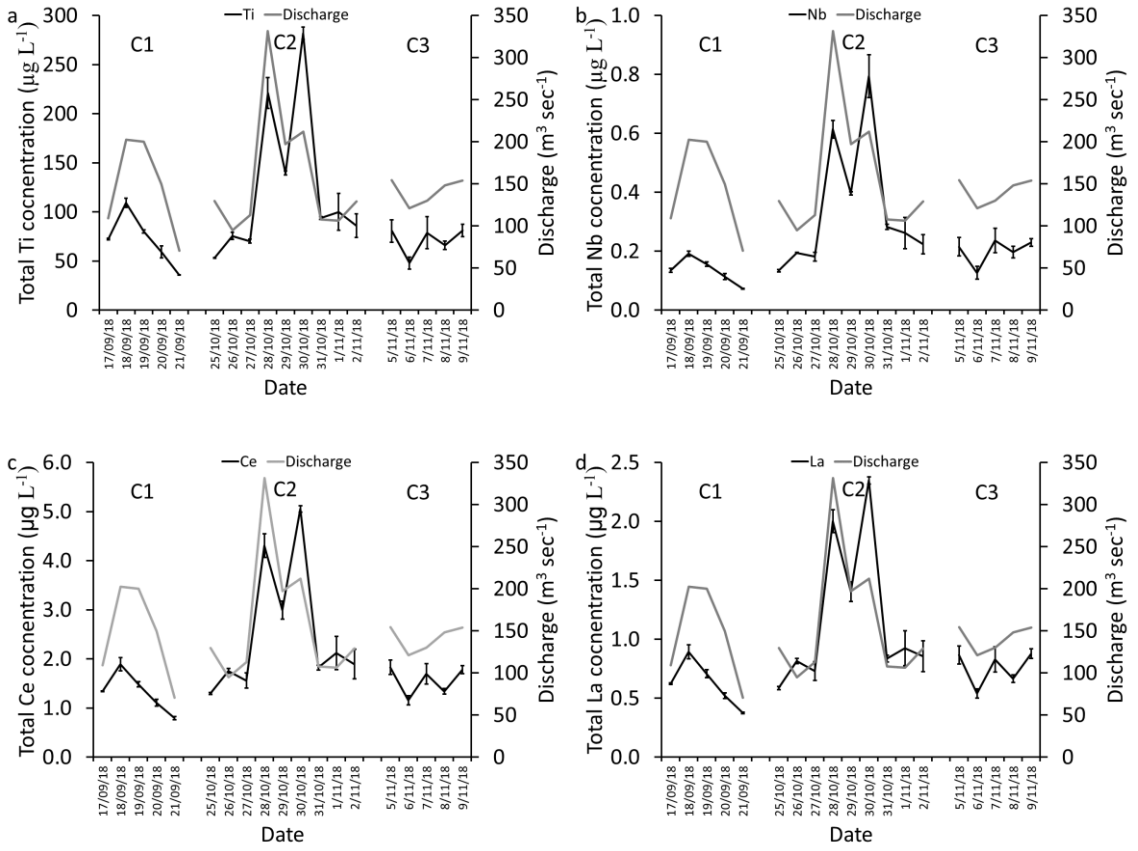

Figure 2.1 Pollutographs (i.e., graphs of pollutant concentrations vs. time) of (a) Ti, (b) Nb, (c) Ce, and (d) La in the Broad River water during the three sampling campaigns.

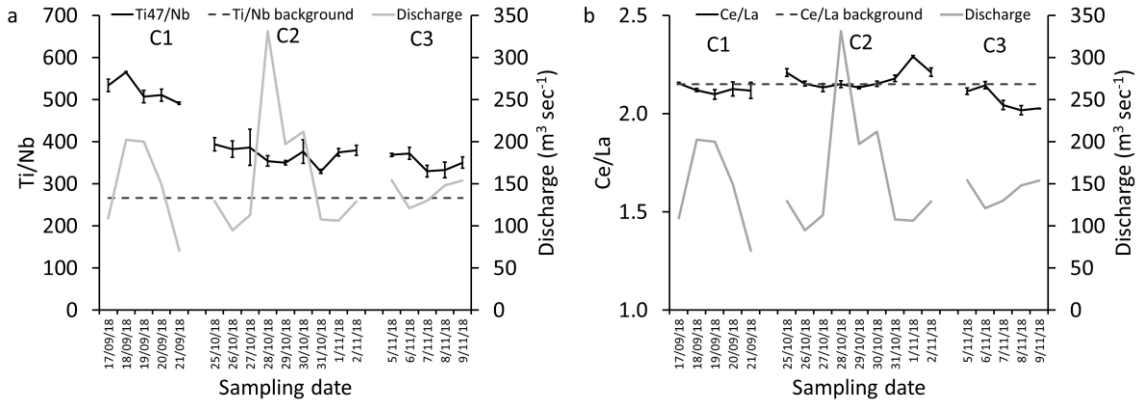

Figure 2.2 Elemental ratios of (a) Ti/Nb and (b) Ce/La in the Broad River bulk water samples during the three sampling campaigns. The background Ti/Nb and Ce/La ratios are average ratios of eight water samples collected in from water bodies near the sampling site in the absence of rainfall events.

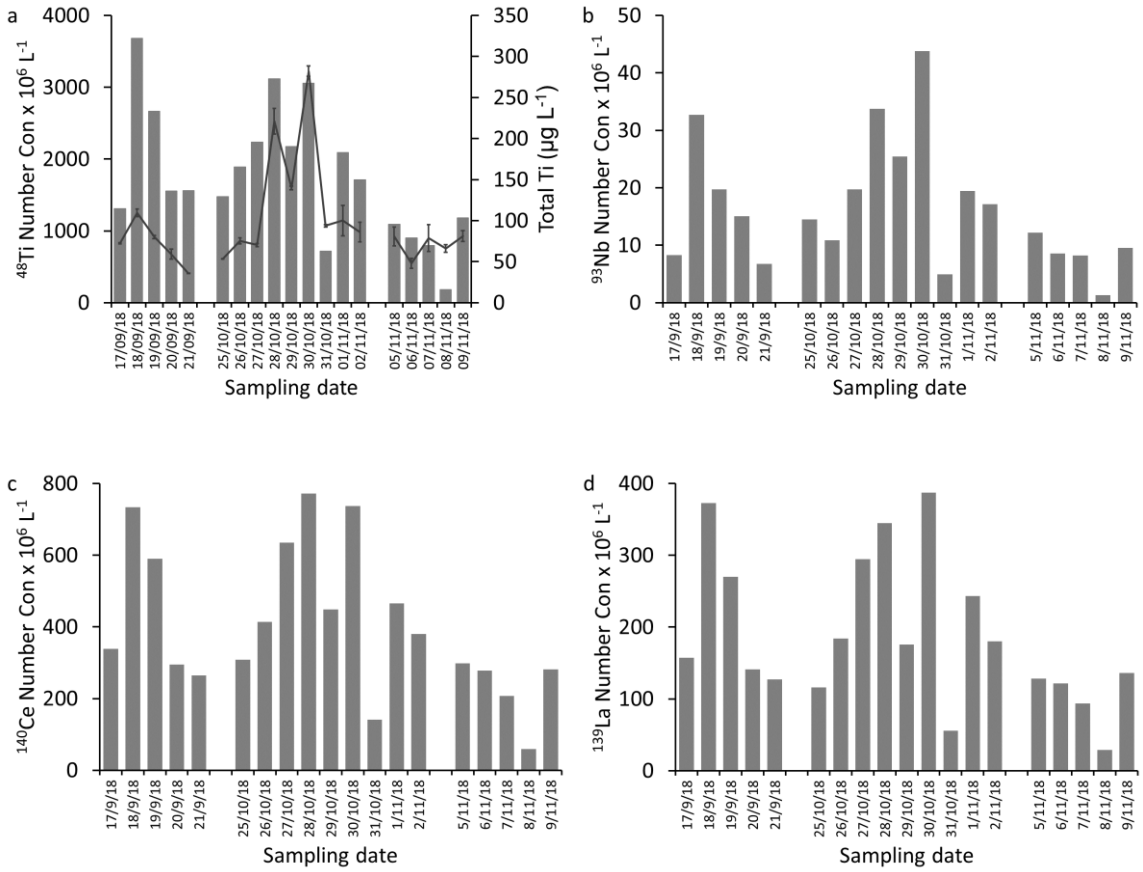

Figure 2.3 Number concentration of (a) Ti-, (b) Nb-, (c) Ce- and (d) La-containing particles in the Broad River water during the three sampling campaigns.

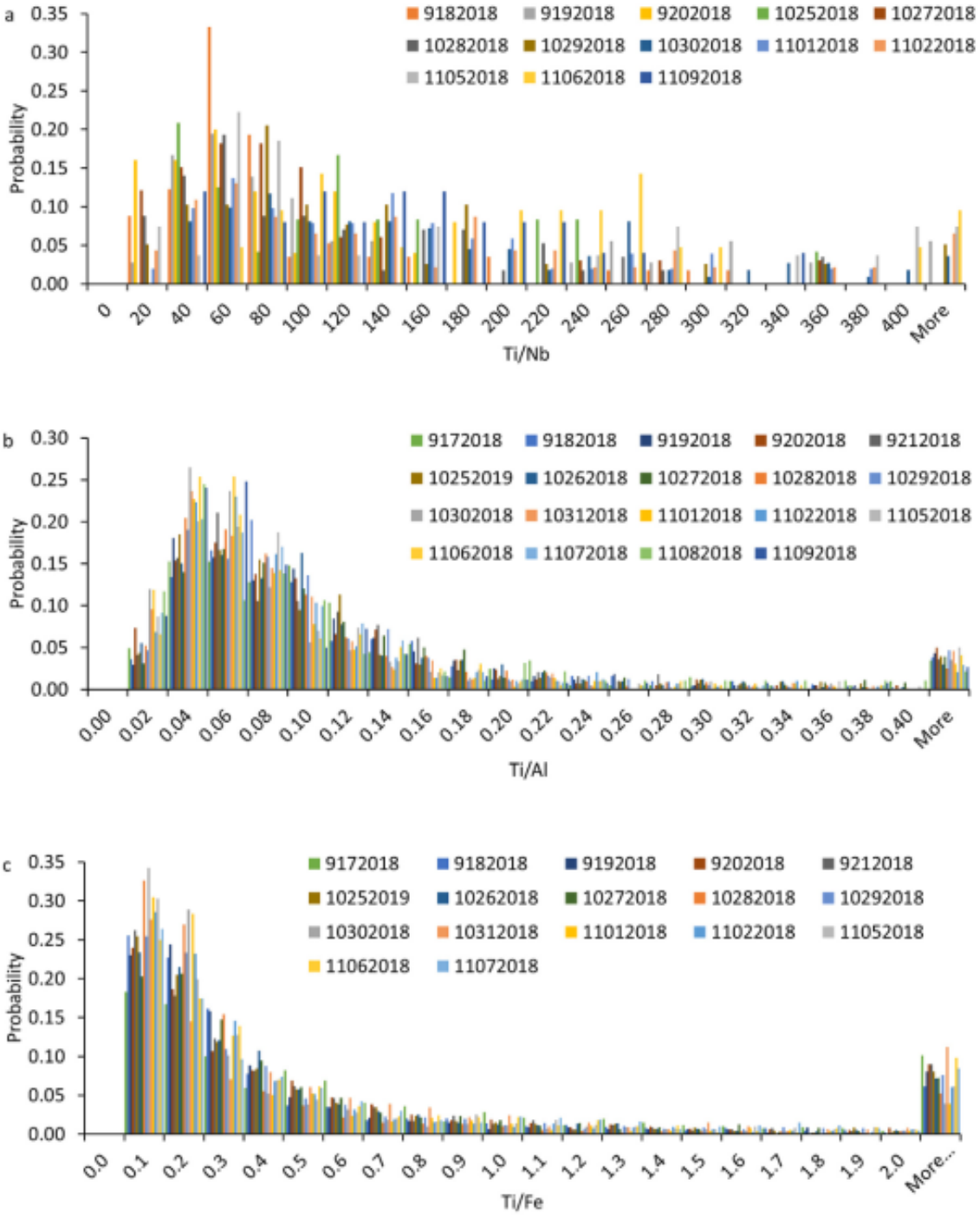

Figure 2.4 Elemental ratio distributions of (a) Ti/Nb, (b) Ti/Al, and (c) Ti/Fe in Ti-containing particles on a single particle basis measured by single particle-inductively coupled plasmatime of flight-mass spectrometer (SP-ICP-TOF-MS). For Ti/Nb, only samples that contained at least 20 particles containing Ti- and Nb-are presented in panel a.

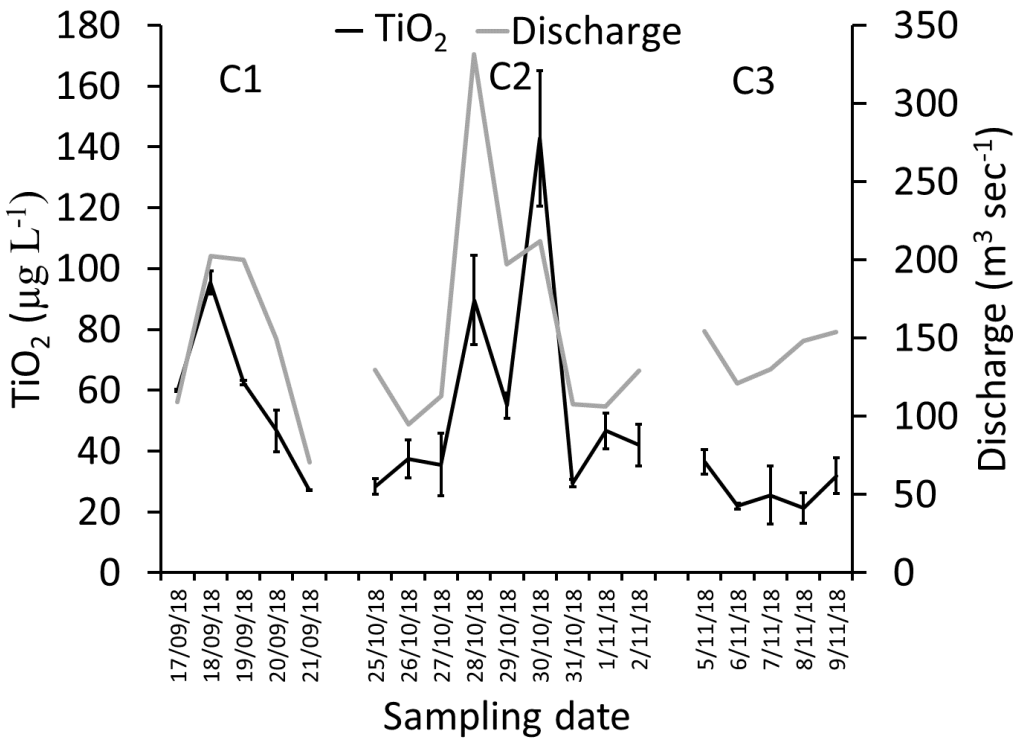

Figure 2.5 The calculated TiO_2 concentrations in the Broad River water during the three sampling campaigns.

References

1. Müller, A.; Österlund, H.; Marsalek, J.; Viklander, M. The pollution conveyed by urban runoff: A review of sources. Sci. Tot. Environ. **2020,** 709, 136125.
2. Kiser, M. A.; Westerhoff, P.; Benn, T.; Wang, Y.; Perez-Rivera, J.; Hristovski, K. Titanium nanomaterial removal and release from wastewater treatment plants. Environ. Sci. Technol. **2009,** 43, 6757-6763.
3. Loosli, F.; Wang, J.; Rothenberg, S.; Bizimis, M.; Winkler, C.; Borovinskaya, O.; Flamigni, L.; Baalousha, M. Sewage spills are a major source of engineered titanium dioxide release into the environment. Environ. Sci. Nano. **2019,** 6, 763-777.
4. Gondikas, A. P.; von der Kammer, F.; Reed, R. B.; Wagner, S.; Ranville, J. F.; Hofmann, T. Release of TiO_2 nanoparticles from sunscreens into surface waters: a one-year survey at the Old Danube recreational lake. Environ. Sci. Technol. **2014,** 48 (10), 5415-5422.
5. Reed, R. B.; Martin, D. P.; Bednar, A. J.; Montano, M. D.; Westerhoff, P.; Ranville, J. F. Multi-day diurnal measurements of Ti-containing nanoparticle and organic sunscreen chemical release during recreational use of a natural surface water. Environ. Sci. Nano. **2017,** 4 (1), 69-77.
6. Baalousha, M.; Yang, Y.; Vance, M. E.; Colman, B. P.; McNeal, S.; Xu, J.; Blaszczak, J.; Steele, M.; Bernhardt, E.; Hochella JR, M. F. Outdoor urban nanomaterials: The emergence of a new, integrated, and critical field of study. Sci. Tot. Environ. **2016,** 557-558, 740-753.
7. Gohler, D.; Stintz, M.; Hillemann, L.; Vorbau, M. Characterization of nanoparticle release from surface coatings by the simulation of a sanding process. Annal. Occup. Hygiene. **2010,** 54 (6), 615-624.
8. Koponen, I. K.; Jensen, K. A.; Schneider, T. Comparison of dust released from sanding conventional and nanoparticle-doped wall and wood coatings. J. Expos. Sci. Environ. Epidemiol. **2011,** 21 (4), 408-418.
9. Nored, A. W.; Chalbot, M. C.; Kavouras, I. G. Characterization of paint dust aerosol generated from mechanical abrasion of TiO_2 -containing paints. J. Occup. Environ. Hyg. **2018,** 15 (9), 629-640.
10. Parker, N.; Keller, A. A. Variation in Regional Risk of Engineered Nanoparticles: nanoTiO_2 as a Case Study. Environ. Sci. Nano. **2019,** 6, 444-455.
11. Wang, J.; Nabi, M. M.; Mohanty, S. K.; Afrooz, A. N.; Cantando, E.; Aich, N.; Baalousha, M. Detection and quantification of engineered particles in urban runoff. Chemosphere **2020,** 248, 126070.
12. Lützhøft, H. C. H.; Hartmann, N. B.; Brinch, A.; Kjølholt, J.; Baun, A. Environmental Effects of Engineered Nanomaterials: Estimations of Predicted No-Effect Concentrations (PNECs);978-87-93352-70-4; The Danish Environmental Protection Agency: Copenhagen, Denmark, 15.
13. Mueller, N. C.; Nowack, B. Exposure Modeling of Engineered Nanoparticles in the Environment. Environ. Sci. Technol. **2008,** 42 (12), 4447-4453.
14. Gondikas, A.; von der Kammer, F.; Kaegi, R.; Borovinskaya, O.; Neubauer, E.; Navratilova, J.; Praetorius, A.; Cornelis, G.; Hofmann, T. Where is the nano? Analytical approaches for the detection and quantification of TiO_2 engineered nanoparticles in surface waters. Environ. Sci. Nano. **2018,** 5 (2), 313-326.

15. Peters, R. J.; van Bemmel, G.; Milani, N. B.; den Hertog, G. C. U.; ndas, A. K.; van der Lee, M.; Bouwmeester, H. Detection of nanoparticles in Dutch surface waters. Sci. Tot. Environ. **2018,** 621, 210-218.
16. Neal, C.; Jarvie, H.; Rowland, P.; Lawler, A.; Sleep, D.; Scholefield, P. Titanium in UK rural, agricultural and urban/industrial rivers: Geogenic and anthropogenic colloidal/sub-colloidal sources and the significance of within-river retention. Sci. Tot. Environ. **2011,** 409 (10), 1843-1853.
17. Barksdale, J. Titanium, its occurrence, chemistry, and technology. Soil Sci. **1950,** 70 (5), 414.
18. Craigie, N. Principles of elemental chemostratigraphy: a practical user guide; Springer International Publishing: Cham, Switzerland, 2018.
19. Zack, T.; Kronz, A.; Foley, S. F.; Rivers, T. Trace element abundances in rutiles from eclogites and associated garnet mica schists. Chem. Geol. **2002,** 184 (1-2), 97-122.
20. NC DEQ Broad River basin restoration priorities; 09.
21. Stewart, S. R.; Berg, R. HURRICANE FLORENCE;AL062018; National Hurricane Center: May 30, 19.
22. Hendriks, L.; Gundlach-Graham, A.; Hattendorf, B.; Günther, D. Characterization of a new ICP-TOFMS instrument with continuous and discrete introduction of solutions. J. Anal. At. Spectrom. **2017,** 32 (3), 548-561.
23. Pace, H. E.; Rogers, N. J.; Jarolimek, C.; Coleman, V. A.; Higgins, C. P.; Ranville, J. F. Determining Transport Efficiency for the Purpose of Counting and Sizing Nanoparticles via Single Particle Inductively Coupled Plasma Mass Spectrometry. Anal. Chem. **2011,** 83 (24), 9361-9369.
24. Tanner, M. Shorter signals for improved signal to noise ratio, the influence of Poisson distribution. J. Anal. Atom. Spectrom. **2010,** 25 (3), 405-407.
25. Antignano, A.; Manning, C. E. Rutile solubility in H_2O, H_2O-SiO_2, and H_2O-$NaAlSi_3O_8$ fluids at 0.7-2.0 GPa and 700-1000 ºC: Implications for mobility of nominally insoluble elements. Chem. Geol. **2008,** 255 (1), 283-293.
26. USGS Mineral Commodity Summaries 2019: US Geological Survey; U.S. Geological Survey: 19.
27. Lim, K. J.; Engel, B. A.; Tang, Z.; Choi, J.; Kim, K.-S.; Muthukrishnan, S.; Tripathy, D. Automated web GIS based hydrograph analysis tool, WHAT. J. Am. Wat. Res. Assoc. **2005,** 41 (6), 1407-1416.
28. Galfi, H.; Österlund, H.; Marsalek, J.; Viklande, M. Mineral and Anthropogenic Indicator Inorganics in Urban Stormwater and Snowmelt Runoff: Sources and Mobility Patterns. Water. Air. Soil Pollut. **2017,** 228 (7), 1-18.
29. Tian, P.; Li, Y.; Yang, Z. Effect of rainfall and antecedent dry periods on heavy metal loading of sediments on urban roads. Front. Earth Sci. China. **2009,** 3 (3), 297-302.
30. Yuan, Q.; Guerra, H.; Kim, Y. An investigation of the relationships between rainfall conditions and pollutant wash-off from the paved road. Water **2017,** 9 (4), 232.
31. Pereira, E.; Baptista-Neto, J. A.; Smith, B. J.; McAllister, J. J. The contribution of heavy metal pollution derived from highway runoff to Guanabara Bay sediments - Rio de Janeiro / Brazil. An. Acad. Bras. Cienc. **2007,** 79 (4), 739-750.
32. Schiff, K. C.; Tiefenthaler, L. L. Anthropogenic versus natural mass emissions from an urban watershed. Southern California Coastal Water Research Project, Annual Report, Long Beach California USA. In Southern California Coastal Water Research Project

Annual Report 1999-2000. WeisbergS., Elmore, D., Eds.; Southern California Coastal Water Research Project: Westminster, CA, 2001; pp 63-70.
33. Baalousha, M.; Wang, J.; Mahmudun Nabi, M.; Loosli, F.; Valenca, R.; Mohanty, S. K.; Afrooz, N.; Cantando, E.; Aich, N. Stormwater green infrastructures retain high concentrations of TiO_2 engineered (nano)-particles. J. Hazard. Mater. **2020,** 122335.
34. José, C. G.; Wyllie, P. J. Ilmenite (high Mg, Mn, Nb) in the carbonatites from the Jacupiranga complex, Brazil. Am. Mineral. **1983,** 68, 960-971.
35. Chemours Titanium Dioxide For Coating; 18.
36. Shandilya, N.; Le Bihan, O.; Bressot, C.; Morgeneyer, M. Emission of Titanium Dioxide Nanoparticles from Building Materials to the Environment by Wear and Weather. Environ. Sci. Technol. **2015,** 49 (4), 2163-2170.
37. Lee, P. K.; Yu, S.; Chang, H. J.; Cho, H. Y.; Kang, M. J.; Chae, B. G. Lead chromate detected as a source of atmospheric Pb and Cr (VI) pollution. Sci. Rep. **2016,** 6, 36088.
38. Wilczynska-Michalik, W.; Rzeznikiewicz, K.; Pietras, B.; Michalik, M. Fine and ultrafine TiO_2 particles in aerosol in Krakow (Poland). Mineralogia **2014,** 45 (3-4), 65-77.
39. Westerhoff, P.; Song, G.; Hristovski, K.; Kiser, M. A. Occurrence and removal of titanium at full scale wastewater treatment plants: implications for TiO_2 nanomaterials. J. Environ. Monit. **2011,** 13 (5), 1195-1203.
40. Markus, A. A.; Krystek, P.; Tromp, P. C.; Parsons, J. R.; Roex, E. W. M.; Voogt, P. d.; Laane, R. W. P. M. Determination of metal-based nanoparticles in the river Dommel in the Netherlands via ultrafiltration, HR-ICP-MS and SEM. Sci. Tot. Environ. **2018,** 631-632, 485-495.
41. Donovan, A. R.; Adams, C. D.; Ma, Y.; Stephan, C.; Eichholz, T.; Shi, H. Single particle ICP-MS characterization of titanium dioxide, silver, and gold nanoparticles during drinking water treatment. Chemosphere **2016,** 144, 148-153.
42. Verplanck, P. L.; Furlong, E. T.; Gray, J. L.; Phillips, P. J.; Wolf, R. E.; Esposito, K. Evaluating the Behavior of Gadolinium and Other Rare Earth Elements through Large Metropolitan Sewage Treatment Plants. Environ. Sci. Technol. **2010,** 44 (10), 3876-3882.
43. Horowitz, A. J.; Elrick, K. A.; Smith, J. J. Monitoring urban impacts on suspended sediment, trace element, and nutrient fluxes within the City of Atlanta, Georgia, USA: program design, methodological considerations, and initial results. Hydrol. Process. An Int. J. **2008,** 22 (10), 1473-1496.
44. Jovanovic, B.; Guzman, H. M. Effects of titanium dioxide (TiO_2) nanoparticles on caribbean reef-building coral (Montastraea faveolata). Environ. Toxicol. Chem. **2014,** 33 (6), 1346-1353.

Chapter 3

Temporal **V**ariation in TiO_2 **E**ngineered **P**article **C**oncentrations in the Broad River **D**uring **D**ry and **W**et **W**eathers.

Nabi, M.M., Wang, J., Goharian, E., Baalousha, M.," Temporal variation in TiO_2 engineered particle concentrations in the Broad River during dry and wet weathers.", Sci. Total Environ., 807 (2022), p. 151081

3.1 Abstract

Titanium dioxide (TiO_2) engineered particles are widely used in the urban environment as pigments in paints, and as active ingredients in photocatalytic coatings. Consequently, studies are necessary to quantify TiO_2 engineered particle concentrations and their temporal variability in surface waters to gain better understanding about their abundance and environmental fate in order to minimize their potential environmental impacts. The objective of this study was to determine the temporal variability in the concentration of TiO_2 engineered particles in the Broad River, Columbia, South Carolina, United States during dry and wet weather conditions and to examine the relationship between flow discharge, water quality indicators, and the concentration of TiO_2 engineered particles. TiO_2 engineered particle concentration in the Broad River water was determined by mass balance calculation using bulk titanium concentration and the increase in Ti/Nb ratio above the natural background ratio. The relative abundance of single metal and multi-metal Ti-bearing particles was determined by single particle-inductively coupled plasma-time of flight-mass spectrometer (SP-ICP-TOF-MS). Additionally, the elemental ratios of Ti/Nb, Ti/Al, and Ti/Fe within multi-metal Ti-bearing particles were determined at the single particle level. Discharge, bulk elemental concentrations (*e.g.,* Ti, Al, Fe, and Nb), bulk elemental ratios (*e.g.,* Ti/Al, Ti/Fe, and Ti/Nb), TiO_2 engineered particle concentration, and turbidity displayed the same trend of rise and fall following storm events. Linear relationships were established between turbidity and TiO_2 engineered particle concentrations in the Broad River for different flow regimes. However, no correlation was observed between TiO_2 engineered particle concentrations and flow discharge, dissolved oxygen, pH, or ionic strength. The established correlations between

turbidity and TiO_2 engineered particle concentrations are important as they can be used to translate the continuously monitored turbidity to TiO_2 concentrations.

3.2 Introduction

Field data on the temporal variability in titanium dioxide (TiO_2) engineered particle concentrations in urban surface waters during and after storm events remains scarce, despite the wide use of TiO_2 engineered particles in the urban environment as pigments (*e.g.*, 100-300 nm) and as engineered nanoparticles (*e.g.*, 1-100 nm) in self-cleaning surfaces [1]. For instance, paint, which contain up to 10% TiO_2 particles, demand is estimated at 5.3 billion liters $year^{-1}$ in 2019 in the United States, a third of which (*e.g.*, 1.77 billion liters) is used for exterior paint [2]. These uses of TiO_2 engineered particles result in their release and deposition on surfaces in the urban environment which later can be washed off by rainfall and surface runoff [3]. Consequently, several studies identified TiO_2 engineered particles in urban media such as fine and ultrafine atmospheric particulate matter [4], dust dry deposition [5], road dust, sludge from storm drains, and roadside soils [6], bridge runoff [3], rain and surface water [7,8], and stormwater green infrastructure [9]. Most studies reported the occurrence, without providing estimated concentrations, of TiO_2 engineered particles in environmental samples based on measuring total Ti concentrations and identifying few particles in a given sample using transmission electron microscopy (TEM) [4,5]. Other studies estimated the concentrations of TiO_2 engineered particles in environmental samples based on environmental fate modeling [10,11]. Nonetheless, recent studies reported quantitative measured concentrations of TiO_2 engineered particles in environmental samples such as sewage spills [12], stormwater runoff [3], stormwater green infrastructure [9], and surface water [7,8,13]. These studies focused on developing approaches to detect and quantify TiO_2

engineered particle concentrations in environmental samples and did not investigate the event-scale temporal variability or the relationship between TiO_2 engineered particle concentrations and environmental parameters such as flow discharge, temperature, pH, dissolved oxygen, turbidity, or suspended solids.

In most cases, contaminant, including TiO_2 engineered particle, in urban rivers are not characterized by a constant concentration, but rather by the episodic or random occurrence of rainfall events, snowmelt, and/or return flows and subsequent high river flows [13]. For instance, a recent environmental fate modeling study suggested that stormwater runoff could result in high variability in TiO_2 engineered nanoparticle concentrations in urban rivers, with high flow events generating a large proportion of the total annual TiO_2 engineered nanoparticle loads in rivers [11]. Variables affecting contaminant load in rivers, thus may affect TiO_2 engineered particle concentrations, include antecedent rainfall, duration of the rainfall event, rainfall intensity of the event, succession of rainfall events, time of rise and fall of the hydrograph, runoff duration, peak discharge and total runoff [14]. Between rainfall events, contaminants in the catchment, including TiO_2 engineered particles, tend to build up via dust blown in by wind, tire wear residue, paint and road marking wear, etc. Thus, the longer period between the antecedent and current rainfall events, the greater the mass of an individual contaminant available for wash-off from surfaces in the basin. In response to the changing intensity, duration, and frequency of rainfall events, some or all the available contaminants are washed off and transported to receiving surface waters [15,16]. While the contaminant mass can increase by storm events, higher peak flows and discharges may end up displaying lower concentrations due to dilution effects.

This study aims to **(1)** quantify the temporal variability in TiO_2 engineered particle concentrations in the Broad River, Columbia, South Carolina, United States during dry and wet weather conditions under rainfall events of various characteristics, **(2)** evaluate the impact of rainfall events characteristics on TiO_2 engineered particle concentrations, and **(3)** determine the correlation between TiO_2 engineered particle concentrations, flow discharge, and environmental indicators with particular emphasis on turbidity as a surrogate for suspended sediment concentration.

3.3 Materials and Methods

3.3.1 Sampling

The Broad River is a principal tributary of the Congaree River, about 240 km long in western North Carolina and northern South Carolina in the Unites States. The Broad River originates in the Blue Ridge Mountains of eastern Buncombe Country, North Carolina, and flows generally south-southeastwardly, through or along the boundaries of Rutherford, Polk, and Cleveland Counties in North Carolina, and Cherokee, York, Union, Chester, Fairfield, Newberry, and Richland Counties in South Carolina. The broad River joins the Saluda River near the City of Columbia in South Carolina to form the Congaree River. The total drainage area of the Broad River is approximately 14,035 km^2 [17]. Land use throughout the Broad River basin is a mix of commercial and residential properties with agricultural (row crops and pasture) and forested land in the headwaters. There are permitted 14 major wastewater treatment plants (WWTP), 30 minor WWTPs, 20 animal

operation facilities, 92 general and individual stormwater facilities in the Broad river basin [17].

Water samples were collected from the Broad River, Columbia, SC 29201 (34°00'10.4"N 81°03'18.4"W) during a range of hydrologic settings including wet weather conditions with different rainfall intensities and during a dry period (**Table B.1**). The period March 2019 to April 2019 experienced typical rain conditions in Columbia, South Carolina, United States with average rainfall of approximately 50 to 100 mm per month, whereas the period of August to September 2019 experienced dry condition with average rainfall of < 25 mm per month, majority of which occurred during the month of September [18]. The precipitation data was collected from the United States Geological Survey (USGS) gauge station number 021695045 (34°00'24"N 81°01'18"W), nearly 3.5 km from the water sampling location. The flow discharge data also was collected from the USGS, station number 02162035 (34°02'54"N 81°04'24"W), which is located nearly 4.5 km upstream of the sampling location (**Figure B.1**).

3.3.2 Sampling site and elemental analysis

Water samples were collected from the Broad River, Columbia, SC 29201 (34°00'10.4"N 81°03'18.4"W) in a 1 L high-density polyethylene bottles (Thermo Scientific, Rockwood, TN, United States). Prior to use, bottles were soaked in 10% nitric acid (Acros Organics, Czech Republic) for at least 24 hours followed by soaking in ultrapure water (UPW, PURELAB Option-Q, ELGA, UK) for 24 hours, air dried, and then double-bagged. In the field, the sampling bottles were rinsed three times in the surface water before filling with the water sample. Samples were individually double-bagged and

returned to the lab the same day, where they were stored at 4°C in the dark until further analysis. All samples were digested with HF:HNO_3 (3:1) mixture (ACS grade acids distilled in the laboratory) and analyzed for total elemental concentrations using Perkin Elmer NexION 350D ICP-MS according to the protocols described in detail in elsewhere [13,19]. The method limit of detection and quantification are summarized in **Table B.2**.

3.2.3 Hydrograph separation

In order to estimate the flow contribution of the storm, first the baseflow (dry flow) should be separated from the direct runoff of the storm event. The baseflow in a river is often attributed to the gradual snowmelt, groundwater discharge to the river, or urban or agricultural return flow to the river. The direct runoff in a river is the portion of the total discharge that is produced by rainfall. In this study, we used the Web based Hydrograph Analysis Tool (WHAT) [20] to separate the total discharge to direct runoff and baseflow.

3.3.4 Calculation of total TiO_2 engineered particle concentration

The concentration of TiO_2 engineered particles in the river water was calculated according to Eq. 1 assuming that all Ti occur in particulate form, that Nb occurs only in natural Ti-bearing particles with constant Ti/Nb ratio, that anthropogenic Ti occur as pure TiO_2 particles [13,19,21–23].

$$[TiO_2]_{engineered\ particles} = \frac{TiO_{2\ MM}}{Ti_{\ MM}}\left[Ti_{sample} - Nb_{sample}.\left(\frac{Ti}{Nb}\right)_{background}\right] \qquad (Eq.1)$$

Where, $[TiO_2]_{engineered\ particles}$ is the concentration of TiO_2 engineered particles, $Ti_{\ MM}$ and $TiO_{2\ MM}$ are the molar masses of Ti and TiO_2, Ti_{sample} and Nb_{sample} are the concentrations of Ti and Nb in a given sample, $Ti/Nb_{background}$ is the natural background

elemental concentration ratio of Ti/Nb. Background Ti/Nb ratio was calculated on eight reference samples collected from Lake Katherine and Gills creek in Columbia, SC in the absence of rainfall events [19]. Elemental ratios (*e.g.,* Ti/Nb) have been recently implemented to quantify the total concentration of TiO_2 engineered particles in wastewater treatment plants [24], urban runoff [3], stormwater green infrastructure [9], surface waters [13,19].

3.3.5 Multi-element single particle analysis

The water samples were shaken vigorously prior extraction to avoid particle losses by sedimentation and to obtain a representative subsample. Ten mL aliquots were transferred into acid-washed 15 mL centrifuge tubes (Fisher Scientific, San Nicolás de los Garza, Nuevo León, Mexico). The transferred samples were bath sonicated for 2 h (Branson, Model 2800, 40 kHz, Danbury, CT, United States), then centrifuged at 775 g for 5 min (Eppendorf Centrifuge 5810R, Hamburg, Germany) to remove large particles (> 1000 nm assuming natural particle density, $\rho = 2.5$ g cm^{-3}) to prevent clogging of the ICP-TOF-MS introduction system. The top 7 mL supernatant was decanted and stored at 4°C in the dark till analysis by SP-ICP-TOF-MS. The theoretical size of the extracted fractions corresponds to particles < 725 nm for TiO_2 particles ($\rho = 4.2$ g cm^{-3}). All samples were bath sonicated again for 15 min immediately prior to SP-ICP-TOF-MS analysis. All samples were diluted 100 folds in ultrahigh purity water prior to the analysis. The Ti recovery of the particle extraction method was calculated as the total mass of Ti single particles to the total mass of Ti in the bulk water samples and varied between 1.6 to 11.2%.

Single particle analysis was performed using an ICP-TOF-MS (TOFWERK, Thun, Switzerland) to determine all isotopes within a single particle simultaneously [25]. Element

specific instrument sensitivities were measured with a multi-element solution mix prepared from a multi-element solution (0, 1, 2, 5, and 10 μgL^{-1} multi element standard, diluted in 1% HCl, BDH Chemicals, Radnor, PA, USA). The transport efficiency was calculated via the known size approach [26] using both Au ENMs with a certified particle size of 60 nm (NIST RM8013 Au, Gaithersburg, MD, USA) and Au standard solutions (0, 1, 2, 5, and 10 μgL^{-1}, diluted in 1% HCl, BDH Chemicals, West Chester, PA, USA) prepared in UPW. Using a standard tuning solution, the ICP-TOF-MS mass spectra were calibrated using $^{18}H_2O^+$, $^{59}Co^+$, $^{115}In^+$, $^{140}Ce^+$, and $^{238}U^+$ target isotopes in TofDAQ view. Particle/baseline signal separation, particle signals, particle mass, and particle number concentration were determined from mass-calibrated ICP-TOF-MS spectra using Python script in Tofware as described elsewhere [19]. The data for each isotope were treated separately, but the time stamps were kept throughout data processing for every isotope, allowing for identification of isotope correlations in a single particle. The elemental mass detection limit for SP-ICP-TOF-MS analysis is summarized in **Table B.2**. Procedural blanks were analyzed together with the samples. Only 15 Ti spikes were detected in the procedural blanks corresponding to a particle number concentration of 3.20×10^4 Ti-bearing particles L^{-1} and a total particle mass concentration of 1.21×10^{-4} $\mu g\ L^{-1}$, which are negligible compared to those measured in the river water samples (see results and discussion).

3.4 Results and Discussion

3.4.1 Rainfall-runoff characteristics

Five rainfall events were monitored during the period 03/20/2019 to 04/19/2019 (**Table B.1**) in addition to a dry period (09/23/2019 to 09/27/2019). Rainfall intensity varied from 0.25 to 28 mm day^{-1}. The antecedent dry days (ADD) varied from 0 to 15 days. The two rainfall events between 03/20/2019 and 04/04/2019 were characterized by relatively long ADDs (7 and 15 days), whereas the rainfall events between 04/05/2019 and 04/19/2019 were characterized by short ADDs (0 to 2 days). Among these 5 rainfall events, only the last two events lasted for more than a day, while the duration of the rainfalls on March 25th, April 2nd and 5th was less than a day. The heaviest rainfall event occurred on April 2nd (28.2 mm per day), followed by the rainfall during the first day (April 12th) of the last event, and the rainfall event on April 5th event. In general, higher intensity of rainfall happens during the less frequent and shorter duration of storm events.

The events' hydrograph and time series of river discharge at the Broad River show that the river's flow regime is highly sensitive to the storms and reaches to its peak value in a short period during the rainfall events, *i.e.* the basin's time of concertation and time of peak is relatively small (**Figure 3.1**). The river's discharge between 04/07/2019 and 04/17/2019 was higher than that between 03/20/2019 and 04/06/2019 and during the drought period between 09/23/2019 and 09/27/2019. This is because rain events between 04/05/2019 and 04/19/2019 were preceded by short antecedent dry periods, whereas those between 03/20/2019 and 04/04/2019 were preceded by longer antecedent dry periods (**Table B.1**). Antecedent meteorological and hydrogeological conditions determine the

hydrological response of a basin, as the smaller ADD means higher soil moisture in the basin and less capacity of infiltration during the next storm [14,16]. Thus, under dry conditions, the water storage capacity of a catchment is higher than under wet conditions when the surface and subsurface storage are likely to be saturated. As the pore size fills with water, the infiltration capacity of the soil profile decreases. Any additional rainfall occurring after soil saturation becomes runoff immediately, even if the rainfall intensity is very small [27]. Thus, rainfall events of similar magnitudes, but different ADD and soil moisture, can result in runoffs of different magnitudes. Moreover, the evapotranspiration rates are lower during the wet seasons. These collectively result in higher runoff following rainfall events during wet conditions, while rainfall events during dry conditions produce low runoff amounts, or may not produce any measurable runoff, unless if the intensity of rainfall is significant [27,28].

3.4.2 Time-flow-concentration trend plots

The temporal variability in pollutant concentration was observed through time-flow-concentration graphs (hydro-pollutographs, **Figure 3.2**). The hydrograph and the pollutographs show similar trend of rise and fall of discharge and pollutant concentrations following rainfall events. The major water quality change that occurred during wet-weather events was the substantial increase in turbidity, the other water quality indicators such as temperature, dissolved oxygen, and pH were not sensitive to the changes in flow (**Figure 3.2a, Figure B.2**). Turbidity values measured between 04/10/2019 and 04/19/2019 were higher than those measured between 03/20/2019 and 04/09/2019 and during the dry period 09/23/2019 to 09/27/2019. Increased turbidity regularly occurs during rain events when rainfall and runoff mobilize particles from the riparian zone, upstream locations in the

watershed, and the overall stream network within a basin [29]. Water from rain events and related runoff increase discharge and flow velocity, which in turn, increase shear stress and turbulence, and therefore increase sediment erosion and transport.

Figure 3.2a shows that equal peaks of discharge may have different magnitude of turbidity. For example, the peak on 04/09/2019 (264 m^3 sec^{-1}; 40 FNU) and 04/15/2019 (274 m^3 sec^{-1}; 92 FNU), which can be attributed to variability in suspended sediment concentration during storm events. Many studies found that turbidity in river waters during rainfall events exhibits close positive correlation with suspended sediment concentrations [30,31], and thus many studies used turbidity as a surrogate of suspended sediment loadings in rivers and streams [32–35].

The increases in Ti concentrations coincided (timewise) with increase in turbidity (**Figure 3.2b**), but not with discharge (**Figure 3.2a**). All other elements (*e.g.*, Nb, Al, and Fe) followed the same trend with slight variations in the concentrations during different rain events (**Figure B.3**). These results suggest that suspending sediments is the key driver of metal mobility during rainfall events. Numerous studies reported elemental concentrations to estimate pollution loads during runoff events [36,37]. However, metals may have both natural as well as anthropogenic origins. Metals occur naturally in soils, which is one of the primary sources of suspended sediments. Soil particles are also important constituent of urban dust, thus they are a significant contributor to metal flow into rivers during runoff events. Therefore, elemental concentrations do not allow differentiating natural from anthropogenic contributions.

3.4.3 Time-flow-elemental ratio trend plots

The elemental ratios of Ti/Nb, Ti/Al, and Ti/Fe show similar trend of rise and fall following rainfall events to each other and to turbidity (**Figure 3.3**). The elemental ratio of Ti/Nb varies between 324.8 ± 39.5 (4/19/2019) and 543.2 ± 22.5 (3/25/2019). The elemental ratio of Ti/Al varies between 0.038 ± 0.002 and 0.065 ± 0.003. The elemental ratio of Ti/Fe varies between 0.039 ± 0.002 and 0.114 ± 0.005. The lowest Ti/Al and Ti/Fe occurred on 9/26/2019 and the highest Ti/Al and Ti/Fe occurred on 4/03/2019. These elemental ratios were generally higher than the natural background elemental ratios, indicating Ti-particle contamination. For instance, the Ti/Nb, Ti/Al, and Ti/Fe ratios were generally higher than the reference ratios (*e.g.*, 267 ± 8.9, 0.049 ± 0.003, and 0.037 ± 0.005, respectably) measured in smaller creeks in the sampling area [19], and higher than the average crustal ratios (*e.g.*, 320, 0.049, and, 0.1 respectively) [38]. The increase in the elemental ratios coincided with the increase in the turbidity, suggesting that turbidity (*e.g.*, suspended solids) is the key factor driving the increase in elemental ratios due to anthropogenic particulate Ti contamination.

The concentration of TiO_2 engineered particles were estimated based on Ti/Nb, Ti/Al, and Ti/Fe (**Figure 3.4a**). The concentration of TiO_2 engineered particles follow the same trend using the three elemental ratios, suggesting that these three elemental ratios can be implemented to estimate of TiO_2 engineered particle concentrations in this study. However, some differences are observed between the estimated TiO_2 engineered particle concentrations, which might be attributed to the unique associations and behaviors of these elements within natural Ti-bearing particles (**see further discussion in section 3.4.5**). Although Nb, Fe, and Al occur in natural Ti-bearing particles and can be used as tracers [19],

Nb is the only element that is exclusively associated with Ti [39]. On the other hand, Fe- and Al-bearing particles occurred both as single metal particles and as particles associated with Ti-bearing particles [39]. Thus, Ti/Nb most likely provides the most accurate estimate of TiO_2 engineered particle concentrations.

3.4.4 Turbidity-TiO_2 relationship

In general, increases in turbidity resulted in increases in TiO_2 concentration (**Figure 3.4b**). However, three different associations can be identified. During the dry season both turbidity and TiO_2 concentration were low. During the wet season, a strong (R^2 of 0.94) linear relationship was established between turbidity and TiO_2 concentration for rainfall events that were preceded with short antecedent dry periods, and a weaker (R^2 of 0.47) linear relationship was established between turbidity and TiO_2 concentration for rainfall events that were preceded with long antecedent dry periods. These findings suggest that turbidity can be used as a substitute to predict TiO_2 concentrations within this watershed. However, as shown here, this relationship depends on several factors such as antecedent dry periods and is likely to be site specific. It is worth noting that a strong positive relationship was observed between total suspended solid concentration and turbidity in rivers, which varied for a particular catchment and within a particular period [40–42]. This variation between turbidity and suspended sediment underpins our observation of the variation between turbidity and TiO_2, given that TiO_2 is typically associated with suspended solids.

3.4.5 Characterization of Ti-bearing particles by SP-ICP-TOF-MS

The number concentration of all, single metal, and multi-metal Ti-bearing particles, determined by SP-ICP-TOF-MS, display a similar trend of rise and fall following rainfall events as the TiO_2 engineered particle mass concentrations (**Figure 3.5a**). Approximately, 29 to 83%, (**Figure 3.5b**) of Ti-bearing particles were single metal, that is based on icp-TOF-MS analysis results that these particles did not contain any natural tracers. This can be due to either (**1**) these single metal Ti-bearing particles are pure TiO_2 engineered particles, and/or (**2**) the concentrations of natural tracers in these single metal Ti-bearing particles are below the SP-ICP-TOF-MS size detection limit [39]. The remaining particles (*e.g.,* 17-71%) contained at least one natural tracer such as Fe, Al, Si, Zr, Nb, Th, Ce, Ba, Mn, Pb, Ni, Zn, La, V, U, Ta, Cr, and W, indicating that these particles are most likely naturally occurring particles. This is in good agreement with elemental association between Ti and other elements in natural surface waters and soils in South Carolina, United States [19,39]. This is also in good agreement with the impurities (*e.g.,* Nb, Ta, Sb, W, V, Cr, Mo, and Sn, Zr, Fe, U and Pb) detected in natural TiO_2 minerals (such as rutile and ilmenite) [21,23,43].

The relative abundance of single metal Ti-bearing particles also displays the same trend of rise and fall following rainfall events as the TiO_2 engineered particle concentrations (**Figure 3.5b**). It is worth noting that Nb always occurred in association with Ti-bearing particles, whereas all other natural tracers occurred both in association with Ti-bearing particles and in single metal particles form. This is because Ti and Nb occur in natural titanium minerals such as rutile, anatase, sphene, and/or opaque heavy minerals (*e.g.,* titanomagnetite, magnetite, and ilmenite) [44]. Natural TiO_2 minerals, such as rutile and

ilmenite, have been shown to be the dominant carrier (*e.g.*, > 90-95% of the whole rock content) for Ti, Nb, Ta, Sb, and W as well as an important carrier (*e.g.*, 5-45% of the whole rock content) for V, Cr, Mo, and Sn in TiO_2-bearing metamorphic rocks [21,43].

The relative abundance of single metal particles was higher during the high runoff periods (*e.g.*, 04/11/2019 to 04/19/2019) than those during the low runoff events (*e.g.*, 03/23/2019 to 04/10/2019) and the drought period (*e.g.*, 09/23/2019 to 09/27/2019). These findings indicate the increase in the relative abundance of single metal particles during runoff events can be attributed to TiO_2 engineered particles in the runoff.

The elemental ratio of Ti/Al, Ti/Fe, and Ti/Nb, determined on single particle basis, display the same trend in all samples. Most particles exhibited Ti/Al ratio within the range 0 to 0.4 (72 to 98%, **Figure 3.6a**), Ti/Fe ratio within the range 0 to 2.0 (75 to 95 %, **Figure 3.6b**), and Ti/Nb ratio within the range 0 to 400 (97 to 100%, **Figure 3.6c**). Nonetheless, a small fraction of particles exhibited an elemental Ti/Al elemental ratio > 0.4 (2 to 28), Ti/Fe > 2.0 (15 to 25 %), and Ti/Nb > 400 (0 to 3%). These elemental ratios are typical of natural Ti-bearing minerals. Ti and Fe occur in natural minerals such as: titanomagnetite ($Fe_{3-x}Ti_xO_4$, $0 < Ti/Fe < 0.43$, $0 < x < 1$) which form a complete solid solution series between end members of magnetite (Fe_3O_4, Ti/Fe = 0) ulvöspinel; ulvöspinel (Fe_2TiO_4, Ti/Fe = 0.43); pseudobrookite (Fe_2TiO_5, Ti/Fe = 0.43); ilmenite ($FeTiO_3$, Ti/Fe = 0.86); pseudorutile ($Fe_2Ti_3O_9$, Ti/Fe = 1.29); and ilmenorutile and ferropseudobrookite ($FeTi_2O_5$, Ti/Fe = 1.71); and iron-depleted naturally occurring Ti-particles due to weathering (*e.g.*, Ti/Fe > 2 to 20) [39,45]. Ti and Al occur in natural minerals such as: palygorskite and montmorillonite (Ti/Al = 0.014-0.016); illite (Ti/Al = 0.026); kaolinite and hectorite (Ti/Al = 0.06); vermiculite and corrensite (Ti/Al = 0.090-0.093) (**Figure 3.2**).

Correlation coefficients between pH and Ti/Fe, probability of Ti/Fe > 2.0, and Ti/Al were calculated using Pearson's correlation method and the *p-value* for correlation was calculated using t-test. The elemental ratio of Ti/Fe (**Figure 3.7a)** and the fraction of particles with Ti/Fe > 2.0 (**Figure 3.7b**) increased with pH ($p < 0.05$)**.** This increase in Ti/Fe on the single particle level might be attributed to the selective dissolution of Fe within Ti-bearing particles due to the increase in pH. It has been shown that Fe-Ti oxides might be subject to alteration or weathering (*e.g.,* dissolution) resulting in higher Ti/Fe elemental ratios [45]. For instance, the alteration of ilmenite is accomplished by the removal of structural iron, which results finally in an almost pure TiO_2 phase [46]. The alteration of ilmenite occurs through several intermediate phases, each successively enriched in titanium and depleted in iron (increasing Ti/Fe ratio), to an almost pure form of TiO_2 [45–48]. The alteration of ilmenite results in the formation of pseudorutile, fine leucoxene, and coarse leucoxene (leucoxene is a polycrystalline aggregate of rutile) [45]. Pseudorutile is an intermediary alteration product of ilmenite with the chemical composition $Fe_2O_3.nTiO_2.mH_2O$ ($3 < n < 5$, $1 < m < 2$) [45]. The elemental ratio of Ti/Al increased slightly with pH ($p < 0.05$, **Figure 3.7b**), likely due to the lower dissolution rate of Al oxides relative to Fe oxides. The pH dependence of Ti/Fe, and Ti/Al might explain differences in estimated TiO_2 engineered particle concentrations based on Ti/Al, Ti/Fe, and Ti/Nb.

3.5 Conclusions and Perspectives

This study provides a comprehensive approach for measuring and monitoring TiO_2 engineered particles in urban rivers. Total TiO_2 engineered particle concentrations were estimated using mass balance calculations coupled with increases in Ti/Nb, Ti/Al, and

Ti/Fe elemental ratios above the natural background ratios. Single particle-inductively coupled plasma-time of flight-mass spectrometer (SP-ICP-TOF-MS) was used to characterize Ti-bearing particles at the single particle level. Furthermore, this study provides the basis for comprehensive investigation of nonpoint TiO_2 engineered particle release and concentrations in urban rivers during rainfall events. The elemental concentrations, TiO_2 concentrations, number concentration of the total-, single metal -, and multi-metal -Ti-bearing particles, and the relative abundance of single metal particles displayed temporal variability and increased with increases in runoff following rainfall events. Determining the temporal variability in engineered particle concentrations in surface waters during rainfall events is critical in improving the understanding of the environmental fate of engineered particles in surface waters and in assessing the environmental exposures to engineered particles. Elemental concentrations, ratios, and TiO_2 engineered particle concentrations correlated with turbidity, but not with discharge. A strong linear relationship was established between turbidity and TiO_2 engineered particle concentration. This relationship is important because it can be used as a substitute for the TiO_2 engineered particle concentration determination within the catchment area. Subsequently, this correlation is important for water resources management studies because it enables continuous monitoring of TiO_2 engineered particle in situ, which allows better understanding of TiO_2 engineered particle temporal behavior. Extending these findings to other sites will require parameterization of the turbidity-TiO_2 linear relationship as this correlation is likely to be site specific. Although turbidity measurement is cost effective and quicker than TiO_2 measurement, there is a need to collect higher time resolution data (*e.g.,* minutes to hours) in order to improve the understanding of the

turbidity-TiO_2 relationship. The findings from this study can be employed to develop management strategies to control rainwater pollution at the catchment level.

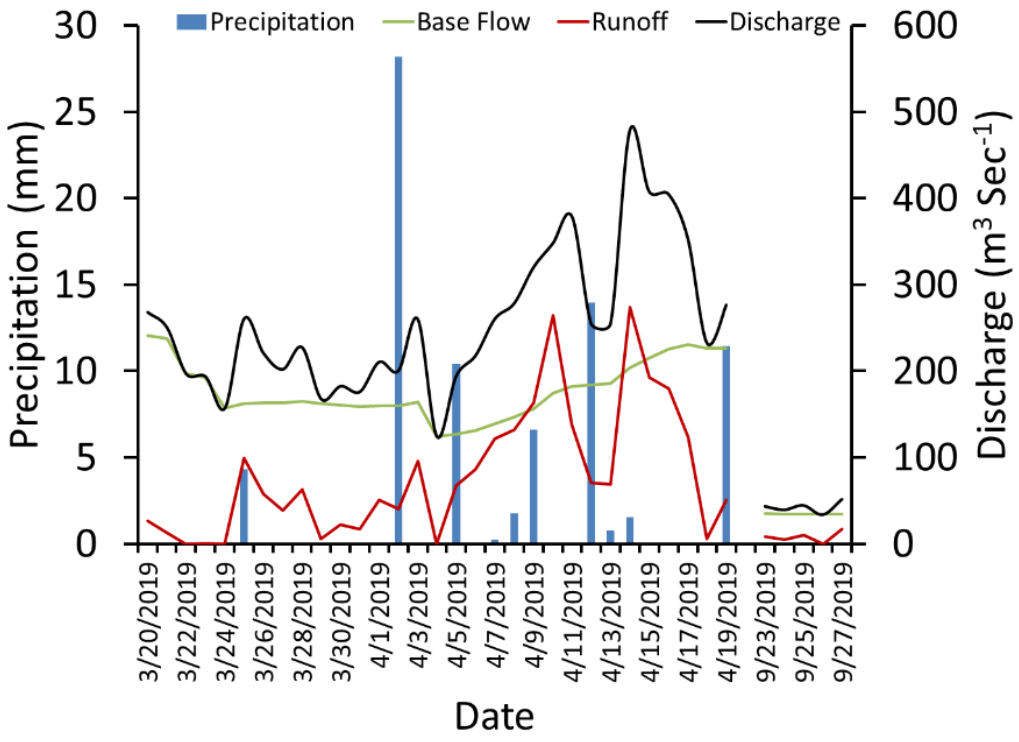

Figure 3.1 Hydrological conditions during the sampling period. March to April was wet weather period, whereas, September was drought conditions

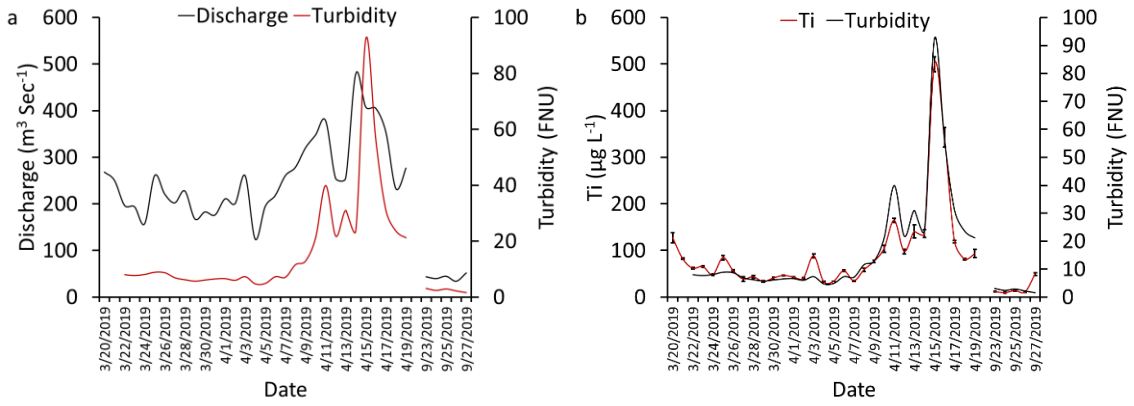

Figure 3.2 Hydrograph and pollutographs (a) discharge-turbidity relationship, (b) Ti concentration-turbidity relationship. FNU: formazin nephelometric units.

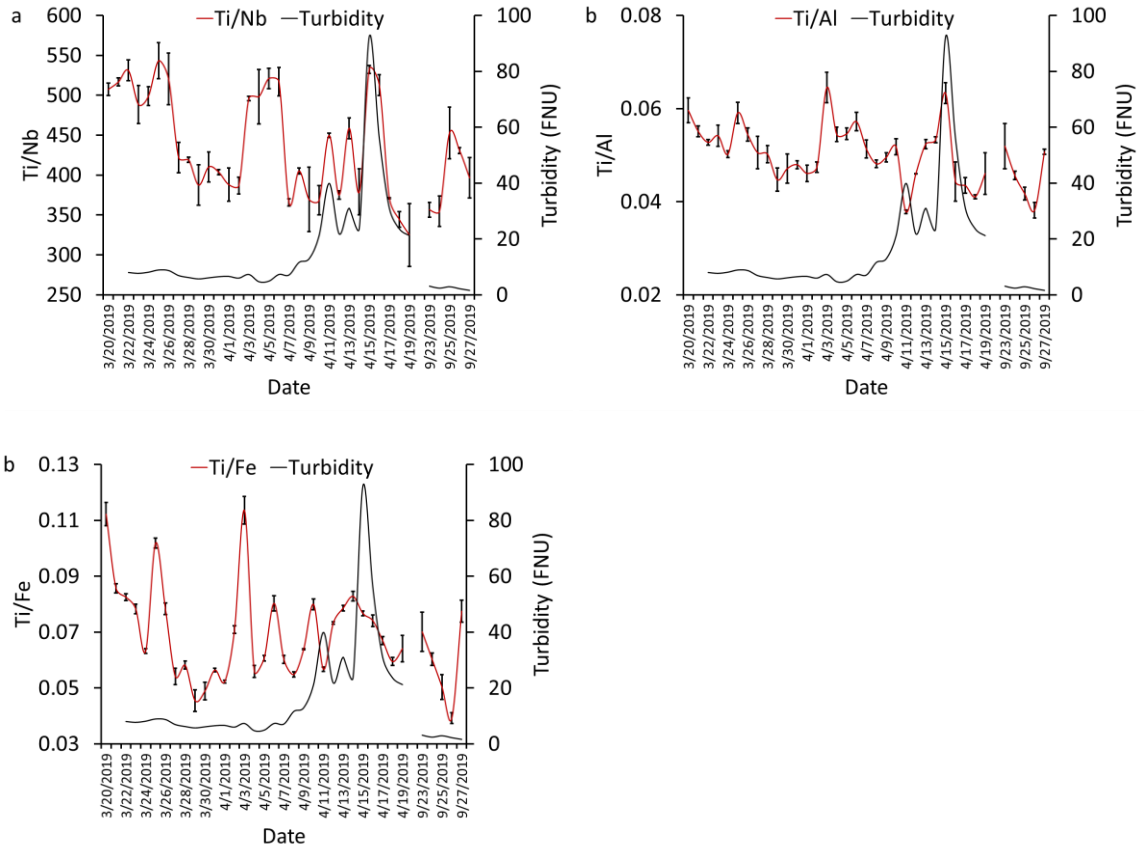

Figure 3.3 Elemental ratio as a function of time (a) Ti/Nb, (b) Ti/Al, and (c) Ti/Fe.

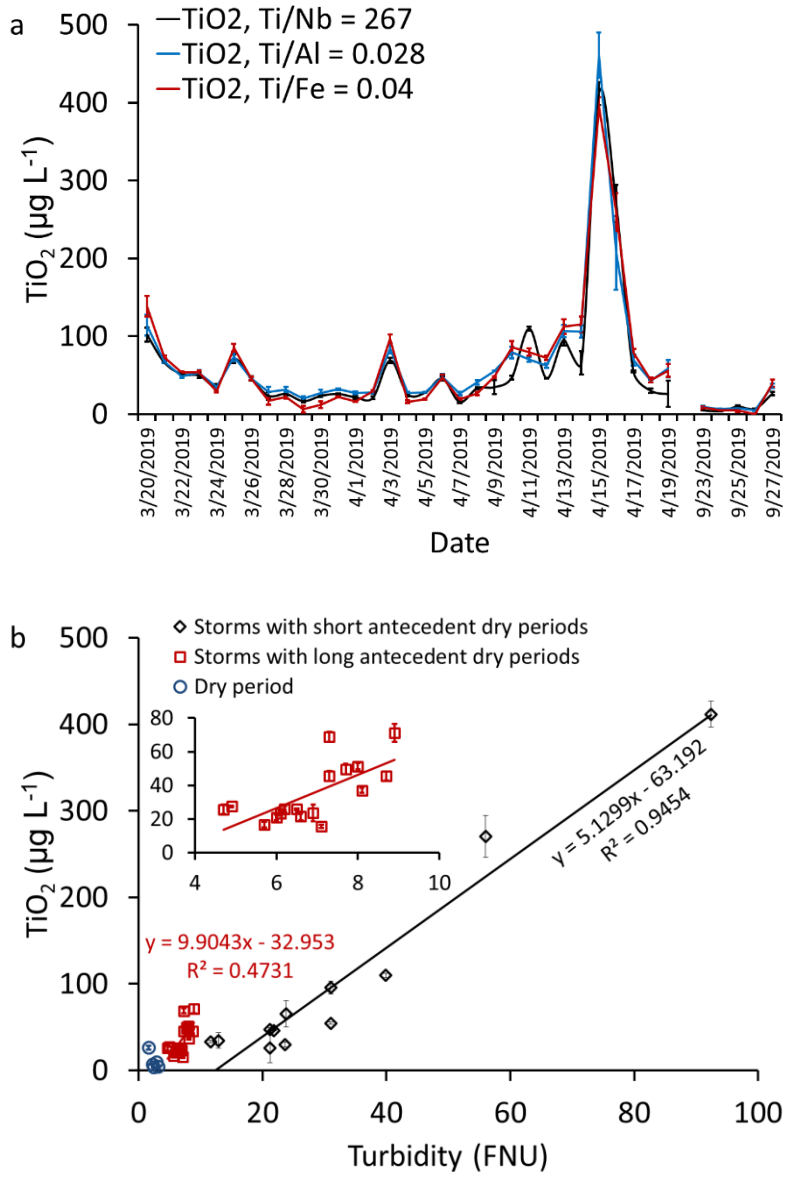

Figure 3.4 (a) TiO_2 concentrations estimated based on Ti/Nb, Ti/Al and Ti/Fe elemental ratios, and (b) Correlation between TiO_2 concentrations estimated based on Ti/Nb and turbidity.

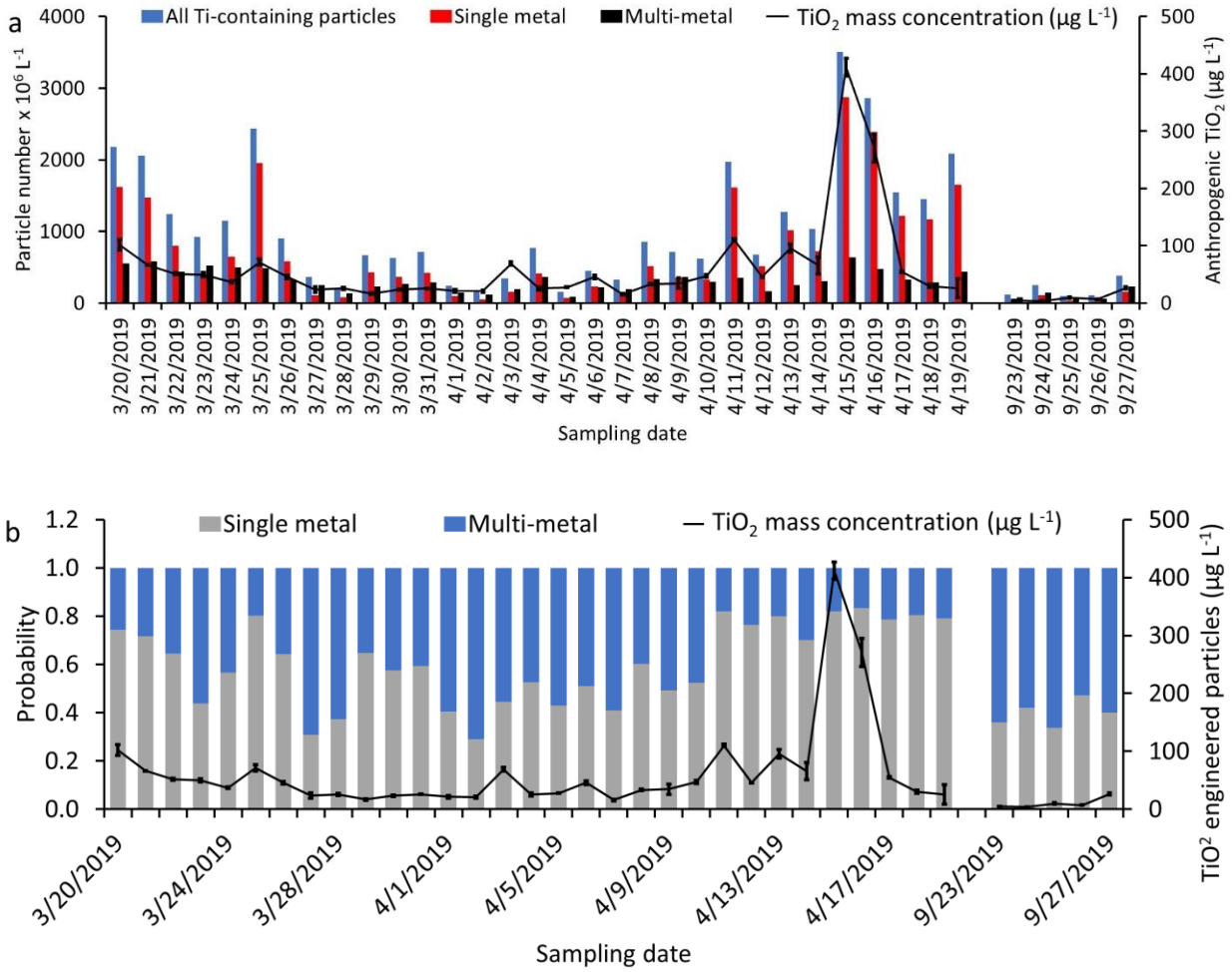

Figure 3.5 Characterization of titanium-bearing particles by single particle-inductively coupled plasma-mass spectrometer (SP-ICP-TOF-MS): (a) number concentration of Ti-bearing particles, and (b) probability of single metal and multi-metal Ti-bearing particles. The term apparently pure indicate all particles detected by SP-ICP-MS that did not contain any natural tracers.

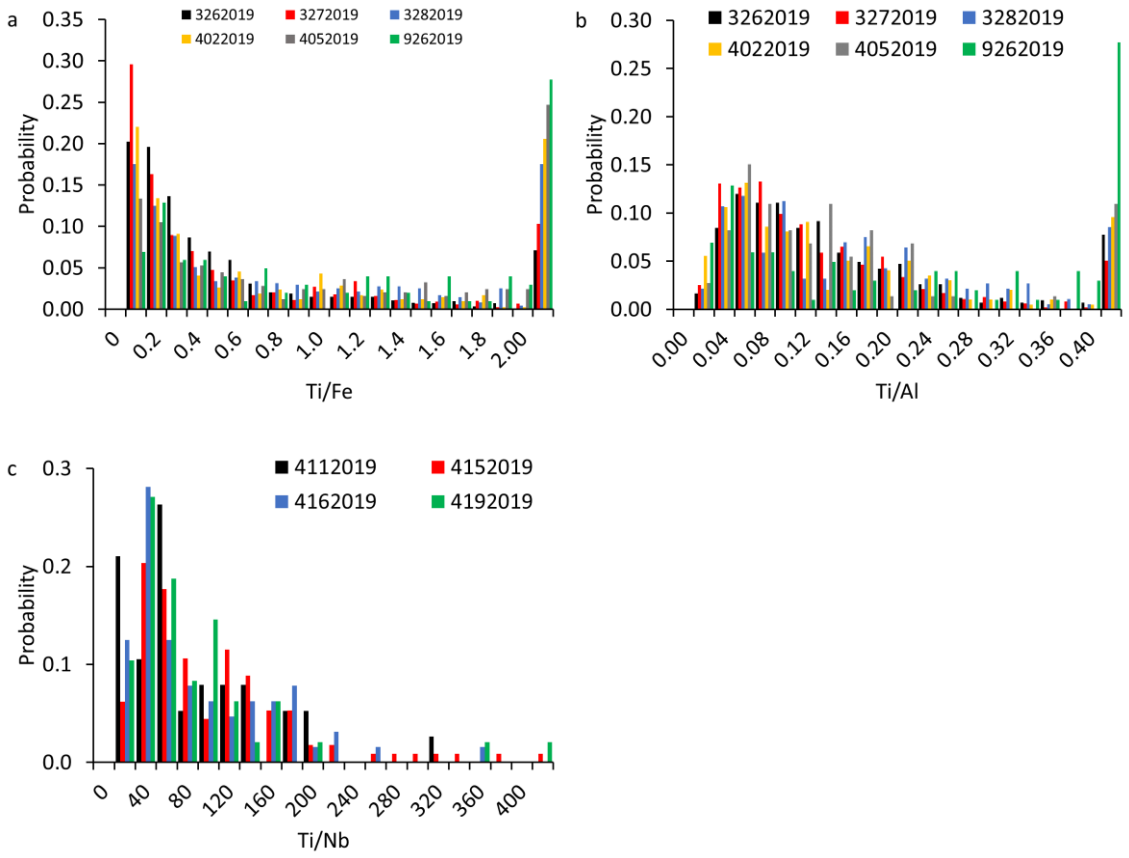

Figure 3.6 Representative elemental ratio distribution on a single particle basis (a) Ti/Fe, (b) Ti/Al, and (c) Ti/Nb

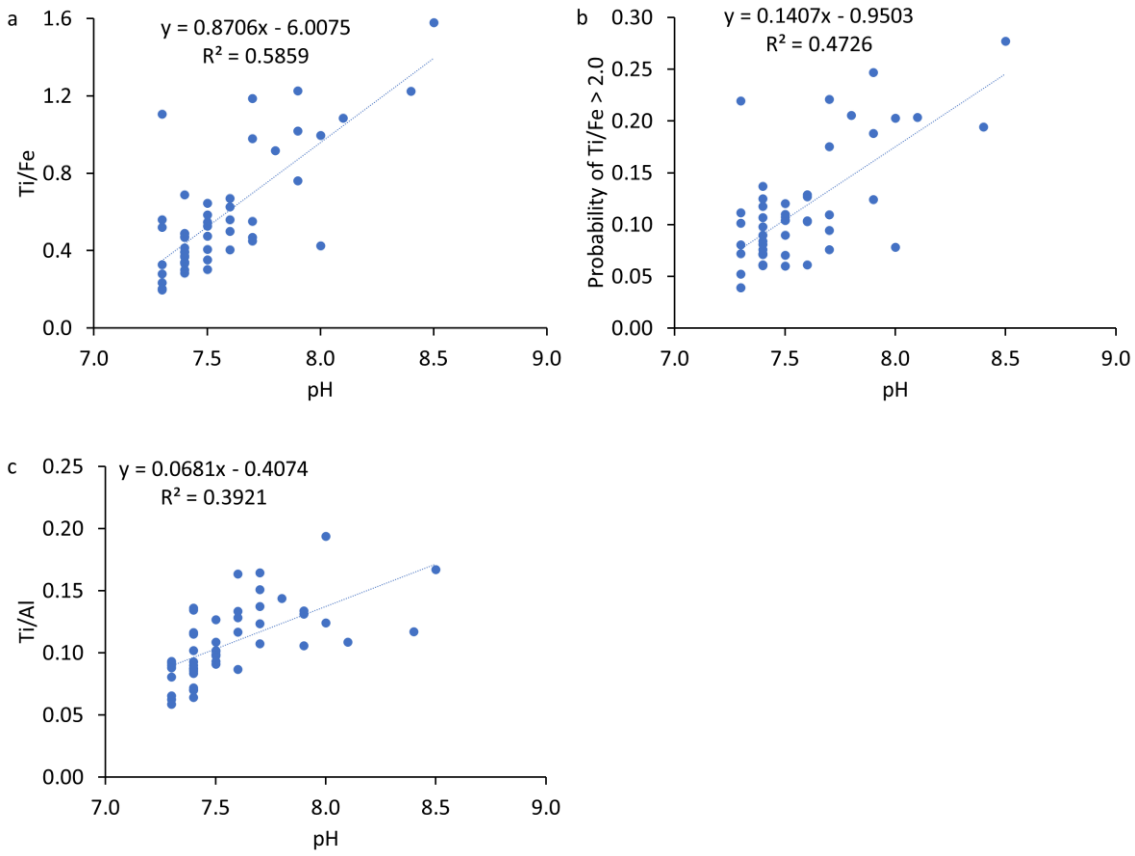

Figure 3.7 Elemental ratio on a single particle level as a function of pH.

References

1. Baalousha M, Yang Y, Vance ME, Colman BP, McNeal S, Xu J, et al. Outdoor urban nanomaterials: The emergence of a new, integrated, and critical field of study. Sci. Tot. Environ 2016; 557-558: 740-753.
2. Coatingsworld. U.S. Demand for Paint & Coatings to Reach 1.4 Billion Gallons in 2019., 2019.
3. Wang J, Nabi MM, Mohanty SK, Afrooz AN, Cantando E, Aich N, et al. Detection and quantification of engineered particles in urban runoff. Chemosphere 2020; 248: 126070.
4. Wilczyńska-Michalik W, Rzeźnikiewicz K, Pietras B, Michalik M. Fine and ultrafine TiO_2 particles in aerosol in Kraków (Poland). Mineralogia 2015; 45.
5. Lee P-K, Yu S, Chang HJ, Cho HY, Kang M-J, Chae B-G. Lead chromate detected as a source of atmospheric Pb and Cr (VI) pollution. Scientific reports 2016; 6: 36088.
6. Adamiec E. Road environments: impact of metals on human health in heavily congested cities of Poland. International journal of environmental research and public health 2017; 14: 697.
7. Azimzada A, Jreije I, Hadioui M, Shaw P, Farner JM, Wilkinson KJ. Quantification and Characterization of Ti-, Ce-, and Ag-Nanoparticles in Global Surface Waters and Precipitation. Environmental Science & Technology 2021; 55: 9836-9844.
8. Wang J-L, Alasonati E, Fisicaro P, Benedetti MF. Titanium nanoparticles fate in small-sized watersheds under different land-uses. Journal of Hazardous Materials 2022; 422: 126695.
9. Baalousha M, Wang J, Nabi MM, Loosli F, Valenca R, Mohanty SK, et al. Stormwater green infrastructures retain high concentrations of TiO_2 engineered (nano)-particles. Journal of hazardous materials 2020; 392: 122335.
10. Gottschalk F, Sun T, Nowack B. Environmental concentrations of engineered nanomaterials: Review of modeling and analytical studies. Environmental Pollution 2013; 181: 287-300.
11. Parker N, Keller AA. Variation in regional risk of engineered nanoparticles: nanoTiO_2 as a case study. Environmental Science: Nano 2019; 6: 444-455.
12. Praetorius A, Gundlach-Graham A, Goldberg E, Fabienke W, Navratilova J, Gondikas A, et al. Single-particle multi-element fingerprinting (spMEF) using inductively-coupled plasma time-of-flight mass spectrometry (ICP-TOFMS) to identify engineered nanoparticles against the elevated natural background in soils. Environmental Science: Nano 2017; 4: 307-314.
13. Nabi MM, Wang J, Baalousha M. Episodic surges in titanium dioxide engineered particle concentrations in surface waters following rainfall events. Chemosphere 2021a; 263: 128261.
14. Onderka M, Krein A, Wrede S, Martínez-Carreras N, Hoffmann L. Dynamics of storm-driven suspended sediments in a headwater catchment described by multivariable modeling. Journal of Soils and Sediments 2012; 12: 620-635.
15. Vercruysse K, Grabowski RC. Temporal variation in suspended sediment transport: linking sediment sources and hydro-meteorological drivers. Earth Surface Processes and Landforms 2019; 44: 2587-2599.

16. Vercruysse K, Grabowski RC, Rickson R. Suspended sediment transport dynamics in rivers: Multi-scale drivers of temporal variation. Earth-Science Reviews 2017; 166: 38-52.
17. SCdhec. Watershed water quality assessment. Broad Rriver basin., Columbia, S.C., 2007.
18. CPC. National weather services. Climate Prediction Center. https://www.cpc.ncep.noaa.gov/. Accessed 19/4/2020.
19. Loosli F, Wang J, Rothenberg S, Bizimis M, Winkler C, Borovinskaya O, et al. Sewage spills are a major source of titanium dioxide engineered (nano)-particle release into the environment. Environmental Science: Nano 2019; 6: 763-777.
20. Lim KJ, Engel BA, Tang Z, Choi J, Kim KS, Muthukrishnan S, et al. Automated web GIS based hydrograph analysis tool, WHAT. JAWRA Journal of the American Water Resources Association 2005; 41: 1407-1416.
21. Gaspar JC, Wyllie PJ. Ilmenite (high Mg, Mn, Nb) in the carbonatites from the Jacupiranga complex, Brazil. American Mineralogist 1983; 68: 960-971.
22. Gondikas AP, von der Kammer F, Reed RB, Wagner S, Ranville JF, Hofmann T. Release of TiO_2 nanoparticles from sunscreens into surface waters: a one-year survey at the Old Danube recreational lake. Environ. Sci. Technol 2014; 48: 5415-5422.
23. Nakashima K, Imaoka T. Niobian and zincian ilmenites in syenites from Cape Ashizuri, Southwest Japan. Mineralogy and Petrology 1998; 63: 1-17.
24. Nabi MM, Wang J, Meyer M, Croteau M-N, Ismail N, Baalousha M. Concentrations and size distribution of TiO_2 and Ag engineered particles in five wastewater treatment plants in the United States. Science of The Total Environment 2021b; 753: 142017.
25. Hendriks L, Gundlach-Graham A, Hattendorf B, Günther D. Characterization of a new ICP-TOFMS instrument with continuous and discrete introduction of solutions. Journal of Analytical Atomic Spectrometry 2017; 32: 548-561.
26. Pace HE, Rogers NJ, Jarolimek C, Coleman VA, Higgins CP, Ranville JF. Determining transport efficiency for the purpose of counting and sizing nanoparticles via single particle inductively coupled plasma mass spectrometry. Analytical chemistry 2011; 83: 9361-9369.
27. Istok J, Boersma L. Effect of antecedent rainfall on runoff during low-intensity rainfall. Journal of Hydrology 1986; 88: 329-342.
28. Penna D, Tromp-van Meerveld H, Gobbi A, Borga M, Dalla Fontana G. The influence of soil moisture on threshold runoff generation processes in an alpine headwater catchment. Hydrology and Earth System Sciences 2011; 15: 689-702.
29. Chen H, Chang H. Response of discharge, TSS, and E. coli to rainfall events in urban, suburban, and rural watersheds. Environmental Science: Processes & Impacts 2014; 16: 2313-2324.
30. Lewis J. Turbidity-controlled suspended sediment sampling for runoff-event load estimation. Water resources research 1996; 32: 2299-2310.
31. Patil S, Barfield B, Wilber G. Turbidity modeling based on the concentration of total suspended solids for stormwater runoff from construction and development sites. World Environmental and Water Resources Congress 2011: Bearing Knowledge for Sustainability, 2011, pp. 477-486.

32. Chanson H, Takeuchi M, Trevethan M. Using turbidity and acoustic backscatter intensity as surrogate measures of suspended sediment concentration in a small subtropical estuary. Journal of environmental management 2008; 88: 1406-1416.
33. Mosbrucker A. High resolution digital elevation model of Mount St. Helens Crater and Upper North Fork Toutle River Basin, Washington, based on an Airborne LiDAR survey of September 2009: US Department of the Interior, US Geological Survey, 2014.
34. Uhrich MA, Bragg HM. Monitoring instream turbidity to estimate continuous suspended-sediment loads and yields and clay-water volumes in the upper North Santiam River Basin, Oregon, 1998-2000. Vol 3: US Department of the Interior, US Geological Survey, 2003.
35. Wass P, Marks S, Finch J, Leeks GJL, Ingram J. Monitoring and preliminary interpretation of in-river turbidity and remote sensed imagery for suspended sediment transport studies in the Humber catchment. Science of the Total Environment 1997; 194: 263-283.
36. Hussain J, Husain I, Arif M, Gupta N. Studies on heavy metal contamination in Godavari river basin. Applied Water Science 2017; 7: 4539-4548.
37. Sakson G, Brzezinska A, Zawilski M. Emission of heavy metals from an urban catchment into receiving water and possibility of its limitation on the example of Lodz city. Environmental monitoring and assessment 2018; 190: 1-15.
38. Rudnick R, Gao S, Holland H, Turekian K. Composition of the continental crust. The crust 2003; 3: 1-64.
39. Baalousha M, Wang J, Erfani M, Goharian E. Elemental fingerprints in natural nanomaterials determined using SP-ICP-TOF-MS and clustering analysis. Science of The Total Environment 2021; 792: 148426.
40. Daphne LHX, Utomo HD, Kenneth LZH. Correlation between turbidity and total suspended solids in Singapore rivers. Journal of Water Sustainability 2011; 1: 313-322.
41. Packman J, Comings K, Booth D. Using turbidity to determine total suspended solids in urbanizing streams in the Puget Lowlands. 1999.
42. Sun H, Cornish PS, Daniell T. Turbidity-based erosion estimation in a catchment in South Australia. Journal of Hydrology 2001; 253: 227-238.
43. Zack T, Kronz A, Foley SF, Rivers T. Trace element abundances in rutiles from eclogites and associated garnet mica schists. Chemical Geology 2002; 184: 97-122.
44. Craigie N. Principles of elemental chemostratigraphy. Advances in Oil and Gas Exploration & Production, Rudy Swennen. A Practical User Guide. p189. DOI: https://doi.org/10.1007/978-3-319-71216-1 2018.
45. Weibel R. Alteration of detrital Fe-Ti oxides in Miocene fluvial deposits, central Jutland, Denmark. Bulletin of the Geological Society of Denmark 2003; 50: 141-208.
46. Morad S, Adin Aldahan A. Alteration of detrital Fe-Ti oxides in sedimentary rocks. Geological Society of America Bulletin 1986; 97: 567-578.
47. Morad S. SEM study of authigenic rutile, anatase and brookite in Proterozoic sandstones from Sweden. Sedimentary Geology 1986; 46: 77-89.
48. Mücke A, Chaudhuri JB. The continuous alteration of ilmenite through pseudorutile to leucoxene. Ore geology reviews 1991; 6: 25-44.

Chapter 4

Urban Runoff Drives Titanium Dioxide Engineered Particle Concentrations in Urban Watersheds: Field Measurements

Nabi, M.M., Wang, J., Goharian, E., Baalousha, M.," Urban runoff drives titanium dioxide engineered particle concentrations in urban watersheds: field measurements".

4.1 Abstract

Urban runoff is a significant source of pollutants, including incidental and engineered nanoparticles to receiving surface waters. The aim of this study is to investigate the impact of urbanization on the concentrations of TiO_2 engineered particles in urban surface waters. The study area boundaries are limited to the Lower Saluda and Nicholas Creek-Broad River from upstream, and outlet of upper Congaree River at Columbia, South Carolina, United States from downstream. This sampling area captures a significant footprint of the urban area of the City of Columbia. Water samples were collected daily from four sites during two rain events. All samples were analyzed for total metal concentrations following acid digestion and for particle number concentration and elemental composition using single particle-inductively coupled plasma-time of flight-mass spectrometer (SP-ICP-TOF-MS). Clustering of multi-metal nanoparticles (mmNPs) demonstrated that Ti-bearing particles were distributed mainly among three clusters, FeTiMn, AlSiFe, and TiMnFe, which are typical of naturally occurring iron oxide, clay, and titanium oxide particles. Thus, anthropogenic Ti concentration was attributed to single-metal nanoparticles, pure TiO_2 particles. The total concentration of anthropogenic TiO_2 in the rivers was determined by mass balance calculation using bulk titanium concentration and increases in Ti/Nb above the natural background ratio. The concentration of anthropogenic TiO_2 increased following the order 0 to 24 $\mu g\ L^{-1}$ in the Lower Saluda River < 0 to 663 $\mu g\ L^{-1}$ in the Broad River < 43 to 1051 $\mu g\ L^{-1}$ in Congaree River at Cayce <58 to 5050 $\mu g\ L^{-1}$ in the Congaree River at Columbia. The concentration of anthropogenic TiO_2 increased with increases in urban runoff. The source of anthropogenic TiO_2 was attributed to diffuse urban runoff. This study demonstrates that diffuse urban runoff results

in high concentration of TiO_2 particles in urban surface waters during and following rainfall events which may pose increased risks to aquatic organisms during these episodic events.

4.2 Introduction

Field Urban runoff is widely recognized as a major vector of pollutants, including engineered and incidental nanoparticles (ENPs and INPs), from the urban environment to receiving surface waters, contributing to the deterioration of urban surface water quality [1]. Yet, there is a limited understanding of the impact of urbanization and urban runoff on the concentrations of engineered particles in urban surface waters [2]. Titanium dioxide (TiO_2) is the most widely used engineered particles in the urban environment both as pigments (*e.g.,* 100-300 nm) in paint and nanosized particles (*e.g.,* 1-100 nm) in self-cleaning surfaces as photocatalysts [3]. For instance, an estimated 5.3 billion liters year^{-1} paint were used in the United States in 2019, 33% of which (e.g., 1.77 billion liters year^{-1}) was used for exterior paint [4]. These uses of TiO_2 result in their release due to wear and tear into the atmosphere and deposition on urban surfaces [5–9]. Rainfall washes the atmospheric deposited particles and carries them into receiving waterbodies. Thus, TiO_2 engineered particles are expected to occur at high concentrations in urban surface waters.

Urban waters receive large amounts of pollution, including TiO_2 engineered particles, from a variety of sources such as industrial discharges, mobile sources (*e.g.,* cars and trucks), residential and commercial wastewater, and polluted stormwater runoff from urban landscape. Recent studies reported high concentrations of TiO_2 engineered particles in road dust (*e.g.,* 0.4-2.5 g·kg^{-1}) [10–16], bridge runoff (*e.g.,* 5-150 µg L^{-1}) [17–19], sanitary sewer overflows impacted surface waters (*e.g.,* 1-100 µg L^{-1}) [20,21], urban runoff impacted surface waters (*e.g.,* 20 to 140 µg L^{-1}) [22], and industrial discharge impacted surface waters (*e.g.,*

133 to 266 μg L^{-1}) [23,24]. Additionally, a recent modeling study predicted even higher concentrations TiO_2 ENPs (*e.g.,* 619 to 1490 μg L^{-1}) in urban rivers following rainfalls [25]. However, other studies reported much lower concentrations of TiO_2 engineered particles in surface waters released from sunscreens (*e.g.,* 1.5-42.5 μg L^{-1}) [26–30]. These discrepancies in the reported TiO_2 engineered particle concentrations can be ascribed to differences in sampling areas, the targeted source of TiO_2 engineered particles, and/or methodological differences [2].

Monitoring engineered particle concentrations in the environment is challenging because of the similarities of physicochemical properties – such as composition, size, and shape – and the lower abundance of the engineered particles compared to naturally occurring counterparts [31,32]. For instance, Ti is the ninth most abundant element in the Earth's crust and is mainly found in minerals such as rutile, ilmenite, sphene, and/or opaque heavy minerals (*e.g.,* titanomagnetite, magnetite, and ilmenite) [33]. These minerals always contain trace concentrations of other elements such as Nb, Ta, Sn, Sb, W, V, Cr, Mo, and rare earth elements (REEs) [34,35]. These natural elemental impurities are typically removed from the natural Ti-bearing minerals during the manufacturing of TiO_2 engineered particles [20]. Thus, the introduction of TiO_2 engineered particles into environmental systems will result in increases in the elemental ratios of Ti to those elements naturally occurring in Ti-bearing minerals, which have been used (*e.g.,* Ti/Nb [20,22,36,37], Ti/Al [27], Ti/REEs [27], and Ti/V [23]) to estimate the concentration TiO_2 engineered particles in environmental systems.

Multi element-single article analysis by single particle-inductively coupled plasma-time of flight-mass spectrometer (SP-ICP-TOF-MS) is a promising technique in the nanometrology toolbox that has been implemented to differentiate ENPs from NNPs based

on the subtle differences in their elemental composition [20,38]. The premise of ICP-TOF-MS is that it detects and quantifies all elements within a single particle at low/trace concentrations, and thus, ICP-TOF-MS is the only method that could be implemented to differentiate ENPs from NNPs in environmental systems at the single particle level. However, the ability of the ICP-TOF-MS to "unequivocally" differentiate ENPs from NNPs based on differences in elemental composition at the single particle level is challenged by the minimal detectable element mass (MDM), which is element dependent [39,40]. The MDM that can be attained with SP-ICP-MS depends on the instrument or elemental sensitivity and the background levels that result from both dissolved analyte and instrumental noise (electronic noise and interferences to the monitored isotope) [40].

The overarching aim of this study is to evaluate the impact of urbanization on the concentrations of TiO_2 engineered particles in urban surface waters. To do this, we collected spatiotemporally resolved water samples from three Rivers within the urban zone of the city of Columbia, South Carolina, United States. We then characterized these water samples for total elemental concentrations using ICP-TOF-MS, estimated the concentrations of anthropogenic TiO_2 engineered particles using mass balance calculations and shifts in elemental ratios above the natural background ratios, and determined particle elemental composition at the single particle level using SP-ICP-TOF-MS.

4.3 Materials and Methods

4.3.1 Study area

The confluence of the Lower Saluda and Broad Rivers forming the Congaree River at Columbia, South Carolina was selected as the study area to investigate the impact of urbanization on the concentrations of TiO_2 engineered particles **(Figure 4.1)**. Water samples were collected between 27/4/2020 and 12/5/2020 from four locations within the limits of Columbia, South Carolina, United States, including the Lower Saluda River and the Broad River upstream of their confluence, and from Congaree River at Columbia and Cayce downstream of the Saluda and Broad Rivers' confluence. The Lower Saluda River (S) samples were collected near Hope ferry landing (34°02'45.7"N 81°11'27.3"W), approximately 2.7 kms downstream of Lake Murray reservoir dam and 12.9 km upstream of the Lower Saluda and Broad Rivers' confluence. The Broad River (B) water samples were collected near Columbia rowing club (34°02'36.9"N 81°04'23.7"W), which is approximately 4.5 km upstream of the Saluda and Broad Rivers' confluence. The Congaree River Columbia samples were collected at West Columbia Riverwalk (33°59'35.4"N 81°03'1.8"W, Co), which is approximately 1.5 km downstream of the Saluda and Broad confluence. The Congaree River Cayce samples were collected at Thomas Newman public boat landing (33°56'57.3"N 81°01'44.1"W, C), which is approximately 6.8 km downstream of the Saluda and Broad Rivers confluence. This sampling area captures a significant footprint of the urban area - accounting for approximately 50% - of the city of Columbia, South Carolina, United States. A detailed description of the sampling locations including

land use, industrial-commercial activities, mining activities, wastewater and storm water facilities in the watershed is provided in the supplementary information section C.1.

Precipitation data for the Broad and Congaree River sampling locations was collected from the USGS station number 021695045 (34°00'24"N 81°01'18"W), nearly 6.3 km from the Broad River sampling location, and nearly 3.1 km from the Congaree River Columbia sampling location and 6.4 km from the Congaree River Cayce sampling location. Rainfall and discharge data for the Lower Saluda River sampling location were collected from USGS station number 02168504 (34°03'03"N 81°12'35"W) immediately after the dam and nearly 1.8 km upstream from the Lower Saluda River sampling location. The discharge data for the Broad, and Congaree Rivers was collected from the USGS stations' number 02162035 (34°02'54"N 81°04'24"W), and 02169500 (33°59'35"N 81°03'00"W), nearly 5.3 km upstream of the Broad River sampling location and 0.05 km upstream from the Congaree River Columbia sampling location and 5.3 km upstream from the Congaree River Cayce sampling location, respectively.

4.3.2 Sample collection, digestion, and elemental analysis

Surface water samples were collected from the Broad, Lower Saluda and Congaree Rivers in 250-mL high density polyethylene bottles (Thermo Scientific, Rockwood, TN, United States). Prior to use, bottles were acid-washed in 10% nitric acid (Sigma Aldrich, St. Louis, MO, United States) for at least 24 hours, and soaked in ultrahigh purity water (PURELAB Option-Q, ELGA, High Wycombe, UK) for 24 hours, air dried, and then double-bagged. In the field, sampling bottles were rinsed three times in the surface water

and then filled with the water sample, samples were individually double-bagged, and returned to the lab the same day and were stored in the dark at 4ºC.

The bulk river water samples were digested using an acid mix, including H_2O_2, HNO_3, and HF, following the digestion protocol described elsewhere and summarized in the Appendix C.2 [17,22,37]. Elemental concentrations in the digested river water samples were determined by ICP-TOFR ICP-TOF-MS (TOFWERK, Switzerland) using TOFPilot 2.8.8 software. The instrument operating conditions are presented in **Table C.3**. Mass spectra calibration and standard tuning procedure were performed before analysis for instrument maintenance. Dissolved multi-element standards were prepared in 1% HNO_3 from commercially available ICP standards (BDH Chemicals, Radnor, PA, USA), with concentrations ranging from 0.001 to 100 μg L^{-1}. Internal standards (ICP Internal Element Group Calibration Standard, BDH Chemicals, Radnor, PA, USA) were monitored at the same time for quality control. The isotopes measured were ^{27}Al, ^{49}Ti, ^{57}Fe, ^{90}Zr, ^{93}Nb, ^{139}La, ^{140}Ce, ^{141}Pr, ^{142}Nd, ^{152}Sm, ^{153}Eu, ^{158}Gd, ^{159}Tb, ^{164}Dy, ^{165}Ho, ^{166}Er, ^{169}Tm, ^{174}Yb, and ^{175}Lu. All isotopes were analyzed in collision/reaction mode.

The USGS reference material BHVO-2 Hawaiian basalts were digested following the same procedure described above. The elemental analysis of the reference material demonstrated high recovery (approximately 100%) for most elements. The precision of our method was within 8% for all isotopes and within 4% for those isotopes without REEs, and the accuracy was better than 89% for most elements, including Ti and Nb. Full procedural digestion blanks was < 6.8% samples' analyte signal for all reported element in this study and < 2.8% samples' analyte signal for titanium and niobium (**Table C.4**). Therefore,

blanks are insignificant to the calculations of Ti concentrations or total Ti/Nb elemental ratios.

4.3.3 Particle composition on single particle basis

The multi-elemental composition of particles of individual particles in a select set of water samples (*e.g.,* 30/4/2020, 1/5/2020, 2/5/2020, and 5/5/2020) representing the start, rising limp, peak, and end of the first runoff event in the studied river system was determined using SP-ICP-TOF-MS. The river water samples were shaken well prior to extraction to resuspend any settled particles and to obtain a representative subsample. The extraction procedure is the same as that used in previous studies [17,22,37]. Briefly, 10 mL aliquots of the river water samples were transferred into acid-washed 15 mL centrifuge tubes. Then the samples were sonicated and centrifuged to obtain the < 1 μm particle size fraction (assuming natural particle density of 2.5 g cm^{-3}). The extracted particles were stored in fridge at 4 °C before SP-ICP-TOF-MS analysis. The theoretical size of the extracted fractions corresponds to particles < 1000 nm for natural particles (r = 2.5 g cm^{-3}), and < 725 nm for TiO_2 particles (r = 4.2 g cm^{-3}). All samples were bath sonicated again for 15 min and were diluted by a factor of 100 prior to SP-ICP-TOF-MS analysis.

Same as total elemental analysis, the instrument was calibrated and tuned daily before single particle analysis. Transport efficiency was calculated based on analysis of certified Au ENPs (NIST RM8013 Au, Gaithersburg, MD, USA) and ionic Au standards [41]. Other element dissolved calibrations were performed with a series of mixed multi-element standards (0, 1, 2, 5, and 10 μgL^{-1}, BDH Chemicals, Radnor, PA, USA). Particle

signals were separated from baseline using TOFpilot V2.10 and reported in time-elapsed format.

The detected particles were classified into single- and multi-metals (smNPs and mmNPs). The smNPs were considered as their own clusters because the particle mass and number concentrations are not sufficient to cluster smNPs. The mmNPs were classified into clusters of NPs of similar elemental composition using a two stage - intra- and inter-sample - agglomerative hierarchical clustering algorithm in MATLAB following the method described elsewhere [42]. Briefly, intra-sample hierarchical clustering was performed - using average correlation distance - on all metal masses in each NP to generate clusters that best account for variance in NP metallic composition in each sample. This step generates a cluster dendrogram for each sample, which was divided into major clusters using a distance cutoff. A cluster representative was determined for each major cluster as the mean of metal mass in individual NPs within each cluster taking into account all elements that occurred in at least 5 percent of NPs within the cluster. For each major cluster, the mass fraction of a given metal in each particle was determined as the mass of that metal divided by the sum of masses of all metals in that NP. The inter-sample clustering was performed on the major cluster representatives identified in the intra-sample clustering to group/cluster the similar NP major clusters identified in the different samples. This step generates a cluster dendrogram for intra-sample cluster representatives, which was divided into major clusters using a distance cutoff as performed for the intra sample clusters. The mean intra-sample cluster composition was determined as the mean of metal mass fraction in all NPs in the cluster and was compared across samples. Select elemental ratios were determined on a particle-per-particle basis taking into account all particles containing the

two elements and the elemental ratio distribution was determined. The number concentration (NP g^{-1}) of the total, smNPs, mmNPs, and cluster members were determined according to the SP-ICP-MS theory.

4.3.4 Estimation of TiO2 engineered particle concentration

The concentration of TiO_2 engineered particles was calculated based on mass balance calculations according to Eq. 1

$$[TiO_2]_{engineered\ particles} = \frac{TiO_{2\ MM}}{Ti_{\ MM}}\left[Ti_{sample} - Nb_{sample}.\left(\frac{Ti}{Nb}\right)_{background}\right] \qquad (Eq.1)$$

Where, $[TiO_2]_{\text{engineered particles}}$ is the concentration of TiO_2 engineered particles, $Ti_{\ MM}$ and $TiO_{2\ MM}$ are the molar masses of Ti and TiO_2, Ti_{sample} and Nb_{sample} are the concentrations of Ti and Nb in a given sample, $Ti/Nb_{background}$ is the natural background elemental concentration ratio of Ti/Nb. Background Ti/Nb was calculated on eight reference samples collected from Lake Katherine and Gills creek in Columbia, SC in the absence of rainfall events [20]. Eq 3 assumes that all Ti occurs in particulate form, engineered Ti occurs as pure TiO_2 engineered particles, and that the natural background Ti/Nb is constant throughout the sampling period. These assumptions are justified for the following reasons. Ti occurrence in the surface waters is expected to occur solely in solid phases because of the very low solubility of TiO_2 [43]. While Ti has numerous industrial applications, from metal alloying to aerospace applications to biomedical devices, approximately 95% of the mined Ti is refined into nearly pure TiO_2 through the treatment of Ti-bearing ores with carbon, chlorine, or sulfuric acid [44]. Additionally, TiO_2 engineered particle contain trace amount of Nb, which was below the ICP-MS detection limit (*e.g.,* < 7 ng L^{-1}) for TiO_2 concentration upto 10,000 mg L^{-1} [22]. On the other hand, natural TiO_2 minerals are the dominant carriers

(*e.g.,* > 90-95% of the whole rock content) of Ti and Nb. The elemental ratio of Ti/Fe, Ti/Al, Ti/Ce, Ti/Zr, and Ti/Nb, determined by SP-ICP-TOF-MS, in naturally occurring particles in the Broad, Lower Saluda, and Congaree Rivers were found to be constant throughout the sampling campaigns (see discussion below and supplementary information).

4.3.5 Discharge hydrographs and baseflow estimation

The discharge was separated into baseflow and direct runoff using tool "WHAT: Web-based Hydrograph Analysis Tool". 'WHAT' is able to connect to the USGS database and query and analyze streamflow data based on its USGS gauge number. The baseflow and direct runoff separation for the Broad, Lower Saluda and Congaree River was performed for the USGS station number 02162035, 02168504 and 02169500, respectively. For baseflow separation, recursive digital filter has been used with aquifer type of perennial streams with porous aquifer.

4.4 Results and Discussion

4.4.1 Precipitation, discharge, runoff, and water quality

Five A significant rain event occurred on 30/4/2020 resulting in 16.8 mm, 15.7 mm, and 16.8 mm rainfall in the Broad, Lower Saluda, and Congaree River watersheds respectively. Smaller rain events of 0.5, 0.5 and 1.0 mm occurred on 29/4/2020, 5/5/2020, and 10/5/2020 in the Broad, Lower Saluda, and Congaree River watersheds respectively (**Table C.5**). Moreover, major rainfall events of 40.2 mm and 9.7 mm occurred on

29/4/2020 in the upstream region of the Broad River at Ashville, NC and Knoxville, TN respectively [45,46]; and 54.5 mm and 3.1 mm occurred on 29/4/2020 and 30/4/2020 in the upstream region of the Lower Saluda River at Rock reservoir, Cleveland, SC [47]. These rain events resulted in increases in release from upstream reservoirs and as a result increases in the discharge in the Lower Saluda, Broad, and Congaree Rivers (**Table C.5**; **Figure C.1**). During this period, water level behind the Lake Murray dam was about 109 m above datum, which is very close to the top of conservation (flood control level of ~109.1 m) of the dam. The discharge in the Lower Saluda River is dominated by regulated releases from the Lake Murray reservoir based on the required hydroelectric generation and flood control regulations. Thus, the discharge in the Lower Saluda River displayed sharp increases between 30/4/2020 and 1/5/2020 and between 4/5/202 and 9/5/2020 due to releases from the Lake Murray reservoir in anticipation of the rain events to keep water level behind the dam below flood zone level (**Table C.5**; **Figure C.1**). Lake Murray is a man-made reservoir of approximately 200 km^2 in size with a maximum depth of approximately 53 m, an average depth of approximately 14 m, and a residence time of approximately 417 days [48,49]. The majority of the inflow to Lake Murray comes from the releases from upstream dams on Saluda River as well as the rainfall over the lake. Local tributaries, which are mostly rural basins, contribute minimally to the storage behind the Lake Murray dam. Thus, the urban contribution at the sampling point to the total discharge is minimal.

The discharge in the Broad and the Congaree Rivers displayed typical hydrographs of natural river discharges. The Broad River is regulated to some degree by the presence of at least 10 hydroelectric facilities and two thermoelectric power plants (**Table C.1**) [50]. The upstream of Broad River from sampling point is regulated using the Parr reservoir

dam, approximately 40 km upstream of the sampling location, which operates in modified run-of-river mode and operates continuously to pass the Broad River flow. These facilities allow a natural river flow to downstream [51]. The retention time of Parr Reservoir is on average about 3 days and varies between 0.8 and 29.3 days based on a maximum and minimum monthly flow of 530 and 15 m^3 sec^{-1}, respectively [52]. The nearest dam to the sampling location is the Broad River diversion dam (low head, a constructed barrier in a river with a hydraulic height not exceeding 7.6 m), approximately 4 km upstream of the Broad River sampling site. This dam diverts the flow (long term average diversion of approximately 11.7 m^3 sec^{-1}) of the Broad River toward the canal of the Columbia Hydroelectric Project. The rainfall resulted in runoff discharges in the Broad and Congaree Rivers between 30/4/2020 and 4/5/2020 and between 5/5/2020 and 9/5/2020 with peak discharge on 1/5/2020 and 7/5/2020. Direct runoff accounted for < 6%, 9-77%, 8-75% of the total discharge in the Lower Saluda, Broad, and Congaree River, respectively. The highest runoff contribution (*e.g.,* direct runoff/total discharge) in the Broad and Congaree Rivers occurred on 1/5/2020. There has been no urban runoff contribution (*i.e.,* baseline flow occurred) on 27/4/2020, 10/5/2020 and 12/5/2020 in the Broad and Congaree Rivers. The average annual discharge rates at the Broad River and Congaree River Columbia sampling sites are approximately 163.08 m^3 sec^{-1} and 243.86 m^3 sec^{-1}. We estimated the urban contribution from the city of Columbia between the Broad and Congaree Rivers' sampling sites as the difference between the sum of the discharge at the Congaree River sampling location and the water withdrawal at the Broad River diversion dam (approximately 255.56 m^3 sec^{-1}) and the sum of the discharge at the Broad River and Lower

Saluda River sampling locations (approximately 225.68 m^3 sec^{-1}). Thus, the average annual runoff contribution of the city of Columbia is approximately 29.88 m^3 sec^{-1}.

The pH varied in a narrow range between 6.4 and 7.8 and was similar in all samples (**Figure C.2a**). The conductivity varied between 48 and 119 μs cm^{-1} with higher values on 27/4/2020 and 28/4/2020 and relatively stable values of around 55 μs cm^{-1} between 29/4/2020 and 12/5/2020 (**Figure C.2b**). The water temperature in the Lower Saluda River water was lower than those in the Broad and Congaree Rivers as the water comes from deep in Lake Murray reservoir (**Figure C.2c**).

4.4.2 Total Ti, Nb, and TiO_2 concentrations

Titanium and Niobium concentrations in the Lower Saluda, Broad, and Congaree Rivers during the sampling period are presented in **Figure 4.2a and b**. Titanium concentrations vary randomly within a narrow range in the Lower Saluda River between 13 and 60 μg L^{-1} (**Figure 4.2a**) and does not follow a specific trend in relation to the discharge. In contrast, titanium concentrations vary within a broader range in the Broad and Congaree Rivers at Columbia and Cayce (8 to 926 μg L^{-1}, 95 to 5976 μg L^{-1}, and 58 to 1170 μg L^{-1}, respectively). The concentrations of Ti in the Broad River follow the discharge trend and continue rising after the second discharge peak. The reason for the increase in Ti concentration after the second discharge peak is unknown. The concentrations of Ti in the Congaree River at Columbia and Cayce display a bimodal distribution and follow closely the rise and fall of the discharge. The highest Ti concentration in the Congaree River at Columbia and Cayce was measured on 1/5/2020 and 2/5/2020, respectively. Generally, Ti concentrations decrease following the order: Congaree River at Columbia > Congaree

River at Cayce > Broad River > Lower Saluda River, which is ascribed to differences in Ti load into these rivers due to differences in urban runoff contribution to the total discharge. The Nb concentration follow the same trend as Ti (**Figure 4.2b**). Ti and Nb pollutographs in the Broad and Congaree Rivers display a mobility pattern driven by the transport of solids [53]; that is the Ti and Nb concentrations are low during low flows, increase with increasing flow due to the transportation of more solids, and then decline with diminishing flow and supply of solids on the catchment surfaces (**Figure 4.2**).

In the Lower Saluda River, the Ti/Nb ratio vary between 238.8 ± 12.1 and 346.7 ± 2.4 and does not follow specific trend with the discharge (**Figure 4.2c**). In the Broad and Congaree Rivers, the Ti/Nb display a bimodal distribution and increase with increases in the discharge/runoff. The Ti/Nb values increase following the order Lower Saluda River < Broad River < Congaree River at Columbia < Congaree River at Cayce. This trend in Ti/Nb ratio is attributed to the introduction of anthropogenic pure Ti-bearing particles between the sampling sites, which can be ascribed to urban runoff from the City of Columbia. The concentration of the anthropogenic Ti-bearing particles was estimated using mass balance and assuming that they occurred as pure TiO_2 particles. The estimated anthropogenic TiO_2 concentrations vary between 0 and 24 μg L^{-1} in the Lower Saluda River, 0 and 663 μg L^{-1} in Broad River, 58 and 5050 μg L^{-1} in Congaree River at Columbia, and 43 to 1051 μg L^{-1} in the Congaree River at Cayce; and follow the same trend with discharge/direct runoff as the total Ti concentration (**Figure 4.2d**).

4.4.3 Particle number concentrations and elemental composition

The number concentration of Ti-bearing particles is generally higher in the Broad and Congaree Rivers compared to those in the Lower Saluda River (**Figure 4.3a**). The relative abundance of smTi-NPs is generally higher during the discharge event than at the end of the event (**Figure 4.3b**). All other elements follow the same trend as Ti-bearing particles (**Figure C.3**). The mass distributions of Ti-bearing particles vary within the same range (*e.g.,* 0 to 20 fg) in all samples (**Figure 4.4**). However, the mass distribution of Ti-bearing particles in the Broad and Congaree Rivers display a shift toward larger masses compared to those in the Lower Saluda River, with a higher fraction of particles with mass > 20 fg. The mass distribution of Ti-bearing particles in the Congaree River at Columbia is intermediate between those in the Broad and the Lower Saluda Rivers due to the mixing of the two Rivers upstream of this sampling location (**Figure 4.4**). The mass distribution of Ti-bearing particles shifts toward higher mass during high discharge (1/5/2020 and 2/5/2020) compared to those at low discharge (30/4/2020 and 5/5/2020).

Clustering analysis of the mmNPs identified 29 mmNP clusters. Six of these 29 clusters - FeTiMn, AlSiFe, CeLaNd, TiMnFe, MnCeBa, and ZrYTh – occur in all samples and account for > 99.4% of the total number of mmNPs in all samples (**Figure C.5**). The elemental composition of these clusters is dominated by one element and contain minor or trace concentrations of other elements (**Figure 4.5**) [54]. The Ti containing particles are distributed among three clusters: FeTiMn, AlSiFe, and TiMnFe, which account for > 99% of all Ti-bearing mmNPs (**Figure C.5**). The elemental ratio of Ti/Fe, Ti/Al, Ti/Ce, Ti/Zr, and Ti/Nb are similar in all samples and are in good agreement with those measured in natural soils and surface waters (**Figure C.6-8**) [20,54,55]. The mean Ti/Nb ratio in all Ti and

Nb containing particles in all samples vary between (mean ± standard deviation of the ratios calculated at the single particle level) 218 ± 195 and 295 ± 280.

4.5 Discussion

The lowest Ti concentration in the Lower Saluda, Broad, and Congaree (Co) Rivers are 13.3 ± 0.2 μg L^{-1}, 8.2 ± 0.1 μg L^{-1}, and 94.8 ± 27.1 μg L^{-1} respectively and occurred during base flow dominated condition when base flow accounted for 90.5%, 100%, and 68% of the total discharge, respectively (**Figure 4.2a**). The highest Ti concentration In the Lower Saluda, Broad, and Congaree (Co) Rivers are 39.2 ± 6.7 μg L^{-1}, 233.4 ± 8.1 μg L^{-1} and 5975.7 ± 88.8 μg L^{-1} respectively and coincided with the peak discharge during the first runoff event on 1/5/2020 (**Figure 4.2a**). The low concentration of Ti in the Saluda River, which is characterized by low urban runoff contribution to the total discharge, and the increase in Ti concentration from the Broad River to the Congaree River, which are characterized by high urban runoff contribution to the total discharge, suggest that urban runoff is the key driver of Ti concentrations in the Broad and Congaree Rivers. The Ti concentrations measured in this study are higher than those previously measured in rivers (*e.g,* 0.6 to 1.6 μg L^{-1}) [56], urban runoff (*e.g.,* 10 to 15 μg L^{-1}) following the release of TiO_2 particles from exterior facades [57], and urban wet and dry runoff (*e.g.,* 15 to 200 μg L^{-1}) [17]. Nonetheless, higher Ti concentrations (*e.g.,* 12.7 mg L^{-1}) were reported in highway runoff in Pullman, Washington [19]. Additionally, high Ti concentrations (*e.g.,* 150 to1600 mg kg^{-1}) were reported in different road-environment samples (*e.g.,* road dust, sludge from storm drains, and roadside soil), which were suspected to be of anthropogenic origin such as the

use of alkali metal titanates as inorganic fillers for the purpose of stabilizing the friction coefficient [58].

Titanium in urban runoff can be attributed to natural and/or anthropogenic sources. Significant quantities of Ti-bearing particles occur in the urban environment due to the soil erosion and atmospheric deposition of soil particles on surfaces in the urban environment [59]. On the other hand, TiO_2 engineered particles are widely used in many applications in the urban environment as pigment in paint and coatings [60,61] and as ENPs in self-cleaning surfaces which have been shown to be released by wear and weathering [5–9]. Several studies reported the occurrence of TiO_2 engineered (nano)-particles in road dust, atmospheric particulate matter [62,63], and urban runoff [17]. Naturally occurring TiO_2 minerals are the dominant carriers (*e.g.,* > 90-95% of the whole rock content) of Ti and Nb [34]. In contrast, commercial TiO_2 particles are typically refined into nearly pure TiO_2 through the treatment of Ti-bearing ores using carbon, chlorine, or sulfuric acid [22,64]. Thus, the elemental ratio of Ti/Nb was used to determine whether the increased Ti concentration is due to natural or anthropogenic Ti inputs. The Ti/Nb in most samples i higher than the natural background ratio determined in a previous study (**Figure 4.2c**) [20], suggesting that all sampling locations received anthropogenic Ti inputs. The lowest Ti/Nb ratios occurred in the Lower Saluda River (239 ± 12) and coincided with the average water background Ti/Nb determined in nearby water bodies (266 ± 9) [20]. The higher (*e.g.,* 280-346) Ti/Nb values in the Lower Saluda River indicate a potential small anthropogenic contribution of TiO_2 engineered particles, potentially from atmospheric deposition or urban runoff from nearby roads and bridges. The lowest Ti/Nb in the Broad and Congaree Rivers (177 ± 36, 408 ± 17, and 435 ± 19, respectively) occurred at the base flow conditions. On the other hand, the highest

Ti/Nb ratios (503 ± 5, 596 ± 11, and 688 ± 31) occurred at the peak of the discharge events on 1/5/2020 and 7/5 2020, suggesting that the discharge/urban runoff is the driver of the increase in Ti/Nb during/following rainfall events. The lower Ti/Nb ratios in the Lower Saluda River than in the Broad and Congaree Rivers are ascribed to the smaller urban runoff contribution to the Lower Saluda River discharge at the sampling location along with sedimentation of anthropogenic Ti-bearing particles in Lake Murray, and thus low input of anthropogenic Ti to the Lower Saluda River.

The anthropogenic Ti-containing particles from urban runoff can occur as smNPs such as those used in building paint, road marking, and photocatalytic surfaces or as mmNPs as those released from traffic-related emissions such as Ti used as fillers in brake pads. Thus, SP-ICP-TOF-MS analysis was used to determine the elemental composition of Ti-bearing particles. The SP-ICP-TOF-MS analysis show higher relative abundance of smTi-bearing NPs during the runoff event than at the end of the runoff event (**Figure 4.3b**) in all sampling sites, which can be ascribed to the increased contribution of pure TiO_2 particles to the total concentration of Ti-bearing particles during the runoff event. The clustering and elemental ratio analysis ahow that > 99% of mm-Ti-bearing particles occurred in three clusters (FeTiMn, AlSiFe, TiMnFe), which are typical of naturally occurring particles such as titanomagnetite (Ti/Fe =0 to 0.43), ilmenite (Ti/Fe = 0.86), pseudorutile (Ti/Fe = 1.29), Ilmenorutile (Ti/Fe = 1.71), or altered pseudorutile (Ti/Fe > 1.71) (**Figure C.6a and C.7a**), clays (Ti/Al = 0 to 0.4, **Figure C.6a and C.7a**), or titanium oxide particles containing Al and Fe (**Figure C.8**). These findings suggest that the majority of anthropogenic Ti-bearing particles are pure TiO_2 particles. It is worth noting that other clusters such as Zn, Cu, Cr, W, Ni, Sn-rich particle clusters were identified more frequently

in the Broad and Congaree Rivers than in the Lower Saluda River (**Figure C.5**). These particles are typical of traffic related emissions detected in bridge runoff in Columbia, South Carolina [36]. However, the number of the detected particles are relatively small and thus these clusters are not discussed further.

Consequently, the total TiO_2 engineered particle concentrations were determined using mass balance calculations and shifts in Ti/Nb above the natural background values (**Figure 4.2d**). The lower concentrations of TiO_2 engineered particles in the Lower Saluda River compared to the Broad and Congaree Rivers can be attributed to the removal of suspended sediments and anthropogenic TiO_2 particles within the Lake Murray reservoir by sedimentation given the long water residence time of approximately 417 days [48,49]. This is consistent with the decreases in turbidity from upstream to downstream Lake Murray reservoir [48,49]. This is also consistent with the smaller masses of Ti-bearing particles in the Lower Saluda River compared to those in the Broad and Congaree Rivers (**Figure 4.4**). Additionally, the low TiO_2 concentration in the Lower Saluda River can be attributed to the absence or small urban runoff contribution (~ 6%) to the discharge at the Lower Saluda River sampling location. In contrast, the Broad River is a natural free flowing river which transport a higher sediment load transport into the Broad River sampling location from the large upstream Broad River watershed. Additionally, the Broad River sampling site is approximately 480 m downstream of a major highway in South Carolina – that is the interstate I20 bridge – which discharges directly into the Broad River. Our previous study demonstrated that bridge runoff contains high concentrations of anthropogenic TiO_2 particles [65].

The increase in TiO_2 concentration from the Broad River to the Congaree River for most sampling dates suggests that the majority of anthropogenic TiO_2 is introduced into the Broad and Congaree Rivers at the urban interface area of the city Columbia, SC, and is ascribed to urban runoff and associated particulate wash off from impervious surfaces. This is consistent with the significant contribution of urban runoff to the total discharge in the Broad River (*e.g.,* 9-77%) and the Congaree Rivers (*e.g.,* 8-75%) as well as the high concentrations of TiO_2 in bridge and urban runoff [17]. The Broad River sample was collected downstream of the I20 highway, the Congaree River at Columbia sample was collected downstream of I176, I126, the Jarvis Klapman Boulevard, and the Gervais Bridge, and the Congaree River at Cayce sample was collected downstream of Blossom Street. All these Bridges have an AADT > 20,000, which result in a substantial release of TiO_2 to the studied river system (**Table C.2**). For instance, the Blossom Street Bridge (AADT = 27,500) runoff has been shown to contain up to 101.1 ± 1.4 μg TiO_2 L^{-1} [36]. It is expected that Bridges with higher traffic density will release higher concentrations of TiO_2 to the studied river system. The lower TiO_2 concentration in the Congaree River than in the Broad River between 10/5/2020 and 12/5/2020 could be due to dilution effect.

The higher TiO_2 concentrations during the first discharge peak in the Congaree River is attributed to the relatively longer antecedent dry period (**Table C.5**) prior to the first rainfall event. Longer antecedent dry periods lead to higher contaminant accumulation on impervious surfaces in the watershed. The heavy rain event on the 29/4/2020 and 30/4/2020 throughout the watershed might have transported the accumulated contaminants from the impervious surfaces into the river system. Similar increases in the Ti concentrations [22] and particulate matter associated contaminants (*e.g.,* metals)

concentrations [66,67] with increases in antecedent dry period were observed for road runoff and urban runoff, respectively.

Although we attributed TiO_2 to urban runoff, other sources of TiO_2 engineered particles into surface waters include recreational activities in the watershed [68], industrial discharge [23], or construction activities [69], effluents from wastewater treatment plant (WWTP) [70], and sanitary sewer overflows [20]. The recreational source (*e.g.,* use of sunscreen during bathing) can be ruled out because there was not any recreational activities in the three rivers during the sampling period due to 'coronavirus stay-at-home order' in South Carolina [71,72]. The industrial and construction sources also can be ruled out as there was no known industrial discharge sources and construction activities near the sampling location which would result in a continuous discharge of TiO_2 particles to surface water. The human waste source is an insignificant source of TiO_2 to the river system during the sampling period because of the small size (1.1 ± 0.0 to 2.1 ± 0.1) of the gadolinium anomaly (**Figure C.9**). Gadolinium anomaly is widely used to track effluent from wastewater treatment plants [73]. Previous studies reported gadolinium anomaly sizes between 1.0 and 30.0 (**Table C.6**) in river streams, and an anomaly > 1.5 has been used as an indicator of wastewater treatment effluent in river streams. Consequently, the observed TiO_2 engineered particles contamination in this study is attributed to rainfall events followed by runoff introduction in the rivers, suggesting that the source of TiO_2 particles here is diffuse urban runoff across the Broad and Congaree Rivers' watersheds.

4.6 Conclusion

The daily monitoring of the total elemental concentrations, bulk elemental ratios, the number particle concentration, and the multi-element composition of single particles in the Saluda-Broad-Congaree Rivers' ecosystem highlights the presence, transient nature, and transport of anthropogenic TiO_2 engineered particle in this urban river ecosystem. The concentration of TiO_2 engineered particle was lowest (0 to 24 μg L^{-1}) in the Lower Saluda River which had the lowest urban footprint. The TiO_2 engineered particle concentration increased from the Broad River (0 to 663 μg L^{-1}) to the Congaree River (53 to 5050 μg L^{-1}) indicating a continuous and increased introduction of TiO_2 engineered into the Broad and Congaree Rivers with urban runoff from the urban area of the city of Columbia, South Carolina. Increases in TiO_2 concentrations were transient and coincided with rainfall with highest concentrations at or near the peak of the discharge. Thus, the urban environment represents a major source of TiO_2 engineered particle into surface waters. The high TiO_2 concentrations in the Broad-Congaree Rivers may pose environmental risk in this River ecosystem, and in other urban rivers, during and following rainfall events, in particular at and near peak discharge. Higher concentrations of TiO_2 engineered particles, and thus higher environmental risks, can be expected in more highly urbanized watersheds than the studied urban river ecosystem. The impact of these TiO_2 engineered particles on river organisms should be further evaluated, including investigating the effect of TiO_2 engineered particles on several organisms in the trophic chain using environmentally relevant concentrations and considering frequent pulse *vs.* chromic exposure. The design of this study highlights the importance of selecting sampling sites and monitoring the spatiotemporal variations in engineered particle concentrations in surface waters for a more

comprehensive understanding of the environmental fate, behavior, and risk assessment of engineered particles. To provide even a more detailed understanding of TiO_2 engineered particle fate and transport in urban ecosystems, future studies could include additional sampling sites, collect samples at higher time resolution or over longer sampling periods, collect data following storm events with various intensities and antecedent dry periods, collect and analyze sediments samples to determine particle sedimentation and deposition in the river system.

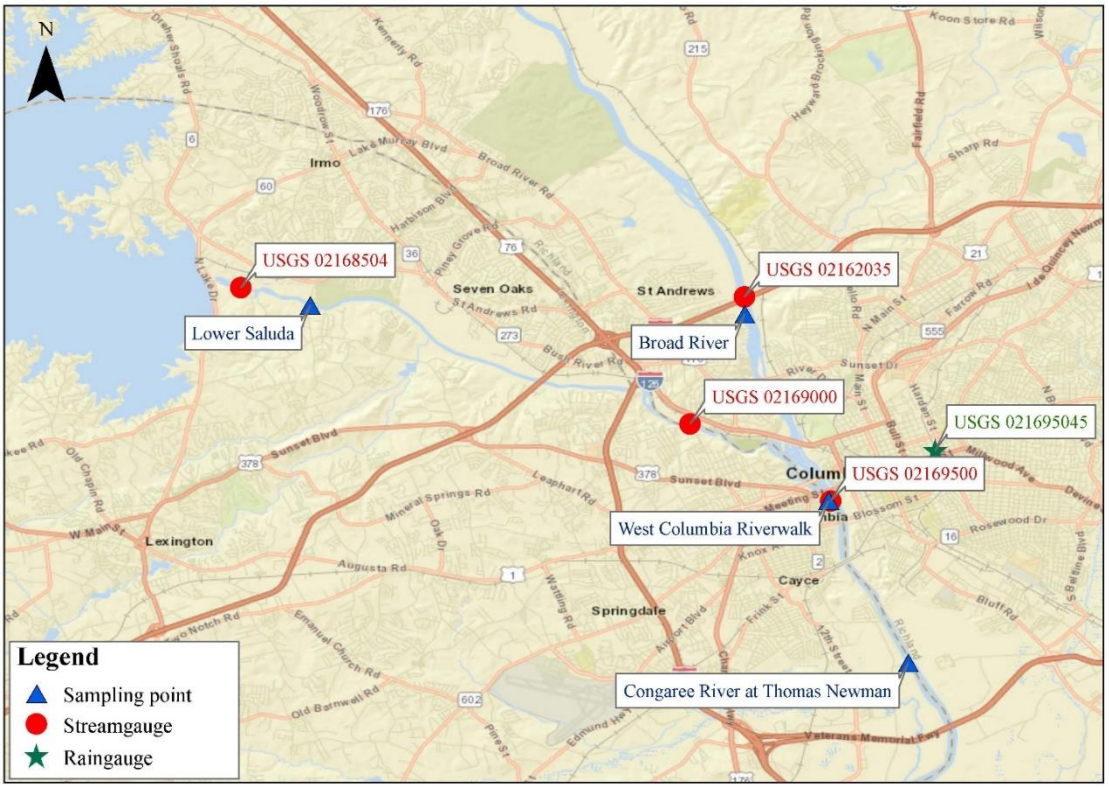

Figure 4.1 Map of the Congaree River, Columbia (Co); Congaree River, Cayce (C); Lower Saluda River (S) and Broad River (B) sampling locations.

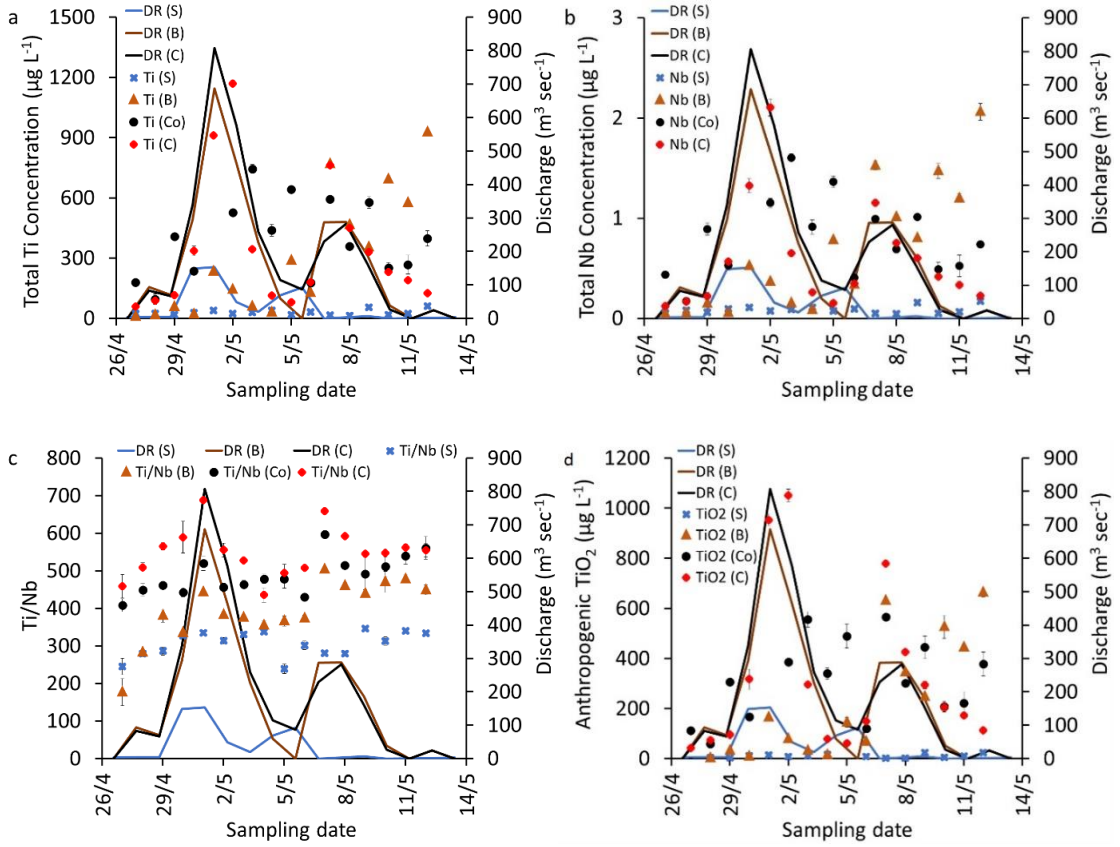

Figure 4.2 Pollutographs of (a and b) the total concentrations of Ti and Nb, (c) Ti/Nb, and (d) the estimated anthropogenic TiO_2 cocnentrations in the Lower Saluda River (S), the Broad River (B), and the Congaree River at Columbia (Co) and Cayce (C) during the sampling campaign. DR (S) refers to direct runoff in the Lower Saluda River, DR (B) refers to direct runoff in the Broad River, and DR (Co) refers to direct runoff in the Congaree River at Columbia. The highest Ti, Nb, and TiO_2 cocnentrations in the Congaree River at Columbia was 5976 ± 89, 11.5 ± 0.5, 5050 ± 143 µg L^{-1} on 1/5/2020 and are not displayed in the Figure.

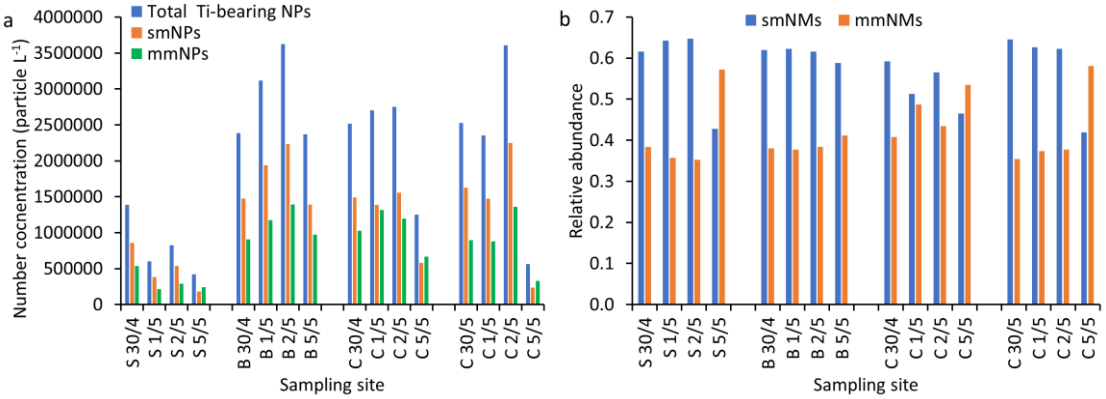

Figure 4.3 (b) Number concentration of total, single metal (sm) and multi-metal (mm), and (b) the relative abundance of sm- and mm- Ti-bearing nanoparticles in the Lower Saluda River (S), Broad River (B), Congaree River at Columbia (Co), and Congaree River at Cayce (C). The number concentrations were corrected by subtracting the number of particles detected in the procedural blanks.

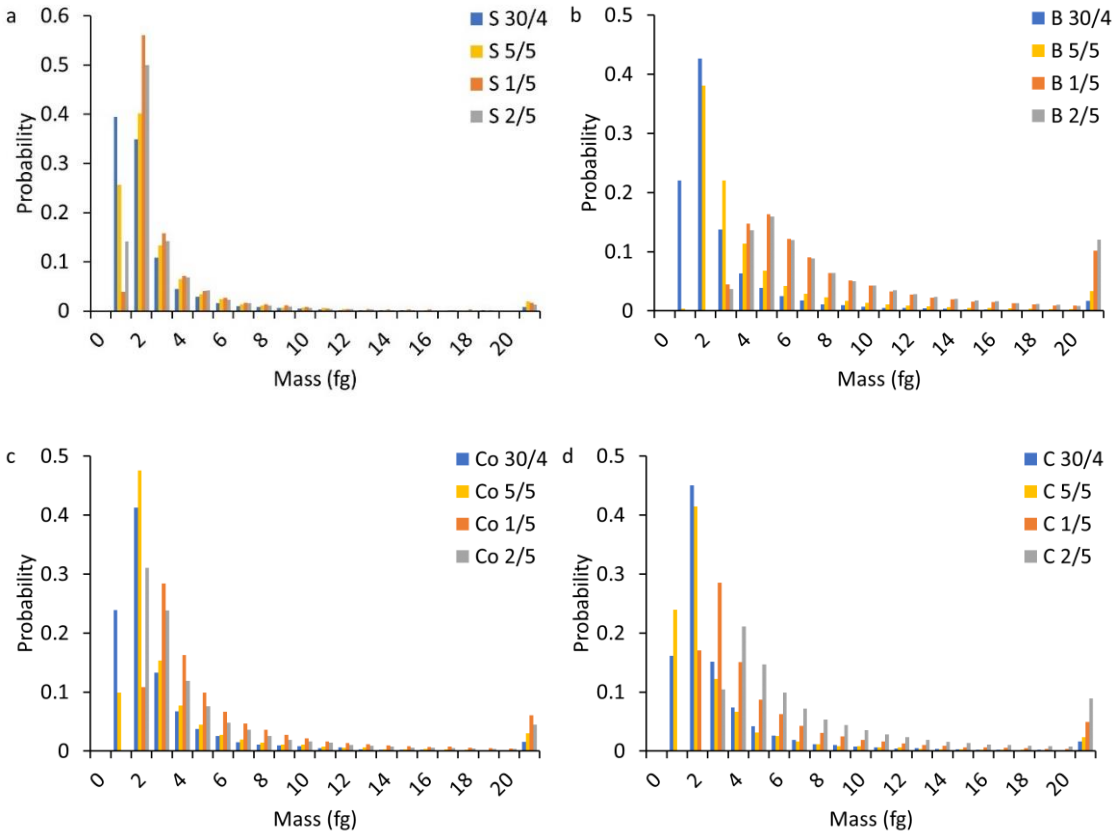

Figure 4.4 Mass distribution of Ti-containing particles in the: (a) Lower Saluda River, (b) Broad River, (c) Congaree River at Columbia, (d) Congaree River at Cayce. S: Lower Saluda River, B: Broad River, Co: Congaree River at Columbia, and C: Congaree River at Cayce.

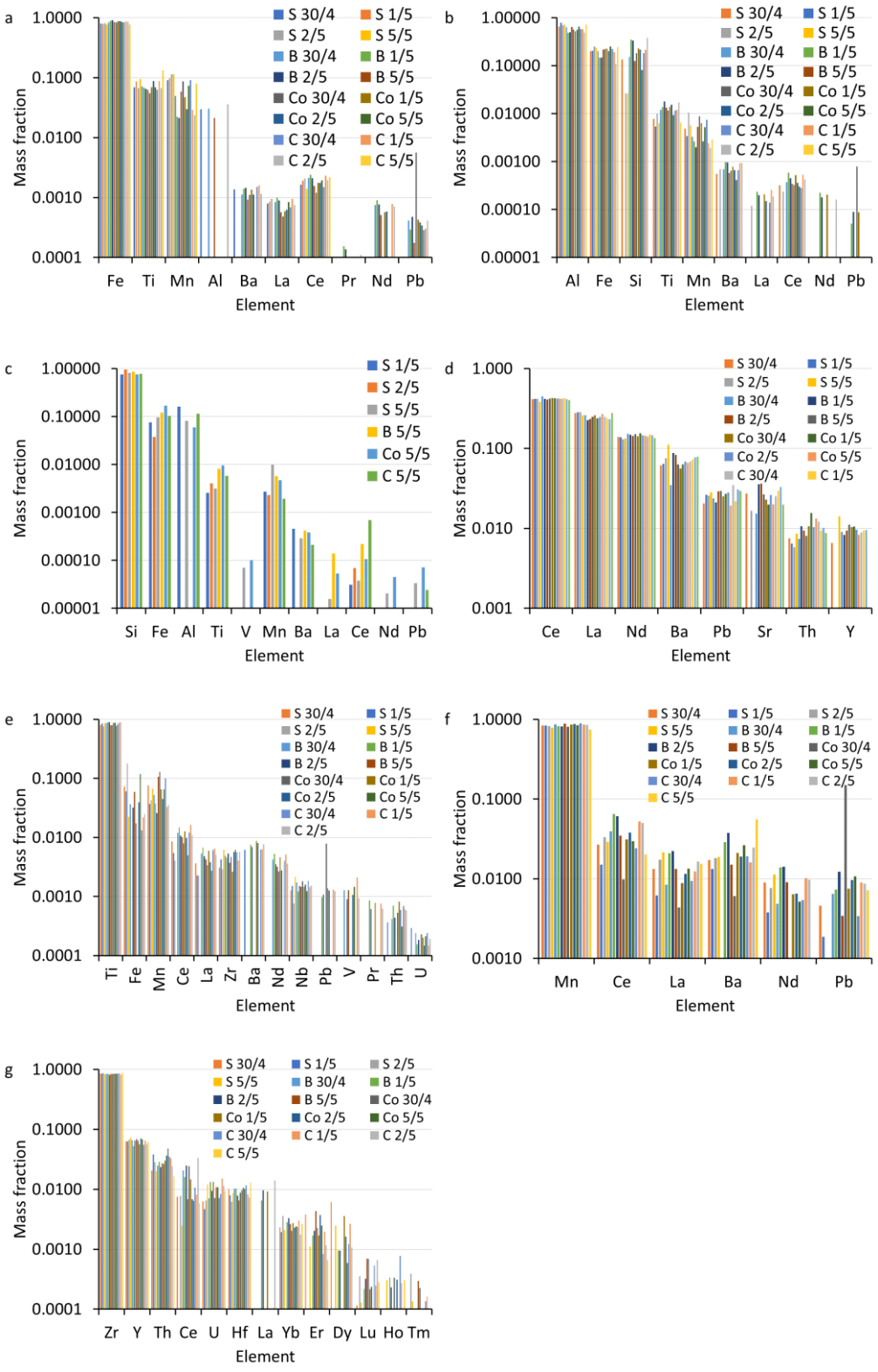

Figure 4.5 Elemental composition of the dominant clusters: (a) Fe-, (b) Al-, (c) Si-, (d) Ce-, (e) Ti-, (f) Mn-, and (g) Zr- rich particle cluster. Standard error was <0.05 for all elements. Note that the Al and Si-rich mmNP clusters are two clusters within the AlSiFe cluster. S:

Lower Saluda River, B: Broad River, Co: Congaree River at Columbia, and C: Congaree River at Cayce.

References:

1. Müller, A., Österlund, H., Marsalek, J. & Viklander, M. The pollution conveyed by urban runoff: A review of sources. Science of the Total Environment 709, 136125 (2020).
2. Kammer, F. von der et al. Analysis of engineered nanomaterials in complex matrices (environment and biota): General considerations and conceptual case studies. Environ. Toxicol. Chem. 31, 32–49 (2012).
3. Baalousha, M. et al. Outdoor urban nanomaterials: The emergence of a new, integrated, and critical field of study. Science of the Total Environment 557–558, 740–753 (2016).
4. Coatingsworld. Paint and coatings demand by market U.S. 2019 | Statista. (2019). Available at: https://www.statista.com/statistics/684695/united-states-paint-and-coatings-demand-by-market/. (Accessed: 22nd April 2020)
5. Göhler, D., Stintz, M., Hillemann, L. & Vorbau, M. Characterization of Nanoparticle Release from Surface Coatings by the Simulation of a Sanding Process. Ann. Occup. Hyg. 54, 615–624 (2010).
6. Koponen, I. K., Jensen, K. A. & Schneider, T. Comparison of dust released from sanding conventional and nanoparticle-doped wall and wood coatings. J. Expo. Sci. Environ. Epidemiol. 21, 408–418 (2011).
7. Nored, A. W., Chalbot, M. C. G. & Kavouras, I. G. Characterization of paint dust aerosol generated from mechanical abrasion of TiO_2-containing paints. J. Occup. Environ. Hyg. 15, 629–640 (2018).
8. Shandilya, N., Le Bihan, O., Bressot, C. & Morgeneyer, M. Evaluation of the Particle Aerosolization from n-TiO_2 Photocatalytic Nanocoatings under Abrasion. J. Nanomater. 2014, 185080 (2014).
9. Shandilya, N., Le Bihan, O. & Morgeneyer, M. A Review on the Study of the Generation of (Nano)particles Aerosols during the Mechanical Solicitation of Materials. J. Nanomater. 2014, (2014).
10. Tou, F. et al. Multi method approach for analysis of road dust particles: elemental ratios, SP-ICP-TOF-MS, and TEM. ESNano (2022, Rev.)
11. Thorpe, A. & Harrison, R. M. Sources and properties of non-exhaust particulate matter from road traffic: A review. Sci. Total Environ. 400, 270–282 (2008).
12. Gietl, J. K., Lawrence, R., Thorpe, A. J. & Harrison, R. M. Identification of brake wear particles and derivation of a quantitative tracer for brake dust at a major road. Atmos. Environ. 44, 141–146 (2010).
13. Wåhlin, P., Berkowicz, R. & Palmgren, F. Characterisation of traffic-generated particulate matter in Copenhagen. Atmos. Environ. 40, 2151–2159 (2006).
14. Apeagyei, E., Bank, M. S. & Spengler, J. D. Distribution of heavy metals in road dust along an urban-rural gradient in Massachusetts. Atmos. Environ. 45, 2310–2323 (2011).
15. Pant, P. & Harrison, R. M. Estimation of the contribution of road traffic emissions to particulate matter concentrations from field measurements: A review. Atmos. Environ. 77, 78–97 (2013).
16. Adachi, K. & Tainosho, Y. Characterization of heavy metal particles embedded in tire dust. Environ. Int. 30, 1009–1017 (2004).

17. Wang, J. et al. Detection and quantification of engineered particles in urban runoff. Chemosphere 248, 126070 (2020).
18. USGS. Characterization of Stormwater Runoff from Bridges in North Carolina and the Effects of Bridge Deck Runoff on Receiving Streams. (2011).
19. Bourcier, D. R., Hindin, E. & Cook, J. C. Titanium and tungsten in highway runoff at pullman, washington. Int. J. Environ. Stud. 15, 145–149 (1980).
20. Loosli, F. et al. Sewage spills are a major source of titanium dioxide engineered (nano)-particle release into the environment. Environ. Sci. Nano 6, 763–777 (2019).
21. Saharia, A. M., Zhu, Z., Aich, N., Baalousha, M. & Atkinson, J. F. Modeling the transport of titanium dioxide nanomaterials from combined sewer overflows in an urban river. Sci. Total Environ. 696, 133904 (2019).
22. Nabi, M. M., Wang, J. & Baalousha, M. Episodic surges in titanium dioxide engineered particle concentrations in surface waters following rainfall events. Chemosphere 263, 128261 (2021).
23. Slomberg, D. L. et al. Anthropogenic Release and Distribution of Titanium Dioxide Particles in a River Downstream of a Nanomaterial Manufacturer Industrial Site. Front. Environ. Sci. 0, 76 (2020).
24. Vidmar, J., Zuliani, T., Milačič, R. & Ščančar, J. Following the Occurrence and Origin of Titanium Dioxide Nanoparticles in the Sava River by Single Particle ICP-MS. Water 14, 959 (2022).
25. Parker, N. & Keller, A. A. Variation in regional risk of engineered nanoparticles: nanoTiO_2 as a case study. Environ. Sci. Nano 6, 444–455 (2019).
26. Rand, L. N. et al. Quantifying temporal and geographic variation in sunscreen and mineralogic titanium-containing nanoparticles in three recreational rivers. Sci. Total Environ. 743, 140845 (2020).
27. Gondikas, A. P. et al. Release of TiO_2 nanoparticles from sunscreens into surface waters: A one-year survey at the old danube recreational lake. Environ. Sci. Technol. 48, 5415–5422 (2014).
28. David Holbrook, R. et al. Titanium distribution in swimming pool water is dominated by dissolved species. Environ. Pollut. 181, 68–74 (2013).
29. Yang, Y. et al. Prospecting nanomaterials in aqueous environments by cloud-point extraction coupled with transmission electron microscopy. Sci. Total Environ. 584–585, 515–522 (2017).
30. Venkatesan, A. K. et al. Detection and Sizing of Ti-Containing Particles in Recreational Waters Using Single Particle ICP-MS. Bull. Environ. Contam. Toxicol. 100, 120–126 (2018).
31. Praetorius, A. et al. Single-particle multi-element fingerprinting (spMEF) using inductively-coupled plasma time-of-flight mass spectrometry (ICP-TOFMS) to identify engineered nanoparticles against the elevated natural background in soils. Environ. Sci. Nano 4, 307–314 (2017).
32. Wang, H., Adeleye, A. S., Huang, Y., Li, F. & Keller, A. A. Heteroaggregation of nanoparticles with biocolloids and geocolloids. Adv. Colloid Interface Sci. 226, 24–36 (2015).
33. Barksdale, J. Titanium, Its Occurrence, Chemistry, and Technology: Soil Science. in 414 (1950).

34. Zack, T., Kronz, A., Foley, S. . & Rivers, T. Trace element abundances in rutiles from eclogites and associated garnet mica schists. Chem. Geol. 184, 97–122 (2002).
35. Craigie, N. Principles of Elemental Chemostratigraphy. Springer International Publishing (Springer International Publishing, 2018). doi:10.1007/978-3-319-71216-1
36. Wang, J., Nabi, M.M., Mahdi, E, Goharian, E, Baalousha, M. Identification and Quantification of Anthropogenic Nanomaterials in Urban Rainfall and Runoff Using Single Particle-Inductively Coupled Plasma-Time of Flight-Mass Spectrometry (In preparation).
37. Nabi, M. M. et al. Concentrations and size distribution of TiO_2 and Ag engineered particles in five wastewater treatment plants in the United States. Sci. Total Environ. 753, 142017 (2021).
38. Praetorius, A. et al. Single-particle multi-element fingerprinting (spMEF) using inductively-coupled plasma time-of-flight mass spectrometry (ICP-TOFMS) to identify engineered nanoparticles against the elevated natural background in soils. Environ. Sci. Nano 4, 307–314 (2017).
39. Lee, S. et al. Nanoparticle size detection limits by single particle ICP-MS for 40 elements. Environ. Sci. Technol. 48, 10291–10300 (2014).
40. Hadioui, M. et al. Lowering the Size Detection Limits of Ag and TiO_2 Nanoparticles by Single Particle ICP-MS. Anal. Chem. 91, 13275–13284 (2019).
41. Pace, H. E. et al. Determining Transport Efficiency for the Purpose of Counting and Sizing Nanoparticles via Single Particle Inductively Coupled Plasma Mass Spectrometry. Anal. Chem. 83, 9361–9369 (2011).
42. Baalousha, M., Wang, J., Erfani, M. & Goharian, E. Elemental fingerprints in natural nanomaterials determined using SP-ICP-TOF-MS and clustering analysis. Sci. Total Environ. 792, 148426 (2021).
43. Antignano, A. & Manning, C. E. Rutile solubility in H_2O, H_2O–SiO_2, and H_2O–$NaAlSi_3O_8$ fluids at 0.7–2.0 GPa and 700–1000 °C: Implications for mobility of nominally insoluble elements. Chem. Geol. 255, 283–293 (2008).
44. U.S. Geological Survey. Mineral Commodity Summaries. Mineral Commodity Summaries (2019). doi:10.3133/70202434
45. U.S. Geological Survey (USGS). USGS Current Conditions for USGS 03451500 FRENCH BROAD RIVER AT ASHEVILLE, NC. Available at: https://waterdata.usgs.gov/nwis/dv?cb_00045=on&format=html&site_no=03451500&referred_module=sw&period=&begin_date=2020-04-20&end_date=2020-05-10. (Accessed: 8th January 2021)
46. City of Knoxville. Rainfall Data - City of Knoxville. Available at: https://knoxvilletn.gov/government/city_departments_offices/engineering/stormwater_engineering_division/rainfall_data. (Accessed: 8th January 2021)
47. U.S. Geological Survey (USGS). USGS Current Conditions for USGS 02162285 TABLE ROCK RESERVOIR NR CLEVELAND, SC. Available at: https://waterdata.usgs.gov/nwis/dv?cb_00045=on&format=html&site_no=02162285&referred_module=sw&period=&begin_date=2020-04-27&end_date=2020-05-12. (Accessed: 10th January 2021)
48. SCDHEC. Saluda River/Lake Murray watershed. Available at: https://scdhec.gov/sites/default/files/docs/HomeAndEnvironment/Docs/03050109-13.pdf. (Accessed: 16th August 2021)

49. SCE & G, S. C. Saluda Project (FERC No. 516): Lake Murray Water Quality Report.
50. National Park Service & U.S. Department of the Interior. Assessment of Water Resources and Watershed Conditions in Congaree National Park, South Carolina. (2010).
51. Federal Energy Regulatory Commission. ENVIRONMENTAL ASSESSMENT FOR HYDROPOWER LICENSE. (2020).
52. SCE & G, S. C. South Carolina Electric & Gas COL Application Part 3-Environmental Report.
53. Galfi, H., Österlund, H., Marsalek, J. & Viklander, M. Mineral and Anthropogenic Indicator Inorganics in Urban Stormwater and Snowmelt Runoff: Sources and Mobility Patterns. Water. Air. Soil Pollut. 228, 1–18 (2017).
54. Wu, J. et al. Metal-Containing Nanoparticles in Low-Rank Coal-Derived Fly Ash from China: Characterization and Implications toward Human Lung Toxicity. Environ. Sci. Technol. 55, 6644–6654 (2021).
55. Gondikas, A. et al. Where is the nano? Analytical approaches for the detection and quantification of TiO_2 engineered nanoparticles in surface waters. Environ. Sci. Nano 5, 313–326 (2018).
56. Markus, A. A. et al. Determination of metal-based nanoparticles in the river Dommel in the Netherlands via ultrafiltration, HR-ICP-MS and SEM. Sci. Total Environ. 631–632, 485–495 (2018).
57. Kaegi, R. et al. Synthetic TiO_2 nanoparticle emission from exterior facades into the aquatic environment. Environ. Pollut. 156, 233–239 (2008).
58. Adamiec, E. Road environments: Impact of metals on human health in heavily congested cities of Poland. Int. J. Environ. Res. Public Health 14, (2017).
59. Pereira, E., Baptista-Neto, J. A., Smith, B. J. & McAllister, J. J. The contribution of heavy metal pollution derived from highway runoff to Guanabara Bay sediments - Rio de Janeiro / Brazil. An. Acad. Bras. Cienc. 79, 739–750 (2007).
60. Chemours. Ti-PureTM Solutions for Coatings: Applications. (2018). Available at: https://www.tipure.com/en/applications/coatings?_ga=2.22333115.1280235886.1586571265-1482119140.1586571265. (Accessed: 10th April 2020)
61. Shandilya, N., Le Bihan, O., Bressot, C. & Morgeneyer, M. Emission of titanium dioxide nanoparticles from building materials to the environment by wear and weather. Environ. Sci. Technol. 49, 2163–2170 (2015).
62. Lee, P. K. et al. Lead chromate detected as a source of atmospheric Pb and Cr (VI) pollution. Sci. Rep. 6, 1–10 (2016).
63. Wilczyńska-Michalik, W., Rzeźnikiewicz, K., Pietras, B. & Michalik, M. Fine and ultrafine TiO_2 particles in aerosol in Kraków (Poland). Mineralogia 45, 65–77 (2014).
64. Survey, U. S. G. Mineral Commodity Summaries. Mineral Commodity Summaries (2019). doi:10.3133/70202434
65. Wang, J., Nabi, M. M., Erfani, M., Goharian, E. & Baalousha, M. Identification and quantification of anthropogenic nanomaterials in urban rain and runoff using single particle-inductively coupled plasma-time of flight-mass spectrometry. Environ. Sci. Nano 9, 714–729 (2022).
66. Tian, P., Li, Y. & Yang, Z. Effect of rainfall and antecedent dry periods on heavy metal loading of sediments on urban roads. Front. Earth Sci. China 3, 297–302 (2009).

67. Yuan, Q., Guerra, H. & Kim, Y. An Investigation of the Relationships between Rainfall Conditions and Pollutant Wash-Off from the Paved Road. Water 9, 232 (2017).
68. Reed, R. B. et al. Multi-day diurnal measurements of Ti-containing nanoparticle and organic sunscreen chemical release during recreational use of a natural surface water. Environ. Sci. Nano 4, 69–77 (2017).
69. Kaegi, R. et al. Release of TiO_2 – (Nano) particles from construction and demolition landfills. NanoImpact 8, 73–79 (2017).
70. Kiser, M. A. et al. Titanium nanomaterial removal and release from wastewater treatment plants. Environ. Sci. Technol. 43, 6757–6763 (2009).
71. City of West Columbia City Council. West Columbia City Operated Parks Closed to Reduce Potential COVID-19 Exposure - City of West Columbia. Available at: https://westcolumbiasc.gov/2020/03/west-columbia-city-operated-parks-closed-to-reduce-potential-covid-19-exposure/. (Accessed: 8th January 2021)
72. City of Columbia. City of Columbia coronavirus (COVID-19) update - Stay at Home Order issued - Tuesday, March 24 at 10 a.m. Available at: https://www.como.gov/CMS/pressreleases/view.php?id=6656. (Accessed: 8th January 2021)
73. Verplanck, P. L. et al. Evaluating the behavior of gadolinium and other rare earth elements through large metropolitan sewage treatment plants. Environ. Sci. Technol. 44, 3876–3882 (2010).

Chapter 5

Temporal Variability in TiO_2 Engineered Particle Concentrations in Rural Edisto River

Nabi, M.M., Wang, J., Journey, C.A., Bradley, P.M., Baalousha, M.," Temporal variability in TiO_2 engineered particle concentrations in rural Edisto River", Chemosphere, 297 (2022), p. 134091

5.1 Abstract

Titanium dixoide (TiO_2) is the most extensively used engineered nanomaterial (ENM) to date, yet its occurrence, concentrations, temporal variability, and fate in natural environmental systems are poorly understood. We conducted a three-year field-monitoring of the TiO_2 concentrations in a rural river basin (Edisto River, < 1% urban land cover) in South Carolina, United States. The total concentrations of Ti, Nb, Al, Fe, Ce, and La in the Edisto River trended higher during spring/summer compared to autumn/winter. Upward trending Ti/Nb in the spring/summer compared to near-background autumn/winter ratios of 266 indicated agricultural prep and growing season related increases in TiO_2 engineered particles. In contrast, downward trending of the Ti/Al and Ti/Fe in the spring and summer compared to the near-background autumn/winter ratios of 0.05 indicated greater mobilization of Fe and Al, relative to Ti during spring/summer. Surface-water concentrations of TiO_2 engineered particles varied between 0 and 128.7 ± 3.9 μg TiO_2 L^{-1}. Increases in TiO_2 concentrations over the spring/summer were associated with increases in phosphorous, orthophosphate, nitrate, ammonia, anthropogenic gadolinium, water temperature, suspended sediments, organic carbon, and alkalinity, and with decreases in dissolved oxygen. The association between these contaminants together with the timing of the increases in their concentrations is consistent with diffuse wastewater source, such as reuse application overspray, biosolids fertilization, or leaking sewers or septic tanks, as the driver of instream concentrations; however, other diffuse sources cannot be ruled out. The findings of this study indicate spatially-distributed (non-point source) releases can result in high concentrations of TiO_2 ENMs, which may pose higher risks to rural stream aquatic ecosystems during the agricultural season. The results illustrate the importance of

monitoring seasonal variations in ENM concentrations in surface waters for a more representative assessment of ecosystem risk.

5.2 Introduction

Titanium dixoide (TiO_2) is the most extensively used engineered nanomaterial (ENM) to date, yet its occurrence, measured concentrations, and fate in natural environmental systems are poorly understood [1]. The global consumption of TiO_2 as engineered particles, including engineered nanomaterials (1-100 nm particles) and pigments (100-300 nm particles), is projected to reach 8.8 million metric tons by 2025 [1]. The major applications of TiO_2 are architectural and industrial paints and coatings (60%), plastic (28%), paper (5%), and other applications (7%) such as photocatalyst, food additive, cosmetics, and sunblocks [2]. These applications result in environmental releases of TiO_2 engineered particles from diverse sources [3–10]. Consequently, TiO_2 engineered particles are widely distributed in the environment [3, 4, 7, 8, 11]. Many studies investigated the presence and concentrations of ENMs in various technical and environmental compartments such as wastewater treatment plants [5, 12, 13], construction and demolition landfills [10], urban runoff [6], and biosolids [11]. Additionally, fewer studies investigated the release of ENMs from localized point sources such as manufacturing facilities [3], painted surfaces [9], municipal wastewater treatment plants [5,13], sewage spills [4], and sunscreens [7,8] to surface waters. However, studies on the potential contribution of more spatially-distributed (non-point) wastewater sources, such as agriculture-applied biosolids and septic tank discharges, to the fluxes of ENMs in river surface waters are scarce, despite the demonstrated presence of ENMs in raw sewage, sewage sludge, and biosolids-amended soils [12,14,15].

In the United States, approximately 7 million dry tons of biosolids are produced annually, and 55% of the produced biosolids (based on 2004 data) are used for agriculture, silviculture, land restoration, and other land applications [16,17]. Seventy-four percent of land-applied biosolids are used for crop agriculture. Biosolids (sewage sludges) are widely recognized as important vectors of chemicals, including heavy metals [18], nutrients [19], as well as ENMs [12,15,20] to amended agricultural soils and nearby surface waters [21–23]. Titanium oxides, iron oxides, silver and zinc sulfides, and other metal containing particles have been reported in sewage sludge and sludge-amended soils [18, 24–26]. Yang et al., (2014) estimated an average TiO_2 concentration in biosolid amended soils in Texas, USA of 2382 ± 422 mg kg^{-1} [22]. Additionally, more than 21 million households in the United States, most commonly in rural areas, use septic systems – not a public sewer – to trap and filter toilet waste [27]. Septic tanks also are widely recognized as an important source of chemicals to ground and surface waters [28,29]. Although it is well recognized that septic tank and agricultural discharges contributes to the loading of contamiants, including TiO_2 [24,30,31], in river surface water, there are currently no field data on the occurrence and concentrations in surface water receiving agricultural discharges.

Available studies have documented the presence of TiO_2 ENMs in biosolids, biosolids-amended agricultural soils, and other environmental compartments based on elemental analysis of total Ti combined with electron microscopic identification of TiO_2 particles, without estimating the relative fractions of engineered and natural Ti particles [8]. Ti, the 9th most abundant element in the Earth's crust, is mainly found in natural rutile, ilmenite minerals, and/or opaque heavy minerals such as titanomagnetite and magnetite [32], with trace concentrations of other elements always present [33]. More than 90 to 95 percent

of the whole rock content of Ti, Nb, Ta, Sb, and W has been attributed to rutile and ilmenite minerals, along with 5 to 45 percent of the whole rock content of V, Cr, Mo, and Sn [34]. Natural Ti-containing particles derived from weathering have similar elemental ratios, associations, and compositions to the parent rocks. Elemental impurities inherent in natural Ti minerals; such as Al, Si, Fe, Mn, Ce, La, Zr, Nb, Pb, Ba, Th, Ta, W, and U [4,35]; are removed by dissolution and reprecipitation during manufacturing of TiO_2 engineered particles. Elevated ratios of Ti to trace elements in Ti-containing minerals have been used to estimate concentrations of TiO_2 engineered particles in sewage spills [4], urban runoff [6], and surface waters [36]. However, there is currently no data on the occurrence and seasonal variability of TiO_2 ENMs in streams receiving discharges from predominantly agricultural watersheds with biosolid applications.

The aims of this study are to investigates the seasonal variability in TiO_2 ENM concentrations and to explore the relationship between TiO_2 and other contaminant concentrations in a rural river basin (Edisto River, South Carolina) with limited urban development (< 1%). The concentration of TiO_2 ENM was monitored biweekly/monthly over a period of three years in the Edisto River at the USGS 02175000 Edisto River sampling site.

5.3 Materials and Methods

5.3.1 Edisto River watershed

The Edisto River basin is situated entirely within the state of South Carolina and is one of the longest free-flowing (unimpounded) black water rivers in the United States

(**Figure D.1**) [37–39]. The Edisto River basin originates in the sandhill region of west central South Carolina, encompasses over 8030 km^2, flows through the upper and lower coastal plain regions, runs into the coastal zone region, and discharges into the Atlantic Ocean. The river meanders approximately 250 miles through the coastal plains of South Carolina [40]. The Edisto River basin encompasses more than eight thousand stream km, 44.5 km^2 of lakes and ponds, and 81 km^2 of estuary. The basin is primarily rural in character with 45% forested land, 29% agricultural land, 15% forested wetland, 5% barren, 3% water, 2% nonforested wetland (saturated marshland), and 1% urban land [40]. The urban land percentage is comprised chiefly of the City of Orangeburg and a portion of the City of Aiken. The city of Orangeburg is 21.5 km^2, with a population of 14,000 according to the 2010 United State census. The city of Orangeburg is located on the North Fork of the Edisto River, 68 km upstream of the sampling site. The city of Aiken is 53.9 km^2, with a population of 29,650 according to the 2010 United State census. The city of Aiken is located on the South Fork of the Edisto River, 140 km upstream of the sampling site. There are 13 permitted wastewater treatment plants (WWTP) along the Edisto River (**Figure D.1b**), and 24 landfill facilities and 52 mining facilities (mainly sand, clay and limestone) in the river basin [40]. Approximatly, 40% of homes in South Carolina rely on septic tanks for wastewater treatment and this number is expected to be even higher in the Edisto River basin given the rural nature of the area [27,41,42]. The discharge data and stream samples were collected from USGS station 02175000 (33°01'40"N 80°23'30"W) and the rainfall data were from the NOAA station ‘Charleston international airport’ (32°53'59"N 80°02'25"W), approximately 36 km from the sampling location.

5.3.2 Sample collection and analysis

Water samples from the Edisto River were collected at the USGS 2175000 Edisto River sampling site, which is located near Givhans Ferry state park, SC (Latitude: 33º 01' 40", Longitude: 80º 23' 30"), approximately 3.9 kms downstream of the confluence of Edisto River and Four Hole swamp. Edisto river water samples were collected approximately monthly between 14/09/2017 and 20/10/2020. Composite depth-integrated samples were collected from about 10 different locations from the middle of the river channel immediately upstream (*e.g.*, 1-2 m) of the bridge located on Highway 61 with average annual daily traffic density of 4300. Water samples were collected in 1 L high-density polyethylene bottles (HPDE, Thermo Scientific, USA) according to USGS guidelines for the water samples collection [43]. The bottles were acid washed prior to the sample collection by soaking in 10% nitric acid (Acros Organics, Czech Republic) for at least 24 hours followed by soaking in ultrapure water (UPW, PURELAB Option-Q, ELGA, UK) for 24 hours, air dried, and then double-bagged. Before filling with the water samples in the field, the sampling bottles were rinsed three times with surface water. The individual samples were double bagged and brought back on ice to the lab on the same day, where they were stored at 4°C in the dark until further analysis. The samples were digested in HF:HNO_3 (3:1) acid mixture (ACS grade acids distilled in the laboratory). The total elemental concentration of the digested samples was analyzed using a Perkin Elmer NexION 350D ICP-MS according to the protocols described in detail in the supplementary information section (section D.1, D.2, and D.3, **Table D.2**) [4]. A selected subset of water samples was analyzed using single particle-inductively coupled plasma-time of flight-mass spectrometer (SP-ICP-TOF-MS, **Table D.1**) to determine the elemental ratios of Ti/Nb in

natural Ti-containing particles, as described in detail in the supplementary information section (section D.4) and elsewhere [36].

5.3.3 Calculation of TiO_2 engineered particle concentration

The concentration of TiO_2 engineered particles in the Edisto river surface water was calculated based on mass balance according Eq. 1

$$[TiO_2]_{engineered\ particles} = \frac{TiO_{2\ MM}}{Ti_{\ MM}}\left[Ti_{sample} - Nb_{sample}.\left(\frac{Ti}{Nb}\right)_{background}\right] \qquad (Eq.2)$$

Where, $[TiO_2]_{\text{engineered particles}}$ is the concentration of TiO_2 engineered particles, $Ti_{\ MM}$ and $TiO_{2\ MM}$ are the molar masses of Ti and TiO_2, Ti_{sample} and Nb_{sample} are the concentrations of Ti and Nb in a given sample, $Ti/Nb_{background}$ is the natural background elemental concentration ratio of Ti/Nb. The background Ti/Nb ratio (255.7 ± 8.9) was estimated as that observed during the drought low-flow period of the summer of 2019 (05/23/2019 no rainfall or surface runoff). We hypothesize that under such conditions the contribution of anthropogenic Ti to the suspended sediments in the Edisto River is negligible.

There are three assumptions for Eq 1: 1) all Ti was in particulate form, 2) anthropogenic Ti occurred only as pure TiO_2 engineered particles, and 3) the natural background elemental ratio of Ti/Nb was constant through the sampling period. These assumptions are supported by the following. TiO_2 has very low solubility and, consequently, Ti is expected to occur only in particulate form in the Edisto river surface water [44]. Mined Ti bearing ores (approx. 95%) are treated to yield nearly pure TiO_2 for use in numerous industrial applications [45]. The concentration of Nb in commercially available TiO_2 engineered particles has been shown to be below the ICP-MS detection limit (*e.g.*, <

7 ng L^{-1}) for TiO_2 concentrations up to 1000 µg L^{-1} [6]. On the other hand, natural TiO_2 minerals are the dominant carriers (*e.g.*, > 90-95% of the whole rock content) of Ti and Nb [46]. The elemental ratio of Ti/Nb, Ti/Fe, and Ti/Al in naturally occurring particles in the Edisto River waters were found to be constant throughout the sampling campaigns (*see results and discussion section 5.4.3*).

5.3.4 Base flow and runoff separation

"WHAT: Web-based Hydrograph Analysis Tool" (WHAT), an online based web tool, was used to separate the discharge into base flow and direct runoff [47]. WHAT is linked to the USGS National Water Information System (NWIS [48]) database. The USGS station number 02175000 was used for the separation of base flow and direct runoff (both overland flow and shallow groundwater discharge), and the following method and conditions applied: Method: Recursive digital filter, Aquifer type: Perennial streams with porous aquifer, Filter parameter: 0.98, BFImax: 0.80, Date range: 16/04/1957 to 20/10/2020.

5.4 Results and Discussion

5.4.1 Precipitation and discharge

Precipitation was recorded on 362 days during the sampling period from 14/09/2017 to 20/10/2020, with the highest rainfall (124 mm) observed on 19/5/2018 within 35.9 kilometers of the Givhans gage (**Figure D.2**). River discharge varied markedly during the sampling period. The maximum discharge was 320.0 m^{-3} s^{-1} on 27/02/2020, and the minimum discharge was 9.6 m^{-3} s^{-1} on 01/10/2019. The discharge was split into base

flow and direct runoff using WHAT [47]. The maximum base flow was 210.7 m^{-3} s^{-1} on 13/03/2020, and the minimum base flow was 8.2 m^{-3} s^{-1} on 13/10/2019. The maximum direct runoff was 157.5 m^{-3} s^{-1} on 12/02/2020, and the minimum direct runoff was 0 m^{-3} s^{-1} on several dates. Most of the collected samples had a runoff contribution, except those collected on 08/05/2018, 12/06/2018, 20/08/2018, 20/03/2019, 29/04/2019, 23/05/2019, 19/03/2020, and 05/05/2020. South Carolina experienced a drought between 19/03/2019 and 10/12/2019, resulting in lower discharge in the Edisto River during summer and fall 2019 (9.6-70.8 m^3 sec^{-1}) compared to the same period in 2018 (13.2-184.3 m^3 sec^{-1}) and 2020 (21.1-194.2 m^3 sec^{-1}) (**Figure D.2**) [49].

5.4.2 Water chemistry

The physicochemical parameters of the Edisto River water exhibited seasonal variations throughout the sampling period (**Figure D.3**). Air and water temperature, nitrate and ammonia, phosphorous, organic carbon, alkalinity, and suspended sediments followed the same trend with higher values during the spring and summer (April to October) and lower values during the fall and winter (November to March, **Figure D.3a-f**). The air and water temperature varied from 6.4 to 32.5 and 7.3 to 29.3 ºC, respectively (**Figure D.3a**). Nitrate and ammonia ranged from 0 to 0.83 mg L^{-1} and 0 to 0.04 mg L^{-1}, respectively (**Figure D.3b**). Phosphorous and orthophosphate varied from 0.02 to 0.11 mg L^{-1} and 0.02 to 0.14 mg L^{-1}, respectively (**Figure D.3c**). Organic carbon ranged from 3.0 to 20.4 mg L^{-1} (**Figure D.3d**). Alkalinity ranged from 9.3 to 25.9 mg L^{-1} $CaCO_3$ (**Figure D.3e**). Suspended sediment concentrations ranged from 2.0 to 33.0 mg L^{-1} (**Figure D.3f**).

Dissolved oxygen varied between 5.0 and 12.1 mg L^{-1} (63 to 105% saturation) and followed the opposite trend with lower values during the spring and summer and higher values during the fall and winter (**Figure D.3g**). This seasonal variation in O_2 may be attributed to both natural and anthropogenic factors [50]. Key natural factors that might influence DO concentrations include stream discharge, flow velocity, temperature, channel gradient, channel bottom substrate, and degree of channel confinement [51]. Anthropogenic factors that influence instream DO include organic and nutrient discharges (*e.g.,* from wastewater agricultural activities) [52,53]. Electrical conductivity varied between 49 and 113 µs cm^{-1} (**Figure D.3h**) and the pH varied between 5.5 and 6.9 (**Figure D.3i**). Conductivity and pH did not exhibit a consistent temporal trend.

The crustal normalized REE pattern indicates the presence of Gd anomaly (Gd/Gd*) in the Edisto River water (**Figure D.4a**). The size of Gd anomaly varied between 0.95 and 1.8 (**Figure D.4b**) with a peak in 2018 and a higher peak in 2020 and no increases in 2019. The geogenic ratio of Gd/Gd* should be close to one and any values exceeding at least 1.3 represent anthropogenic Gd input [54,55]. Despite the small size of the Gd anomaly, the manifestation of these anomalies in 2018 and 2020 and their absence during the drought period of 2019 are strong indications that these anomalies are true Gd contamination signatures. REE distribution patterns of surface water and groundwater from industrialized and highly populated areas show anthropogenic gadolinium anomalies as a result of the use of Gd compounds as a contrast agent in magnetic resonance imaging [55]. The Gd compounds enter the surface water mostly via wastewater sources such as wastewater treated effluent discharge directly as permitted point sources or indirectly through reuse application overspray, sewage spills, leaking sewage pipes, and leaking or improperly

designed septic tanks [55,56]. These results indicate a possible contribution of wastewater sources to the discharge in the Edisto River in the spring/summer of 2018 and 2020. The notably higher concentrations of suspended sediment, anthropogenic Gd, and Ti during 2020 may be due in part to the precedent 2019 dry conditions, with limited runoff and associated increased land accumulation of these constituents between 19/03/2019 and 10/12/2019 and subsequent elevated runoff during 2020.

The spring/summer timing of the increases in P, N, OC, Alkalinity, SPM, and Gd anomaly (*e.g.*, spring and summer) and the concurrent decreases in DO coincides with the agriculture season and with the application of biosolids on agricultural fields (**Table D.5**) [57], is consistent with agriculture-linked spatially-distributed wastewater sources (e.g., land application of biosolids/wastewater effluent reuse overspray) as drivers of these contaminants in the Edisto River as discussed in more detail in section 5.4.5.

5.4.3 Elemental concentrations and ratios

The concentrations of Ti, Nb, Al, Fe, Ce and La followed the same seasonal trend of increases during the spring and summer compared to fall and winter (**Figure 5.1**), suggesting a common environmental driver. Elemental ratios (*e.g.,* Ti/Nb, Ti/Al, Ti/Fe, and Ce/La), however, exhibited different patterns (**Figure 5.2a-d**). Except during the 2019 spring/summer drought, Ti/Nb trended higher between February and August, with lower values between September and January (**Figure 5.2a**). The lowest Ti/Nb ratio (255.7 ± 8.9) was observed during the drought period of summer 2019 in the absence of precipitation-driven surface runoff (**Figure 5.2a**). This value was consistent with a natural background ratio of Ti/Nb (266.4 ± 8.9) in our previous study in the tributaries of the Congaree River

[4]. Thus, 255.7 was used herein as the natural background Ti/Nb ratio to estimate natural and anthropogenic Ti concentrations. The Ti/Al and Ti/Fe ratios followed the opposite trend compared to that of Ti/Nb (**Figure 5.2b and c**). This might be due to the co-release of Al and Fe with Ti from the same source such as sewage spills, biosolids, or urban runoff [4–6,36]. The Ce/La ratio exhibited limited variability (*e.g.*, 2.0 ± 0.01 to 2.4 ± 0.02), with an average observed value (2.2 ± 0.1) consistent with the average crustal Ce/La (2.13) and the average background water Ce/La (2.15 ± 0.01) [4]. This pattern indicates little anthropogenic Ce or La contamination (**Figure 5.2d**). The near constant Ce/La ratio and the high concentration of Ce and La in the Edisto River water during high discharge indicates a significant introduction of natural particles during runoff events in the Edisto River.

Given the significant contribution of natural particles, as indicated by the high Ce and La concentrations, and the presence of Nb in natural titanium minerals, observed differences in Ti/Nb elemental ratios in Edisto River bulk water samples plausibly may result from **1)** variability in the elemental ratios within naturally-occurring Ti-containing particles, or **2)** variability in the introduction of anthropogenic Ti-containing particles which do not contain Nb [51]. Strong associations between Ti and Nb in titanium minerals and no apparent explanation for seasonal changes in Ti and Nb contents of natural mineral sources suggest that these variations are due to anthropogenic Ti-contamination. To further test this hypothesis, the elemental associations and variability in Ti/tracer ratios in natural Ti-containing particles collected within the basin was investigated by SP-ICP-TOF-MS (**Table D.6**). Despite the significant differences in bulk water Ti/Nb ratios (varied between 243 ± 29 to 417 ± 4) in the selected Edisto River samples, the elemental ratios of Ti/Nb in multi-element Ti-bearing particles did not vary substantially (varied between 212 ± 185

and 263 ± 183). Thus, the observed variability in Edisto River bulk sample Ti/Nb ratios is attributed to seasonal differences in the supply of anthropogenic, Nb-free, Ti-particles to the stream.

5.4.4 Concentration and co-occurrence of TiO_2 and other contaminants

The estimated TiO_2 engineered particle concentrations based on shifts in Ti/Nb elemental ratios varied between 0 µg L^{-1} and 128.5 ± 3.9 µg L^{-1} (**Figure 5.3a**). These TiO_2 concentrations are similar to those measured in other surface waters in South Carolina receiving sewage spills, such as Gills Creek and Stoops Creek (1 to 100 µg L^{-1}) [4], and receiving urban runoff such as the Broad River (20 to 150 µg L^{-1}) [36]. However, these TiO_2 concentrations are notably higher than those (*e.g.*, 0.55 to 6.5 µg L^{-1}) reported in surface water from the Dommel River in the Netherlands and Ribble/Wyre and upper Severn rivers UK. [58–60].

The TiO_2 pollutograph followed the same trends of rise and fall as those of phosphorus, orthophosphate, nitrate, ammonia, anthropogenic Gd, temperature, and SPM (**Figure 5.3a-e**); and the opposite trend as that of organic carbon and DO (**Figure 5.3f-g**). The co-occurrence of TiO_2 with phosphorous and nitrogen (**Figure 5.3a and b**), recognized agriculture-related contaminants, suggest that the release of TiO_2 is possibly associated with agricultural runoff. The concentration of nitrogen in streams draining fields with applied sewage sludge has been shown to follow the same trend as those shown here [61]. The co-occurrence of TiO_2 with anthropogenic Gd (**Figure 5.3c**), a recognized wastewater contaminant, suggests that the release of TiO_2 is associated with human-waste. Together these co-occurrences suggest that the release of TiO_2 is associated with human waste

disposal, such as discharges to the stream and sewage sludge land application on adjacent agricultural fields.

The rise and fall of TiO_2 particles with temperature is likely due to seasonal effect such as agricultural land application and associated release of TiO_2 during the spring and summer seasons. The co-occurrence of TiO_2 with SPM (**Figure 5.3e**) is likely to be due to the heteroaggregation of TiO_2 particles with the suspended solids. The negative correlation between TiO_2 and DO (**Figure 5.3g**) is also consistent with co-release of TiO_2 with wastewater discharge and/or runoff of biosolids from agricultural fields. Apart from the impact on DO, organic matter and discharge (mentioned in section 5.4.2), water temperature also influences the size of particles in suspension and their tendency to settle. Higher water temperature promotes more breakable flocs (in terms of size reduction) formation and, thus, supports suspension of smaller particles, including TiO_2-containing particles, in the stream water [62].

5.4.5 Potential source of TiO_2 in the Edisto River

Releases of TiO_2 into the Edisto River might originate from various sources including 1) treated sewage [12,13], 2) sewage spills [4], 3) urban runoff [36], and/or 4) agricultural runoff from fields amended with biosolids or irrigated with reuse water. Below we discuss the likely contribution of these sources to TiO_2 concentrations in the Edisto River.

Thirteen WWTP were identified along the Edisto River (**Table D.8**). The effluent volume varies from 0.11 to 18.5 x 10^6 L day^{-1} (0.0013 to 0.21 m^3 sec^{-1}) with a total effluent volume of all WWTPs of 32.1 x 10^6 L day^{-1} (0.37 m^3 sec^{-1}). The largest WWTP along the Edisto River is Orangeburg WWTP, with an effluent volume of 18.5 x 10^6 L day^{-1} (0.21

m^3 sec^{-1}) and located at approximately 75 km upstream the sampling site. The total effluent volume from all WWTPs is negligible (< 4%) compared to the lowest discharge of 9.6 m^3 sec^{-1} at the sampling site and would result in significant dilution (*e.g.,* > 25 folds in the worst-case scenario) of WWTP effluent. Given the low concentration of TiO_2 engineered particles in WWTP effluents in the USA (*e.g.,* 1-50 µg L^{-1}) [5,12,13], this would result in TiO_2 concentrations of < 2.0 µg L^{-1}, much lower than the surface-water TiO_2 concentrations observed in this study. Therefore, WWTP effluent is estimated to be a minor contributor to total concentrations of TiO_2 in the Edisto River.

Fifty-three sewage spills were identified in the Edisto River watershed. These occurred mainly in Orangeburg and Aiken Counties, the largest urban areas in the Edisto River watershed and the closest to the sampling location (**Table D.9**). The total volumes of sewage spills were 81,386, 187,756, and 162,773 L in 2018, 2019, and 2020, respectively. The short duration (*e.g.,* 5 minutes to 14 hours) and small volumes (*e.g.,* 1,100 minutes to 50000 L, **Table D.9**) of these sewage spills, and their distance from the sampling site (*e.g.,* 75 and 140 km for Orangeburg and Aiken, respectively) result in significant dilution of any associated TiO_2 releases to background level concentrations at the sampling site. Therefore, sewage spills occurring in the rural areas of Orangeburg and Aiken cities are also unlikely to be significant contributors to TiO_2 loads observed at the sampling site in the Edisto River.

Urban land use represents only 1% of the Edisto watershed area and is comprised of the City of Orangeburg (21.5 km^2) and a portion of the City of Aiken (total area of Aiken is 53.9 km^2), located at approximately 68 and 140 km, respectively upstream of the sampling site. This is likely to result in significant dilution of any TiO_2 emitted from Aiken

and/or Orangeburg to the background level at the sampling site. Paul et al (2001) reported that urban runoff varies between 20 and 55% of total rainfall in the impervious urban corridor depending on percentage of infiltration, evapotranspiration and imperviousness [63]. Consequently, the total urban runoff generated from both cities would vary in the range from 23.1 to 63.4 x 10^6 L day^{-1} (0.27 to 0.73 m^3 sec^{-1}) assuming average annual rainfall of 47 and 48 inches in Orangeburg and Aiken cities respectively in the same day [64]. The total urban runoff from both cities is negligible compared to the lowest discharge of 9.6 m^3 sec^{-1} at the sampling site and would result in significant dilution (*e.g.*, 13 to 35 folds in the worst-case scenario) of urban runoff. The concentration of TiO_2 engineered particles in urban runoff in the USA ranges from 5 to 150 µg L^{-1} [6]. Therefore, the resulting TiO_2 concentration would be between 4.3 to 11.5 µg L^{-1} in the stream water adjacent to the urban areas, well below the in-stream TiO_2 concentrations observed in this study. Thus, urban source is unlikely to account for the total TiO_2 load at the sampling site.

Bridge runoff also could contribute to in-stream TiO_2 concentrations [6]. One bridge (State road 18-19) was identified near (3.4 km) and upstream of the sampling site. The average daily traffic in 2019 on this bridge was 250 vehicles per day [65]. This average daily traffic is much lower (~ 358 times less) than that reported for bridges in a recent study [6] in which TiO_2 engineered particles in bridge runoff estimated to vary between 5 to 150 µg L^{-1}. Based on that report, the in-stream TiO_2 concentration associated with bridge runoff from State road 18-19 was estimated to be < 0.5 µg L^{-1} (in the worst case scenario) at the bridge and to decrease downstream due to dilution. Thus bridge runoff also is unlikely to contribute substantially to total TiO_2 loads observed at the sampling site.

Approximately 33,929 dry U.S. tons of total solids is generated in SC annually, with land application estimated at 12,758 dry U.S. tons (*e.g.,* 38% of the total solids) per year [16]. Therefore, the total solids applied annually on land in South Carolina is estimated to be approximately 5.5 x 10^6 µg solids m^{-1} of agricultural land. The concentration of TiO_2 in sewage sludge in the United States is estimated at 1.67 to 10.0 kg TiO_2 ton^{-1} dry weight (**Table D.10**) [13]. Thus, the estimated TiO_2 mass applied annually on land in SC is approximatly 21 to 130 tons TiO_2 (or 21 x 10^{12} to 13 x 10^{13} µg TiO_2). Accordingly, the estimated TiO_2 mass applied annually on land in the Edisto River watershed is estimated to be approximately 1,100 to 6,600 µg TiO_2 per square meter of agricultural land, a substantial potential contributor to TiO_2 loads in the Edisto River. Therefore, based on this preliminary source apportionment, the seasonal patterns in in-stream TiO_2 concentrations and elemental ratios and the co-occurrence of TiO_2 and agriculture and sewage related contaminants (*e.g.,* increased phosphorous, nitrogen, and anthropogenic Gd and decreased DO) in the Edisto River are most easily reconciled with seasonally-intensive human-waste biosolid applications on agricultural land against a non-seasonal background signal from normal-operation and episodic bypass effluent discharges from the limited number of upstream WWTP point-sources and numerous spatially-distributed (functionally non-point source) upstream residential on-site septic discharges.

5.5 Conclusions

This study demonstrated seasonal variability in TiO_2 concentrations in a rural river in South Carolina, United States. This study is the first to characterize and quantify engineered particles in a river reach draining a rural watershed with less than 1% urban

land cover and concomitantly few WWTP point-source discharges. In this setting, long-term monitoring of the concentration of TiO_2 engineered particles was required to discern the temporal variability in surface-water TiO_2 ENM and to establish the background natural Ti/Nb ratio. Using the elemental ratio approach, the total, natural, and engineered Ti concentrations were quantified in Edisto river water. The elemental ratio of Ti/Nb varied from 255.7 ± 8.9 to 464.5 ± 2.8. The lowest measured Ti/Nb ratios, observed in the absence of runoff and precipitation during the drought 2019, were in good agreement with average Ti/Nb ratios in sediments upstream in the Edisto river basin and with previously established natural background ratios in tributaries of the Congaree River (*e.g.,* 266.4 ± 8.9) [17]. Thus, this Ti/Nb elemental ratio (*e.g.,* 255.7±8.9) was employed as the natural background ratio to calculate natural and anthropogenic Ti concentrations by mass-balance.

The Edisto River TiO_2 ENM concentration ranged from 0 to 128.7 ± 3.9 μg L^{-1}. The concentrations of TiO_2 ENMs increased during the spring and summer seasons and decreased during the fall and winter seaons, which concided with increases and decreases in phosphorous, nitrogen, ammonia, organic carbon, anthropogenic Gd. While the source(s) of TiO_2 ENM loading to the stream was not specifically identified, seasonal patterns in the instream concentrations and elemental ratios are most easily reconciled with seasonally-intensive biosolid application on agricultural land against a non-seasonal background signal from normal-operation and episodic bypass effluent discharges from the limited number of upstream wastewater treatment facility point-sources and numerous spatially-distributed (non-point source) upstream residential on-site septic discharges, because: **1)** WWTP effluent discharge and by-pass sewage spills are small contributors (< 4%) to the Edisto River discharge at the Givhans gage, **2)** no seasonal pattern in effluent

discharge and by-pass events was observed during the study period, **3)** the increase in TiO_2 concentrations during the spring and summer, coincided with the onset of the growing season and the timing of agricultural biosolids application, and **4)** TiO_2 co-associated with other agriculture-runoff and wastewater signatures such as nutrients and anthropogenic gadolinium, respectively.

The instream TiO_2 concentrations observed in the current study are higher than the PNEC for TiO_2 ENMs to freshwater organisms (*e.g.*, 1-18 µg L^{-1}). Further, fluvial transport of TiO_2 engineered particles from the Edisto River as well as other rivers to the ocean could lead to bioaccumulation in estuarine and coastal microflora and induce coral bleaching and coral population declines [66,67]. Further research is needed on the occurence and temporal variability in TiO_2 ENM concentrations in streambed sediments to better understand the fate, transport, and potential aquatic effects of TiO_2 ENM on rural stream ecosystems and estuarine and coastal receptors.

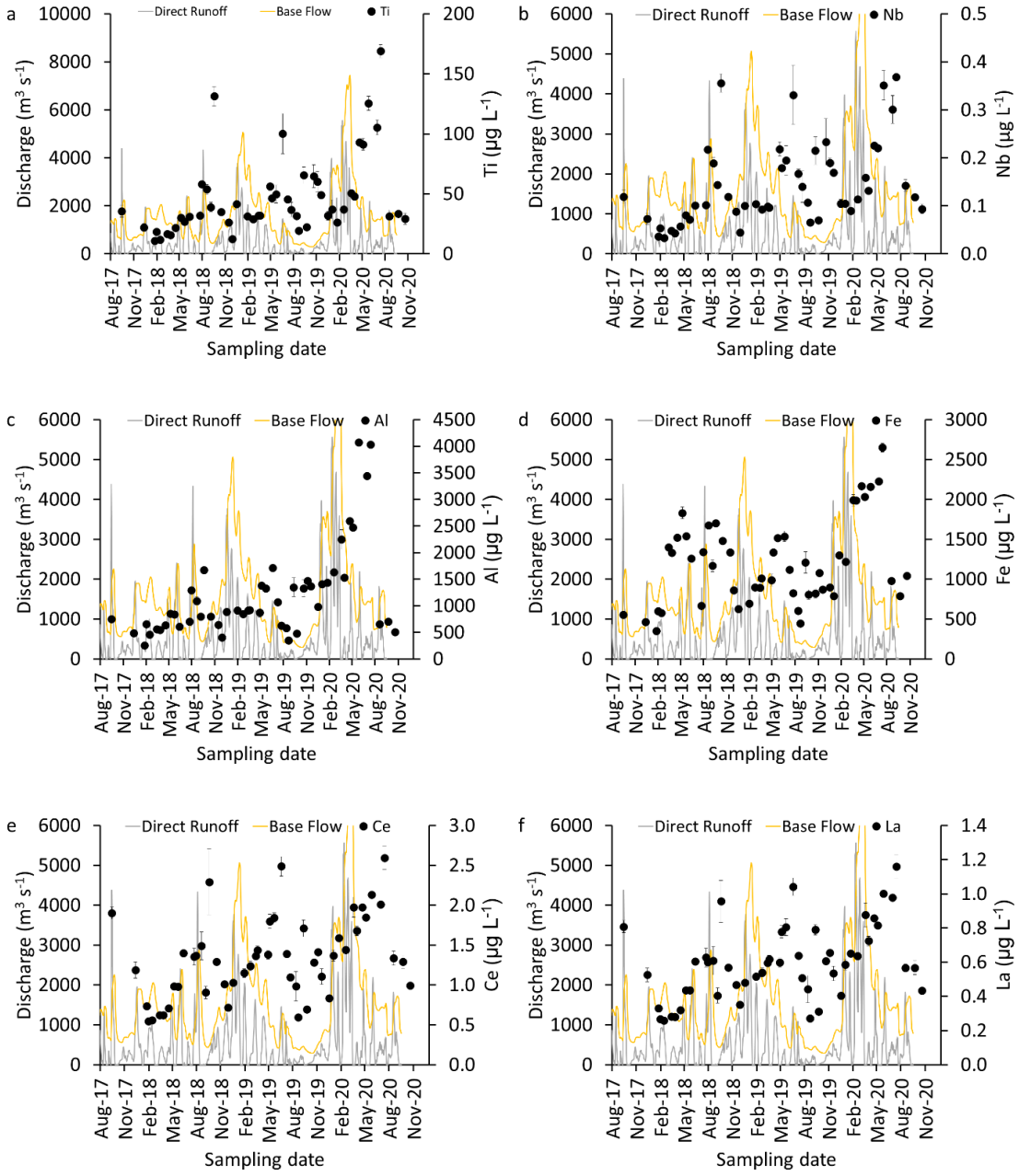

Figure 5.1 Temporal variation in (a) Ti, (b) Nb, (c) Al, (d) Fe, (e) Ce, and (f) La concentration in the Edisto River water at the sampling site.

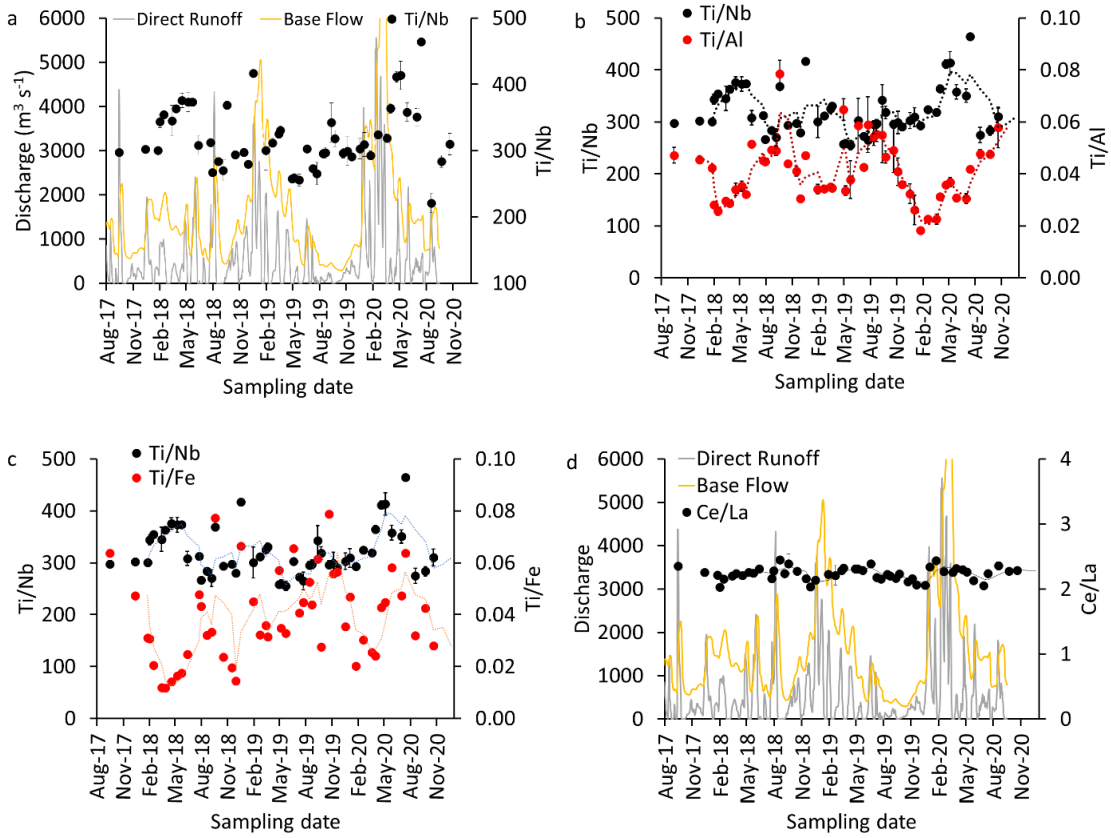

Figure 5.2 Temporal variability of elemental ratios of (a) Ti/Nb, (b) Ti/Al, (c) Ti/Fe, and (d) Ce/La in the Edisto River water at the sampling site.

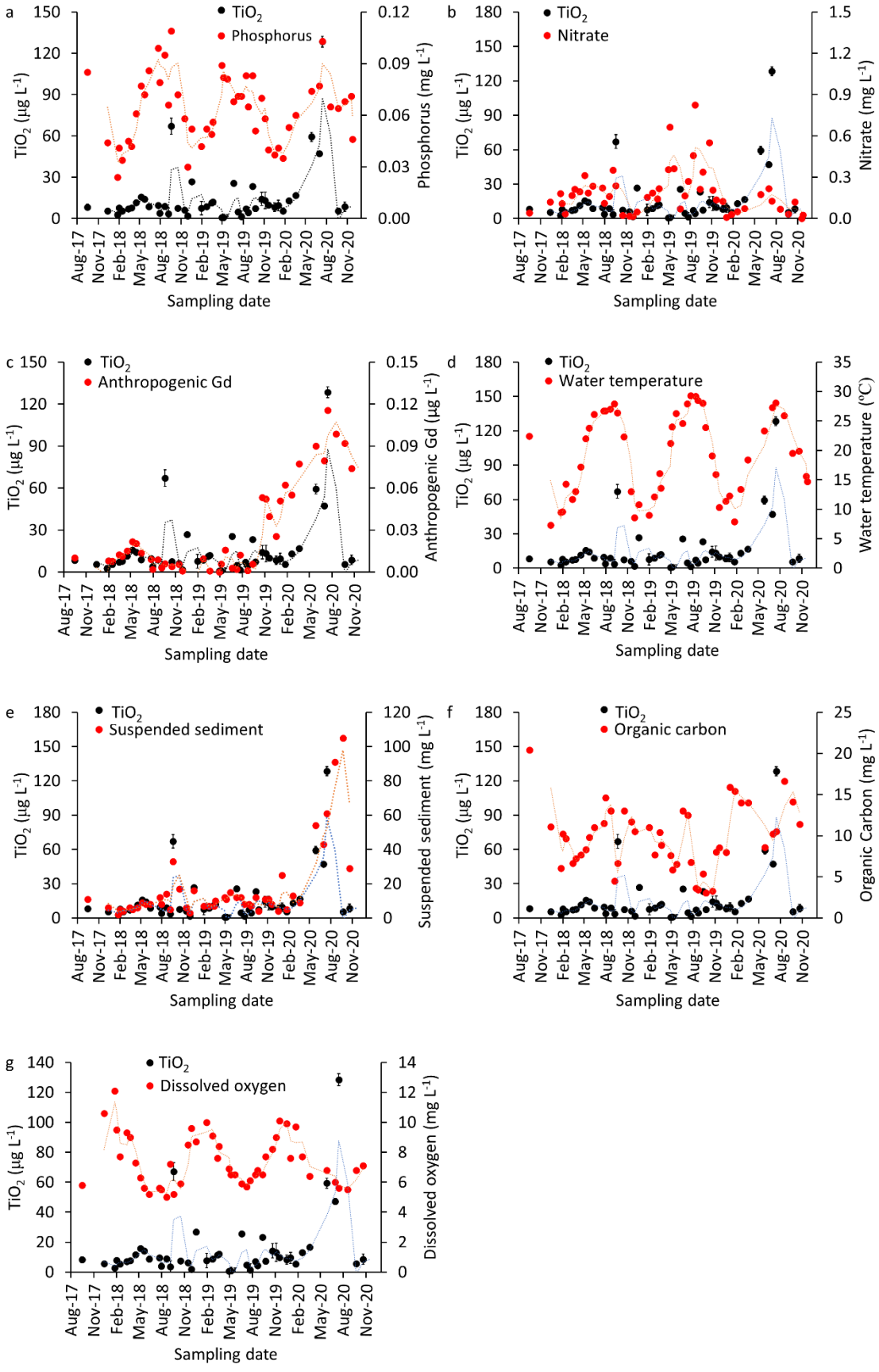
a
TiO2
Phosphorus
TiO2 (µg L-1)
Phosphorus (mg L-1)
b
TiO2
Nitrate
TiO2 (µg L-1)
Nitrate (mg L-1)
c
TiO2
Anthropogenic Gd
TiO2 (µg L-1)
Anthropogenic Gd (µg L-1)
d
TiO2
Water temperature
TiO2 (µg L-1)
Water temperature (°C)
e
TiO2
Suspended sediment
TiO2 (µg L-1)
Suspended sediment (mg L-1)
f
TiO2
Organic carbon
TiO2 (µg L-1)
Organic Carbon (mg L-1)
g
TiO2
Dissolved oxygen
TiO2 (µg L-1)
Dissolved oxygen (mg L-1)
Aug-17
Nov-17
Feb-18
May-18
Aug-18
Nov-18
Feb-19
May-19
Aug-19
Nov-19
Feb-20
May-20
Aug-20
Nov-20
Sampling date

Figure 5.3 TiO_2 engineered particle concentrations compared to (a) phosphorus, (b) nitrate, (c) anthropogenic Gd, (d) water temperature, (e) suspended sediment, (f) organic carbon, and (g) dissolved oxygen in the Edisto River water at the sampling site.

References:

1. Piccinno, F.; Gottschalk, F.; Seeger, S.; Nowack, B., Industrial production quantities and uses of ten engineered nanomaterials in Europe and the world. Springer Netherlands: 2012; 14, 1-11.
2. Linak, E.; Inoguchi, Y., Chemical Economics Handbook: Titanium Dioxide‖. Menlo Park, CA, SRI Consulting 2005.
3. Slomberg, D. L.; Auffan, M.; Guéniche, N.; Angeletti, B.; Campos, A.; Borschneck, D.; Aguerre-Chariol, O.; Rose, J., Anthropogenic release and distribution of titanium dioxide particles in a river downstream of a nanomaterial manufacturer industrial site. Frontiers in Environmental Science 2020.
4. Loosli, F.; Wang, J.; Rothenberg, S.; Bizimis, M.; Winkler, C.; Borovinskaya, O.; Flamigni, L.; Baalousha, M., Sewage spills are a major source of titanium dioxide engineered (nano)-particle release into the environment. Environmental Science: Nano 2019, 6, (3), 763-777.
5. Nabi, M. M.; Wang, J.; Meyer, M.; Croteau, M.-N.; Ismail, N.; Baalousha, M., Concentrations and size distribution of TiO_2 and Ag engineered particles in five wastewater treatment plants in the United States. Science of The Total Environment 2021, 753, 142017.
6. Wang, J.; Nabi, M. M.; Mohanty, S. K.; Afrooz, A. N.; Cantando, E.; Aich, N.; Baalousha, M., Detection and quantification of engineered particles in urban runoff. Chemosphere 2020, 248, 126070.
7. Gondikas, A. P.; von der Kammer, F.; Reed, R. B.; Wagner, S.; Ranville, J. F.; Hofmann, T., Release of TiO_2 nanoparticles from sunscreens into surface waters: a one-year survey at the Old Danube recreational lake. Environ. Sci. Technol 2014, 48, (10), 5415-5422.
8. Rand, L. N.; Bi, Y.; Poustie, A.; Bednar, A. J.; Hanigan, D. J.; Westerhoff, P.; Ranville, J. F., Quantifying temporal and geographic variation in sunscreen and mineralogic titanium-containing nanoparticles in three recreational rivers. Science of The Total Environment 2020, 743, 140845.
9. Kaegi, R.; Ulrich, A.; Sinnet, B.; Vonbank, R.; Wichser, A.; Zuleeg, S.; Simmler, H.; Brunner, S.; Vonmont, H.; Burkhardt, M.; Boller, M., Synthetic TiO_2 nanoparticle emission from exterior facades into the aquatic environment. Environ. Pollut 2008, 156, (2), 233-239.
10. Kaegi, R.; Englert, A.; Gondikas, A.; Sinnet, B.; von der Kammer, F.; Burkhardt, M., Release of TiO_2–(Nano) particles from construction and demolition landfills. NanoImpact 2017, 8, 73-79.
11. Baalousha, M.; Wang, J.; Nabi, M. M.; Loosli, F.; Valenca, R.; Mohanty, S. K.; Afrooz, N.; Cantando, E.; Aich, N., Stormwater green infrastructures retain high concentrations of TiO_2 engineered (nano)-particles. Journal of hazardous materials 2020, 392, 122335.
12. Westerhoff, P.; Song, G.; Hristovski, K.; Kiser, M. A., Occurrence and removal of titanium at full scale wastewater treatment plants: implications for TiO_2 nanomaterials. J. Environ. Monit 2011, 13, (5), 1195-1203.

13. Kiser, M. A.; Westerhof, P.; Benn, T.; Wang, Y.; Perez-Rivera, J.; Hristovski, K., Titanium Nanomaterial Removal and Release from Wastewater Treatment Plants. Environ. Sci. Technol 2009, 43, 6757-6763.
14. Kiser, M. A.; Ladner, D. A.; Hristovski, K. D.; Westerhoff, P. K., Nanomaterial Transformation and Association with Fresh and Freeze-Dried Wastewater Activated Sludge: Implications for Testing Protocol and Environmental Fate. Environ. Sci. Technol 2012, 46, (13), 7046-7053.
15. Kiser, M. A.; Ryu, H.; Jang, H.; Hristovski, K.; Westerhoff, P., Biosorption of nanoparticles to heterotrophic wastewater biomass. Wat. Res 2010, 44, (14), 4105-4114.
16. Biosolids, N. E.; Association, R., A national biosolids regulation, quality, end use & disposal survey. NEBRA, Tamworth, NH 2007.
17. Agency, U. S. E. P., Biosolids generation, use, and disposal in the United States. In Office of Wastewater Management: 1999.
18. Tou, F.; Yang, Y.; Feng, J.; Niu, Z.; Pan, H.; Qin, Y.; Guo, X.; Meng, X.; Liu, M.; Hochella, M. F., Environmental risk implications of metals in sludges from waste water treatment plants: the discovery of vast stores of metal-containing nanoparticles. Environmental science & technology 2017, 51, (9), 4831-4840.
19. Zhang, M.; Heaney, D.; Henriquez, B.; Solberg, E.; Bittner, E., A four-year study on influence of biosolids/MSW cocompost application in less productive soils in Alberta: nutrient dynamics. Compost science & utilization 2006, 14, (1), 68-80.
20. Westerhoff, P. K.; Kiser, M. A.; Hristovski, K., Nanomaterial removal and transformation during biological wastewater treatment. Environ. Eng. Sci 2013, 30, (3), 109-117.
21. Smith, I. M.; Hall, K. J.; Lavkulich, L. M.; Schreier, H., Trace Metal Concentrations in an Intensive Agricultural Watershed in British Columbia, Canada JAWRA Journal of the American Water Resources Association 2007, 43, (6), 1455-1467.
22. Yang, Y.; Wang, Y.; Westerhoff, P.; Hristovski, K.; Jin, V. L.; Johnson, M.-V. V.; Arnold, J. G., Metal and nanoparticle occurrence in biosolid-amended soils. Science of the total environment 2014, 485, 441-449.
23. Clarke, R.; Peyton, D.; Healy, M. G.; Fenton, O.; Cummins, E., A quantitative risk assessment for metals in surface water following the application of biosolids to grassland. Science of the Total Environment 2016, 566, 102-112.
24. Gottschalk, F.; Sonderer, T.; Scholz, R. W.; Nowack, B., Modeled Environmental Concentrations of Engineered Nanomaterials (TiO_2, ZnO, Ag, CNT, Fullerenes) for Different Regions. Environ. Sci. Technol 2009, 43, (24), 9216-9222.
25. Kim, B.; Park, C. S.; Murayama, M.; Hochella, M. F., Discovery and Characterization of Silver Sulfide Nanoparticles in Final Sewage Sludge Products. Environ. Sci. Technol 2010, 44, (19), 7509-7514.
26. Kim, B.; Levard, C. m.; Murayama, M.; Brown, G. E.; Hochella, M. F., Integrated Approaches of X-Ray Absorption Spectroscopic and Electron Microscopic Techniques on Zinc Speciation and Characterization in a Final Sewage Sludge Product. J. Environ. Quality 2014, 43, (3), 908-916.
27. Bureau, U. S. C., Historical Census of Housing Tables: Sewage Disposal. In 1990.
28. Arnade, L. J., Seasonal correlation of well contamination and septic tank distance. Groundwater 1999, 37, (6), 920-923.

29. Paul, J. H.; McLaughlin, M. R.; Griffin, D. W.; Lipp, E. K.; Stokes, R.; Rose, J. B., Rapid movement of wastewater from on-site disposal systems into surface waters in the Lower Florida Keys. Estuaries 2000, 23, (5), 662-668.
30. Clarke, R.; Healy, M. G.; Fenton, O.; Cummins, E., A quantitative risk ranking model to evaluate emerging organic contaminants in biosolid amended land and potential transport to drinking water. Human and Ecological Risk Assessment: An International Journal 2016, 22, (4), 958-990.
31. Boxall, A.; Tiede, K.; Chaudhry, Q.; Aitken, R.; Jones, A.; Jefferson, B.; Lewis, J., Current and future predicted exposure to engineered nanoparticles. Safety of Nanomaterials Interdisciplinary Research Centre Report 2007, 1-13.
32. Barksdale, J., Titanium, its occurrence, chemistry, and technology. Soil Science 1950, 70, (5), 414.
33. Craigie, N., Principles of elemental chemostratigraphy. Advances in Oil and Gas Exploration & Production, Rudy Swennen. A Practical User Guide. p189. DOI: https://doi.org/10.1007/978-3-319-71216-1 2018.
34. Zack, T.; Kronz, A.; Foley, S. F.; Rivers, T., Trace element abundances in rutiles from eclogites and associated garnet mica schists. Chemical Geology 2002, 184, (1-2), 97-122.
35. Gondikas, A.; von der Kammer, F.; Kaegi, R.; Borovinskaya, O.; Neubauer, E.; Navratilova, J.; Praetorius, A.; Cornelis, G.; Hofmann, T., Where is the nano? Analytical approaches for the detection and quantification of TiO_2 engineered nanoparticles in surface waters. Environmental Science: Nano 2018, 5, (2), 313-326.
36. Nabi, M. M.; Wang, J.; Baalousha, M., Episodic surges in titanium dioxide engineered particle concentrations in surface waters following rainfall events. Chemosphere 2021, 263, 128261.
37. U.S. Geological Survey, National Land Cover Database (NLCD) 2011 Edition. In 2014.
38. Bradley, P. M.; Journey, C. A.; Chapelle, F. H.; Lowery, M. A.; Conrads, P. A., Flood hydrology and methylmercury availability in Coastal Plain rivers. Environ. Sci. Technol. 2010, 44, (24), 9285-9290.
39. Feaster, T. D.; Benedict, S. T.; Clark, J. M.; Bradley, P. M.; Conrads, P. A. Scaling up watershed model parameters—Flow and load simulations of the Edisto River Basin, South Carolina, 2007-09; 2328-0328; US Geological Survey: 2014.
40. South Carolina Department of Health and Environmental Control, Watershed Water Quality Assessment - Edisto River Basin.; South Carolina Department of Health and Environmental Control, Bureau of Water: Columbia, South Carolina, 2012.
41. Sowah, R.; Zhang, H.; Radcliffe, D.; Bauske, E.; Habteselassie, M., Evaluating the influence of septic systems and watershed characteristics on stream faecal pollution in suburban watersheds in G eorgia, USA. Journal of applied microbiology 2014, 117, (5), 1500-1512.
42. EPA, Septic Systems Overview In 2021.
43. Wilde, F. D.; Radtke, D. B., Handbooks for Water-resources Investigations: National field manual for the collection of water-quality data. Field measurements. US Department of the Interior, US Geological Survey: 1998.

44. Antignano, A.; Manning, C. E., Rutile solubility in H_2O, H_2O–SiO_2, and H_2O–$NaAlSi_3O_8$ fluids at 0.7–2.0 GPa and 700–1000 C: implications for mobility of nominally insoluble elements. Chemical Geology 2008, 255, (1-2), 283-293.
45. Wilburn, D. R., National Minerals Information Center.
46. Gaspar, J. C.; Wyllie, P. J., Ilmenite (high Mg, Mn, Nb) in the carbonatites from the Jacupiranga complex, Brazil. American Mineralogist 1983, 68, (9-10), 960-971.
47. Lim, K. J.; Engel, B. A.; Tang, Z.; Choi, J.; Kim, K. S.; Muthukrishnan, S.; Tripathy, D., Automated web GIS based hydrograph analysis tool, WHAT. JAWRA Journal of the American Water Resources Association 2005, 41, (6), 1407-1416.
48. U.S. Geological Survey USGS National Water Information System: Mapper (NWISmapper). http://maps.waterdata.usgs.gov/mapper/index.html (January 12, 2016),
49. NIDIS, Drought.gov, https://www.drought.gov/drought/states/south-carolina, (accessed 20 May 2020). In.
50. Bellos, D.; Sawidis, T., Chemical pollution monitoring of the river pinios (Thessalia—Greece). Journal of environmental management 2005, 76, (4), 282-292.
51. Ice, G.; Sugden, B., Summer dissolved oxygen concentrations in forested streams of northern Louisiana. Southern Journal of Applied Forestry 2003, 27, (2), 92-99.
52. Joyce, K.; Todd, R.; Asmussen, L.; Leonard, R., Dissolved oxygen, total organic carbon and temperature relationships in southeastern US coastal plain watersheds. Agricultural Water Management 1985, 9, (4), 313-324.
53. Santhi, C.; Williams, J.; Dugas, W.; Arnold, J.; Srinivsan, R.; Hauck, L. In Water quality modeling of Bosque River Watershed to support TMDL analysis, Total Maximum Daily Load (TMDL): Environmental Regulations, Proceedings of 2002 Conference, 2002; American Society of Agricultural and Biological Engineers: 2002; p 33.
54. Moeller, P.; Paces, T.; Dulski, P.; Morteani, G., Anthropogenic Gd in surface water, drainage system, and the water supply of the city of Prague, Czech Republic. Environmental science & technology 2002, 36, (11), 2387-2394.
55. Knappe, A.; Möller, P.; Dulski, P.; Pekdeger, A., Positive gadolinium anomaly in surface water and ground water of the urban area Berlin, Germany. Geochemistry 2005, 65, (2), 167-189.
56. Oppenheimer, J. A.; Badruzzaman, M.; Jacangelo, J. G., Differentiating sources of anthropogenic loading to impaired water bodies utilizing ratios of sucralose and other microconstituents. Water Research 2012, 46, (18), 5904-5916.
57. Lu, Q.; He, Z. L.; Stoffella, P. J., Land application of biosolids in the USA: A review. Applied and Environmental Soil Science 2012, 2012.
58. Donovan, A. R.; Adams, C. D.; Ma, Y.; Stephan, C.; Eichholz, T.; Shi, H., Single particle ICP-MS characterization of titanium dioxide, silver, and gold nanoparticles during drinking water treatment. Chemosphere 2016, 144, 148-153.
59. Markus, A.; Krystek, P.; Tromp, P.; Parsons, J.; Roex, E.; de Voogt, P.; Laane, R., Determination of metal-based nanoparticles in the river Dommel in the Netherlands via ultrafiltration, HR-ICP-MS and SEM. Science of the total environment 2018, 631, 485-495.
60. Neal, C.; Jarvie, H.; Rowland, P.; Lawler, A.; Sleep, D.; Scholefield, P., Titanium in UK rural, agricultural and urban/industrial rivers: Geogenic and anthropogenic colloidal/sub-colloidal sources and the significance of within-river retention. Sci. Tot. Environ 2011, 409, (10), 1843-1853.

61. Showers, W. J.; Usry, B.; Fountain, M.; Fountain, J.; McDade, T.; DeMaster, D. Nitrate Flux from Ground to Surface Waters Adjacent to the Neuse River Wastewater Treatment Plant; Water Resources Research Institute of the University of North Carolina: 2006.
62. Cortecci, G.; Boschetti, T.; Dinelli, E.; Cidu, R.; Podda, F.; Doveri, M., Geochemistry of trace elements in surface waters of the Arno River Basin, northern Tuscany, Italy. Applied Geochemistry 2009, 24, (5), 1005-1022.
63. Paul, M. J.; Meyer, J. L., Streams in the urban landscape. Ann. Rev. Ecol. Sys 2001, 333-365.
64. Office, S. C. S. C., Climate data of Orangeburg and Aiken County. In.
65. SCDOT, 2019 sverage daily traffic for dorchester county. https://www.scdot.org/travel/pdf/trafficcounts/2019/Dorchester.pdf. In SCDOT Road Data Services: 2021.
66. Corinaldesi, C., Marcellini, F., Nepote, E., Damiani, E. and Danovaro, R. 2018. Impact of inorganic UV filters contained in sunscreen products on tropical stony corals (Acropora spp.). Science of The Total Environment 637-638, 1279-1285.
67. Jovanović, B. and Guzmán, H.M. 2014. Effects of titanium dioxide (TiO_2) nanoparticles on caribbean reef-building coral (Montastraea faveolata). Environmental toxicology and chemistry 33(6), 1346-1353.

Chapter 6

Conclusion

6.1 Conclusion

The overall aim of this PhD dissertation was to develop analytical approaches to overcome the challenges in detecting, quantifying and characterizing ENPs in surface waters focusing on chemical nature, concentration, size and morphology of the nanoparticles, and monitoring titanium dioxide engineered particles in rural and urban surface waters. This overarching goal was achieved by addressing the following specific objectives: 1) evaluating the applicability of elemental ratios (e.g., Ti to Nb, Ce to La, Ti to Fe and Ti to Al) to quantify ENPs in the surface waters; 2) characterizing the elemental composition of Ti-containing particles in the surface waters on a single particle basis using SP-ICP-TOF-MS; 3) quantifying and characterizing TiO_2 engineered nanoparticles in the surface waters; 4) investigating the environmental factors (e.g., rain events, rain intensities, total runoff, draught etc.) determining the occurrence and concentrations of TiO_2 engineered particle concentrations in the surface waters; (5) determining the correlation between TiO_2 engineered particle concentrations, flow discharge, and environmental indicators; (6) evaluating the impact of urbanization on the concentrations of TiO_2 engineered particles in urban surface waters; (7) exploring the relationship between TiO_2 and other contaminant concentrations in a rural river basin with limited urban development (< 1%).

Natural nanoparticles form after weathering of parent rocks, and display similar elemental compositions, associations, and ratios as those of the parent rocks. Therefore, characterization of naturally occurring Ti-containing particles by single particle-inductively coupled plasma-mass spectrometer (SP-ICP-TOF-MS) demonstrated that natural Ti-particles contain other elements such as Al, Si, Fe, Mn, Ce, La, Zr, Nb, Pb, Ba,

Th, Ta, W, and U. These natural elemental impurities are typically removed from the natural Ti-containing minerals by dissolution and reprecipitation during the manufacturing of TiO_2 engineered particles. Therefore, mobilization of TiO_2 engineered particles with urban runoff to receiving surface waters increased the elemental ratios of Ti to the elements naturally associated with Ti-containing minerals. Therefore, the concentrations of TiO_2 engineered particle were estimated by mass balance calculations using total titanium concentrations and increases in Ti/Nb ratios above the natural background ratios in the surface waters. The overall conclusions of these studies are summarized below:

6.1.1 Summary of findings

Characterizing and quantifying the concentrations of titanium dioxide engineered particles in the Broad River, Columbia, South Carolina, United States during and following rainfall events in 2018 and offering a methodological framework for monitoring titanium-based nanoparticles in complex surface water and environmental matrices:

1. Identifying the natural background of elemental ratio of Ti/Nb is quite complicated for large urban rivers such as the Broad River, because there are many sources of TiO_2 engineered particles release to surface waters in large urban rivers such as urban runoff, sewage spills, wastewater treatment effluent, and resuspension of contaminated sediment
2. The continuous introduction of TiO_2 engineered particles into surface waters result in a shift in the natural elemental ratios toward higher values. The elemental ratio of Ti/Nb in the Broad River ranged from 330 to 565 and followed the same trend

of rise and fall as the discharge/runoff, suggesting introduction of TiO_2 engineered particle to the Broad River water with urban runoff.

3. The TiO_2 engineered particle concentrations varied between 20 and 140 µg L^{-1} during the sampled events. which are in the same order of magnitude as the predicted no effect concentration (PNEC) for TiO_2 pigments (*e.g.*, 127-184 µg L^{-1}) and is higher than the PNEC for TiO_2 ENPs to freshwater organisms (*e.g.*, 1-18 µg L^{-1}). Transport of TiO_2 engineered particles with river water to the ocean could also pose a significant risk for coral reefs. TiO_2 ENPs have been shown to bioaccumulate in microflora and induce coral bleaching, which could contribute to an overall decrease in coral populations.

The temporal variability in the concentration of TiO_2 engineered particles in the Broad River, Columbia, South Carolina, United States during dry and wet weather conditions in 2019 and examining the relationship between flow discharge, water quality indicators, and the concentration of TiO_2 engineered particles:

1. This study provides the basis for comprehensive investigation of nonpoint TiO_2 engineered particle release and concentrations in urban rivers during rainfall events.
2. The elemental concentrations, TiO_2 engineered particle concentrations, number concentration of the total-, single metal -, and multi-metal -Ti-bearing particles, and the relative abundance of single metal particles displayed temporal variability and increased with increases in runoff following rainfall events
3. A strong linear relationship was established between turbidity and TiO_2 engineered particle concentration. This relationship is important because it can be used as a

substitute for the TiO_2 engineered particle concentration determination within the catchment area.

The impact of urbanization on the concentrations of TiO_2 engineered particles in urban surface waters in 2020:

1. The daily monitoring of the total elemental concentrations, bulk elemental ratios, the number particle concentration, and the multi-element composition of single particles in the Saluda-Broad-Congaree Rivers' ecosystem highlights the presence, transient nature, and transport of anthropogenic TiO_2 engineered particle in this urban river ecosystem.
2. The concentration of anthropogenic TiO_2 increased following the order 0 to 24 µg L^{-1} in the Lower Saluda River < 0 to 663 µg L^{-1} in the Broad River < 43 to 1051 µg L^{-1} in Congaree River at Cayce <58 to 5050 µg L^{-1} in the Congaree River at Columbia. The concentration of anthropogenic TiO_2 increased with increases in urban runoff. The source of anthropogenic TiO_2 was attributed to diffuse urban runoff.
3. Clustering of multi-metal nanoparticles (mmNPs) demonstrated that Ti-bearing particles were distributed mainly among three clusters, FeTiMn, AlSiFe, and TiMnFe, which are typical of naturally occurring iron oxide, clay, and titanium oxide particles. Thus, anthropogenic Ti concentration was attributed to single-metal nanoparticles, pure TiO_2 particles.
4. The high TiO_2 engineered particle concentrations in the Broad-Congaree Rivers may pose environmental risk in this River ecosystem, and in other urban rivers, during and following rainfall events, in particular at and near peak discharge.

Higher concentrations of TiO_2 engineered particles, and thus higher environmental risks, can be expected in more highly urbanized watersheds than the studied urban river ecosystem.

The seasonal variability in TiO_2 engineered particles concentrations between 2017 and 2020 to explore the relationship between TiO_2 and other contaminant concentrations in the rural Edisto River in South Carolina, United States with limited urban development (< 1%):

1. This study is the first to characterize and quantify engineered particles in a river reach draining a rural watershed with less than 1% urban land cover and concomitantly few WWTP point-source discharges. Long term monitoring of the concentration of TiO_2 engineered particles in rural Edisto River reach with fewer potential sources of TiO_2 engineered particles is useful to establish the background natural Ti to Nb ratio. The elemental ratio of Ti to Nb in the Edisto River varied from 256 to 465. Since, the lowest measured elemental ratio of Ti to Nb occurred in the absence of runoff and precipitation contribution during the draught period of summer 2019, this Ti/Nb elemental ratio (*e.g.*, 256) is established as the natural background ratio to calculate natural and anthropogenic Ti concentrations by mass-balance calculations.
2. The Edisto River stream TiO_2 engineered particle concentration ranged from 0 to 129 µg L^{-1}. The concentrations of TiO_2 engineered particle increased during the spring and summer seasons and decreased during the fall and winter seasons, which coincided with increases and decreases in phosphorous, nitrogen, ammonia, organic carbon, anthropogenic Gd.

3. The source of TiO_2 load was not specifically identified but is most likely to result from biosolid application on agricultural land in the region because: (**i)** WWTP effluent and by-pass sewage spills are likely to be a small contributor to TiO_2 concentrations in the Edisto River *i.e.*, < 4% of the Edisto River discharge, (**ii)** no seasonal pattern in effluent discharge and by-pass events was observed during the study period, **(iii)** the increase in TiO_2 concentrations during the spring and summer, which coincides with the agriculture season and with the application of biosolids on agricultural fields, and (**iv)** the co-occurrence of TiO_2 with agriculture runoff and wastewater related contaminants such as nutrients and anthropogenic gadolinium, respectively.

The design of these studies highlights the importance of selecting sampling sites and monitoring the spatiotemporal variations in engineered particle concentrations in surface waters for a more comprehensive understanding of the environmental fate, behavior, and risk assessment of engineered particles.

6.2 Outlook

The overall outcome of these results suggests that the characterization of ENPs is complex and cannot be described by quantifying the elemental bulk concentration of NPs in the environmental compartments, that had been the approach adopted in many studies in the literature. Rather, ENP should be characterized by identifying and taking into account both the bulk and natural NPs concentration in the complex environmental matrices including surface waters.

There are episodic surges in titanium dioxide engineered particle concentrations in surface water during and following rainfall events as discussed above. Additional research is needed to further understand the impact of rainfall characteristics and the hydrogeological factors on the higher resolution temporal variability in TiO_2 engineered particle concentrations in surface waters. Further research is needed on the occurrence and temporal variability in TiO_2 engineered particle concentrations in the riverbed sediments to further understand the fate of TiO_2 engineered particle concentrations in river stream. High frequency sampling could be carried out during recreational activities in a lake to evaluate the real time dispersity of TiO_2 ENP substances in a dynamic environmental system. This could help understanding the representativeness of the grabbed samples for NP studies to the system as a whole at a given point of time. Better sampling representativeness could be obtained by using sampling schemes that integrate across multiple widths and depths of the stream cross section as well.

Considering the strong linear relationship found between turbidity and TiO_2 engineered particle concentrations in our study, future studies should attempt to extend this finding to other sites incorporating required site parameterization of the turbidity-TiO_2 linear relationship as this correlation is likely to be site specific. Although turbidity measurement is cost effective and quicker than TiO_2 engineered particle measurement, there is a need to collect higher time resolution data (*e.g.*, minutes to hours) in order to improve the understanding of the turbidity-TiO_2 relationship. The findings from this study can be employed to develop management strategies to control rainwater pollution at the catchment level.

Considering the wide range of TiO_2 engineered particle concentrations in the surface waters, future studies should investigate the impact of these TiO_2 engineered particles on river organisms, including investigating the effect of TiO_2 engineered particles on several organisms in the trophic chain using environmentally relevant concentrations and considering frequent pulse *vs.* chromic exposure. To provide even a more detailed understanding of TiO_2 engineered particle fate and transport in stream water ecosystems, future studies could include additional sampling sites, collect samples at higher time resolution or over longer sampling periods, collect data following storm events with various intensities and antecedent dry periods, collect and analyze sediments samples to determine particle sedimentation and deposition in the river system.

The dissertation research described in this thesis is a valuable contribution to the field of environmental TiO_2 ENP characterization. SP-ICP-TOF-MS proved to be a valuable tool in each of these projects and is expected to continue advancing this area of research in future work.

References

1. Zänker, H. & Schierz, A. Engineered Nanoparticles and Their Identification Among Natural Nanoparticles. Annu. Rev. Anal. Chem. 5, 107–132 (2012).
2. Mrowiec, B. Nanomaterials in the environment. E3S Web of Conferences 22, (2017).
3. EPA. Nanotechnology for site remediation fact sheet. Solid waste and emergency response. (2008).
4. Huang, S. H. & Chen, D. H. Rapid removal of heavy metal cations and anions from aqueous solutions by an amino-functionalized magnetic nano-adsorbent. J. Hazard. Mater. 163, 174–179. (2009).
5. Buzea, C., Pacheco Blandino, I. I. & Robbie, K. Nanomaterials and nanoparticles: Sources and toxicity. Biointerphases 2, (2007).
6. Benn, T., Cavanagh, B., Hristovski, K., Posner, J. D. & Westerhoff, P. The release of nanosilver from consumer products used in the home. J. Environ. Qual. 39, 1875–1882 (2010).
7. Baalousha, D. M. Developing Analytical Methods for the Detection and Quantification of Engineered Nanoparticle Release in Complex Environmental Matrices. (2017). Available at: https://calendar.buffalo.edu/event/171117ewrebaalousha/.
8. Cision. Titanium Dioxide (TiO_2) - A Global Market Overview. (2016).
9. Loosli, F. et al. Sewage spills are a major source of titanium dioxide engineered (nano)-particle release into the environment. Environ. Sci. Nano 6, 763–777 (2019).
10. Piccinno, F., Gottschalk, F., Seeger, S. & Nowack, B. Industrial production quantities and uses of ten engineered nanomaterials in Europe and the world. J. Nanoparticle Res. 14, 1109 (2012).
11. Peters, R. J. B. et al. Detection of nanoparticles in Dutch surface waters. Sci. Total Environ. 621, 210–218 (2018).
12. Coatingsworld. Demand for Paint and coatings to reach 1.4 Billion Gallons in 2019 | Statista. (2019). Available at: https://www.statista.com/statistics/684695/united-states-paint-and-coatings-demand-by-market/. (Accessed: 22nd April 2020)
13. Grand View Research. No Title. (2018). Available at: https://www.grandviewresearch.com/industry-analysis/%0Atraffic-road-marking-coatings-market/request. (Accessed: 22nd April 2020)
14. ASTM. ASTM D7942 - 15 Standard Specification for Thermoplastic Pavement Markings in Non Snow Plow Areas. (2015). Available at: https://www.astm.org/Standards/D7942.htm. (Accessed: 22nd April 2020)
15. Weir, A., Westerhoff, P., Fabricius, L., Hristovski, K. & von Goetz, N. Titanium Dioxide Nanoparticles in Food and Personal Care Products. Environ. Sci. Technol. 46, 2242–2250 (2012).
16. Linak, E. & Inoguchi, Y. Chemical Economics Handbook: Titanium Dioxide. (SRI Consulting, Menlo Park, 2005).

17. Wang, J. et al. Detection and quantification of engineered particles in urban runoff. Chemosphere 248, 126070 (2020).
18. Baalousha, M. et al. Stormwater green infrastructures retain high concentrations of TiO_2 engineered (nano)-particles. J. Hazard. Mater. 392, 122335 (2020).
19. Westerhoff, P., Song, G., Hristovski, K. & Kiser, M. A. Occurrence and removal of titanium at full scale wastewater treatment plants: Implications for TiO_2 nanomaterials. J. Environ. Monit. 13, 1195–1203 (2011).
20. Nowack, B. & Mueller, N. C. Exposure modeling of engineered nanoparticles in the environment. EMPA Act. 41, 63 (2008).
21. Lützhøft, H., Hartmann, N., Brinch, A. & Kjølholt, J. Environmental Effects of Engineered Nanomaterials: Estimations of Predicted No-Effect Concentrations (PNECs). (2015).
22. Dahle, J. T. & Arai, Y. Environmental geochemistry of cerium: applications and toxicology of cerium oxide nanoparticles. Int. J. Environ. Res. Public Health 12, 1253–1278 (2015).
23. Dale, J. G., Cox, S. S., Vance, M. E., Marr, L. C. & Hochella, M. F. Transformation of Cerium Oxide Nanoparticles from a Diesel Fuel Additive during Combustion in a Diesel Engine. Environ. Sci. Technol. 51, 1973–1980 (2017).
24. Dahle, J. T. & Arai, Y. Environmental geochemistry of cerium: Applications and toxicology of cerium oxide nanoparticles. International Journal of Environmental Research and Public Health 12, 1253–1278 (2015).
25. Gottschalk, F., Sun, T. & Nowack, B. Environmental concentrations of engineered nanomaterials: Review of modeling and analytical studies. Environ. Pollut. 181, 287–300 (2013).
26. Balusamy, B. & Uyar, T. Toxicity of lanthanum oxide (La_2O_3) nanoparticles in aquatic environments. Environ. Sci. Process. Impacts (2015). doi:10.1039/C5EM00035A
27. Cao, J. et al. Controllable syntheses of hexagonal and lamellar mesostructured lanthanum oxide. Mater. Lett. 59, 408–411 (2005).
28. Blay, V. et al. Engineering zeolites for catalytic cracking to light olefins. ACS Catal. 7, 6542–6566 (2017).
29. VA: U.S. Geological Survey (USGS), U. W. S. S. R. Runoff: Surface and Overland Water Runoff. Available at: https://www.usgs.gov/special-topic/water-science-school/science/runoff-surface-and-overland-water-runoff?qtscience_center_objects=0#qt-science_center_objects. (Accessed: 30th April 2019)
30. He, W., Odnevall Wallinder, I. & Leygraf, C. A laboratory study of copper and zinc runoff during first flush and steady-state conditions. Corros. Sci. 43, 127–146 (2001).
31. Nabi, M. M., Wang, J. & Baalousha, M. Episodic increases in titanium dioxide engineered particle concentrations in the Broad River following rainfall events (In Preparation). (2020).
32. Parker, N. & Keller, A. A. Variation in regional risk of engineered nanoparticles: nano TiO_2 as a case study. Environ. Sci. Nano 6, 444–455 (2019).
33. Onderka, M., Krein, A., Wrede, S., Martínez-Carreras, N. & Hoffmann, L. Dynamics of storm-driven suspended sediments in a headwater catchment described by multivariable modeling. J. Soils Sediments 2012 124 12, 620–635 (2012).
34. Chemours Titanium Dioxide For Coating; 18.

35. Vercruysse, K. & Grabowski, R. C. Temporal variation in suspended sediment transport: linking sediment sources and hydro-meteorological drivers. Earth Surf. Process. Landforms 44, 2587–2599 (2019).
36. Vercruysse, K., Grabowski, R. C. & Rickson, R. J. Suspended sediment transport dynamics in rivers: Multi-scale drivers of temporal variation. Earth-Science Rev. 166, 38–52 (2017).
37. Smail, E. A., Webb, E. A., Franks, R. P., Bruland, K. W. & Sañudo-Wilhelmy, S. A. Status of Metal Contamination in Surface Waters of the Coastal Ocean off Los Angeles, California since the Implementation of the Clean Water Act. Environ. Sci. Technol. 46, 4304–4311 (2012).
38. Neal, C. et al. Titanium in UK rural, agricultural and urban/industrial rivers: Geogenic and anthropogenic colloidal/sub-colloidal sources and the significance of within-river retention. Sci. Total Environ. 409, 1843–1853 (2011).
39. Markus, A. A.; Krystek, P.; Tromp, P. C.; Parsons, J. R.; Roex, E. W. M.; Voogt, P. d.; Laane, R. W. P. M. Determination of metal-based nanoparticles in the river Dommel in the Netherlands via ultrafiltration, HR-ICP-MS and SEM. Sci. Tot. Environ. **2018,** 631-632, 485-495.
40. Taylor, K. G. & Owens, P. N. Sediments in urban river basins: A review of sediment-contaminant dynamics in an environmental system conditioned by human activities. Journal of Soils and Sediments 9, 281–303 (2009).
41. Smith, I. M., Hall, K. J., Lavkulich, L. M. & Schreier, H. Trace metal concentrations in an intensive agricultural watershed in British Columbia, Canada. J. Am. Water Resour. Assoc. 43, 1455–1467 (2007).
42. Yang, Y. et al. Metal and nanoparticle occurrence in biosolid-amended soils. Sci. Total Environ. 485–486, 441–449 (2014).
43. De La Rosa, G., Laura López-Moreno, M., Hernandez-Viezcas, J., Montes, M. O. & Peralta-Videa, J. R. Toxicity and biotransformation of ZnO nanoparticles in the desert plants Prosopis juliflora-velutina, Salsola tragus and Parkinsonia florida. Int. J. Nanotechnol 8,
44. Judy, J. D. & Bertsch, P. M. Bioavailability, Toxicity, and Fate of Manufactured Nanomaterials in Terrestrial Ecosystems. in Advances in Agronomy 123, 1–64 (Academic Press Inc., 2014).
45. Kim, B., Murayama, M., Colman, B. P. & Hochella, M. F. Characterization and environmental implications of nano- and larger TiO_2 particles in sewage sludge, and soils amended with sewage sludge. J. Environ. Monit. 14, 1129–1137 (2012).
46. US EPA. Biosolids Generation, Use, and Disposal in The United States. (US EPA Washington, DC, USA, 1999).
47. North East Biosolids and Residuals Association (NEBRA). A national biosolids regulation, quality, end use & disposal survey. Final report. Tamworth (NH). (2007).
48. Baertsch, C., Paez-Rubio, T., Viau, E. & Peccia, J. Source tracking aerosols released from land-applied class B biosolids during high-wind events. Appl. Environ. Microbiol. 73, 4522–4531 (2007).
49. Tou, F. et al. Environmental Risk Implications of Metals in Sludges from Waste Water Treatment Plants: The Discovery of Vast Stores of Metal-Containing Nanoparticles. Environ. Sci. Technol. 51, 4831–4840 (2017).

50. Martínez, F., Casermeiro, M. A., Morales, D., Cuevas, G. & Walter, I. Effects on run-off water quantity and quality of urban organic wastes applied in a degraded semi-arid ecosystem. Sci. Total Environ. 305, 13–21 (2003).
51. Westerhoff, P. et al. Characterization, Recovery Opportunities, and Valuation of Metals in Municipal Sludges from U.S. Wastewater Treatment Plants Nationwide. Environ. Sci. Technol. 49, 9479–9488 (2015).
52. You, G. et al. Investigation of the rheological behavior of activated sludge in response to CeO_2 nanoparticles and potential mechanism. Environ. Sci. Pollut. Res. 25, 29725–29733 (2018).
53. Kim, B., Park, C. S., Murayama, M. & Hochella, M. F. Discovery and characterization of silver sulfide nanoparticles in final sewage sludge products. Environ. Sci. Technol. 44, 7509–7514 (2010).
54. Gottschalk, F., Sonderer, T., Scholz, R. W. & Nowack, B. Modeled environmental concentrations of engineered nanomaterials (TiO_2, ZnO, Ag, CNT, fullerenes) for different regions. Environ. Sci. Technol. 43, 9216–9222 (2009).
55. Rand, L. N. et al. Quantifying temporal and geographic variation in sunscreen and mineralogic titanium-containing nanoparticles in three recreational rivers. Sci. Total Environ. 743, 140845 (2020).
56. Bureau, U. C. Historical Census of Housing Tables: Sewage Disposal. (1990).
57. Arnade, L. J. Seasonal Correlation of Well Contamination and Septic Tank Distance. Ground Water 37, 920–923 (1999).
58. Paul, J. H. et al. Rapid movement of wastewater from on-site disposal systems into surface waters in the Lower Florida Keys. Estuaries 23, 662–668 (2000).
59. Boxall, A. et al. Current and future predicted environmental exposure to engineered nanoparticles. (Central Science Laboratory, 2007).
60. Clarke, R., Healy, M. G., Fenton, O. & Cummins, E. A quantitative risk ranking model to evaluate emerging organic contaminants in biosolid amended land and potential transport to drinking water. http://dx.doi.org/10.1080/10807039.2015.1121376 22, 958–990 (2016).
61. Westerhoff, P. et al. Low risk posed by engineered and incidental nanoparticles in drinking water. Nat. Nanotechnol. 13, 661–669 (2018).
62. Gondikas, A. P. et al. Release of TiO_2 Nanoparticles from Sunscreens into Surface Waters: A One-Year Survey at the Old Danube Recreational Lake. Environ. Sci. Technol. 48, 5415–5422 (2014).
63. Nakashima, K. & Imaoka, T. Niobian and Zincian ilmenites in syenites from Cape Ashizuri, Southwest Japan. Miner. Pet. 63, 1–17 (1998).
64. José, C. G. . & Wyllie, P. J. Ilmenite (high Mg, Mn, Nb) in the carbonatites from the Jacupiranga complex, Brazil. Am. Miner. 68, 960–971 (1983).
65. Praetorius, A. et al. Single-particle multi-element fingerprinting (spMEF) using inductively-coupled plasma time-of-flight mass spectrometry (ICP-TOFMS) to identify engineered nanoparticles against the elevated natural background in soils. Environ. Sci. Nano 4, 307–314 (2017).
66. Laycock, A., Coles, B., Kreissig, K. & Rehkämper, M. High precision 142 Ce/ 140 Ce stable isotope measurements of purified materials with a focus on CeO_2 nanoparticles. J. Anal. At. Spectrom. 31, 297–302 (2016).

67. Salminen, R. et al. FOREGS Geochemical Atlas of Europe, Part I* Background Information, Methodology, and Maps. Geol. Surv. Finland, Espoo (2005).
68. Yi, Z., Loosli, F., Wang, J., Berti, D. & Baalousha, M. How to distinguish natural versus engineered nanomaterials: insights from the analysis of TiO_2 and CeO_2 in soils. Environ. Chem. Lett. 18, 215–227 (2020).
69. Gallego-Hernández, A. L. et al. Identification of inhalable rutile and polycyclic aromatic hydrocarbons (PAHs) nanoparticles in the atmospheric dust. Environ. Pollut. 260, 114006 (2020).
70. Pradas Del Real, A. E. et al. Searching for relevant criteria to distinguish natural vs. anthropogenic TiO_2 nanoparticles in soils. Environ. Sci. Nano 5, 2853–2863 (2018).
71. Wagner, S., Gondikas, A., Neubauer, E., Hofmann, T. & von der Kammer, F. Spot the Difference: Engineered and Natural Nanoparticles in the Environment-Release, Behavior, and Fate. Angew. Chemie Int. Ed. 53, n/a-n/a (2014).
72. Regelink, I. C., Weng, L., Koopmans, G. F. & van Riemsdijk, W. H. Asymmetric flow field-flow fractionation as a new approach to analyse iron-(hydr)oxide nanoparticles in soil extracts. Geoderma 202–203, 134–141 (2013).
73. Hamon, R. E. et al. Geochemical indices allow estimation of heavy metal background concentrations in soils. Global Biogeochem. Cycles 18, n/a-n/a (2004).
74. Müller, A.; Österlund, H.; Marsalek, J.; Viklander, M. The pollution conveyed by urban runoff: A review of sources. Sci. Tot. Environ. **2020,** 709, 136125.
75. Kiser, M. A.; Westerhoff, P.; Benn, T.; Wang, Y.; Perez-Rivera, J.; Hristovski, K. Titanium nanomaterial removal and release from wastewater treatment plants. Environ. Sci. Technol. **2009,** 43, 6757-6763.
76. Reed, R. B.; Martin, D. P.; Bednar, A. J.; Montano, M. D.; Westerhoff, P.; Ranville, J. F. Multi-day diurnal measurements of Ti-containing nanoparticle and organic sunscreen chemical release during recreational use of a natural surface water. Environ. Sci. Nano. **2017,** 4 (1), 69-77.
77. Baalousha, M.; Yang, Y.; Vance, M. E.; Colman, B. P.; McNeal, S.; Xu, J.; Blaszczak, J.; Steele, M.; Bernhardt, E.; Hochella JR, M. F. Outdoor urban nanomaterials: The emergence of a new, integrated, and critical field of study. Sci. Tot. Environ. **2016,** 557-558, 740-753.
78. Gohler, D.; Stintz, M.; Hillemann, L.; Vorbau, M. Characterization of nanoparticle release from surface coatings by the simulation of a sanding process. Annal. Occup. Hygiene. **2010,** 54 (6), 615-624.
79. Koponen, I. K.; Jensen, K. A.; Schneider, T. Comparison of dust released from sanding conventional and nanoparticle-doped wall and wood coatings. J. Expos. Sci. Environ. Epidemiol. **2011,** 21 (4), 408-418.
80. Nored, A. W.; Chalbot, M. C.; Kavouras, I. G. Characterization of paint dust aerosol generated from mechanical abrasion of TiO_2 -containing paints. J. Occup. Environ. Hyg. **2018,** 15 (9), 629-640.
81. Gondikas, A.; von der Kammer, F.; Kaegi, R.; Borovinskaya, O.; Neubauer, E.; Navratilova, J.; Praetorius, A.; Cornelis, G.; Hofmann, T. Where is the nano? Analytical approaches for the detection and quantification of TiO_2 engineered nanoparticles in surface waters. Environ. Sci. Nano. **2018,** 5 (2), 313-326.
82. Barksdale, J. Titanium, its occurrence, chemistry, and technology. Soil Sci. **1950,** 70 (5), 414.

83. Craigie, N. Principles of elemental chemostratigraphy: a practical user guide; Springer International Publishing: Cham, Switzerland, 2018.
84. Zack, T.; Kronz, A.; Foley, S. F.; Rivers, T. Trace element abundances in rutiles from eclogites and associated garnet mica schists. Chem. Geol. **2002,** 184 (1-2), 97-122.
85. NC DEQ Broad River basin restoration priorities; 09.
86. Stewart, S. R.; Berg, R. HURRICANE FLORENCE;AL062018; National Hurricane Center: May 30, 19.
87. Hendriks, L.; Gundlach-Graham, A.; Hattendorf, B.; Günther, D. Characterization of a new ICP-TOFMS instrument with continuous and discrete introduction of solutions. J. Anal. At. Spectrom. **2017,** 32 (3), 548-561.
88. Pace, H. E.; Rogers, N. J.; Jarolimek, C.; Coleman, V. A.; Higgins, C. P.; Ranville, J. F. Determining Transport Efficiency for the Purpose of Counting and Sizing Nanoparticles via Single Particle Inductively Coupled Plasma Mass Spectrometry. Anal. Chem. **2011,** 83 (24), 9361-9369.
89. Tanner, M. Shorter signals for improved signal to noise ratio, the influence of Poisson distribution. J. Anal. Atom. Spectrom. **2010,** 25 (3), 405-407.
90. Antignano, A.; Manning, C. E. Rutile solubility in H_2O, H_2O-SiO_2, and H_2O-$NaAlSi_3O_8$ fluids at 0.7-2.0 GPa and 700-1000 ºC: Implications for mobility of nominally insoluble elements. Chem. Geol. **2008,** 255 (1), 283-293.
91. USGS Mineral Commodity Summaries 2019: US Geological Survey; U.S. Geological Survey: 19.
92. Lim, K. J.; Engel, B. A.; Tang, Z.; Choi, J.; Kim, K.-S.; Muthukrishnan, S.; Tripathy, D. Automated web GIS based hydrograph analysis tool, WHAT. J. Am. Wat. Res. Assoc. **2005,** 41 (6), 1407-1416.
93. Galfi, H.; Österlund, H.; Marsalek, J.; Viklande, M. Mineral and Anthropogenic Indicator Inorganics in Urban Stormwater and Snowmelt Runoff: Sources and Mobility Patterns. Water. Air. Soil Pollut. **2017,** 228 (7), 1-18.
94. Tian, P.; Li, Y.; Yang, Z. Effect of rainfall and antecedent dry periods on heavy metal loading of sediments on urban roads. Front. Earth Sci. China. **2009,** 3 (3), 297-302.
95. Yuan, Q.; Guerra, H.; Kim, Y. An investigation of the relationships between rainfall conditions and pollutant wash-off from the paved road. Water **2017,** 9 (4), 232.
96. Pereira, E.; Baptista-Neto, J. A.; Smith, B. J.; McAllister, J. J. The contribution of heavy metal pollution derived from highway runoff to Guanabara Bay sediments - Rio de Janeiro / Brazil. An. Acad. Bras. Cienc. **2007,** 79 (4), 739-750.
97. Schiff, K. C.; Tiefenthaler, L. L. Anthropogenic versus natural mass emissions from an urban watershed. Southern California Coastal Water Research Project, Annual Report, Long Beach California USA. In Southern California Coastal Water Research Project Annual Report 1999-2000. WeisbergS., Elmore, D., Eds.; Southern California Coastal Water Research Project: Westminster, CA, 2001; pp 63-70.
98. Shandilya, N.; Le Bihan, O.; Bressot, C.; Morgeneyer, M. Emission of Titanium Dioxide Nanoparticles from Building Materials to the Environment by Wear and Weather. Environ. Sci. Technol. **2015,** 49 (4), 2163-2170.
99. Lee, P. K.; Yu, S.; Chang, H. J.; Cho, H. Y.; Kang, M. J.; Chae, B. G. Lead chromate detected as a source of atmospheric Pb and Cr (VI) pollution. Sci. Rep. **2016,** 6, 36088.

100. Wilczynska-Michalik, W.; Rzeznikiewicz, K.; Pietras, B.; Michalik, M. Fine and ultrafine TiO_2 particles in aerosol in Krakow (Poland). Mineralogia **2014,** 45 (3-4), 65-77.
101. Donovan, A. R.; Adams, C. D.; Ma, Y.; Stephan, C.; Eichholz, T.; Shi, H. Single particle ICP-MS characterization of titanium dioxide, silver, and gold nanoparticles during drinking water treatment. Chemosphere **2016,** 144, 148-153.
102. Verplanck, P. L.; Furlong, E. T.; Gray, J. L.; Phillips, P. J.; Wolf, R. E.; Esposito, K. Evaluating the Behavior of Gadolinium and Other Rare Earth Elements through Large Metropolitan Sewage Treatment Plants. Environ. Sci. Technol. **2010,** 44 (10), 3876-3882.
103. Horowitz, A. J.; Elrick, K. A.; Smith, J. J. Monitoring urban impacts on suspended sediment, trace element, and nutrient fluxes within the City of Atlanta, Georgia, USA: program design, methodological considerations, and initial results. Hydrol. Process. An Int. J. **2008,** 22 (10), 1473-1496.
104. Jovanovic, B.; Guzman, H. M. Effects of titanium dioxide (TiO_2) nanoparticles on caribbean reef-building coral (Montastraea faveolata). Environ. Toxicol. Chem. **2014,** 33 (6), 1346-1353.
105. Coatingsworld. U.S. Demand for Paint & Coatings to Reach 1.4 Billion Gallons in 2019., 2019.
106. Adamiec E. Road environments: impact of metals on human health in heavily congested cities of Poland. International journal of environmental research and public health 2017; 14: 697.
107. Azimzada A, Jreije I, Hadioui M, Shaw P, Farner JM, Wilkinson KJ. Quantification and Characterization of Ti-, Ce-, and Ag-Nanoparticles in Global Surface Waters and Precipitation. Environmental Science & Technology 2021; 55: 9836-9844.
108. Wang J-L, Alasonati E, Fisicaro P, Benedetti MF. Titanium nanoparticles fate in small-sized watersheds under different land-uses. Journal of Hazardous Materials 2022; 422: 126695.
109. Nabi MM, Wang J, Baalousha M. Episodic surges in titanium dioxide engineered particle concentrations in surface waters following rainfall events. Chemosphere 2021a; 263: 128261.
110. SCdhec. Watershed water quality assessment. Broad Rriver basin., Columbia, S.C., 2007.
111. CPC. National weather services. Climate Prediction Center. https://www.cpc.ncep.noaa.gov/. Accessed 19/4/2020.
112. Loosli F, Wang J, Rothenberg S, Bizimis M, Winkler C, Borovinskaya O, et al. Sewage spills are a major source of titanium dioxide engineered (nano)-particle release into the environment. Environmental Science: Nano 2019; 6: 763-777.
113. Nabi MM, Wang J, Meyer M, Croteau M-N, Ismail N, Baalousha M. Concentrations and size distribution of TiO_2 and Ag engineered particles in five wastewater treatment plants in the United States. Science of The Total Environment 2021b; 753: 142017.
114. Istok J, Boersma L. Effect of antecedent rainfall on runoff during low-intensity rainfall. Journal of Hydrology 1986; 88: 329-342.
115. Penna D, Tromp-van Meerveld H, Gobbi A, Borga M, Dalla Fontana G. The influence of soil moisture on threshold runoff generation processes in an alpine headwater catchment. Hydrology and Earth System Sciences 2011; 15: 689-702.

116. Chen H, Chang H. Response of discharge, TSS, and E. coli to rainfall events in urban, suburban, and rural watersheds. Environmental Science: Processes & Impacts 2014; 16: 2313-2324.
117. Lewis J. Turbidity-controlled suspended sediment sampling for runoff-event load estimation. Water resources research 1996; 32: 2299-2310.
118. Patil S, Barfield B, Wilber G. Turbidity modeling based on the concentration of total suspended solids for stormwater runoff from construction and development sites. World Environmental and Water Resources Congress 2011: Bearing Knowledge for Sustainability, 2011, pp. 477-486.
119. Chanson H, Takeuchi M, Trevethan M. Using turbidity and acoustic backscatter intensity as surrogate measures of suspended sediment concentration in a small subtropical estuary. Journal of environmental management 2008; 88: 1406-1416.
120. Mosbrucker A. High resolution digital elevation model of Mount St. Helens Crater and Upper North Fork Toutle River Basin, Washington, based on an Airborne LiDAR survey of September 2009: US Department of the Interior, US Geological Survey, 2014.
121. Uhrich MA, Bragg HM. Monitoring instream turbidity to estimate continuous suspended-sediment loads and yields and clay-water volumes in the upper North Santiam River Basin, Oregon, 1998-2000. Vol 3: US Department of the Interior, US Geological Survey, 2003.
122. Wass P, Marks S, Finch J, Leeks GJL, Ingram J. Monitoring and preliminary interpretation of in-river turbidity and remote sensed imagery for suspended sediment transport studies in the Humber catchment. Science of the Total Environment 1997; 194: 263-283.
123. Hussain J, Husain I, Arif M, Gupta N. Studies on heavy metal contamination in Godavari river basin. Applied Water Science 2017; 7: 4539-4548.
125. Sakson G, Brzezinska A, Zawilski M. Emission of heavy metals from an urban catchment into receiving water and possibility of its limitation on the example of Lodz city. Environmental monitoring and assessment 2018; 190: 1-15.
126. Rudnick R, Gao S, Holland H, Turekian K. Composition of the continental crust. The crust 2003; 3: 1-64.
127. Baalousha M, Wang J, Erfani M, Goharian E. Elemental fingerprints in natural nanomaterials determined using SP-ICP-TOF-MS and clustering analysis. Science of The Total Environment 2021; 792: 148426.
128. Daphne LHX, Utomo HD, Kenneth LZH. Correlation between turbidity and total suspended solids in Singapore rivers. Journal of Water Sustainability 2011; 1: 313-322.
129. Packman J, Comings K, Booth D. Using turbidity to determine total suspended solids in urbanizing streams in the Puget Lowlands. 1999.
130. Sun H, Cornish PS, Daniell T. Turbidity-based erosion estimation in a catchment in South Australia. Journal of Hydrology 2001; 253: 227-238.
131. Weibel R. Alteration of detrital Fe-Ti oxides in Miocene fluvial deposits, central Jutland, Denmark. Bulletin of the Geological Society of Denmark 2003; 50: 141-208.
132. Morad S, Adin Aldahan A. Alteration of detrital Fe-Ti oxides in sedimentary rocks. Geological Society of America Bulletin 1986; 97: 567-578.
133. Morad S. SEM study of authigenic rutile, anatase and brookite in Proterozoic sandstones from Sweden. Sedimentary Geology 1986; 46: 77-89.

134. Mücke A, Chaudhuri JB. The continuous alteration of ilmenite through pseudorutile to leucoxene. Ore geology reviews 1991; 6: 25-44.
135. Kammer, F. von der et al. Analysis of engineered nanomaterials in complex matrices (environment and biota): General considerations and conceptual case studies. Environ. Toxicol. Chem. 31, 32–49 (2012).
136. Coatingsworld. Paint and coatings demand by market U.S. 2019 | Statista. (2019). Available at: https://www.statista.com/statistics/684695/united-states-paint-and-coatings-demand-by-market/. (Accessed: 22nd April 2020)
137. Shandilya, N., Le Bihan, O., Bressot, C. & Morgeneyer, M. Evaluation of the Particle Aerosolization from n-TiO_2 Photocatalytic Nanocoatings under Abrasion. J. Nanomater. 2014, 185080 (2014).
138. Shandilya, N., Le Bihan, O. & Morgeneyer, M. A Review on the Study of the Generation of (Nano)particles Aerosols during the Mechanical Solicitation of Materials. J. Nanomater. 2014, (2014).
139. Tou, F. et al. Multi method approach for analysis of road dust particles: elemental ratios, SP-ICP-TOF-MS, and TEM. ESNano (2022, Rev.)
140. Thorpe, A. & Harrison, R. M. Sources and properties of non-exhaust particulate matter from road traffic: A review. Sci. Total Environ. 400, 270–282 (2008).
141. Gietl, J. K., Lawrence, R., Thorpe, A. J. & Harrison, R. M. Identification of brake wear particles and derivation of a quantitative tracer for brake dust at a major road. Atmos. Environ. 44, 141–146 (2010).
142. Wåhlin, P., Berkowicz, R. & Palmgren, F. Characterisation of traffic-generated particulate matter in Copenhagen. Atmos. Environ. 40, 2151–2159 (2006).
143. Apeagyei, E., Bank, M. S. & Spengler, J. D. Distribution of heavy metals in road dust along an urban-rural gradient in Massachusetts. Atmos. Environ. 45, 2310–2323 (2011).
144. Pant, P. & Harrison, R. M. Estimation of the contribution of road traffic emissions to particulate matter concentrations from field measurements: A review. Atmos. Environ. 77, 78–97 (2013).
145. Adachi, K. & Tainosho, Y. Characterization of heavy metal particles embedded in tire dust. Environ. Int. 30, 1009–1017 (2004).
146. USGS. Characterization of Stormwater Runoff from Bridges in North Carolina and the Effects of Bridge Deck Runoff on Receiving Streams. (2011).
147. Bourcier, D. R., Hindin, E. & Cook, J. C. Titanium and tungsten in highway runoff at pullman, washington. Int. J. Environ. Stud. 15, 145–149 (1980).
148. Saharia, A. M., Zhu, Z., Aich, N., Baalousha, M. & Atkinson, J. F. Modeling the transport of titanium dioxide nanomaterials from combined sewer overflows in an urban river. Sci. Total Environ. 696, 133904 (2019).
149. Slomberg, D. L. et al. Anthropogenic Release and Distribution of Titanium Dioxide Particles in a River Downstream of a Nanomaterial Manufacturer Industrial Site. Front. Environ. Sci. 0, 76 (2020).
150. Vidmar, J., Zuliani, T., Milačič, R. & Ščančar, J. Following the Occurrence and Origin of Titanium Dioxide Nanoparticles in the Sava River by Single Particle ICP-MS. Water 14, 959 (2022).
151. David Holbrook, R. et al. Titanium distribution in swimming pool water is dominated by dissolved species. Environ. Pollut. 181, 68–74 (2013).

152. Yang, Y. et al. Prospecting nanomaterials in aqueous environments by cloud-point extraction coupled with transmission electron microscopy. Sci. Total Environ. 584–585, 515–522 (2017).
153. Venkatesan, A. K. et al. Detection and Sizing of Ti-Containing Particles in Recreational Waters Using Single Particle ICP-MS. Bull. Environ. Contam. Toxicol. 100, 120–126 (2018).
154. Wang, J., Nabi, M.M., Mahdi, E, Goharian, E, Baalousha, M. Identification and Quantification of Anthropogenic Nanomaterials in Urban Rainfall and Runoff Using Single Particle-Inductively Coupled Plasma-Time of Flight-Mass Spectrometry (In preparation).
155. Lee, S. et al. Nanoparticle size detection limits by single particle ICP-MS for 40 elements. Environ. Sci. Technol. 48, 10291–10300 (2014).
156. Hadioui, M. et al. Lowering the Size Detection Limits of Ag and TiO_2 Nanoparticles by Single Particle ICP-MS. Anal. Chem. 91, 13275–13284 (2019).
157. U.S. Geological Survey. Mineral Commodity Summaries. Mineral Commodity Summaries (2019). doi:10.3133/70202434
158. U.S. Geological Survey (USGS). USGS Current Conditions for USGS 03451500 French broad river at Asheville, NC. Available at: https://waterdata.usgs.gov/nwis/dv?cb_00045=on&format=html&site_no=03451500&referred_module=sw&period=&begin_date=2020-04-20&end_date=2020-05-10. (Accessed: 8th January 2021)
159. City of Knoxville. Rainfall Data - City of Knoxville. Available at: https://knoxvilletn.gov/government/city_departments_offices/engineering/stormwater_engineering_division/rainfall_data. (Accessed: 8th January 2021)
160. U.S. Geological Survey (USGS). USGS Current Conditions for USGS 02162285 table rock reservoir nr Cleveland, SC. Available at: https://waterdata.usgs.gov/nwis/dv?cb_00045=on&format=html&site_no=02162285&referred_module=sw&period=&begin_date=2020-04-27&end_date=2020-05-12. (Accessed: 10th January 2021)
161. SCDHEC. Saluda River/Lake Murray watershed. Available at: https://scdhec.gov/sites/default/files/docs/HomeAndEnvironment/Docs/03050109-13.pdf. (Accessed: 16th August 2021)
162. SCE & G, S. C. Saluda Project (FERC No. 516): Lake Murray Water Quality Report.
163. National Park Service & U.S. Department of the Interior. Assessment of Water Resources and Watershed Conditions in Congaree National Park, South Carolina. (2010).
164. Federal Energy Regulatory Commission. Environmental assessment for hydropower license. (2020).
165. SCE & G, S. C. South Carolina Electric & Gas COL Application Part 3-Environmental Report.
166. Wu, J. et al. Metal-Containing Nanoparticles in Low-Rank Coal-Derived Fly Ash from China: Characterization and Implications toward Human Lung Toxicity. Environ. Sci. Technol. 55, 6644–6654 (2021).
167. Kaegi, R. et al. Synthetic TiO_2 nanoparticle emission from exterior facades into the aquatic environment. Environ. Pollut. 156, 233–239 (2008).

168. Chemours. Ti-PureTM Solutions for Coatings: Applications. (2018). Available at: https://www.tipure.com/en/applications/coatings?_ga=2.22333115.1280235886.1586571265-1482119140.1586571265. (Accessed: 10th April 2020)
169. Kaegi, R. et al. Release of TiO_2 – (Nano) particles from construction and demolition landfills. NanoImpact 8, 73–79 (2017).
170. City of West Columbia City Council. West Columbia City Operated Parks Closed to Reduce Potential COVID-19 Exposure - City of West Columbia. Available at: https://westcolumbiasc.gov/2020/03/west-columbia-city-operated-parks-closed-to-reduce-potential-covid-19-exposure/. (Accessed: 8th January 2021)
171. City of Columbia. City of Columbia coronavirus (COVID-19) update - Stay at Home Order issued - Tuesday, March 24 at 10 a.m. Available at: https://www.como.gov/CMS/pressreleases/view.php?id=6656. (Accessed: 8th January 2021)

Appendix A: Supporting Information for Chapter 2

A.1 Gadolinium anomaly

There are two major sources of TiO_2 into rivers: 1) wastewater in the form of effluent or sewage overflows [2] and 2) urban runoff [3]. The crust normalized pattern of REEs shows flat line for all REEs with a slight increase in Gd in all samples (**Figure A3a**), indicating that all REEs originate from natural sources (*e.g.,* soil erosion or river sediments) with a potential presence of anthropogenic Gd. The major anthropogenic source of anthropogenic Gd is domestic sewage effluent, widely recognized as the major source of Gd in polluted streams. Anomalies in REE patterns are commonly quantified by the ratio of the normalized measured concentration of the normalized theoretical concentration (determined by interpolation between neighboring elements) for the anomalous element. Here, we use neodymium (Nd) and samarium (Sm) to extrapolate the background Gd values in the samples, and to quantify Gd anomalies according to Eq. 1 [4].

$$Gd_N/Gd_N^* = Gd_N/10^{(2logSm-logNd)} \quad \text{(Eq. 1)}$$

A size of $Gd_N/Gd_N^* = 1.5$ is commonly used as the benchmark to distinguish between the natural and anthropogenic Gd anomaly. The size of the Gd anomalies varied in the range from $Gd_N/Gd_N^* = 1.0\pm0.01$ and 1.21 ± 0.01 **(Figure A.3b)**, suggesting that there is minimal or absence of Gd anomaly during the C1, C2 and C3 in the Broad river surface water which might be attributed to insignificant (mean: 5.2%) contribution of WWTP effluent discharge into the river stream in comparison to the direct runoff.

Table A.1 Perkin Elmer NexION 350D ICP-MS operating conditions.

Instrument Parameter	Value
Nebulizer Gas Flow	0.85 to 1 L/min
Auxiliary Gas Flow	1.02 L/min
Plasma Gas Flow	16 L/min
ICP RF Power	1600 W
Analog Stage Voltage	-1600 V
Pulse Stage Voltage	1600 V
Discriminator Threshold	12
Deflector Voltage	-9.5 V
Dwell time	50 ms
Sample Flow Rate	0.3 mL/min

Table A.2 TOFWERK ICP-TOF-MS operating conditions.

Instrument parameter	Value				
Plasma Power	1550 V				
Nebulizer Gas Flow	1.1 L/min				
Auxiliary Gas Flow	0.8 L/min				
Cooling Gas Flow	14 L/min				
Injector Diameter	2 mm				
Collision Cell Gas	5 mL/min He with 4.5% H_2				
CCT Bias	-4.34 V				
Notch	Mass	29	32	36.3	41
	Amplitude (V)	1.6	2.0	2.0	1.2
TOF Repetition Rate	33 kHz				
Detected Mass Range	14-275 m/Z				
(CeO/Ce)	< 2.0%				
Data Acquisition	Continuous Mode				
TOF Time Resolution	2 ms				
Sample Flow Rate	0.4 mL/min				

Table A.3 Total daily precipitation (mm) in Columbia, SC during the three sampling campaigns

C1		C2		C3	
Date	Precipitation	Date	Precipitation	Date	Precipitation
9/14/2018	0	10/25/2018	1.0	11/3/2018	0
9/15/2018	39.1	10/26/2018	33.3	11/4/2018	3.6
9/16/2018	41.4	10/27/2018	0	11/5/2018	3.0
9/17/2018	27.7	10/28/2018	0	11/6/2018	1.0
9/18/2018	0	10/29/2018	0	11/7/2018	19.3
9/19/2018	0	10/30/2018	0	11/8/2018	0
9/20/2018	0	10/31/2018	0	11/9/2018	3.6
9/21/2018	0	11/1/2018	0.3		
		11/2/2018	20.1		

Table A.4 Elemental analysis of Concentration of the USGS reference materials BHVO-2 Hawaiian basalts

Concentration (ug/kg)	Mean	Standard Deviation	Recommended values [1]	Precision (%)	Error (%)	Accuracy (%)
^{27}Al	7.55×10^{7}	3.13×10^{6}	7.11×10^{7}	4.15	6.1	93.9
^{47}Ti	1.52×10^{7}	5.73×10^{5}	1.64×10^{7}	3.78	4.1	95.9
^{57}Fe	9.43×10^{7}	3.44×10^{6}	8.67×10^{7}	3.65	8.8	91.2
^{93}Nb	1.57×10^{4}	1.24×10^{2}	1.81×10^{4}	0.79	11.0	89.0
^{139}La	1.38×10^{4}	3.98×10^{2}	1.52×10^{4}	2.89	2.9	97.1
^{140}Ce	3.39×10^{4}	9.29×10^{2}	3.75×10^{4}	2.74	4.3	95.7
^{141}Pr	4.77×10^{3}	1.20×10^{2}	5.34×10^{3}	2.52	4.8	95.2
^{142}Nd	2.23×10^{4}	4.01×10^{2}	2.43×10^{4}	1.80	2.0	98.0
^{152}Sm	5.70×10^{3}	1.24×10^{1}	6.02×10^{3}	0.22	5.3	94.7
^{153}Eu	1.91×10^{3}	1.77×10^{0}	2.04×10^{3}	0.09	6.3	93.7
^{158}Gd	6.33×10^{3}	1.96×10^{2}	6.21×10^{3}	3.10	1.9	98.1
^{159}Tb	9.06×10^{2}	4.12×10^{0}	9.39×10^{2}	0.45	3.5	96.5
^{164}Dy	5.01×10^{3}	3.66×10^{1}	5.28×10^{3}	0.73	5.1	94.9
^{165}Ho	9.42×10^{2}	3.15×10^{1}	9.89×10^{2}	3.34	4.7	95.3
^{166}Er	2.44×10^{3}	4.12×10^{0}	2.51×10^{3}	0.17	3	97.0
^{169}Tm	3.36×10^{2}	2.38×10^{1}	3.35×10^{2}	7.09	0.3	99.7
^{174}Yb	1.92×10^{3}	3.20×10^{1}	1.99×10^{3}	1.67	3.7	96.3
^{175}Lu	3.24×10^{2}	2.61×10^{1}	2.75×10^{2}	8.07	14.2	85.8

Precision (%) = standard deviation/mean * 100

Error (%) = |(Measured concentration – recommended value)| / recommended value * 100

Accuracy = 100 –Error (%)

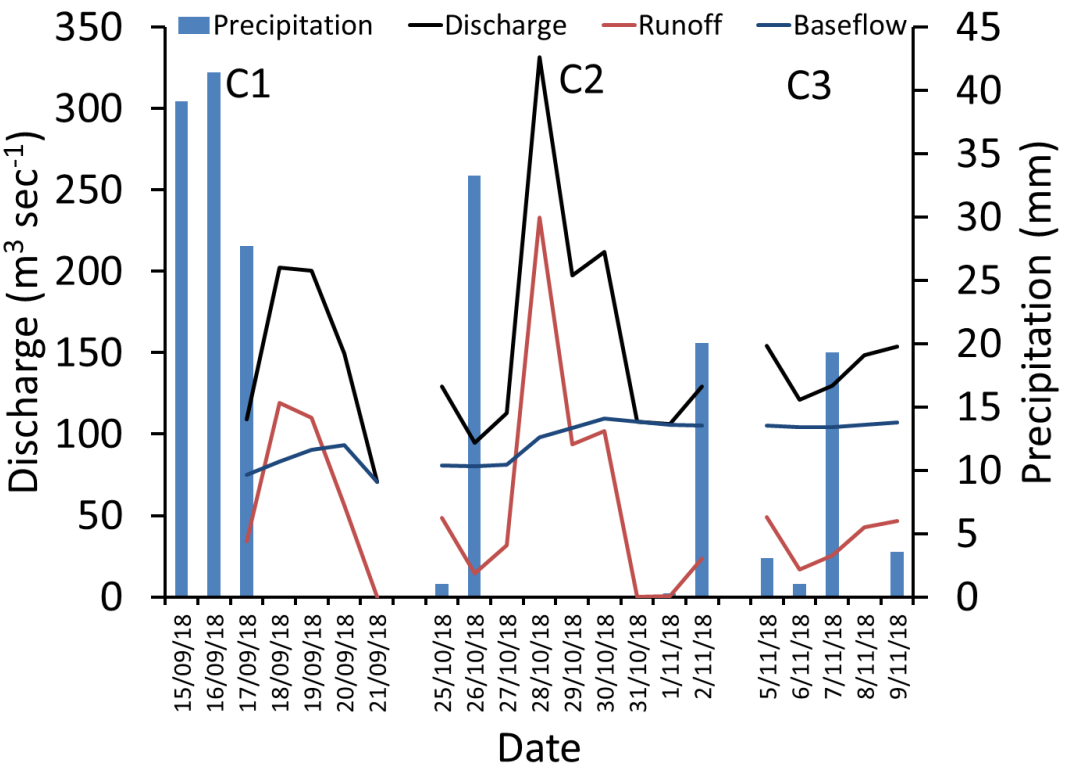

Figure A.1 Precipitation in Columbia, South Carolina and discharge, runoff, and base flow in the Broad River during the sampling events.

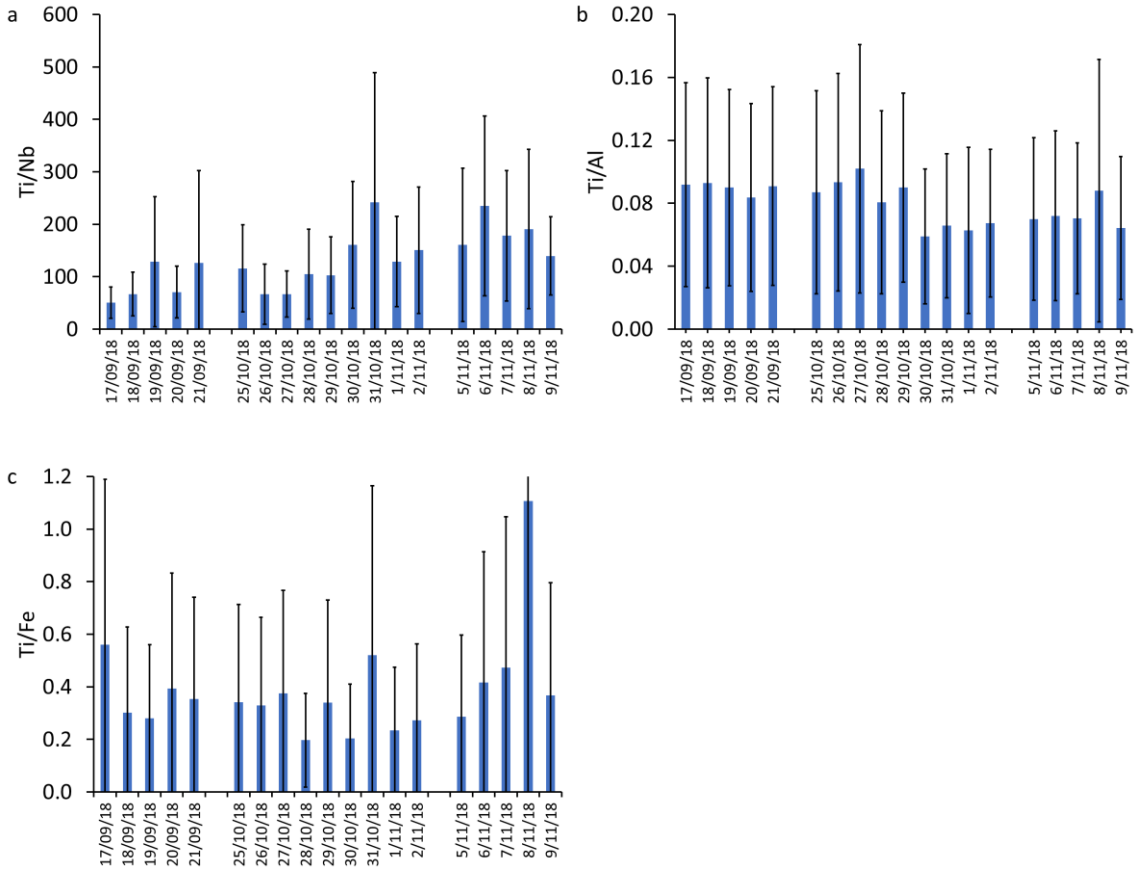

Figure A.2 Elemental ratios of (a) Ti/Nb, (b) Ti/Al, and (b) Ti/Fe in Ti-containing particles on a single particle basis measured by ICP-TOF-MS. Error bars represent the standard deviation of the elemental ratio distribution.

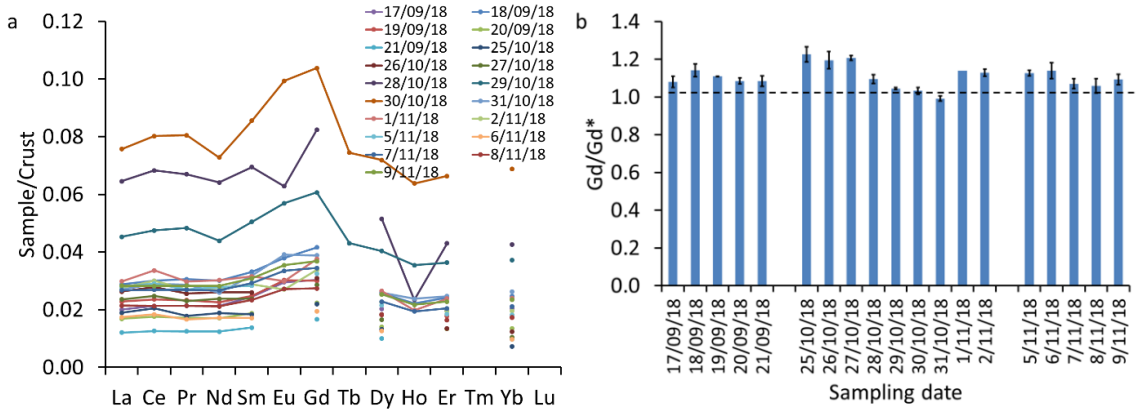

Figure A.3 (a) Crustal normalized rare earth element concentrations and (b) size of gadolinium anomaly calculated based on the equation 1.

References

1. Jochum, K. P.; Weis, U.; Schwager, B.; Stoll, B.; Wilson, S. A.; Haug, G. H.; Andreae, M. O.; Enzweiler, J. Reference values following ISO guidelines for frequently requested rock reference materials. Geostand. Geoanal. Res. 2016, 40 (3), 333-350.
2. Loosli, F.; Wang, J.; Rothenberg, S.; Bizimis, M.; Winkler, C.; Borovinskaya, O.; Flamigni, L.; Baalousha, M. Sewage spills are a major source of engineered titanium dioxide release into the environment. Environ. Sci. Nano. 2019, 6, 763-777.
3. Wang, J.; Nabi, M. M.; Mohanty, S. K.; Afrooz, A. N.; Cantando, E.; Aich, N.; Baalousha, M. Detection and quantification of engineered particles in urban runoff. Chemosphere 2020, 248, 126070.
4. Kulaksiz, S.; Bau, M. Contrasting behaviour of anthropogenic gadolinium and natural rare earth elements in estuaries and the gadolinium input into the North Sea. Earth Planet. Sci. Lett. 2007, 260 (1), 361-371.

Appendix B: Supporting Information for Chapter 3

Table B.1 Characteristics of rainfall events during the sampling period of March and April of 2019.

Rainfall number	Date	Precipitation (mm)	Antecedent dry period (days)
1	03/25/2019	4.3	15
2	04/02/2019	28.2	7
3	04/05/2019	10.4	2
4	04/07/2019	0.25	1
	04/08	1.78	0
	04/09	6.60	0
5	04/12/2019	13.97	2
	04/13	0.76	0
	04/14	1.52	0

Table B.2 Method limit of detection (LoD) and limit of quantification (LoQ) for total elemental analysis using ICP-MS, and elemental mass detection limit (EMDL) for single particle analysis using ICP-TOF-MS for all the isotopes monitored.

	Elemental concentration analysis		Particle analysis
Isotope	LoD (mg/L)	LoQ (mg/L)	EMDL (g)
^{27}Al	0.335	1.015	4.94×10^{-15}
^{47}Ti	0.022	0.063	5.05×10^{-16}
^{57}Fe	3.132	7.179	3.57×10^{-16}
^{93}Nb	0.007	0.021	7.50×10^{-17}
^{139}La	0.006	0.017	3.16×10^{-17}
^{140}Ce	0.008	0.023	3.41×10^{-17}
^{141}Pr	0.006	0.020	2.52×10^{-17}
^{142}Nd	0.003	0.009	6.85×10^{-17}
^{152}Sm	0.008	0.026	7.94×10^{-17}
^{153}Eu	0.008	0.026	3.87×10^{-17}
^{158}Gd	0.006	0.020	8.66×10^{-17}
^{159}Tb	0.008	0.026	2.41×10^{-17}
^{164}Dy	0.008	0.028	6.46×10^{-17}
^{165}Ho	0.005	0.016	1.89×10^{-17}
^{166}Er	0.009	0.031	5.63×10^{-17}
^{169}Tm	0.003	0.011	2.15×10^{-17}
^{174}Yb	0.006	0.019	5.55×10^{-17}
^{175}Lu	0.007	0.023	1.67×10^{-17}

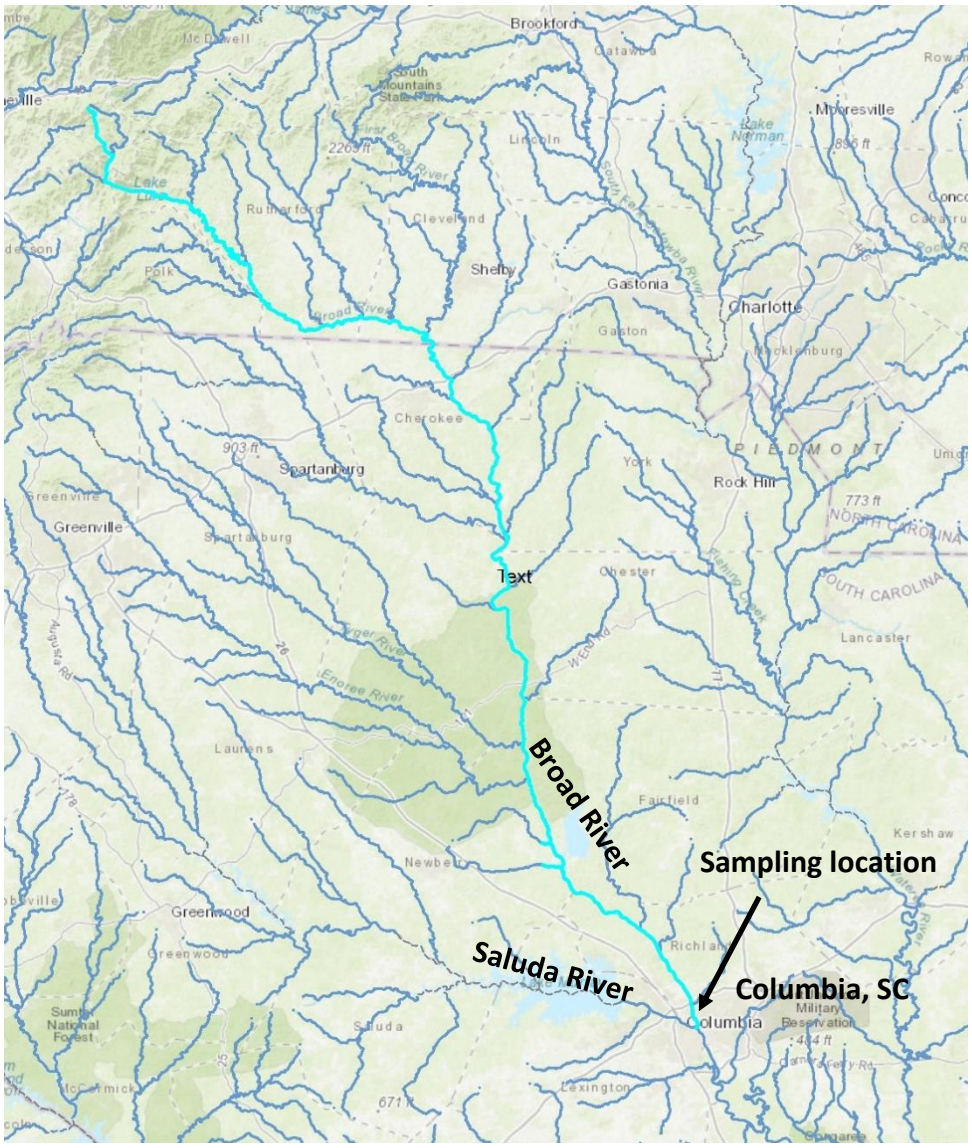

Figure B.1 Map of the Broad River watershed. Samples were collected right before the confluence between the Saluda and the Broad Rivers.

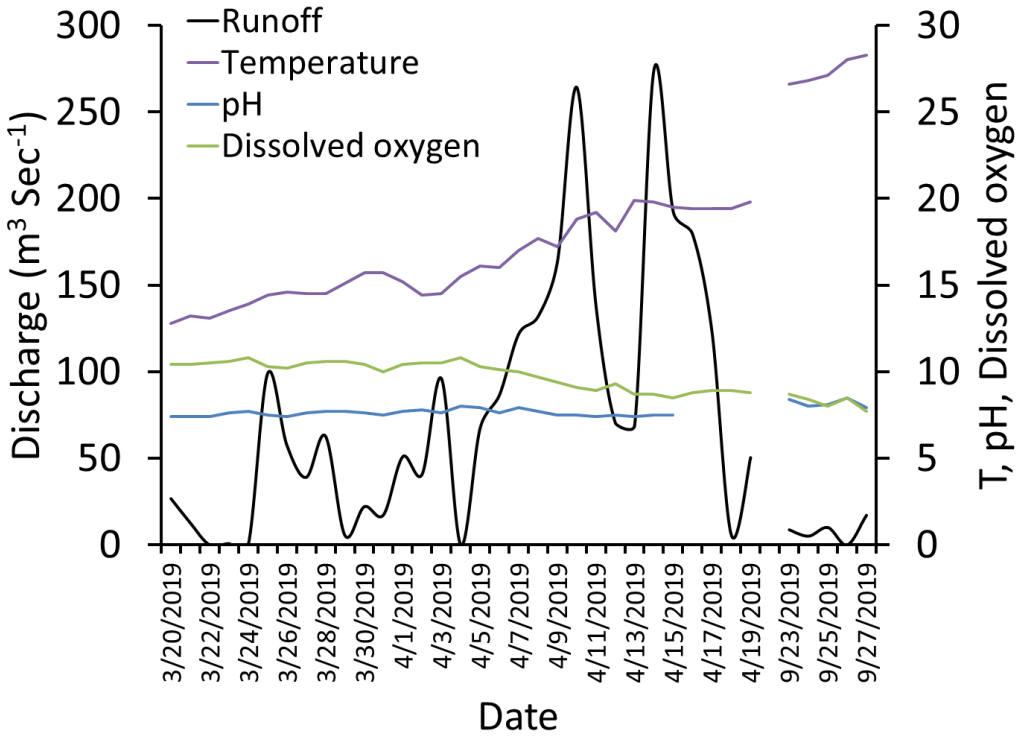

Figure B.2 Time-flow-pH, dissolved oxygen (mg L^{-1}), and water temperature (° C) trend plot.

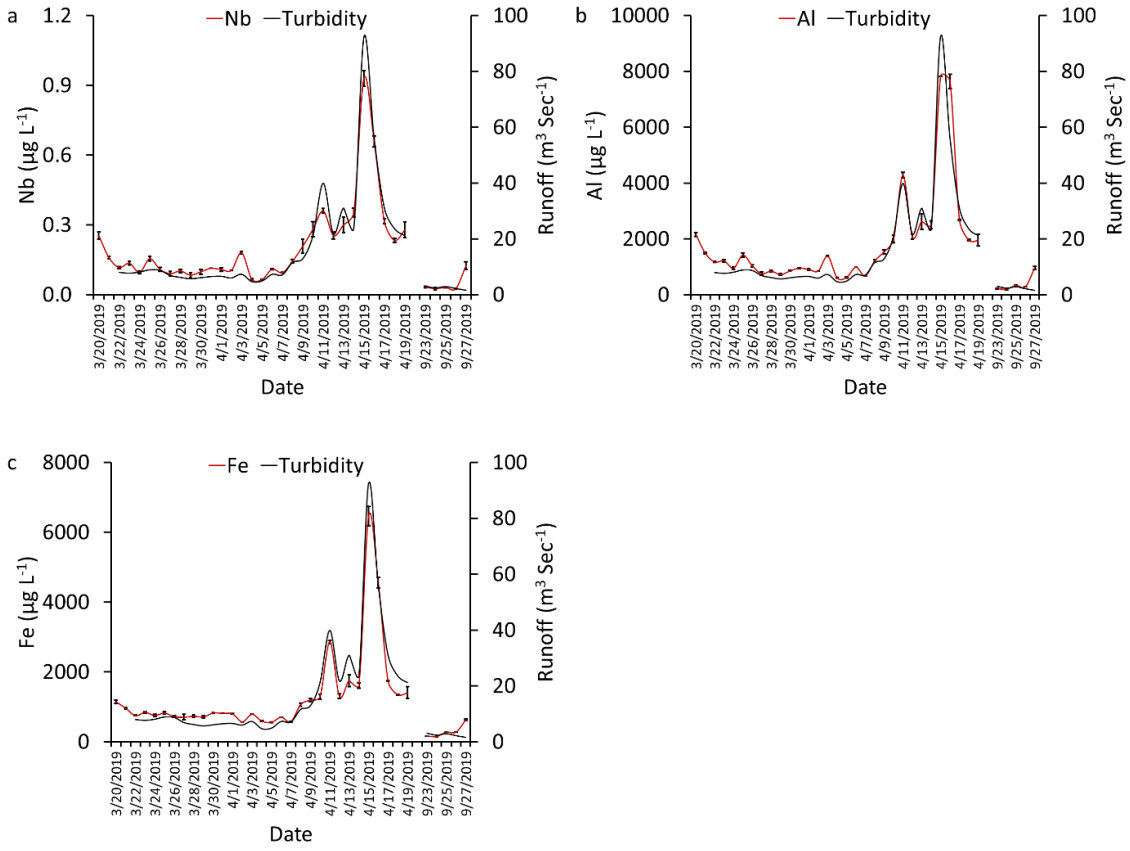

Figure B.3 Pollutographs of elements-turbidity relationships (a) Nb, (b) Al, and (c) Fe. FNU: formazin nephelometric units.

Appendix C: Supporting Information for Chapter 4

C.1 Detailed description of the sampling locations

Saluda River: Water samples were collected from the lower Saluda River, Hope ferry landing, Columbia, SC 29072 (34°02'45.7"N 81°11'27.3"W) which is approximately 2.7 kms downstream from the Lake Murray dam **(Figure 4.1)**. The Lower Saluda River flows out of the Lake Murray dam and merges downstream with the Broad River. Therefore, lower Saluda River is an engineered river controlled from the Lake Murray dam. Lake Murray serves as a retention reservoir for the suspended particulate matters, those come with the stream of upstream Saluda River. The Saluda River is approximately 291 km long, originates in the Blue Ridge Mountains of northwest of Greenville County, South Carolina, and flows generally southeastwardly in South Carolina [1]. The Saluda River basin covers approximately 6535 square kilometers and contains twenty-one (21) watershed [2]. The dominant land use throughout the Saluda River basin is forested (53.7%); agricultural (26.1%); urban (12.9%); water (4.2%) and others (0.1-3.3%): swampland, barren land and marshland. There are permitted 9 major wastewater treatment plants (WWTP); 15 minor WWTPs; 92 industrial, mining and quarrying facilities, 35 municipal separate stormwater facilities in the Saluda River basin [3]. The Saluda River is crossed 26 times by many highways, and three of those highway's bridges cross the Saluda River near the sampling location. The lake Murray dam (34°03'14.4"N 81°13'9.8"W) on highway 6 between the lake Murray and lower Saluda River is situated 2.75km upstream from the sampling

location, and had an estimated AADT of 26,700 in 2019 [4]. The I20 bridge over Saluda River (34°01'31.7"N 81°07'42.9"W) is situated 6.2kms downstream from the sampling location, and had an estimated AADT of 84,000 in 2019 [4]. The interstate I26 bridge (34°01'25.7"N 81°06'12.6"W) over Saluda River is situated 8.4km downstream from the sampling location, and had an estimated AADT of 95,400 in 2019 [5].

Water samples were collected from the Saluda River during a range of hydrologic conditions (**Table C.4**). There had been 20.5 mm rainfall (in total) during the entire sampling campaign with a major rainfall event of 15.7 mm occurred on 30/4/2020 near the sampling location. Major rainfall events of 54.5 mm and 3.1 mm occurred on 29/4/2020 and 30/4/2020 in the upstream region of the Saluda River at Rock reservoir, Cleveland, SC [6]. The rainfall and discharge data were collected from the USGS station number 02168504 (34°03'03"N 81°12'35"W), nearly 1.8 km upstream from the sampling location.

Broad River: Water samples were collected from the Broad River, Columbia rowing club, Columbia, SC 29201 (34°02'36.9"N 81°04'23.7"W) **(Figure 4.1)**. The Broad River is approximately 240 km long, originates in the Blue Ridge Mountains of eastern Buncombe County, North Carolina, and flows generally south-southeastwardly in South Carolina. The total catchment area of the Broad River is approximately 14,000 square kilometers. Apart from the forested land (66%) in the headwaters of the Broad River basin; the dominant land use throughout the Broad River basin is agricultural (23%); urban (9%): commercial and residential; others (2-4%): mining operations, and logging operations. There are permitted 14 major wastewater treatment plants (WWTP), 30 minor WWTPs, 20 animal operation facilities, 92 general and individual stormwater facilities in the Broad River basin 7[7]. The Broad River is crossed 22 times by many highways. There are three

bridges crossing the Broad River near the sampling location. The interstate I20 bridge (34°02'52.5"N 81°04'23.6"W) over Broad River is situated 481m upstream from the sampling location, and had an estimated AADT of 119,100 in 2019 [5]. The Broad River bridge on highway 176 (34°01'33.3"N 81°04'9.9"W) is situated 2 kms downstream from the sampling location, and had an estimated AADT of 24,400 in 2019 [5]. The interstate I126 bridge (34°00'33.7"N 81°03'36.1"W) over Broad River is situated 4km downstream from the sampling location, and had an estimated AADT of 71,800 in 2019 [5].

Water samples were collected from the Broad River during a range of hydrologic conditions (**Table C.4**). There had been 18.8 mm rainfall (in total) during the entire sampling campaign with a major rainfall event of 16.8 mm occurred on 30/4/2020 near the sampling location. Moreover, there were major rainfall events of 40.2 mm and 9.7 mm occurred on 29/4/2020 in the upstream region of the Broad River at Ashville, NC and Knoxville, TN respectively [8,9]. The rainfall data was collected from the USGS station number 021695045 (34°00'24"N 81°01'18"W), nearly 3.1 km from the sampling location. The **discharge** data was collected from the USGS station number 02162035 (34°02'54"N 81°04'24"W), nearly 5.3 km upstream of the sampling location.

Congaree River: Water samples had been collected from the Congaree River at West Columbia Riverwalk, West Columbia, SC 29169 (33°59'35.4"N 81°03'1.8"W) and Thomas Newman public boat landing, Cayce, SC 29033 (33°56'57.3"N 81°01'44.1"W) **(Figure 4.1)**. Thomas Newman public boat landing sampling location is 5.3 km downstream of West Columbia Riverwalk sampling location. The Congaree River basin is formed by the confluence of the Saluda and Broad River basins in central South Carolina near Columbia. Therefore, the Broad River and Saluda River merge to form the Congaree

River, which flows southeasterly for 50 miles and merges with the Wateree River to form the Santee River Basin which finally discharges into the Atlantic Ocean. The Congaree River basin area is 1785 square kilometers and contains four (04) watersheds. In the Congaree River basin, 34.6% is forested land, 26.6% is agricultural land, 19.0% is forested wetland (swamp), 17.9% is urban land, 0.3% is barren land, 1.3% is water, and 0.3% is non-forested wetland (marsh). There are permitted 2 major wastewater treatment plants (WWTP); 4 minor WWTPs; 35 industrial, mining and quarrying facilities; 20 municipal separate stormwater facilities in the Congaree River basin [3]. The Congaree River is crossed 7 times by many highways. There are three bridges crossing the Congaree River near the sampling locations. The Jarvis Klapman Blvd bridge (33°59'57.2"N 81°03'12.3"W) on highway 12 and The Gervais street bridge on highway 1 (33°59'43.8"N 81°03'6.9"W) are situated 729 m and 288 m respectively upstream from the Congaree River, Columbia sampling location, and had an estimated AADT of 22,700 and 28,000 respectively in 2019 [4]. The Blossom street bridge (33°59'17"N 81°02'48"W) on highway 176 over Congaree River is situated 674 m downstream from the Congaree River, Columbia sampling location and 4.6 km upstream from the Congaree River, Cayce sampling location, and had an estimated AADT of 27,500 in 2019 [5].

Congaree River is downstream from the confluence of the Saluda and Broad River, therefore, the prevailed diverse climatic or hydrologic conditions on the upstream of the Saluda and Broad River during the sampling campaign also affected the Congaree River. Moreover, the Congaree River basin's hydrologic conditions had also been diverse during the water samples collection (**Table C.4**). There had been 18.8 mm rainfall (in total) during the entire sampling campaign with a major rainfall event of 16.8 mm occurred on 30/4/2020

near the sampling location. The rainfall data was collected from the USGS station number 021695045 (34°00'24"N 81°01'18"W), nearly 3.1 km from the West Columbia Riverwalk sampling location and 6.4 km from the Thomas Newman public boat landing sampling location. The discharge data were collected from the USGS station number 02169500 (33°59'35"N 81°03'00"W), nearly 0.05 km from the West Columbia Riverwalk sampling location and 5.3 km from the Thomas Newman public boat landing sampling location.

C.2 Sample digestion

The bulk river water samples were digested in 15 mL Teflon vessels (Savillex, Eden Prairie, MN, United States) on custom-made Teflon covered hotplates placed in a box equipped with double-HEPA filtered forced air in a metal-free HEPA filtered air clean lab. 10 mL water aliquots or 5 mL extracted particle suspensions were placed in the vessel and weighed (Mettler Toledo, Excellence Plus, Columbus, OH, United States). Samples were dried at 110°C and treated with 1 mL of 30% H_2O_2 (Fisher Chemical, Fair Lawn, NJ, United States) for 2 h at 70°C to remove organic matters. H_2O_2 was then evaporated, and the sample was digested with 2 mL of HF:HNO_3 (3:1) mixture (ACS grade acids distilled in the laboratory, Sigma Aldrich, St. Louis, MO, United States) for 48 h at 110°C. After evaporation of the acid mixture at 110°C, the residue was reacted with 1 mL of distilled HNO_3 to break up insoluble fluoride salt that may have formed during the sample digestion and HNO_3 was left to evaporate at 110°C. This step was repeated twice before weighing the sample and adding 5 mL of 1% HNO_3. The sample was sonicated for 10 min in a sonication bath (Branson, 2800, 40kHz, Danbury, CT, United States) and warmed for 2 h at 50°C for full dissolution. The solution was transferred to 15 mL polypropylene centrifuge tubes (Fisher Scientific, San Nicolás de los Garza, Nuevo León, Mexico) and

stored at 4°C. Samples were centrifuged (Eppendorf, 5810 R, Hamburg, Germany) for 5 min at 3100 g prior to ICP-MS analysis to remove any undigested minerals.

C.3 Gadolinium anomaly

The major anthropogenic source of anthropogenic Gd is domestic sewage effluent, widely recognized as the major source of Gd in polluted streams. Anomalies in REE patterns are commonly quantified by the ratio of the normalized measured concentration of the normalized theoretical concentration (determined by interpolation between neighboring elements) for the anomalous element. Here, we use neodymium (Nd) and samarium (Sm) to extrapolate the background Gd values in the samples, and to quantify Gd anomalies according to Eq. 1 [11].

$$Gd_N/Gd_N^* = Gd_N/10^{(2logSm-logNd)} \quad \text{(Eq. 1)}$$

A size of $Gd_N/Gd_N^* = 1.5$ is commonly used as the benchmark to distinguish between the natural and anthropogenic Gd anomaly. The size of the Gd anomalies varied in the range from $Gd_N/Gd_N^* = 1.1 \pm 0.0$ and 2.1 ± 0.1 **(Figure C.9)**, suggesting that there is minimal or absence of Gd anomaly during the sampling event in the Saluda, Broad and Congaree River surface water which might be attributed to insignificant (mean: 5.2%) contribution of WWTP effluent discharge into the river stream in comparison to the direct runoff.

Table C.1 Power plants on the Broad River.

Power plant	GPS Coordinates	Type	Distance from the sampling site	Type of dam/water control
Duke Energy -- Cliffside Plant	35°12'47.9"N, 81°45'39.2"W	Thermo	145 km	
Broad River energy, Cherokee	35°4'53.4"N, 81°34'18.9"W	Thermo	124 km	
Power plant 1, Cherokee	35°3'52.2"N, 81°32'41.6"W	Hydro	120 km	Gravity-type concrete spillway
Magna Energy Systems	34°59'57.5"N, 81°56'11.6"W	Hydro	132 km	Low head
Lower Pacolet Hydro	34°55'11.9"N, 81°44'16.2"W	Hydro	115 km	Low head
Lockhart Power Company	34°46'46.3"N, 81°27'24.9"W	Hydro	89 km	Diversion and Low head
Neal Shoals Hydro, Union Hydroelectric project	34°39'51.8"N, 81°26'54.8"W	Hydro	77 km	Low head
SCE&G - Fairfield Pumped Storage, Jenkinsville, SC 29065	34°18'19.7"N, 81°19'54.8"W	Hydro	38 km	Diversion
Virgil C. Summer Nuclear Station	34°17'52.5"N, 81°18'55.9"W	Thermo	36 km	
Parr hydro	34°15'35.2"N, 81°19'50.4"W	Hydro	34 km	low head
Columbia Hydroelectric Project	34°0'8.5"N, 81°3'14.8"W	Hydro	4 km	low head

Table C.2 The annual average daily traffic (AADT) on the bridges crossing the Broad, Saluda and Congaree Rivers near the sampling locations in 2019.

Name of the River	**Highways**	**GPS coordinates**	**Distance from respective sampling location**	**AADT**	**Ref**
Saluda River	The interstate I26 bridge	34°01'25.7"N 81°06'12.6"W	8.4 km downstream	95,400	5
	The I20 bridge	34°01'31.7"N 81°07'42.9"W	6.2 km downstream	84,000	4
	The lake Murray dam	34°03'14.4"N 81°13'9.8"W	2.75 km upstream	26,700	4
Broad river	The interstate I126 bridge	34°00'33.7"N 81°03'36.1"W	4 km downstream	71,800	5
	The Broad River bridge on highway 176	34°01'33.3"N 81°04'9.9"W	2 km upstream	24,400	5
	The interstate I20 bridge	34°02'52.5"N 81°04'23.6"W	481 m upstream	119,000	5
Congaree River	The Jarvis Klapman Blvd bridge	33°59'57.2"N 81°03'12.3"W	729 m upstream Columbia sampling location	22,700	4
	The Gervais Street bridge on highway 1	33°59'43.8"N 81°03'6.9"W	288 m upstream Columbia sampling location	28,000	4
	The Blossom Street bridge	33°59'17"N 81°02'48"W	4.6 km upstream the Cayce sampling location	27,500	5

Table C.3 TOFWERK ICP-TOF-MS operating conditions.

Instrument parameter	**Value**				
Plasma Power	1550 V				
Nebulizer Gas Flow	1.1 L/min				
Auxiliary Gas Flow	0.8 L/min				
Cooling Gas Flow	14 L/min				
Injector Diameter	2.5 mm				
Collision Cell Gas	5 mL/min He with 4.5% H_2				
CCT Bias	-4.15 V				
Notch	Mass	29	32	36.3	41
	Amplitude (V)	1.6	2.0	2.0	1.2
TOF Repetition Rate	33 kHz				
Detected Mass Range	14-275 m/Z				
(CeO/Ce)	< 3.0%				
Data Acquisition	Continuous Mode				
TOF Time Resolution	300 ms for elemental concentration, 2 ms for particle analysis				
Sample Flow Rate	0.4 mL/min				

Table C.4 Elemental analysis of the USGS reference materials BHVO-2 Hawaiian basalts.

Concentration (μg/kg)	Mean	Standard Deviation	Recommended values [10]	Precision (%)	Error (%)	Accuracy (%)
^{27}Al	7.55×10^7	3.13×10^6	7.11×10^7	4.15	6.1	93.9
^{49}Ti	1.52×10^7	5.73×10^5	1.64×10^7	3.78	4.1	95.9
^{57}Fe	9.43×10^7	3.44×10^6	8.67×10^7	3.65	8.8	91.2
^{90}Zr	1.51×10^5	4.45×10^3	1.71×10^5	2.94	11.7	91.9
^{93}Nb	1.57×10^4	1.24×10^2	1.81×10^4	0.79	11.0	89.0
^{139}La	1.38×10^4	3.98×10^2	1.52×10^4	2.89	2.9	97.1
^{140}Ce	3.39×10^4	9.29×10^2	3.75×10^4	2.74	4.3	95.7
^{141}Pr	4.77×10^3	1.20×10^2	5.34×10^3	2.52	4.8	95.2
^{142}Nd	2.23×10^4	4.01×10^2	2.43×10^4	1.80	2.0	98.0
^{152}Sm	5.70×10^3	1.24×10^1	6.02×10^3	0.22	5.3	94.7
^{153}Eu	1.91×10^3	1.77×10^0	2.04×10^3	0.09	6.3	93.7
^{158}Gd	6.33×10^3	1.96×10^2	6.21×10^3	3.10	1.9	98.1
^{159}Tb	9.06×10^2	4.12×10^0	9.39×10^2	0.45	3.5	96.5
^{164}Dy	5.01×10^3	3.66×10^1	5.28×10^3	0.73	5.1	94.9
^{165}Ho	9.42×10^2	3.15×10^1	9.89×10^2	3.34	4.7	95.3
^{166}Er	2.44×10^3	4.12×10^0	2.51×10^3	0.17	3	97.0
^{169}Tm	3.36×10^2	2.38×10^1	3.35×10^2	7.09	0.3	99.7
^{174}Yb	1.92×10^3	3.20×10^1	1.99×10^3	1.67	3.7	96.3
^{175}Lu	3.24×10^2	2.61×10^1	2.75×10^2	8.07	14.2	85.8

Precision (%) = standard deviation/mean * 100

Error (%) = |(Measured concentration – recommended value)| / recommended value * 100

Accuracy = 100 –Error (%)

Table C.5 Total daily precipitation (mm) in the sampling locations, Columbia, SC during the sampling campaign. S: Lower Saluda River, B: Broad River, Co: Congaree River at Columbia, and C: Congaree River at Cayce, ADP: Antecedent dry period

Date	Precipitation (B)	Precipitation (Co and C)	Precipitation (S)	ADP (Days) (C and B)	ADP (Days) (S)
27/4/2020	0	0	0		
28/4/2020	0	0	0		
29/4/2020	0.5	0.5	2.5	5	4
30/4/20020	16.8	16.8	15.7	0	0
1/5/2020	0	0	0		
2/5/2020	0	0	0		
3/5/2020	0	0	0		
4/5/2020	0	0	0		
5/5/2020	0.5	0.5	0	4	
6/5/2020	0	0	1.5		5
7/5/2020	0	0	0		
8/5/2020	1.0	1.0	0.8	2	1
9/5/2020	0	0	0		
10/5/2020	0	0	0		
11/5/2020	0	0	0		
12/5/2020	0	0	0		

Table C.6 Gd anomalies across the world.

SI	Country	Location	Gd_N/Gd_N^* size	Reference
1	USA	River waters in Pennsylvania	1.58 to 4.94	[12]
2	Germany	Rhine River	4.4 to 21	[13]
3	Germany	Wupper River, Leverkussen; Others: Sieg, Rhein, Elbe, and Mosel River	9.1 to 30; other rivers: 1.5 to 3	[14]
4	Germany	Spree, Dahme, Upper Havel River	1.6 to 1.8	[15]
5	France	Vene River	2.1 to 5.25	[16]
6	Czech Republic	Berounka, Vltava, Jizera River	1.1 to 11.3	[17]
7	Japan	Ara, Tama, and Tone River	1.0 to 7.0	[18]
8	Luxembourg	Alzette River	20 to 30	[19]

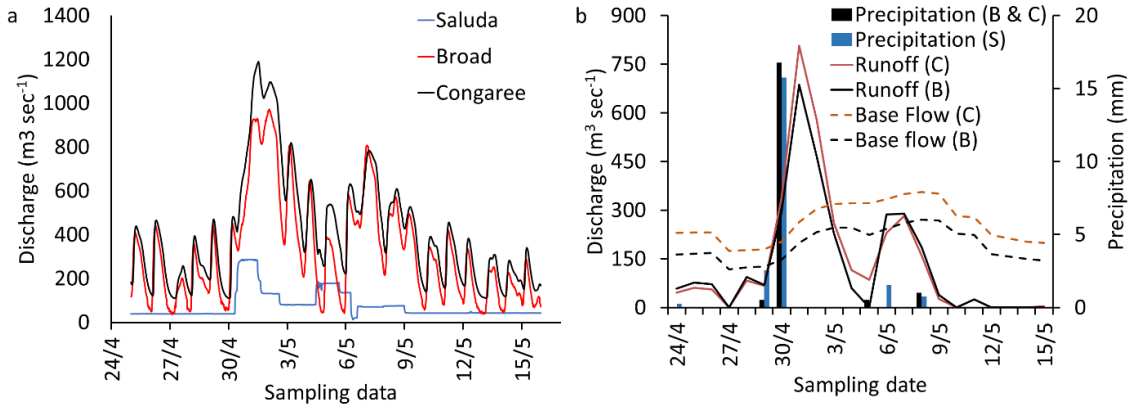

Figure C.1 (a) 15-minutes time resolution discharge in the Saluda, Broad, and Congaree Rivers and (b) the separated runoff and baseflow in the Broad and Congaree Rivers based on daily discharge data together with the precipitation in Columbia, South Carolina near the Lower Saluda River (S), Broad and Congaree River (B & Co).

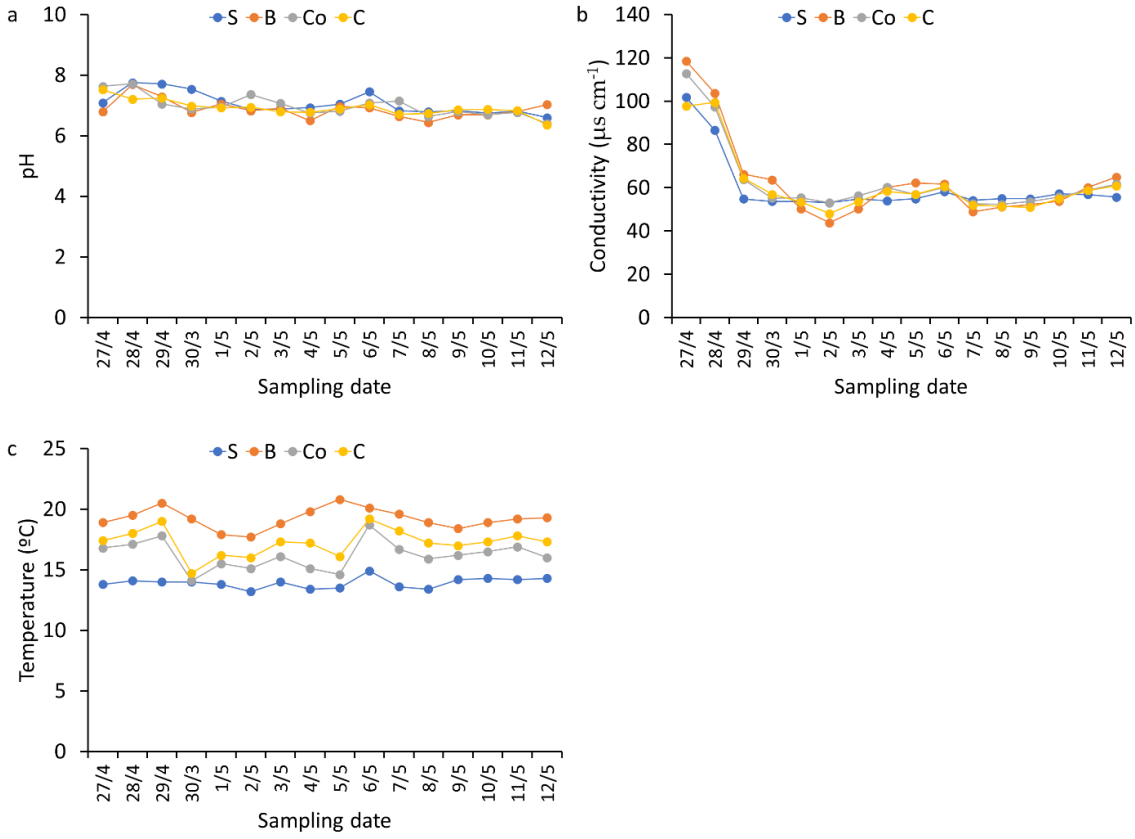

Figure C.2 Water physicochemical properties at the sampling sites during the sampling period (a) pH, (b) conductivity, and (c) temperature. S: Lower Saluda River, B: Broad River, Co: Congaree River at Columbia, and C: Congaree River at Cayce.

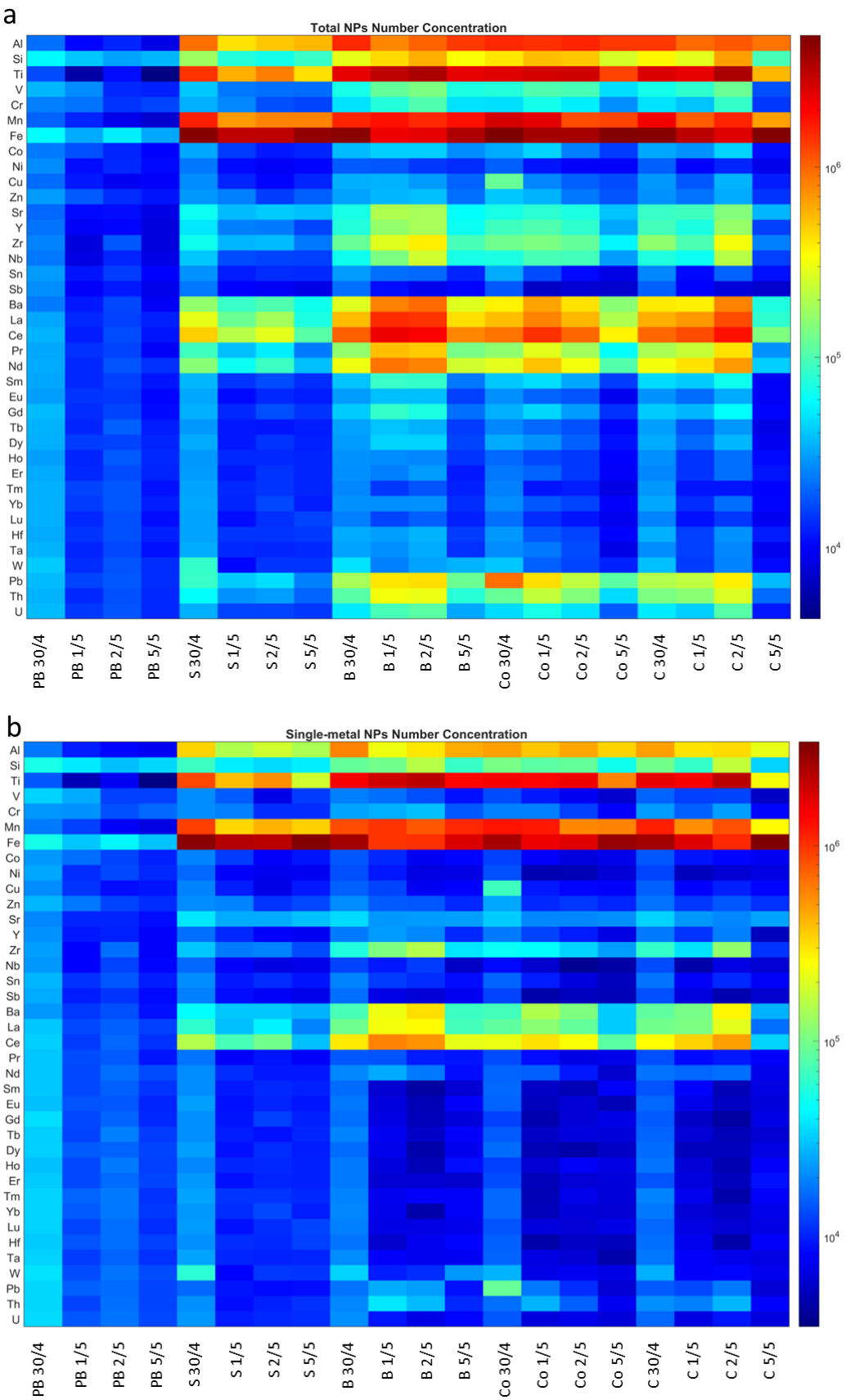
a
Total NPs Number Concentration
Al
Si
Ti
V
Cr
Mn
Fe
Co
Ni
Cu
Zn
Sr
Y
Zr
Nb
Sn
Sb
Ba
La
Ce
Pr
Nd
Sm
Eu
Gd
Tb
Dy
Ho
Er
Tm
Yb
Lu
Hf
Ta
W
Pb
Th
U
10^6
10^5
10^4
PB 30/4
PB 1/5
PB 2/5
PB 5/5
S 30/4
S 1/5
S 2/5
S 5/5
B 30/4
B 1/5
B 2/5
B 5/5
Co 30/4
Co 1/5
Co 2/5
Co 5/5
C 30/4
C 1/5
C 2/5
C 5/5
b
Single-metal NPs Number Concentration
Al
Si
Ti
V
Cr
Mn
Fe
Co
Ni
Cu
Zn
Sr
Y
Zr
Nb
Sn
Sb
Ba
La
Ce
Pr
Nd
Sm
Eu
Gd
Tb
Dy
Ho
Er
Tm
Yb
Lu
Hf
Ta
W
Pb
Th
U
10^6
10^5
10^4
PB 30/4
PB 1/5
PB 2/5
PB 5/5
S 30/4
S 1/5
S 2/5
S 5/5
B 30/4
B 1/5
B 2/5
B 5/5
Co 30/4
Co 1/5
Co 2/5
Co 5/5
C 30/4
C 1/5
C 2/5
C 5/5

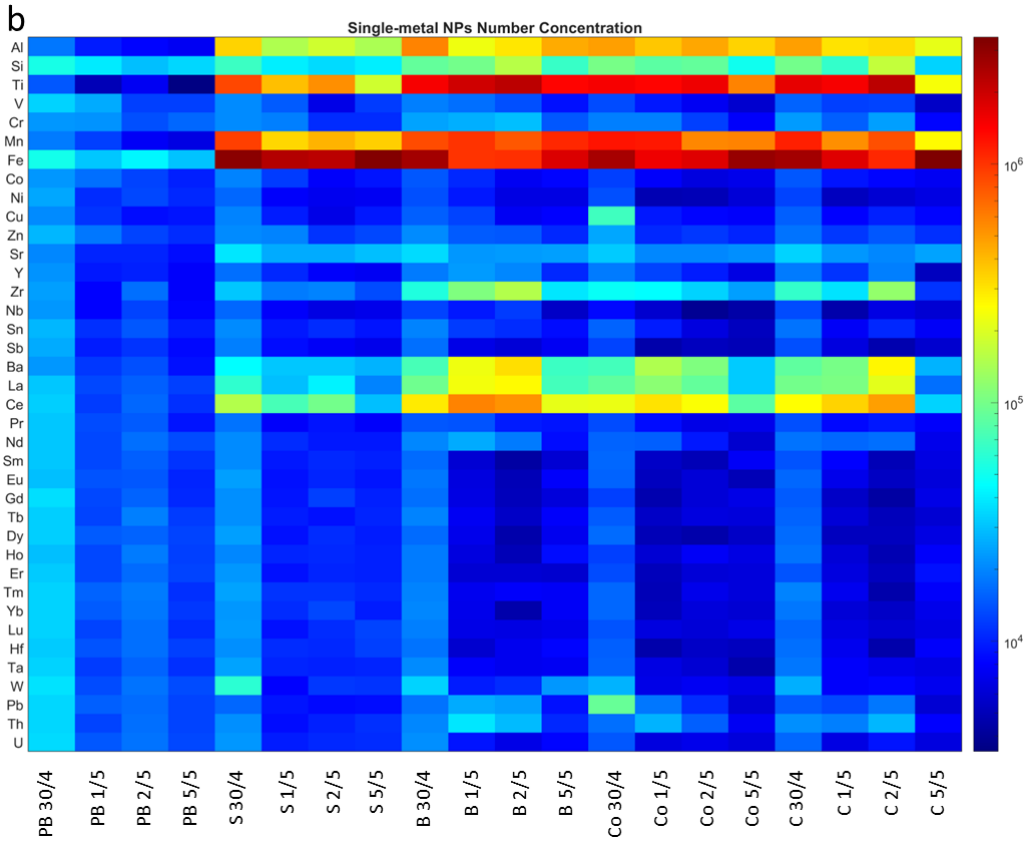

Figure C.3 Uncorrected number concentrations of (a) NPs, (b) smNPs and (c) mmNPs in procedural blanks and the selected River samples. PB: procedural blanks, S: Lower Saluda River, B: Broad River, Co: Congaree River at Columbia, and C: Congaree River at Cayce.

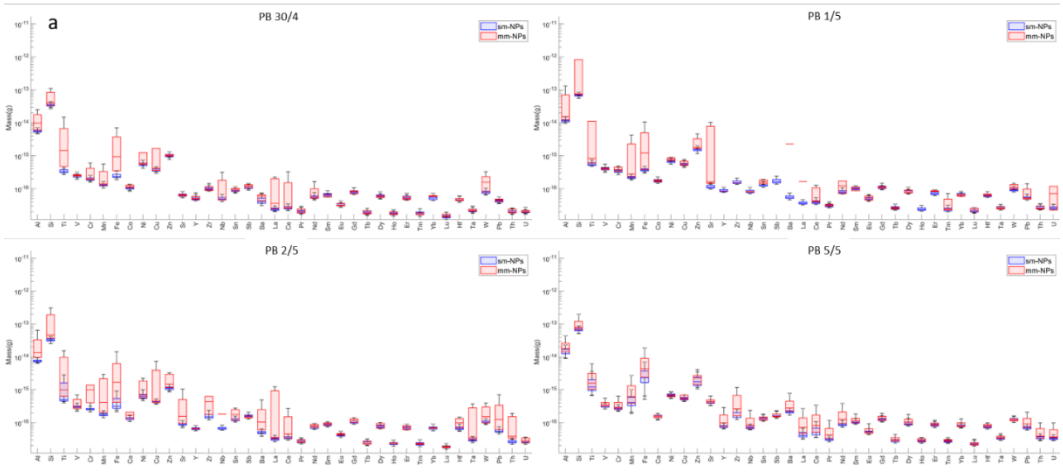

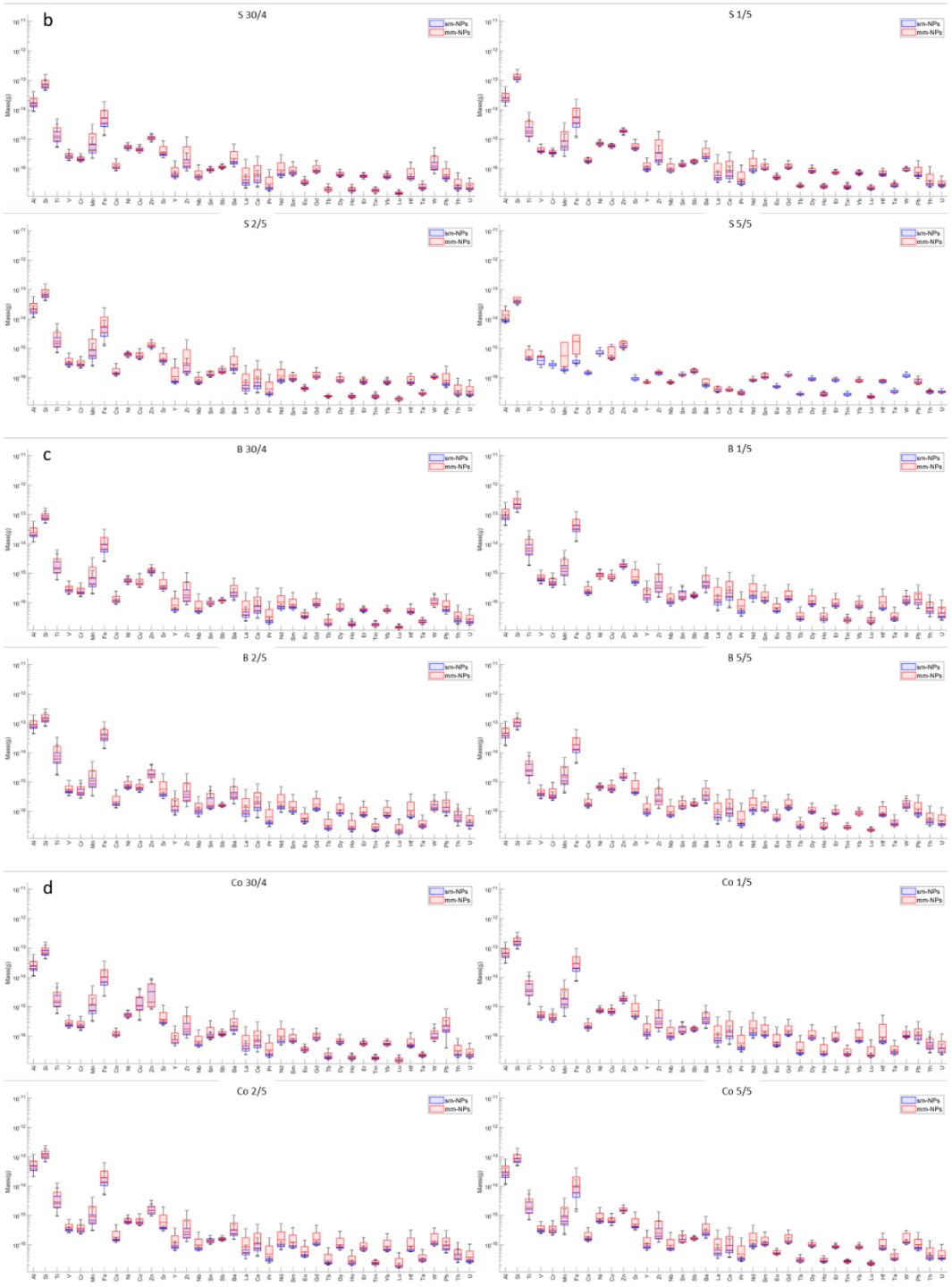
b
S 30/4
S 1/5
S 2/5
S 5/5
c
B 30/4
B 1/5
B 2/5
B 5/5
d
Co 30/4
Co 1/5
Co 2/5
Co 5/5
srn-NPs
mm-NPs
Mass(g)

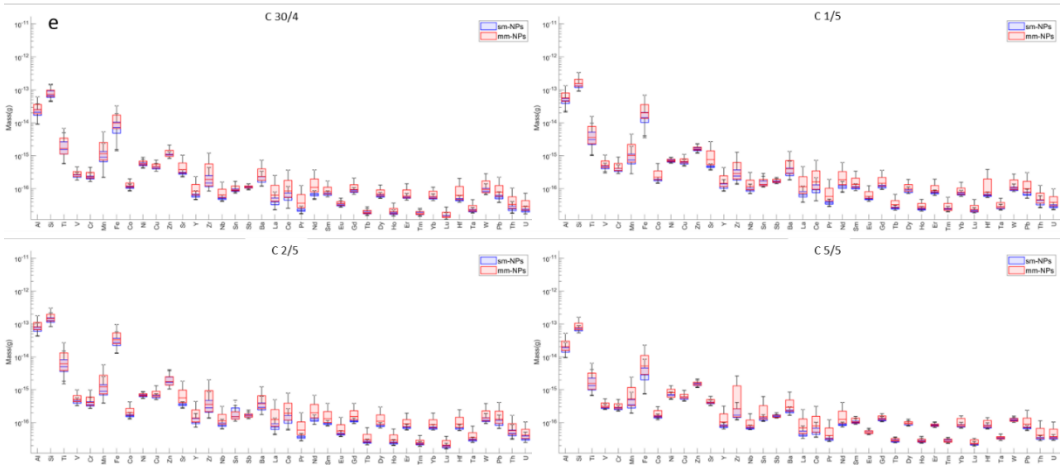

Figure C.4 Mass distribution within individual particles in (a) procedural blanks (PB), (b) Lower Saluda River (S), (c) Broad River (B), (d) Congaree River at Columbia (Co), and (e) Congaree River at Cayce (C).

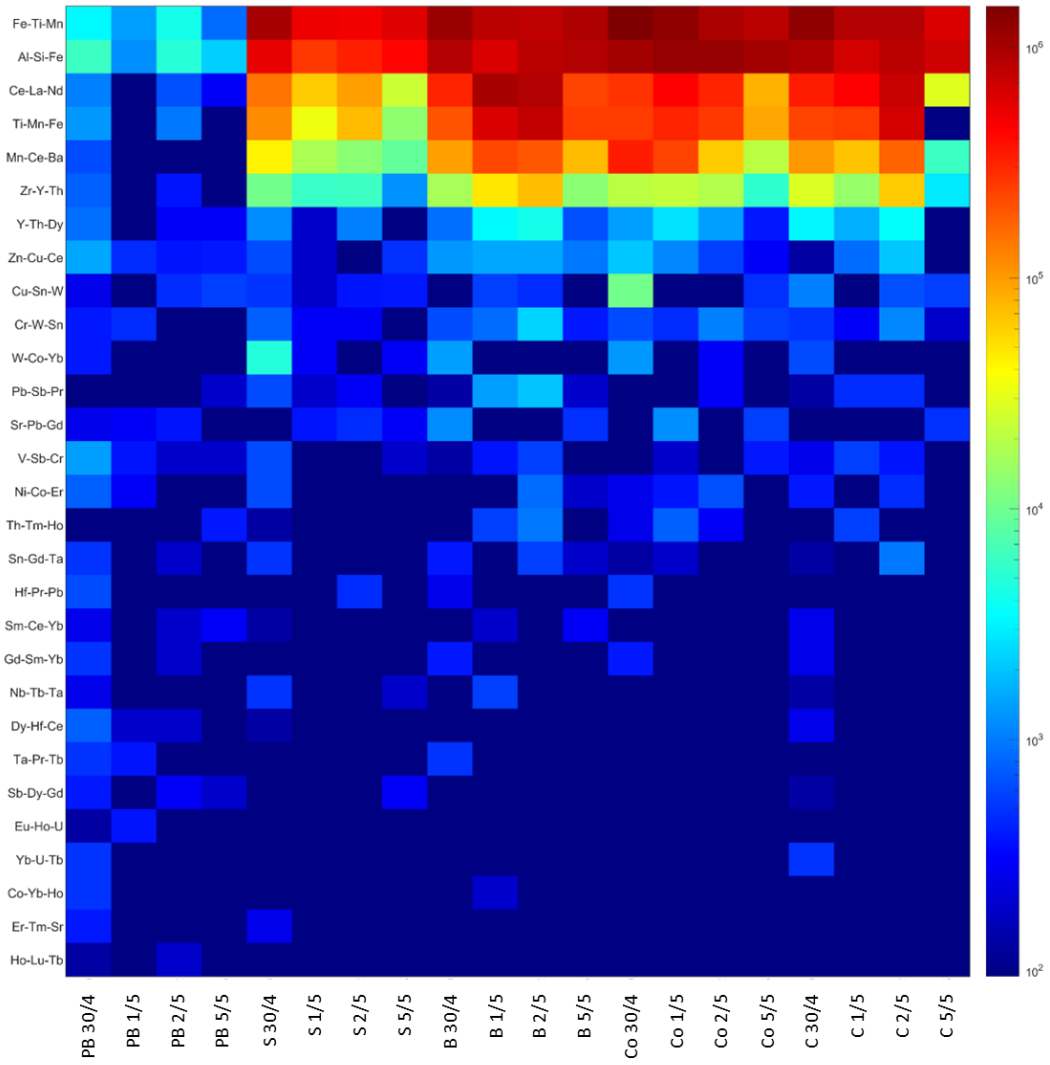

Figure C.5 Number concentrations of the members of mmNP clusters. Clustering parameters were: maximum number of first stage clusters = 30, first and second stage cutoffs were 0.65 and 0.2. PB: procedural blank, S: Lower Saluda River, B: Broad River, Co: Congaree River at Columbia, and C: Congaree River at Cayce.

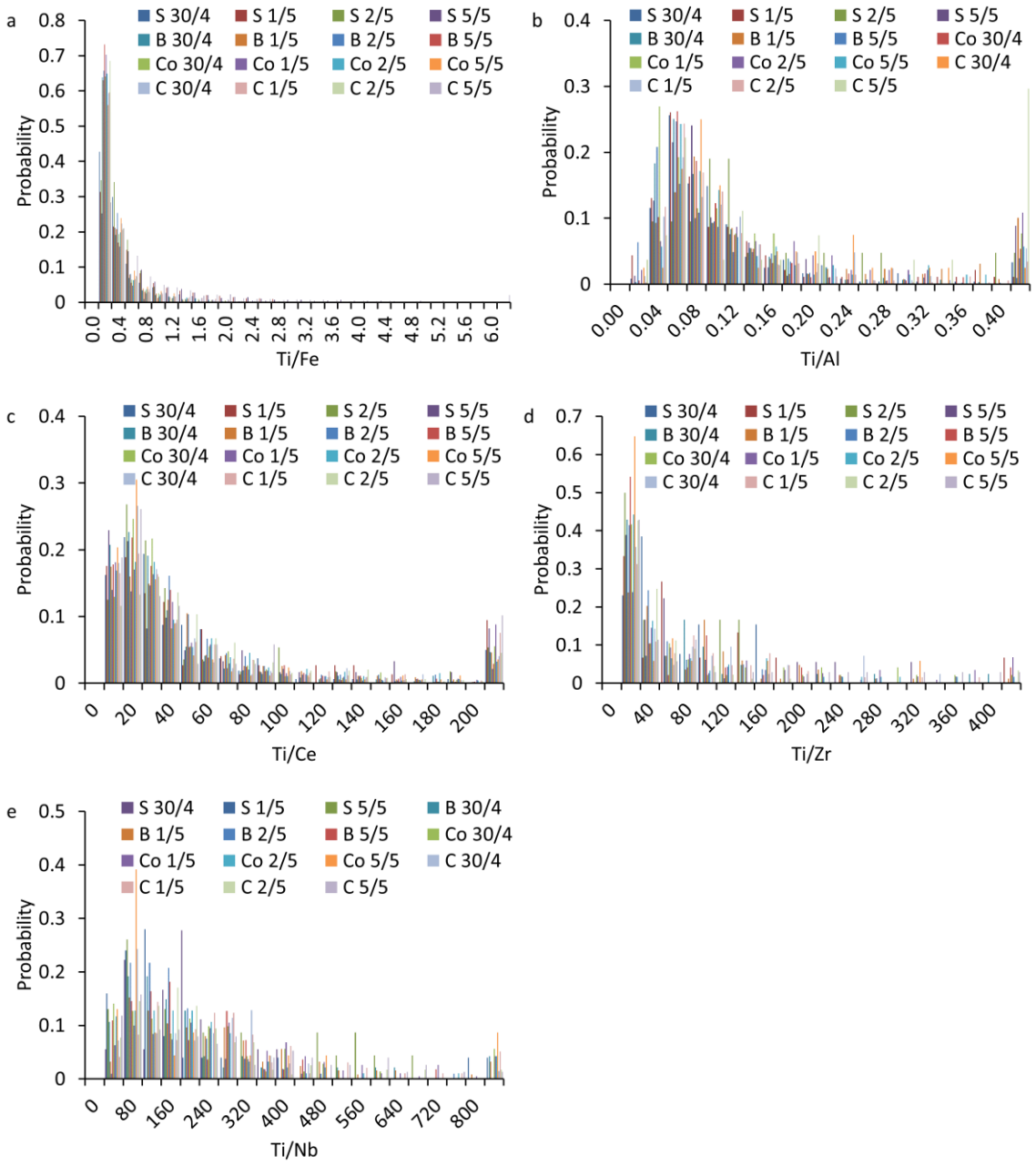

Figure C.6. Elemental ratios of (a) Ti/Fe and (b) Ti/Al, and (c) Ti/Ce, (d) Ti/Zr, and (e) Ti/Nb in Fe-rich clusters. S: Lower Saluda River, B: Broad River, Co: Congaree River at Columbia, and C: Congaree River at Cayce.

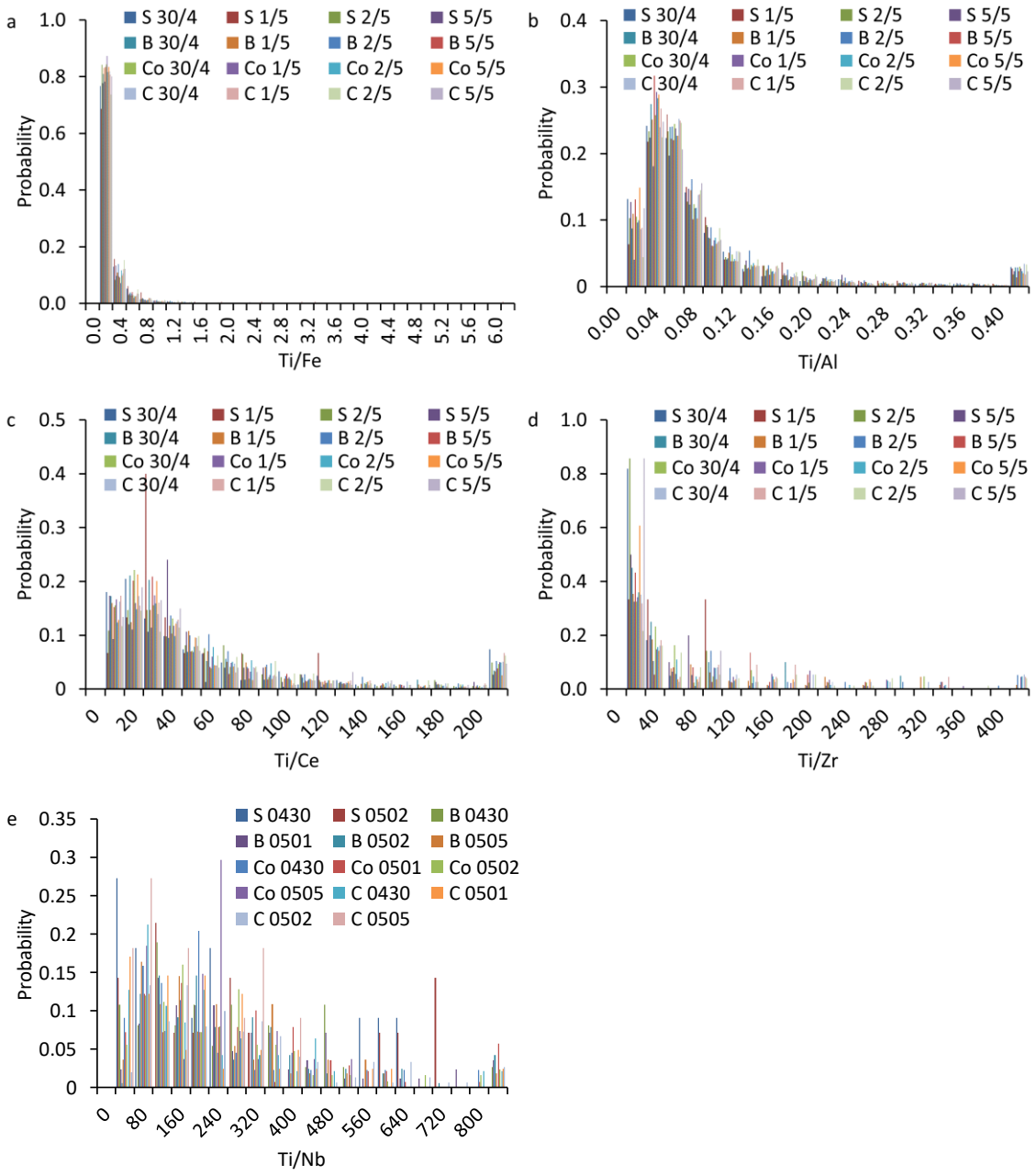

Figure C.7 Elemental ratios of (a) Ti/Fe, (b) Ti/Al, (c) Ti/Ce, (d) Ti/Zr, and (e) Ti/Nb in Al-rich clusters. S: Lower Saluda River, B: Broad River, Co: Congaree River at Columbia, and C: Congaree River at Cayce.

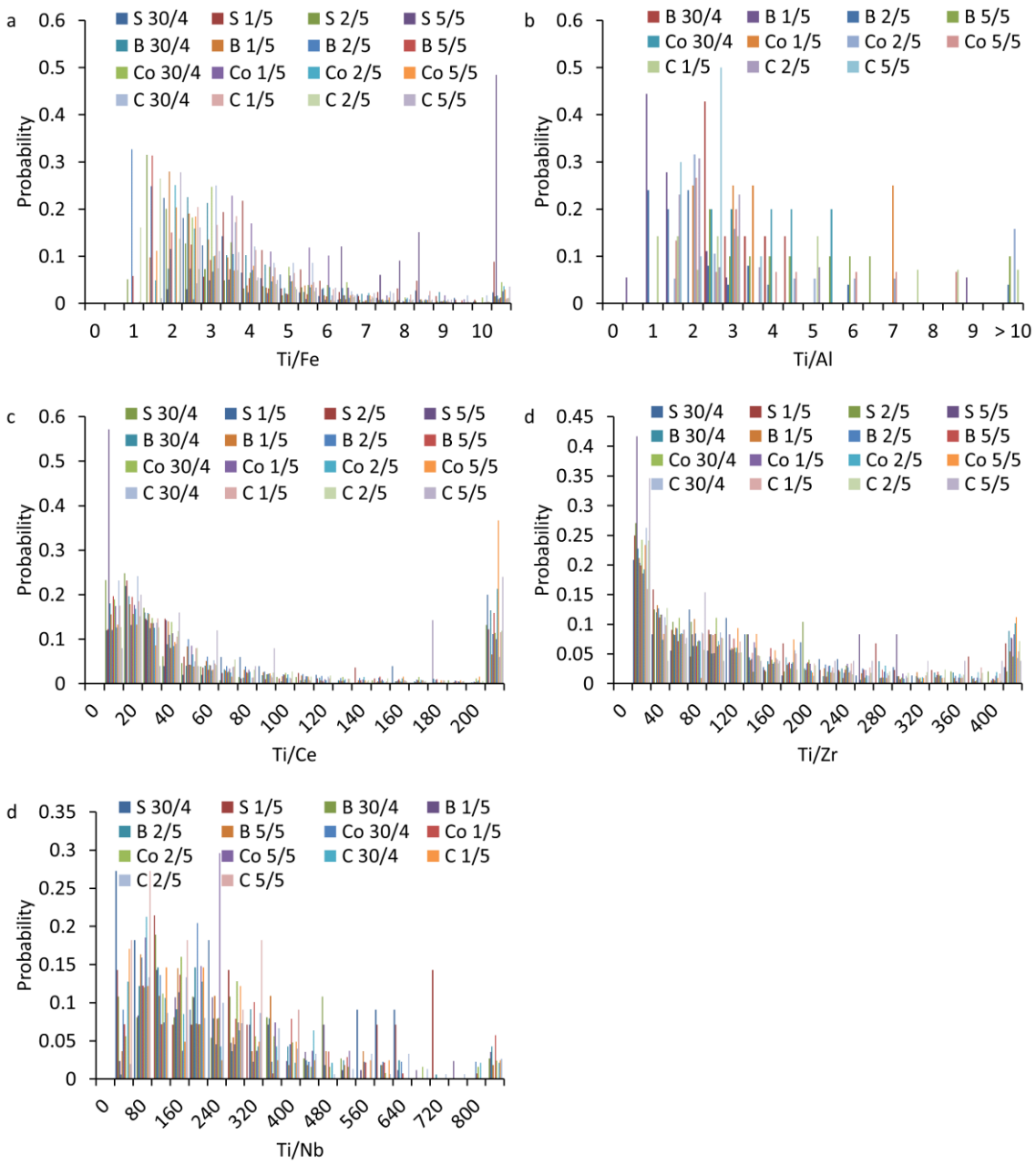

Figure C.8 Elemental ratios of (a) Ti/Fe and (b) Ti/Al, and (c) Ti/Ce, (d) Ti/Zr, and (e) Ti/Nb in Ti-rich clusters. S: Lower Saluda River, B: Broad River, Co: Congaree River at Columbia, and C: Congaree River at Cayce.

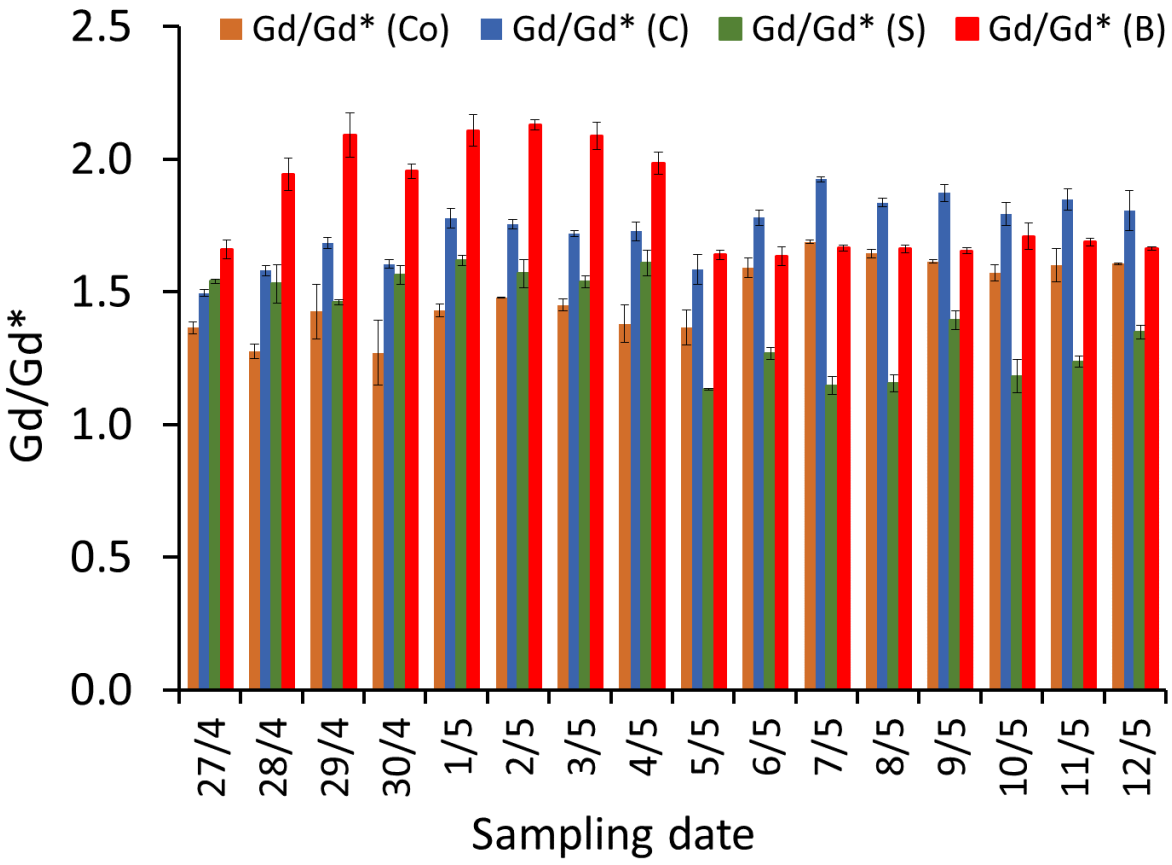

Figure C.9 Gadolinium anomaly in Saluda River (S), Broad River (B), Congaree River, Columbia (Co), Congaree River, Cayce (C) based on the equation 1.

References

1. U.S. Army Corps of Engineers & Stanley Consultants. Saluda River Basin, Charleston district navigability study. (1977).
2. Congaree River Keeper. Lower Saluda River. Available at: https://www.congareeriverkeeper.org/lower-saluda-river. (Accessed: 8th January 2021)
3. SCDHEC. Watershed Water Quality Assessment Saluda River Basin. (2011).
4. SCDOT. Annual average daily traffic. (2019). Available at: https://www.scdot.org/travel/pdf/trafficcounts/2019/Lexington.pdf. (Accessed: 2nd April 2021)
5. SCDOT. Annual average daily traffic. (2019). Available at: https://www.scdot.org/travel/pdf/trafficcounts/2019/Richland.pdf. (Accessed: 1st April 2021)
6. U.S. Geological Survey (USGS). USGS Current Conditions for USGS 02162285 TABLE ROCK RESERVOIR NR CLEVELAND, SC. Available at: https://waterdata.usgs.gov/nwis/dv?cb_00045=on&format=html&site_no=02162285&referred_module=sw&period=&begin_date=2020-04-27&end_date=2020-05-12. (Accessed: 10th January 2021)
7. NC DEQ. Broad river Basin restoration priorities. (2009).
8. U.S. Geological Survey (USGS). USGS Current Conditions for USGS 03451500 FRENCH BROAD RIVER AT ASHEVILLE, NC. Available at: https://waterdata.usgs.gov/nwis/dv?cb_00045=on&format=html&site_no=03451500&referred_module=sw&period=&begin_date=2020-04-20&end_date=2020-05-10. (Accessed: 8th January 2021)
9. City of Knoxville. Rainfall Data - City of Knoxville. Available at: https://knoxvilletn.gov/government/city_departments_offices/engineering/stormwater_engineering_division/rainfall_data. (Accessed: 8th January 2021)
10. Jochum, K. P. et al. Reference Values Following ISO Guidelines for Frequently Requested Rock Reference Materials. Geostand. Geoanalytical Res. 40, 333–350 (2016).
11. Kulaksiz, S. & Bau, M. Contrasting behaviour of anthropogenic gadolinium and natural rare earth elements in estuaries and the gadolinium input into the North Sea. Earth Planet. Sci. Lett. 260, 361–371 (2007).
12. Bau, M., Knappe, A. & Dulski, P. Anthropogenic gadolinium as a micropollutant in river waters in Pennsylvania and in Lake Erie, northeastern United States. Chemie der Erde 66, 143–152 (2006).
13. Kulaksiz, S. & Bau, M. Rare earth elements in the Rhine River, Germany: First case of anthropogenic lanthanum as a dissolved microcontaminant in the hydrosphere. Environ. Int. 37, 973–979 (2011).
14. Bau, M. & Dulski, P. Anthropogenic origin of positive gadolinium anomalies in river waters. Earth Planet. Sci. Lett. 143, 245–255 (1996).
15. Knappe, A., Möller, P., Dulski, P. & Pekdeger, A. Positive gadolinium anomaly in surface water and ground water of the urban area Berlin, Germany. Geochemistry 65, 167–189 (2005).
16. Elbaz-Poulichet, F., Seidel, J. L. & Othoniel, C. Occurrence of an anthropogenic gadolinium anomaly in river and coastal waters of Southern France. Water Res. 36, 1102–1105 (2002).

17. Möller, P., Paces, T., Dulski, P. & Morteani, G. Anthropogenic Gd in surface water, drainage system, and the water supply of the City of Prague, Czech Republic. Environ. Sci. Technol. 36, 2387–2394 (2002).
18. Nozaki, Y., Lerche, D., Alibo, D. S. & Tsutsumi, M. Dissolved indium and rare earth elements in three Japanese rivers and Tokyo Bay: Evidence for anthropogenic Gd and In. Geochim. Cosmochim. Acta 64, 3975–3982 (2000).
19. Hissler, C., Stille, P., Guignard, C., François Iffly, J. & Pfister, L. Rare Earth Elements as hydrological tracers of anthropogenic and critical zone contributions: a case study at the Alzette River basin scale. Procedia Earth Planet. Sci. 10, 349–352 (2014).

Appendix D: Supporting Information for Chapter 5

D.1 Sample digestion for elemental analysis

The bulk water samples were digested in 15 mL Teflon vessels (Savillex, Eden Prairie, MN, United States) on custom-made Teflon covered hotplates placed in a box equipped with double-HEPA filtered forced air in a metal-free HEPA filtered air clean laboratory. Water aliquots (10 mL) were placed in the vessel and weighed (Mettler Toledo, Excellence Plus, Columbus, OH, United States). Samples were dried at 110°C and treated with 1 mL of 30% H_2O_2 (Fisher Chemical, Fair Lawn, NJ, United States) for 2 h at 70°C to remove organic matter. Remaining H_2O_2 was then evaporated and the sample was digested with 2 mL of HF:HNO_3 (3:1) mixture (ACS grade acids distilled in the laboratory, Sigma Aldrich, St. Louis, MO, United States) for 24 h at 110°C. After evaporation of the acid mixture at 110°C, the residue was reacted with 1 mL of distilled HNO_3 to break up insoluble fluoride salt that may have formed during the sample digestion, and HNO_3 was left to evaporate at 110°C. This step was repeated twice before weighing the sample and adding 5 mL of 1% HNO_3. The sample was sonicated for 10 min in a sonication bath (Branson, 2800, 40kHz, Danbury, CT, United States) and warmed for 2 h at 50°C for full dissolution. The solution was transferred to 15 mL polypropylene centrifuge tubes (Fisher Scientific, San Nicolás de los Garza, Nuevo León, Mexico) and stored at 4°C. Samples were centrifuged (Eppendorf, 5810 R, Hamburg, Germany) for 5 min at 3100 g prior to ICP-MS analysis to for removing any undigested minerals.

Full procedural digestion blanks were < 6.8% for all reported element in this study and < 2.8% for titanium and niobium of samples' analyte signal [1]. Therefore, blanks are insignificant to the calculations of Ti concentrations or total Ti/Nb elemental ratios. The elemental concentrations of the USGS reference materials BHVO-2 Hawaiian basalts run as unknowns after digestion following the digestion procedure described above, demonstrate high recovery (approximately 100%) for most elements [1]. The precision of our method was better than 4% for all isotopes and the accuracy was better than 89% for most elements, including Ti and Nb (**Table D.1**) [1].

D.2 Elemental analysis

Elemental concentrations in the digested water samples were determined by Perkin Elmer NexION 350D ICP-MS (**Table D.2**). Standard tuning procedure was performed before analysis for instrument maintenance. Dissolved multi-element standards mixture of ICP Complete Group Calibration Standard (BDH Chemicals, Radnor, PA, USA) and ICP Refractory Element Group Calibration Standard (BDH Chemicals, Radnor, PA, USA) diluted in 1% nitric acid (TraceMetal grade, Fisher Chemical, Fair Lawn, NJ, USA) were used for mass concentration calibration ranging from 0.01 to 1000 µg/L. Internal standards (ICP Internal Element Group Calibration Standard, BDH Chemicals, Radnor, PA, USA) were monitored at the same time for quality control. The isotopes measured were ^{27}Al, ^{49}Ti, ^{57}Fe, ^{93}Nb, ^{139}La, ^{140}Ce, ^{149}Sm, ^{157}Gd, and ^{159}Tb. All isotopes were analyzed in the standard mode.

D.3 Nb concentration in TiO_2 engineered particles

Two commercially available TiO_2 engineered particles 1) P25 TiO_2 ENP with 21 nm primary particle size (Sigma Aldrich, St Louis, MO, USA) and 2) Tiona 595 Rutile titanium dioxide pigment (Glen Burnie, MD, USA) were digested using the same procedure described in the supplementary information (SI.1.1). The Ti and Nb concentration in the digested samples were determined by ICP-MS for target TiO_2 concentrations covering the range of measured TiO_2 concentrations in this study (*e.g.*, 0.01-1000 µg L^{-1}). The Nb concentration was below the ICP-MS detection limit (*e.g.*, 7 ng L^{-1}) for TiO_2 concentrations up to 1000 µg L^{-1}. Therefore, the Nb concentration in TiO_2 engineered particles is negligible for the range of TiO_2 concentrations measured in this study in Edisto River stream water.

D.4 Multi element-single particle analysis

A selected set of Edisto River water samples was analyzed by icpTOF-MS to determine the elemental association and elemental ratios for natural particles and to cross validate the background elemental ratios determined based on the minimum elemental ratio measured in all sampling events.

The Edisto River water samples were shaken well prior extraction to resuspend any settled particles and to obtain a representative subsample. Aliquots (10 mL) were transferred into acid-washed 15 mL centrifuge tubes. The transferred samples were bath sonicated for 2 h (Branson, Model 2800, 40 kHz, Danbury, CT, United States), then centrifuged at 775 g for 5 min to remove large particles (> 1000 nm assuming natural particle density, ρ = 2.5 g cm^{-3}) and prevent clogging of the ICP-TOF-MS introduction

system. The top 7 mL supernatant was decanted and stored at 4°C in the dark till analysis by SP-ICP-TOF-MS. The theoretical size of the extracted fractions corresponds to particles < 1000 nm for natural particles (ρ = 2.5 g cm^{-3}), and < 725 nm for TiO_2 particles (ρ = 4.2 g cm^{-3}). All samples were bath sonicated again for 15 min and were diluted by a factor of 100 prior to SP-ICP-TOF-MS analysis.

Single particle analysis of the diluted particle extracts was performed using an ICP-TOF-MS (TOFWERK, Thun, Switzerland) to determine all isotopes within a single particle simultaneously [3]. Element specific instrument sensitivities were measured with a series of multi-element solutions prepared from a 71-element ICP-MS certified reference standard mixture (0, 1, 2, 5, and 10 µg L^{-1} multi element standard, diluted in 1% HNO_3, BDH Chemicals, Radnor, PA, USA). The transport efficiency was calculated using the known size approach [4] using both Au ENMs with a certified particle size of 60 nm (NIST RM8013 Au, Gaithersburg, MD, USA) prepared in UPW and Au standard solutions (0, 1, 2, 5, and 10 µgL^{-1}, diluted in 1% HCl, BDH Chemicals, West Chester, PA, USA). Using a standard tuning solution, the ICP-TOF-MS mass spectra were calibrated using $^{18}H_2O^+$, $^{59}Co^+$, $^{115}In^+$, $^{140}Ce^+$, and $^{238}U^+$ target isotopes in TofDAQ view (TOFWERK) prior to analysis or in Tofware (TOFWERK) after analysis if mass shifts occurred during analysis. Particle/baseline signal separation, particle signal, mass, and number concentration were determined from mass-calibrated ICP-TOF-MS spectra using Python script in Tofware as described elsewhere [1]. The particle detection threshold was calculated for each isotope according to Eq. 1 [5].

$$\text{Threshold} = \text{Mean} + (3.29\sigma + 2.71) \quad \text{(Eq. 1)}$$

The data for each isotope were treated separately, but the time stamps were kept throughout data processing for every isotope, allowing for identification of isotope correlations in a single particle. For example, an impure particle (*e.g.*, a particle containing multiple elements) generates several isotope signals spikes in each time stamp. An "apparently pure" particle generates one isotope signal spike in a given time stamp. The term "apparently pure" is used in this study as such particles might contain elements at concentrations below the sp-ICP-MS size/mass detection limit. Elemental association and elemental ratio distributions were determined using data filtration in Excel.

D.5 Gadolinium anomaly

There are two major sources of TiO_2 into rivers: 1) wastewater in the form of effluent or sewage overflows [1] and 2) urban runoff [6]. The crust normalized pattern of REEs shows a flat line for all REEs with a slight increase in Gd in all samples (**Figure D.4a**), indicating that all REEs originate from natural sources (e.g., soil erosion or river sediments) with a potential presence of anthropogenic Gd. The major anthropogenic source of Gd is domestic sewage effluent, widely recognized as the major source of Gd in polluted streams. Anomalies in REE patterns are commonly quantified by the ratio of the normalized measured concentration of the normalized theoretical concentration (determined by interpolation between neighboring elements) for the anomalous element. Here, we use neodymium (Nd) and samarium (Sm) to extrapolate the background Gd values in the samples and to quantify Gd anomalies according to Eq. 1 [7].

$$Gd_N/Gd_N^* = Gd_N/10^{(2logSm-logNd)} \quad \text{(Eq. 1)}$$

A size of $Gd_N/Gd_N^* = 1.3$ is commonly used as the benchmark to distinguish between the natural and anthropogenic Gd anomaly.

D.6 Estimating urban runoff from urban areas in the Edisto River basin

There are no data available on the urban runoff generation from the city of Orangeburg and Aiken; therefore, the urban runoff contribution into the Edisto River stream from the city of Orangeburg and Aiken is measured based on the following assumptions:

1. A quarter of the city of Aiken is taken into account due to the fact that only a portion of the City of Aiken is situated in the Edisto River basin.
2. Rainfall affected the entire city of Orangeburg (~21.5 km^2) and a quarter of the city of Aiken (~53.9/4 = 13.48 km^2) at the same time which created the 20-55% runoff [16]
3. 40 years (from 1971 to 2010) mean yearly precipitation in Orangeburg county is 47 inches, and mean yearly precipitation in Aiken county is 48 inches [17]

Therefore, the lower limit of total urban runoff generated from both cities = {(47/365*25.4/1000*21.5*10^9) + (48/365*25.4/1000*53.9/4*10^9)} * 20% = 23,065,983.6 L day^{-1}

And the upper limit of total urban runoff generated from both cities = {(47/365*25.4/1000*21.5*10^9) + (48/365*25.4/1000*53.9/4*10^9)} * 55% = 63,431,454.8 L day^{-1}

D.7 Estimation of land-applied biosolids and the associated TiO_2

The Edisto River basin originates in the sandhill region of the west central South Carolina and covers 8,030 km^2, and 29% of the lands in the basin are used for agricultural purposes. The total number of wastewater treatment plants (WWTPs) in SC is 173 with a total flow of 462 million gallons per day (MGD) (1.75×10^6 m^3 day^{-1}) and total solids used and disposed of 37,400 dry U.S. tons. The land applied biosolids in SC is estimated at 14,063 dry U.S. tons (*e.g.*, 38% of the total generated solids) [18]. The concentration of TiO_2 in sewage sludge in the United States is estimated at 1.67 to 10.0 kg TiO_2 $tons^{-1}$ dry weight (**Table D.8**) [19].

Agricultural land area in South Carolina = 4,800,000 acres = 19,424,928,000 m^2

Agricultural land area in ER watershed = 8,030 km^2 * 29% = 8030 * 29% * 10^6 m^2 = 2,328,700,000 m^2

The lower limit of TiO_2 mass applied on land in South Carolina = 14,063 * 1.67*9.072 * 10^11/1000 = $21.3 * 10^{12}$ µg TiO_2

The upper limit of TiO_2 mass applied on land in South Carolina = 14,063 * 10 * 9.072 * 10^11/1000 = $12.8 * 10^{13}$ µg TiO_2

The lower limit of TiO_2 mass applied on land in Edisto River watershed =$21.3 * 10^{12}$ µg TiO_2 * 2,328,700,000 / (19,424,928,000 * 2,328,700,000) = 1097.5 µg TiO_2 m^{-2}

The upper limit of TiO_2 mass applied on land in Edisto River watershed =$12.8 * 10^{13}$ µg TiO_2 * 2,328,700,000 / (19,424,928,000 * 2,328,700,000) = 6594.4 µg TiO_2 m^{-2}

Table D.1 Elemental analysis of concentration ($\mu g\ kg^{-1}$) of the USGS reference materials BHVO-2 Hawaiian basalts

Concentration (ug/kg)	Mean	Standard Deviation	Recommended values [2]	Precision (%)	Error (%)	Accuracy (%)
^{27}Al	7.55×10^7	3.13×10^6	7.11×10^7	4.15	6.1	93.9
^{47}Ti	1.52×10^7	5.73×10^5	1.64×10^7	3.78	4.1	95.9
^{57}Fe	9.43×10^7	3.44×10^6	8.67×10^7	3.65	8.8	91.2
^{93}Nb	1.57×10^4	1.24×10^2	1.81×10^4	0.79	11.0	89.0
^{139}La	1.38×10^4	3.98×10^2	1.52×10^4	2.89	2.9	97.1
^{140}Ce	3.39×10^4	9.29×10^2	3.75×10^4	2.74	4.3	95.7
^{152}Sm	5.70×10^3	1.24×10^1	6.02×10^3	0.22	5.3	94.7
^{158}Gd	6.33×10^3	1.96×10^2	6.21×10^3	3.10	1.9	98.1
^{159}Tb	9.06×10^2	4.12×10^0	9.39×10^2	0.45	3.5	96.5

Precision (%) = standard deviation/mean * 100

Error (%) = |(Measured concentration – recommended value)| / recommended value * 100

Accuracy = 100 –Error (%)

Table D.2 Perkin Elmer NexION 350D ICP-MS operating conditions.

Instrument Parameter	**Value**
Nebulizer Gas Flow	0.85 to 1 L/min
Auxiliary Gas Flow	1.02 L/min
Plasma Gas Flow	16 L/min
ICP RF Power	1600 W
Analog Stage Voltage	-1600 V
Pulse Stage Voltage	1600 V
Discriminator Threshold	12
Deflector Voltage	-9.5 V
Dwell time	50 ms
Sample Flow Rate	0.3 mL/min

Table D.3 TOFWERK ICP-TOF-MS operating conditions.

Instrument parameter	**Value**				
Plasma Power	1550 V				
Nebulizer Gas Flow	1.1 L/min				
Auxiliary Gas Flow	0.8 L/min				
Cooling Gas Flow	14 L/min				
Injector Diameter	2 mm				
Collision Cell Gas	5 mL/min He with 4.5% H_2				
CCT Bias	-4.34 V				
Notch	Mass	29	32	36.3	41

	Amplitude (V)	1.6	2.0	2.0	1.2
TOF Repetition Rate	33 kHz				
Detected Mass Range	14-275 m/Z				
(CeO/Ce)	< 2.0%				
Data Acquisition	Continuous Mode				
TOF Time Resolution	2 ms				
Sample Flow Rate	0.4 mL/min				
Analysis time	10 min				
Transport efficiency	XX %				

Table D.4 Gd anomalies across the world.

SI	Country	Location	Gd_N/Gd_N^* size	Reference
1	USA	River waters in Pennsylvania	1.58 to 4.94	[8]
2	Germany	Rhine River	4.4 to 21	[9]
3	Germany	Wupper River, Leverkussen; Others: Sieg, Rhein, Elbe, and Mosel River	9.1 to 30; other rivers: 1.5 to 3	[8]
4	Germany	Spree, Dahme, Upper Havel River	1.6 to 1.8	[10]
5	France	Vene River	2.1 to 5.25	[11]
6	Czech Republic	Berounka, Vltava, Jizera River	1.1 to 11.3	[12]
7	Japan	Ara, Tama, and Tone River	1.0 to 7.0	[13]
8	Luxembourg	Alzette River	20 to 30	[14]

Table D.5 Typical biosolids application scenarios [15].

Type of site/vegetation	**Schedule**	**Application frequency**	**Application rate**
Corn	April, May, after harvest	Annually	5 to 10 dry tons per acre
Small grains	March-June, August, fall	Up to 3 times per year	2 to 5 dry tons per acre
Soybeans	April-June, fall	Annually	5 to 20 dry tons per acre
Hay	After each cutting	Up to 3 times per year	2 to 5 dry tons per acre
Forest land	Year round	Once every 2-5 years	5 to 100 dry tons per acre

Range land	Year round	Once every 1-2 years	2 to 60 dry tons per acre
Reclamation sites	Year round	Once	60 to 100 dry tons per acre

Table D.6 Elemental ratios in bulk water samples and in multi-element Ti-bearing particles in a select set of Edisto River water samples. The elemental composition of single particles was determined using SP-ICP-TOF-MS.

Sampling date	Bulk water Ti/Nb*	Ti/Nb**	Ti/Al**	Ti/Fe**	Ce/La**
23/5/18	374 ± 6	230 ± 210	0.15 ± 0.20	1.0 ± 3.1	1.9 ± 1.1
23/7/18	267 ± 3	248 ± 170	0.24 ± 0.37	1.1 ± 3.6	1.9 ± 1.0
5/9/18	270 ± 16	263 ± 183	0.16 ± 0.26	1.1 ± 3.2	2.0 ± 1.1
18/9/18	369 ± 6	226 ± 183	0.18 ± 0.71	0.9 ± 2.4	1.9 ± 0.9
17/12/18	417 ± 4	225 ± 172	0.13 ± 0.20	1.4 ± 5.0	1.9 ± 1.0
29/4/19	258 ± 3	250 ± 309	0.16 ± 0.42	0.6 ± 2.1	2.0 ± 1.1
23/5/19	256 ± 9	235 ± 227	0.20 ± 0.19	0.7 ± 2.4	2.0 ± 1.0
23/7/19	265 ± 17	229 ± 275	0.18 ± 0.32	0.6 ± 1.6	1.9 ± 1.0
11/9/19	243 ± 29	212 ± 185	0.16 ± 0.47	0.9 ± 3.6	2.0 ± 1.0

* Values are reported as mean ± standard deviation of three independent replicates.
** Values are reported as mean ± standard deviation of the ratios in individual particles.

Table D.7-a Pearson correlation between TiO_2 and the parameters reported in Figure 5.1 considering the entire dataset.

	Pearson r =	p- value =	significant
Anthropogenic Gd	0.45	0.001	yes
Phosphorus	0.42	0.003	yes
Suspended sediment	0.37	0.010	yes
Water temperature	0.24	0.099	no
Total nitrogen	0.018	0.905	no
Organic carbon	-0.04	0.799	no
Dissolved oxygen	-0.26	0.079	no

Table D.7-b Pearson correlation between TiO_2 and the parameters reported in Figure 5.1, excluding the data between 16/10/2018 and 17/12/2019.

	Pearson r =	p- value =	significant
Phosphorus	0.52	0.01	yes
Anthropogenic Gd	0.45	0.02	yes
Water temperature	0.38	0.05	Yes
Suspended sediment	0.33	0.10	no
Total nitrogen	0.16	0.43	no
Organic carbon	-0.21	0.31	no
Dissolved oxygen	-0.31	0.13	no

Table D.8 Wastewater treatment plants along the Edisto River and its tributaries

CITY	Facility Name	Approximate distance from sampling site (km)	Average daily flow (Ml/d)
ORANGEBURG	ORANGEBURG STP	75	18.50
BATESBURG	BATESBURG STP	162	5.38
EDGEFIELD	ECW&SA-JOHNSTON PLANT #1	178	2.05
ST GEORGE	ST GEORGE WWTP	31	2.04
BLACKVILLE	BLACKVILLE TOWN OF	96	0.99
BOWMAN	BOWMAN WWS	56	0.89
Holly Hill	HOLLY HILL WWTP	45	0.72
HARLEYVILLE	HARLEYVILLE STP	30	0.45
WAGENER	WAGENER WWTP	128	0.30
BRANCHVILLE	BRANCHVILLE WWTP	53	0.27
SPRINGFIELD	SPRINGFIELD PLANT #1	107	0.23
SPRINGFIELD	SPRINGFIELD PLANT #2	107	0.23
NORWAY	NORWAY WWTP	90	0.11
Total			**32.1**

Table D.9 Sewage spills in the major urban areas (Aiken and Orangeburg) in the Edisto River watershed

CITY	Facility Name	Date (dd/mm/yyyy)	Approximate distance from sampling site (km)	Sewage spill duration (minutes)	Sanitary sewer overflow (l)
ORANGEBURG	ORANGEBURG WWTF	11/11/2020	75	5	11356.2
	ORANGEBURG WWTF	11/11/2020	75	5	5678.1
	ORANGEBURG WWTF	24/9/2020	75	165	11356.2
	ORANGEBURG WWTF	17/9/2020	75	30	5678.1
	ORANGEBURG WWTF	17/9/2020	75	60	3785.4
	ORANGEBURG WWTF	17/9/2020	75	30	3785.4
	ORANGEBURG WWTF	18/5/2020	75	240	3785.4
	ORANGEBURG WWTF	5/3/2020	75	60	3785.4
	ORANGEBURG WWTF	5/3/2020	75	30	3785.4
	ORANGEBURG WWTF	5/3/2020	75	30	3785.4
	ORANGEBURG WWTF	25/2/2020	75	480	3785.4
	ORANGEBURG WWTF	25/2/2020	75	105	3785.4
	ORANGEBURG WWTF	25/2/2020	75	120	3785.4
	ORANGEBURG WWTF	25/2/2020	75	60	7570.8
	ORANGEBURG WWTF	20/2/2020	75	60	3785.4
	ORANGEBURG WWTF	19/2/2020	75	75	3785.4
	ORANGEBURG WWTF	19/2/2020	75	90	3785.4
	ORANGEBURG WWTF	19/2/2020	75	15	3785.4
	ORANGEBURG WWTF	23/12/2019	75	120	3785.4
	ORANGEBURG WWTF	23/12/2019	75	60	3785.4
	ORANGEBURG WWTF	23/12/2019	75	60	3785.4
	BOWMAN TOWN	23/12/2019	45	60	3785.4
	ORANGEBURG WWTF	6/12/2019	75	150	3785.4
	ORANGEBURG WWTF	21/2/2019	75	30	20441.2
	ORANGEBURG WWTF	2/2/2019	75	90	41639.5
	ORANGEBURG WWTF	2/2/2019	75	70	49210.3
	ORANGEBURG WWTF	11/10/2018	75	60	3785.4
	ORANGEBURG WWTF	4/9/2018	75	60	3785.4
	ORANGEBURG WWTF	2/8/2018	75	60	3785.4
	ORANGEBURG WWTF	16/7/2018	75	570	30283.3
	ORANGEBURG WWTF	24/5/2018	75	60	1892.7
	ORANGEBURG WWTF	24/5/2018	75	30	1892.7
	ORANGEBURG WWTF	24/5/2018	75	30	1892.7
	ORANGEBURG WWTF	18/5/2018	75	60	3785.4
	ORANGEBURG WWTF	18/5/2018	75	60	3785.4
	ORANGEBURG WWTF	18/5/2018	75	60	3785.4

	ORANGEBURG WWTF	18/5/2018	75	60	1892.7
	ORANGEBURG WWTF	23/1/2018	75	47	1892.7
	ORANGEBURG WWTF	20/11/2017	75	70	1892.7
AIKEN	AIKEN PSA HORSE CREEK WWTF	9/7/2020	150		
	AIKEN SEWER SYSTEM	19/5/2020	138	420	37854.1
	WAGENER TOWN WWTF	11/5/2020	114	130	30283.3
	AIKEN SEWER SYSTEM	25/4/2020	138	150	1892.7
	AIKEN SEWER SYSTEM	13/2/2020	138	300	1892.7
	AIKEN SEWER SYSTEM	26/12/2019	138	240	1892.7
	AIKEN SEWER SYSTEM	16/12/2019	138	47	1892.7
	WAGENER TOWN WWTF	11/6/2019	114	840	18927.1
	WAGENER TOWN WWTF	11/6/2019	114	240	30283.3
	AIKEN PSA HORSE CREEK WWTF	6/5/2019	150	250	4542.5
	WAGENER TOWN WWTF	30/5/2018	114	50	18927.1
	SHAW INDUSTRIES SEWER COLLECTION SYSTEM	14/10/2017	138	90	1514.2
	NORTH AUGUSTA CITY	3/10/2017	155	600	1135.6
	AIKEN SEWER SYSTEM	13/9/2017	138	05	1892.7
TOTAL					**438350.5**

Table D.10 TiO_2 concentration in sewage sludge

Country	C (µg Ti/ g DW)	C (g TiO_2/ tons DW)	Reference
USA	1000-6000	1,668-10,008	[19]
UK	379-676	632-1,128	[20]
China	971-1,653	1,620-2,757	[21]
Canada	175	292	[22]

DW: dry weight

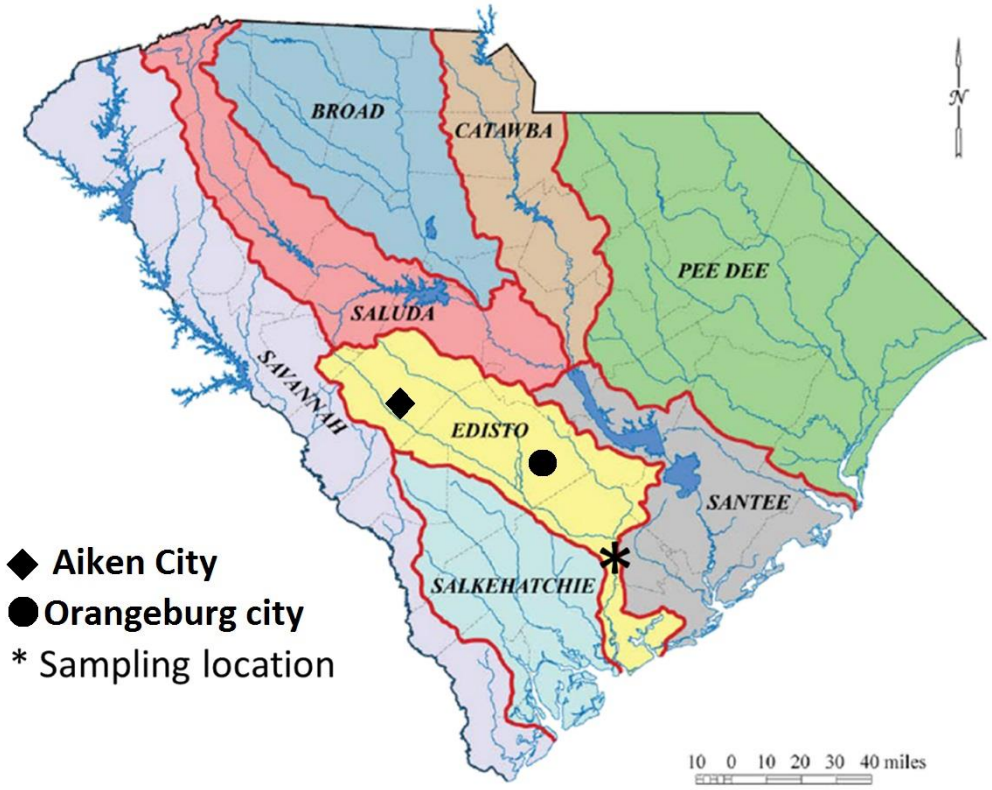

Figure D.1 Sampling location on the Edisto River. Samples were collected at the USGS station 02175000 Edisto River near Givhans, South Carolina.

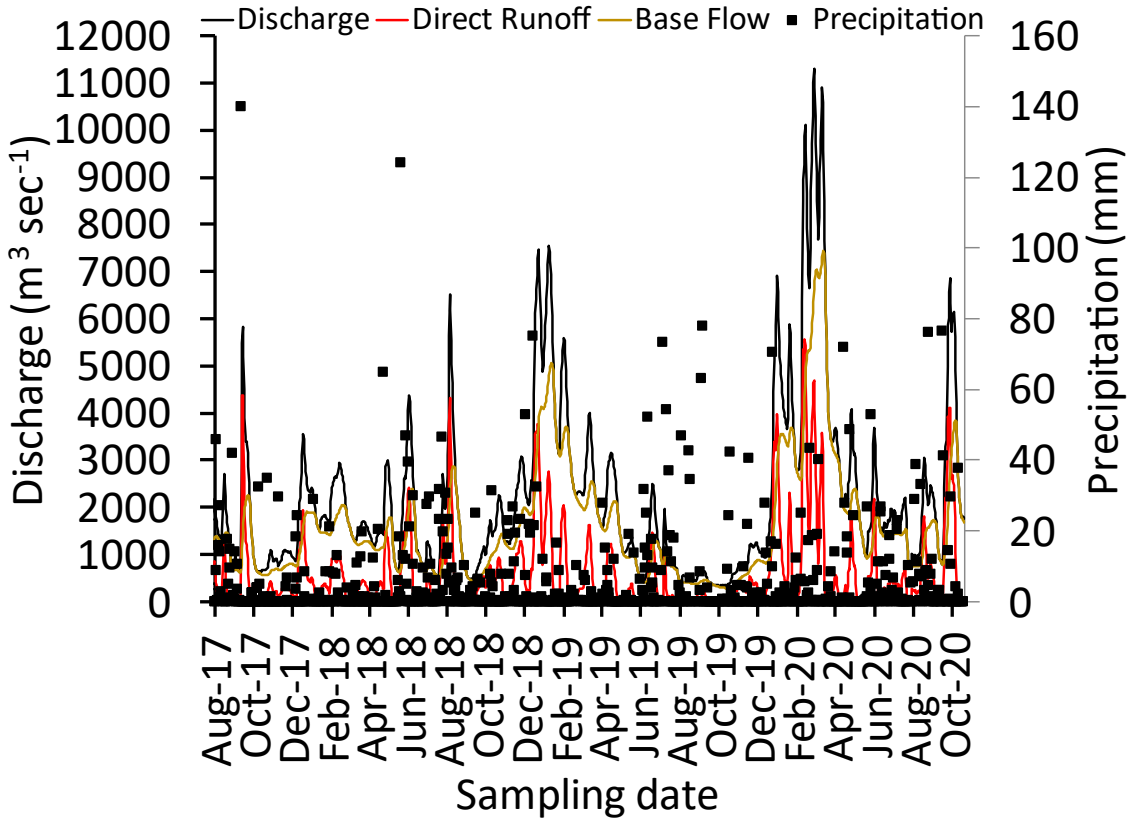

Figure D.2 Precipitation, discharge, base flow, and direct runoff in the Edisto River at the sampling site, USGS 02175000.

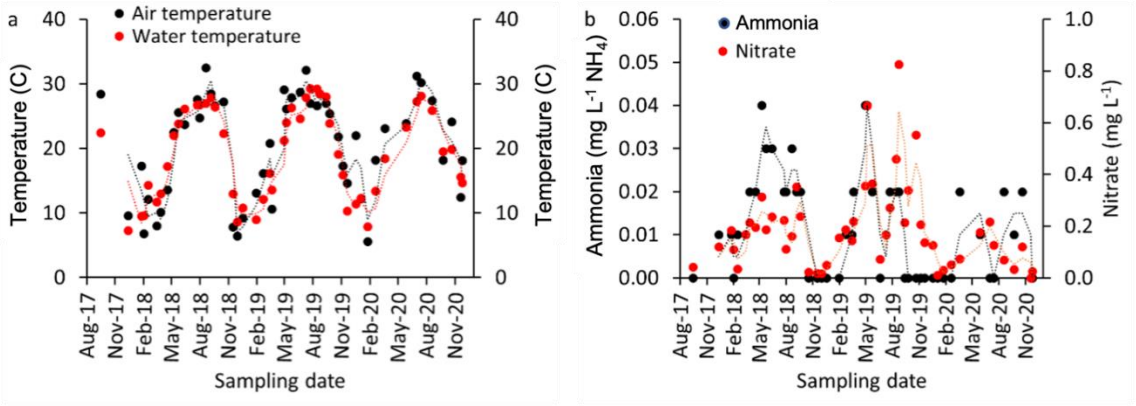

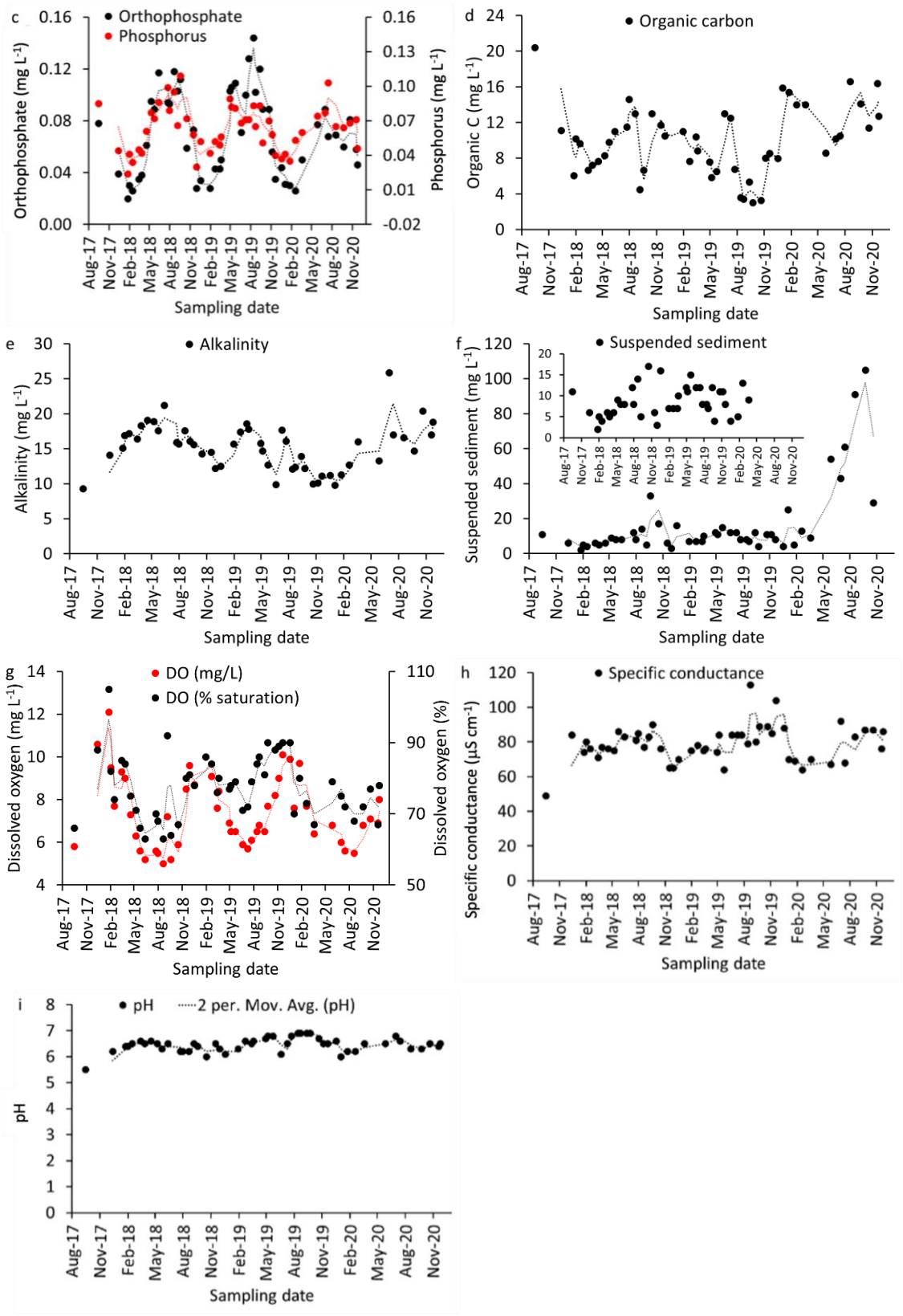

Figure D.3 The physicochemical properties of the Edisto River water at the sampling site: (a) air and water temperature, (b) ammonia and nitrate, (c) phosphorous and

orthophosphate, (d) organic carbon, (e) alkalinity, (f) suspended sediment, (g) dissolved oxygen, (h) specific conductance, and (i) pH.

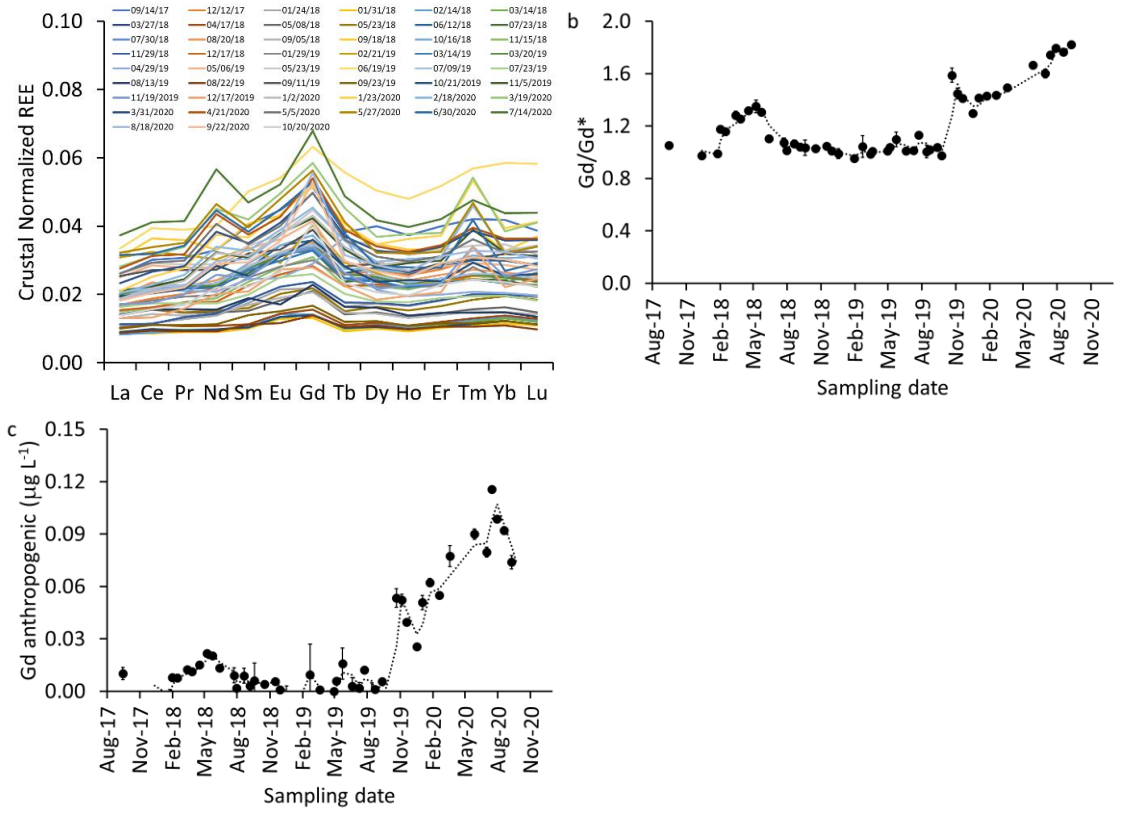

Figure D.4 (a) Crustal normalized REE, and (b) Gadolinium anomaly, and (c) anthropogenic Gd concentration.

References

1. Loosli, F. et al. Sewage spills are a major source of titanium dioxide engineered (nano)-particle release into the environment. Environ. Sci. Nano 6, 763–777 (2019).
2. Jochum, K. P. et al. Reference Values Following ISO Guidelines for Frequently Requested Rock Reference Materials. Geostand. Geoanalytical Res. 40, 333–350 (2016).
3. Hendriks, L., Gundlach-Graham, A., Hattendorf, B. & Günther, D. Characterization of a new ICP-TOFMS instrument with continuous and discrete introduction of solutions. J. Anal. At. Spectrom. 32, 548–561 (2017).
4. Pace, H. E. et al. Determining transport efficiency for the purpose of counting and sizing nanoparticles via single particle inductively coupled plasma mass spectrometry. Anal. Chem. 83, 9361–9369 (2011).
5. Tanner, M. Shorter signals for improved signal to noise ratio, the influence of Poisson distribution. J. Anal. At. Spectrom. 25, 405–407 (2010).
6. Wang, J. et al. Detection and quantification of engineered particles in urban runoff. Chemosphere 248, 126070 (2020).
7. Kulaksiz, S. & Bau, M. Contrasting behaviour of anthropogenic gadolinium and natural rare earth elements in estuaries and the gadolinium input into the North Sea. Earth Planet. Sci. Lett. 260, 361–371 (2007).
8. Bau, M., Knappe, A. & Dulski, P. Anthropogenic gadolinium as a micropollutant in river waters in Pennsylvania and in Lake Erie, northeastern United States. Chemie der Erde 66, 143–152 (2006).
9. Kulaksiz, S. & Bau, M. Rare earth elements in the Rhine River, Germany: First case of anthropogenic lanthanum as a dissolved microcontaminant in the hydrosphere. Environ. Int. 37, 973–979 (2011).
10. Knappe, A., Möller, P., Dulski, P. & Pekdeger, A. Positive gadolinium anomaly in surface water and ground water of the urban area Berlin, Germany. Geochemistry 65, 167–189 (2005).
11. Elbaz-Poulichet, F., Seidel, J. L. & Othoniel, C. Occurrence of an anthropogenic gadolinium anomaly in river and coastal waters of Southern France. Water Res. 36, 1102–1105 (2002).
12. Möller, P., Paces, T., Dulski, P. & Morteani, G. Anthropogenic Gd in surface water, drainage system, and the water supply of the City of Prague, Czech Republic. Environ. Sci. Technol. 36, 2387–2394 (2002).
13. Nozaki, Y., Lerche, D., Alibo, D. S. & Tsutsumi, M. Dissolved indium and rare earth elements in three Japanese rivers and Tokyo Bay: Evidence for anthropogenic Gd and In. Geochim. Cosmochim. Acta 64, 3975–3982 (2000).
14. Hissler, C., Stille, P., Guignard, C., François Iffly, J. & Pfister, L. Rare Earth Elements as hydrological tracers of anthropogenic and critical zone contributions: a case study at the Alzette River basin scale. Procedia Earth Planet. Sci. 10, 349–352 (2014).
15. US EPA. Biosolids technology fact sheet: Land application of biosolid. (2000).
16. Paul, M. J. & Meyer, J. L. Streams in the Urban Landscape. Annu. Rev. Ecol. Syst. 32, 333–365 (2001).
17. South Carolina State Climatology Office. Climate data of Orangeburg and Aiken county. Available at:

http://www.dnr.sc.gov/climate/sco/ClimateData/countyData/county_orangeburg.php. (Accessed: 16th May 2020)
18. North East Biosolids and Residuals Association (NEBRA). A national biosolids regulation, quality, end use & disposal survey. Final report. Tamworth, NH, USA. (2007).
19. Kiser, M. A. et al. Titanium nanomaterial removal and release from wastewater treatment plants. Environ. Sci. Technol. 43, 6757–6763 (2009).
20. Johnson, A. C. et al. An assessment of the fate, behaviour and environmental risk associated with sunscreen TiO_2 nanoparticles in UK field scenarios. Sci. Total Environ. 409, 2503–2510 (2011).
21. Shi, X. et al. Fate of TiO_2 nanoparticles entering sewage treatment plants and bioaccumulation in fish in the receiving streams. NanoImpact 3–4, 96–103 (2016).
22. Khosravi, K., Hoque, M. E., Dimock, B., Hintelmann, H. & Metcalfe, C. D. A novel approach for determining total titanium from titanium dioxide nanoparticles suspended in water and biosolids by digestion with ammonium persulfate. Anal. Chim. Acta 713, 86–91 (2012)

Appendix E

Permissions to Reprint

Episodic surges in titanium dioxide engineered particle concentrations in surface waters following rainfall events

Author: Md Mahmudun Nabi,Jingjing Wang,Mohammed Baalousha
Publication: Chemosphere
Publisher: Elsevier
Date: January 2021

Journal Author Rights

Please note that, as the author of this Elsevier article, you retain the right to include it in a thesis or dissertation, provided it is not published commercially. Permission is not required, but please ensure that you reference the journal as the original source. For more information on this and on your other retained rights, please visit: https://www.elsevier.com/about/our-business/policies/copyright#Author-rights

BACK CLOSE WINDOW

Temporal variation in TiO2 engineered particle concentrations in the Broad River during dry and wet weathers

Author: Md Mahmudun Nabi,Jingjing Wang,Erfan Goharian,Mohammed Baalousha

Publication: Science of The Total Environment

Publisher: Elsevier

Date: 10 February 2022

Temporal variability in TiO2 engineered particle concentrations in rural Edisto River

Author: Md Mahmudun Nabi,Jingjing Wang,Celeste A. Journey,Paul M. Bradley,Mohammed Baalousha

Publication: Chemosphere

Publisher: Elsevier

Date: June 2022

Journal Author Rights

Please note that, as the author of this Elsevier article, you retain the right to include it in a thesis or dissertation, provided it is not published commercially. Permission is not required, but please ensure that you reference the journal as the original source. For more information on this and on your other retained rights, please visit: https://www.elsevier.com/about/our-business/policies/copyright#Author-rights

BACK CLOSE WINDOW